GRI-94/0455

Topical Report

Using Diagenesis Information to Augment Fracture Analysis

Prepared by:
Bureau of Economic Geology
The University of Texas at Austin

Gas Research Institute

Exploration and Production Group
April 1995

GRI-94/0455

USING DIAGENESIS INFORMATION TO AUGMENT FRACTURE ANALYSIS

Topical Report

(January 1993–November 1994)

Prepared by

S. E. Laubach, T. F. Hentz, M. K. Johns, H. Baek, and S. J. Clift

Bureau of Economic Geology

Noel Tyler, Director

The University of Texas at Austin

Austin, Texas 78713-8924

for

Gas Research Institute

Contract No. 5082-211-0708

John Hansen, Project Manager

April 1995

DISCLAIMER

LEGAL NOTICE This work was prepared by the Bureau of Economic Geology as an account of work sponsored by the Gas Research Institute (GRI). GRI, nor members of GRI, nor any person acting on behalf of either:

a. Makes any warranty or representation, expressed or implied, with respect to the accuracy, completeness, or usefulness of the information contained in this report, or that the use of any apparatus, method, or process disclosed in this report may not infringe privately owned rights; or

b. Assumes any liability with respect to the use of, or for damages resulting from the use of, any information, apparatus, method, or process disclosed in this report.

50272-101

REPORT DOCUMENTATION PAGE	1. REPORT NO. GRI-94/0455	2.	3. Recipient's Accession No.

4. Title and Subtitle
Using Diagenesis Information to Augment Fracture Analysis

5. Report Date
April 1995

6.

7. Author(s)
S. E. Laubach, T. F. Hentz, M. K. Johns, H. Baek, S. J. Clift

8. Performing Organization Rept. No.

9. Performing Organization Name and Address
Bureau of Economic Geology
The University of Texas at Austin
University Station, Box X
Austin, Texas 78713-8924

10. Project/Task/Work Unit No.

11. Contract(C) or Grant(G) No.
(C) 5082-211-0708
(G)

12. Sponsoring Organization Name and Address
Gas Research Institute
8600 West Bryn Mawr Avenue
Chicago, IL 60631
Project Manager: John Hansen

13. Type of Report & Period Covered
Topical
January 1993–November 1994

14.

15. Supplementary Notes
Topical report on analysis of natural fractures in low-matrix-permeability, gas-bearing sandstones, including new methods to predict fracture porosity, interpret geophysical well logs, and map natural fracture strikes in the subsurface.

16. Abstract (Limit: 200 words)

This report describes relations between natural fractures and diagenesis that can be used to identify fractured beds, controls on fracture porosity, and fracture strike. By categorizing diagenesis based on the temporal relations of authigenic mineral precipitation and fracture movement, sandstones can be subdivided into those dominated by pre-, syn-, and postkinematic cements. Even sandstones that have virtually all of their rock-framework porosity occluded by synkinematic cement may retain substantial fracture porosity. An estimate of the probable degree of postkinematic mineral occlusion of fracture porosity can be obtained from study of framework authigenic cement volume. A breakthrough technique that uses photomultiplier-based imaging of electron beam-induced luminescence (scanned CL) to detect quartz-filled microfractures in sandstones having synkinematic quartz cement permits fracture strikes to be mapped in areas of the wellbore where no macrofractures are present. Because small specimens can be used to get fracture strike with the scanned CL method, this approach can be applied to samples obtained from wireline-conveyed rotary sidewall coring devices, permitting more fracture-strike data to be collected at reduced cost. Results of this study can be applied by operators to evaluation of prospects for horizontal drilling in highly cemented sandstone formations.

17. Document Analysis a. Descriptors
Texas, Wyoming, Canyon Sandstone, Travis Peak Formation, Frontier Formation, tight gas sandstones, diagenesis, natural fractures, reservoir quality, horizontal drilling, numerical modeling, rock-property testing, well-log analysis

b. Identifiers/Open-Ended Terms
innovative natural fracture mapping methods, description of fractures in tight gas sandstones, fracture toughness testing and point-load testing of sandstone, analysis of geophysical well logs, new classification of diagenesis, integrated diagenetic and structural studies

c. COSATI Field/Group

18. Availability Statement	19. Security Class (This Report)	21. No. of Pages
Release unlimited	Unclassified	189
	20. Security Class (This Page)	22. Price

(See ANSI–Z39.18) *See Instructions on Reverse*

OPTIONAL FORM 272 (4-77)
(Formerly NTIS–35)
Department of Commerce

dominated, volumetrically, by pre-, syn-, and postkinematic cements. This categorization leads to useful insights about the properties of fractures and their relation to sandstone framework porosity. Fracture-prone layers of several different types exist in highly cemented sandstone. Prekinematic cements that localize fractures can be identified with conventional geophysical logs. Fractured beds associated with synkinematic quartz cement tend to preserve fracture porosity in highly cemented sandstones. Methods based on borehole-imaging logs and combinations of acoustic and other logs (an application of data normally collected for stress profile logs) can identify thin, fracture-prone beds in quartz-cemented rocks. However, the current propensity of beds to fracture is only a useful indication of the likelihood of fracture occurrence if the diagenetic context of fracture development is known.

Fracture porosity is mainly controlled by diagenetic history of the rock. Diagenesis information can be used to predict the degree of natural fracture occlusion. In synkinematic cement, competition between fracturing and fracture sealing determines porosity and fracture-network connectivity. Even sandstones that have virtually all of their matrix porosity occluded by synkinematic cement may retain substantial fracture porosity. An estimate of the probable degree of postkinematic mineral occlusion of fracture porosity can be obtained from study of the appropriate rock framework authigenic cement volume.

A breakthrough technique that uses photomultiplier-based imaging of electron beam-induced luminescence (scanned CL) to detect quartz-filled microfractures in sandstones having synkinematic quartz cement permits fracture strikes to be mapped in areas of the wellbore where no macrofractures are present. Because small specimens can be used to get fracture strike with the scanned CL method, this approach can be applied to samples obtained from wireline-conveyed rotary sidewall coring devices, permitting more fracture-strike data to be collected at reduced cost. This report also describes the use of fractures in coal inclusions and axial point-load tests to acquire indirect evidence of macrofracture strike.

Results of this study can be applied by operators to evaluation of prospects for horizontal drilling in highly cemented sandstone formations. Data required include samples of the formation sufficient to characterize cement sequence and microstructure. Such data can normally be acquired from sidewall or full-diameter core. If macrofractures are present, they should also be analyzed, but their presence is not required in order to evaluate beds. Using microstructures to evaluate the timing of fracturing, the proper categorization of cements relative to movement history can be carried out. Analysis of macrofractures in core will greatly improve reliability of this assessment. Results of this study suggest that areas having synkinematic quartz cement and slight or no overprint of postkinematic cement will be most prospective for having open fractures. Scanned CL evidence taken from oriented core or sidewall cores in areas of dense synkinematic quartz cement can provide information on local fracture orientation to guide selection of well drilling direction.

Although this issue has only recently been addressed explicitly by reservoir modelers, the critical role of fracture-lining and fracture-filling minerals in governing fracture porosity (and permeability) and the capacity for fracture porosity to change with variation in effective stress is of fundamental importance. Greater appreciation of the genetic link between evolving fracture porosity and diagenesis illustrated in this study shows that this approach can lead to better extrapolation of fracture attributes.

Technical Approach

The study focuses on opening-mode fractures (veins) in three representative sandstone plays—the Canyon, Travis Peak, and Frontier. Our approach is based on observations of contrasting low-matrix-permeability sandstones that were chosen for study based on existence of a core data base and known diagenetic framework. Core samples from Sonora and Ozona Canyon, Travis Peak, and Frontier Formation sandstones represent diagenetic and natural fracture information from rocks having a range of ages, burial/loading histories, and compositional characteristics. Study focused on core samples in order to eliminate the need to identify and discount spurious uplift- and weathering-related fractures and to facilitate comparison and correlation of diagenetic zones with geophysical log signatures.

Implications

Low-matrix-permeability natural gas reservoirs in sandstones, generally defined as sandstone formations with in situ gas permeability values of 0.1 millidarcy or less, are important parts of the U.S. natural gas resource base, with about 27 percent (349 Tcf of 1,295 Tcf) of the technically recoverable lower 48 supply (National Petroleum Council, 1992; Perry, 1994). Current yearly production is about 2 Tcf, or 12 percent of the lower 48 yearly gas production total (excluding casinghead gas).

Natural fractures are widespread in these reservoirs, and they are responsible for areas of high deliverability. Where natural fractures play a role in gas deliverability, the lack of reliable methods to systematically determine fracture attributes has hindered efficient development of the resource through optimized well placement or directional drilling. As exploration and development increasingly move into reservoirs where natural fractures are key to successful completions, methods to measure or predict natural fracture attributes will be needed in order to achieve desired production levels at acceptable cost.

CONTENTS

Figures

Tables

Appendix Tables

Using Diagenesis Information to Augment Fracture Analysis

Benefits of Research

Low-matrix-permeability natural gas reservoirs in sandstones are important parts of the U.S. natural gas resource base, with about 27 percent (349 Tcf of 1,295 Tcf) of the technically recoverable lower 48 supply (National Petroleum Council, 1992; Perry, 1994). Low permeability in these sandstones is primarily the result of precipitation of authigenic cement that blocks porosity (Dutton and Laubach, 1993). Natural fractures also occur in these sandstones, and operator surveys show that industry believes these features to be important reservoir elements (Hansen, 1993). Yet measuring the role of natural fractures in current natural gas production and assessing the potential for effectively targeting these features with advanced reservoir development technology are hindered by inadequate natural fracture interpretation and characterization methods.

This study presents criteria and methods for systematically characterizing natural fractures in thoroughly cemented sandstone natural gas reservoirs on the basis of relationships between fractures and diagenetic framework. Application of these criteria to four formations in three plays clarifies how sandstone diagenesis information can be used to identify beds that are compositionally susceptible to fracture, recognize controls on fracture porosity, and infer orientation of fractures. In low-matrix-permeability sandstones, knowledge of natural fracture attributes is important in development decisions, but for many plays, information on natural fractures is sparse. This study provides methods to augment fracture characterization that are applicable to most of these units.

Technical Perspective

To efficiently and fully develop geologically complex natural gas reservoirs, information is needed on several key attributes of natural fractures. These include identification or prediction of areas of high fracture abundance, documentation of fracture porosity and permeability patterns and controls, and measurement of fracture strike. These fracture attributes are important because, among other effects, natural fractures can

- enhance or inhibit formation permeability,
- cause drainage anisotropy and reservoir compartmentalization,
- promote near-wellbore hydraulic fracture tortuosity that can have detrimental effects on success of well stimulation, and
- influence growth direction of hydraulic fractures.

Increasingly, natural fractures are viewed as targets for directional drilling because of the potential for enhanced deliverability that open fractures provide. Filled fractures that inhibit matrix flow also need to be considered in development decisions because of their role in promoting reservoir drainage anisotropy and compartmentalization. From a development point of view, assessing the character of natural fractures is critical to (1) deciding the type of well to drill, (2) selecting well spacing patterns that account for permeability anisotropy, (3) planning and evaluating stimulation and completion, and (4) estimating reserves.

As illustrated in table 1 and appendix 1, natural fractures are widespread in natural gas reservoir sandstones, yet attributes such as spacing, porosity, and strike in nearly all major tight gas sandstone plays either are undetermined or have been measured satisfactorily only in small areas. Fractures are commonly an unknown or poorly known quantity in formation evaluation and reservoir modeling simply because fractures may not intersect the wellbore where they can be detected and characterized. Few wellbores intersect fractures owing to the nearly vertical inclination and wide spacing (on the order of meters to tens of meters or more) that typify large opening-mode fractures in flatlying sedimentary rocks. Such fractures have an exceedingly low probability of being intersected by vertical wellbores that are typically less than 18 inches (46 cm) in diameter. Fractures that do not intersect the wellbore are not detectable by geophysical logging methods. The same sampling limitations apply, of course, to whole core.

No models exist that predict the distribution of open pore space (and thus their ability to transmit fluid) in fractures. This fracture attribute is difficult to establish even where core and advanced well-log data are available. Current fracture detection methods—when they yield any information at all—commonly do not provide statistically significant data sufficient to

Table 1. Fractures observed in core.

Formation (basin)	Range of widths	Widths of open fractures	Height (length)	Fracture types	Mineral fill	Fracture strike	References*
Clinton-Medina (Appalachian Basin)	nd	nd	nd	Sealed inclined to vertical extension fractures and open bedding parallel fractures	nd	N55 to 75E NW-SE, E to NE, W to NW	1, 2, 3, 4, 5, 6, 7, 8, 9, 10, 11, 12, 13
Berea (Appalachian Basin)	nd	nd	up to several feet	Subvertical, partly open fractures	nd	NE and NW	14, 7
Cotton Valley (East Texas and Louisiana Basins)	nd	Local; ~0.25 cm	nd	Partly filled subvertical extension fractures confined to individual sandstone beds	Calcite	E to NE	15, 3, 16, 17
Travis Peak (East Texas and Louisiana Basins)	0.5 μm to 0.5 cm	0.5 cm	up to several feet	Open and filled subvertical extension fractures	Quartz, ankerite, calcite, gypsum	E to NE	18, 19, 20, 21, 22, 17, 23, 24, 25
Olmos (Maverick Basin)	nd	nd	nd	Extension fractures and small normal faults	nd	nd	26, 27
Wilcox deltaic (Texas Gulf Coast Basin)	nd	nd	nd	Open and filled extension fractures and normal faults	nd	nd	28
Wilcox Lobo (Texas Gulf Coast Basin)	nd	nd	nd	Extensively fractured and faulted locally	Quartz	variable	29, 30, 32, 33, 34, 35, 36, 37, 38
Vicksburg (Texas Gulf Coast Basin)	nd	nd	nd	Sealed or open fractures and small faults	nd	nd	39, 40
Cherokee-Red Fork (Anadarko Basin)	nd	nd	nd	Unspecified fractures	nd	nd	41
Cleveland (Anadarko Basin)	nd	nd	<1 ft	Subvertical, mineralized extension fractures	nd	300–320	42, 43, 44, 3, 45, 46
Granite Wash (Anadarko Basin)	nd	nd	nd	nd	nd	nd	nd
Davis (Fort Worth Basin)	<0.25 mm	Local	4 inches to several feet	Partly to completely filled vertical to subvertical extension fractures	Calcite	359–020	47
Abo (Permian Basin)	nd		nd	Natural fractures and minor faults	nd	nd	48, 49, 50, 51
Morrow (Permian Basin)	nd		nd	nd		nd	52

Table 1 (cont.)

Formation (basin)	Range of widths	Widths of open fractures	Height (length)	Fracture types	Mineral fill	Fracture strike	References*
Sonora Canyon (Val Verde Basin)	nd	nd	Avg. <4 inches in siderite zones >1 ft in quartz-rich layers	Partly open fractures confined to siderite zones. Partly open fractures not confined to siderite zones	Dickite, calcite, quartz	range of strikes	53, 16, 54, 55, 56, 57
Ozona Canyon (Val Verde Basin)	0.05–1.45 mm	variable	up to 38 cm	Opening mode, vertical	Barite, quartz, ankerite, calcite	nd	58
Dakota (Piceance and San Juan Basins)	nd	nd	nd	Unspecified fractures and faults	nd	nd	59, 60, 61
Cliff House-Point Lookout (San Juan Basin)	nd	nd	nd	Unspecified fractures	nd	nd	3, 62
Pictured Cliffs (San Juan Basin)	nd	nd	nd	Extension fractures confined to individual sandstone beds	Calcite	310–320	59, 63, 64, 65, 66, 67
Muddy (J) (Denver Basin)	nd	nd	nd	Unspecified fractures	nd	nd	68, 69, 70
Mancos "B" (Piceance Basin)	nd	nd	nd	Unspecified fractures localized in sandstone and siltstone layers	nd	nd	3, 71
Mesaverde (Piceance Basin)	nd	nd	nd	At MWX site: partly filled or open vertical natural fractures and faults	Calcite, dickite, quartz, barite	W to NW	72, 73, 74, 75, 76, 77, 78, 79, 80, 81, 82, 83, 61, 84
Upper Almond-Blair (Green River Basin)	nd	nd	nd	Unspecified fractures	Bitumen	nd	3, 85, 86
Frontier (Green River Basin)	<0.25 mm	nd	up to 8 ft	Subvertical, extension fractures, small faults	Calcite, quartz	E to NE, NE to N, N to NW	20, 87, 88, 89, 90, 91

nd = not determined

Table 1 (cont.)

***References**

1 Baumgardner, 1991
2 Engelder, 1985
3 Finley, 1984
4 Laughrey and Harper, 1986
5 Laughrey, 1984
6 Multer, 1963
7 Overbey and Henninger, 1985
8 Overbey and Rough, 1971
9 Schrider and others, 1970
10 Ohio Geological Society, 1985
11 Sitler, 1985
12 Verbeek and Grout, 1983
13 Watts and others, 1972
14 Frantz and others, 1993
15 Dutton and others, 1991b
16 Finley and others, 1990
17 Laubach and others, 1989a
18 CER Corporation and S. A. Holditch & Assoc., 1989
19 CER Corporation and S. A. Holditch & Assoc., 1991
20 Clift and others, 1992
21 Dutton and others, 1991a
22 Laubach and Monson, 1988
23 Laubach, 1988b
24 Laubach, 1989a
25 Laubach, 1989b
26 Snedden and Kersey, 1982
27 Tyler and Ambrose, 1986
28 Laubach, unpub. core description, 1992
29 Henke, 1982
30 Henke, 1985
32 Laubach and others, 1992c
33 O'Brien and Freeman, 1979
34 Railroad Commission of Texas, 1980
35 Railroad Commission of Texas, 1991
36 Robinson and others, 1986
37 Self and others, 1986a
38 Self and others, 1986b
39 Laubach and others, 1992
40 Railroad Commission of Texas, 1990
41 Cornell, 1991
42 Brashear, 1961
43 CER Corporation, 1991b
44 CER Corporation, 1991c
45 Hentz, 1992
46 Landes, 1970
47 Collins and others, 1992
48 Baumgardner and others, 1988
49 Bentz, 1992
50 Broadhead, 1984
51 Scott and others, 1983
52 Craddock and others, 1983
53 Dyke, 1992
54 Hamlin and others, 1992
55 Marin and others, 1993
56 Miller and others, 1991
57 NSI, 1991
58 This report
59 DuChene, 1989
60 Lacy and others, 1992
61 Pittman and Sprunt, 1986
62 Gorham and others, 1979
63 Hower, 1990
64 Laubach and others, 1991
65 Laubach and others, 1992c
66 Laubach and Tremain, 1991
67 Laubach, 1992a
68 Higley and Schmoker, 1989
69 Weimer and others, 1986
70 Weimer and Sonnenberg, 1989
71 Middlebrook and others, 1993
72 Branagan, 1992
73 Brown and others, 1986
74 Lorenz and Finley, 1991
75 Lorenz and Hill, 1991
76 Lorenz, 1987
77 Mallory, 1977
78 Millison, 1962
79 Morrow and others, 1990
80 Myal and Frohne, 1991
81 Myal and Frohne, 1992
82 Northrop and Frohne, 1990
83 Pittman and Sprunt, 1984b
84 Ritzma, 1962
85 Pittman and Dickenson, 1989
86 Yin and others, 1992
87 Dickenson, 1992
88 Dutton and others, 1992
89 Hyman and others, 1991
90 Laubach and others, 1992b
91 Laubach, 1991

Table 2. Fracture characterization methods and their limitations.

Fracture attribute	Characterization method	Limitations of method	References
Porosity	Whole core observation Borehole-imaging logs	Sampling bias No basis for extrapolation	Nelson, 1985 Laubach, 1988
Degree of fracture porosity occlusion	Diagenetic analysis	Requires core but permits extrapolation; macrofractures not required	This report
Permeability	Wellbore flow measurements Inference from well tests	Only pertains to features intersecting wellbore or hydraulic fractures	Aguilera, 1980 van Golf-Racht, 1982
Conventional macrofracture orientation	Oriented cores Borehole-imaging logs Interference tests	Only pertains to features at wellbore or in core	Nelson and others, 1987 Laubach and others, 1991 Aguilera, 1980
New orientation methods	Microfracture/CL imaging	Can be used where no macrofractures are visible	This report
	Fractures in coal inclusions	Useful in Cretaceous fluvial and nearshore marine facies	This report
	Point-load tests	Best in soft, pliant sandstones	This report
Distribution at wellbore	Core Various geophysical logs Fluid loss during drilling	Well-developed techniques	Kulander and others, 1990 Aguilera, 1980 Dyke, 1991
Distribution away from wellbore	Well tests Seismic information Outcrop analogs	Non-unique and ambiguous results in many cases	van Golf-Racht, 1982 Nelson, 1985 Laubach, 1992

establish fracture abundance patterns or to map shifts in fracture orientation within a given unit or from one unit to the next (table 2). In low-matrix-permeability gas sandstone plays, even this information is commonly unavailable because costly borehole-imaging logs and whole core are rarely acquired in more than a few wells in an area. Yet studies of fractures in outcrops of reservoir-facies sandstones show that fracture attributes such as porosity, spacing, and strike can shift with disconcerting abruptness over short vertical and lateral distances (Laubach, 1992a). Moreover, fractures near the wellbore—and even fractures at considerable distance from the wellbore—may have an influence on deliverability and success of completion and stimulation practices that is difficult to anticipate.

To a great extent, the fracture-sampling problem has impeded basic studies of fracture characteristics in reservoir rocks. The fracture-sampling problem applies to study of macrofractures—large, macroscopically visible fractures. Microfractures, which are only visible under magnification, are more common and can be sampled effectively in small volumes of rock. Diagenetic aspects of rocks that may provide insight into properties of fractures can also be sampled in small rock volumes. Although large fractures are rightly viewed as key to fluid flow in fractured rock, indirect methods to infer the properties of large fractures using information that can be obtained from core or geophysical logs have the advantage of avoiding the sampling problem. Are indirect characterization methods feasible and, if so, what fundamental aspect of these rocks is most promising for yielding accurate indirect information on fracture attributes?

subsequently precipitated authigenic quartz in macro- and microfractures at the micron scale. When the beam of primary electrons strikes the sample, photons are generated as a result of electron hole pair recombination (Oxford Instruments, 1993). As the electron beam scans the sample, the intensity of the light emitted changes according to the spatial distribution of electro-optical centers (impurities, defects, etc.). The application of this method permits new insights into timing of fracture growth relative to cement precipitation, patterns of infill of fracture porosity, and identification of microstructures useful for inferring deformation kinematics.

Geologic Setting of Study Units

Canyon Sandstones

The Lower Permian Canyon Sandstones (Wolfcampian Sonora Canyon, lower Leonardian Ozona Canyon) were deposited in the Val Verde Basin, a northwest-trending foreland basin within the Permian Basin of West Texas (Hills and Galley, 1988). The Val Verde Basin forms an asymmetric trough; its deepest part is adjacent to the Ouachita structural belt in the south (fig. 1). The basin is one of a series of foreland basins that formed along the southern margin of the North American plate as a result of processes associated with plate convergence during Ouachita orogenesis (Wuellner and others, 1986; Meckel and others, 1992). The basin is bounded on the north and east by shelflike positive structural features: Central Basin Platform, Ozona Arch, and Eastern Shelf (fig. 1).

The Val Verde Basin became a distinct structural feature during Late Mississippian time, when the Tobosa Basin, the ancestral structure of the Permian Basin, began to separate into several basins and uplifts. Beginning in the Early Permian (Wolfcampian to early Leonardian), deposition of clastic slope wedges (coalesced submarine fan systems), now composing the Sonora and Ozona Canyon, prograded the southern margin of the Eastern Shelf southwestward (Hamlin and others, 1992; Laubach and others, 1994; Hamlin and others, in press). On the basin floor the distal parts of these northeastwardly derived slope wedges merged and interfingered with a continuing influx of Ouachita sediments from the south. Depths to Sonora Canyon reservoirs range from about 2,500 to 8,500 ft, whereas depths to Ozona Canyon reservoirs range from about 2,500 to 7,000 ft.

Travis Peak Formation

The area of study of the Lower Cretaceous Travis Peak Formation of the East Texas Basin (figs. 2 and 3) is on the western flank of the Sabine Arch within the East Texas Basin (Laubach and Jackson, 1990). Other regional structures in the area include the northeast- and east-trending Mexia–Talco fault zone, the east-trending Elkhart–Mount Enterprise fault zone, the east-trending Angelina flexure, and various minor structures caused by movement of salt. Near the center of the Sabine Arch, on the eastern side of the study area, the top of the Travis Peak occurs at 5,600 ft below sea level. The formation dips to the west and southwest on the western side of the Sabine Arch, and in the southern area the top of the Travis Peak is at 9,400 ft below sea level. The Travis Peak Formation is about 1,800 to 2,200 ft thick in East Texas (Tye, 1989).

Carbonates dominated early phases of deposition in the East Texas Basin (Moore, 1983). The earliest progradation of terrigenous clastics in the basin is recorded by the Upper Jurassic–Lower Cretaceous Cotton Valley Group. The Travis Peak Formation represents a second period of fluvial-deltaic progradation (Dutton and others, 1991a, 1991b). The relatively simple diagenetic pattern with depth in this formation, combined with dense well control on fracture-abundance patterns, allows the effects of the principal compositional variable, degree of quartz cementation, to be compared with fracture abundance.

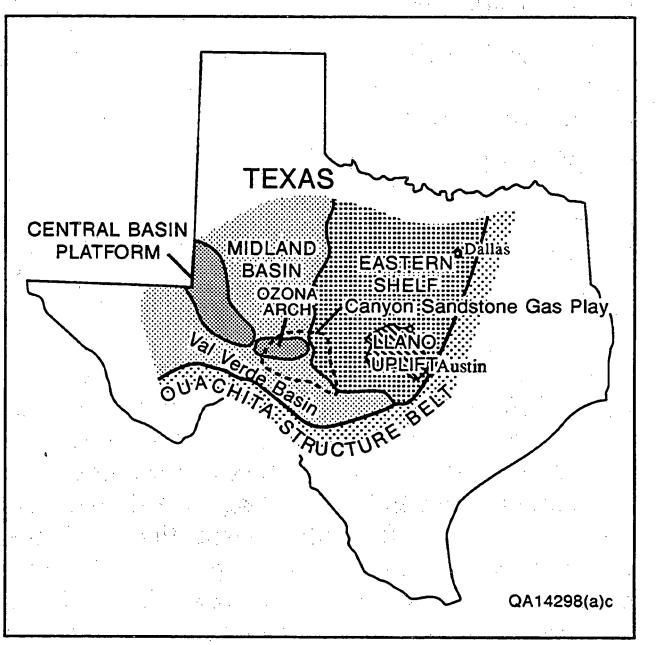

Figure 1. Structural setting of the Canyon Sandstones, Val Verde Basin, Texas.

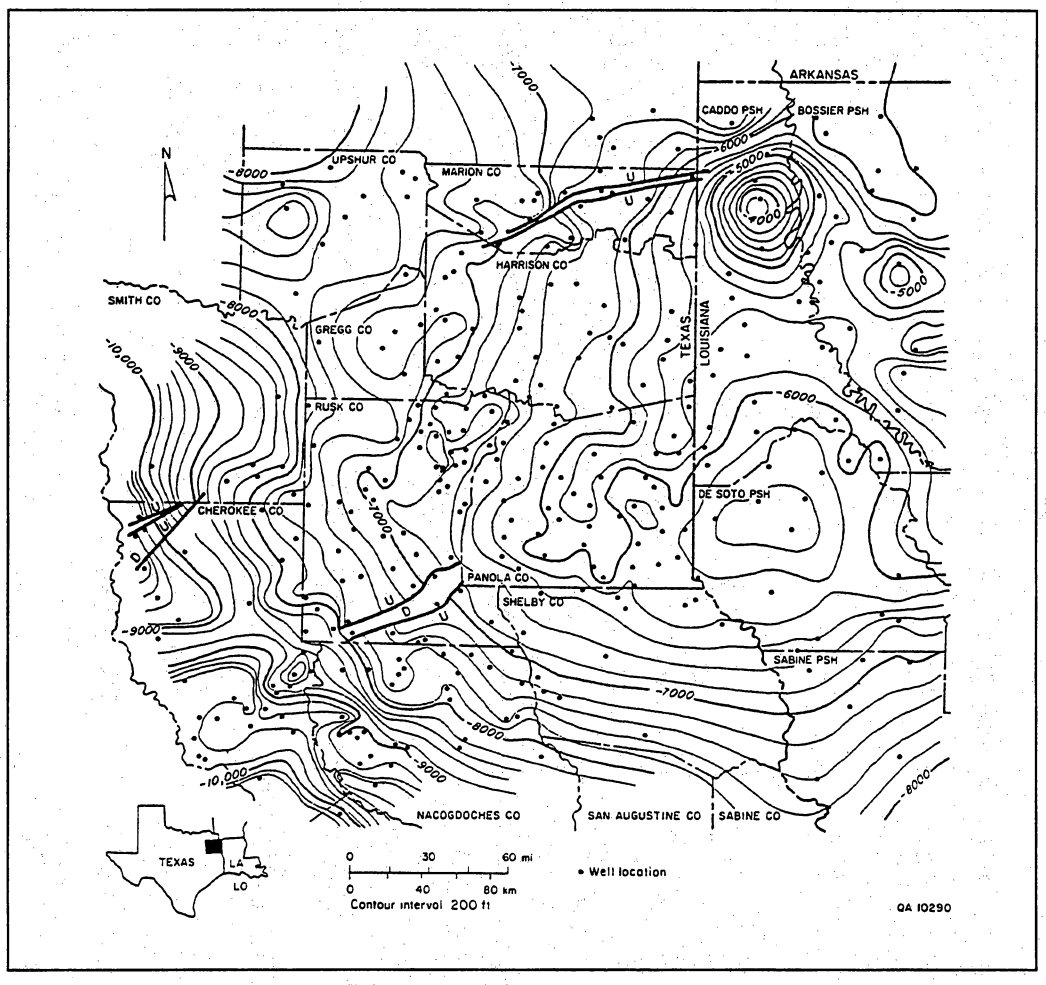

Figure 2. Structural setting of the Travis Peak Formation, East Texas. Structure-contour map, top of Travis Peak Formation. Datum is sea level. From Dutton and others (1991a, 1991b).

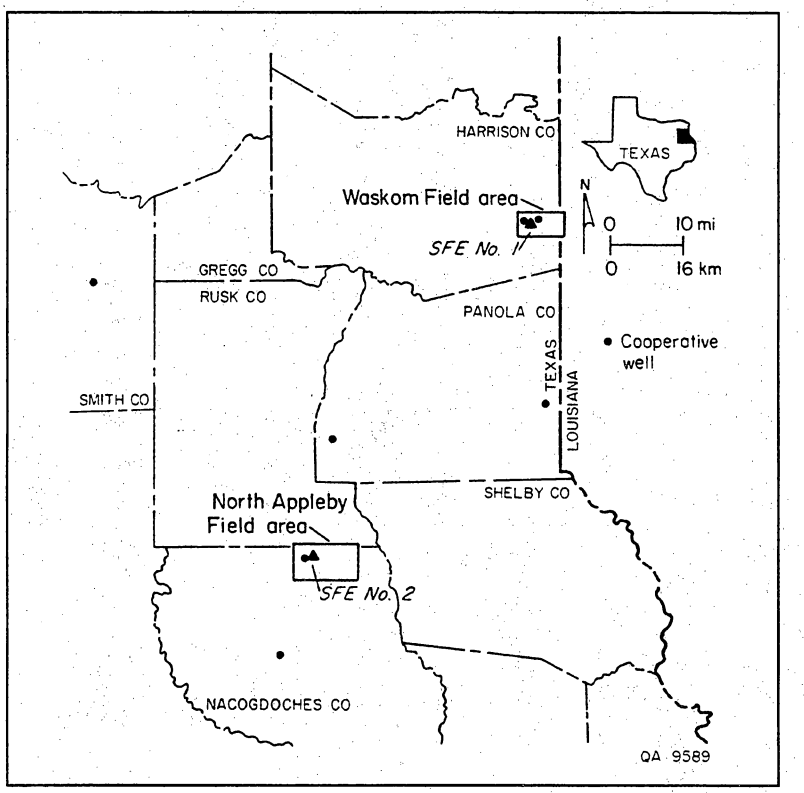

Figure 3. Location of principal GRI research wells in East Texas.

Frontier Formation

The Upper Cretaceous Frontier Formation in the Green River Basin of southwest Wyoming comprises marine and nonmarine sandstone and shale facies, which record early Late Cretaceous foreland-basin sedimentation (fig. 4). Frontier shorelines, composed of wave-dominated deltaic headlands and delta-flank strandplains, prograded eastward into the western interior Cretaceous seaway (Myers, 1977; Winn and others, 1984; Moslow and Tillman, 1986) during Cenomanian and Turonian times (Merewether and others, 1984).

The Green River Basin is within an extensive foreland basin that has been segmented by Laramide uplifts during the Late Cretaceous and early Tertiary. A major structure within the Green River Basin is the Moxa Arch, a broad north-trending uplift (fig. 4) that is a major area of Frontier gas production in the western Green River Basin. Major uplift of the Moxa Arch apparently occurred during the Late Cretaceous (Wach, 1977), related partly to deep-seated thrust-fault movement (Kraig and others, 1987). Uplift largely postdated Frontier deposition, but stratigraphic thinning indicates that some uplift was occurring along the south part of the Moxa Arch during Frontier deposition (Thomaidis, 1973; Wach, 1977; Dutton and others, in press). The present attitude of the Moxa Arch indicates that more recent uplift has been concentrated in the north and has resulted in a southward tilt. Samples in this study are mainly from the vicinity of the Moxa Arch.

Depth to the Frontier Formation increases from north to south along the Moxa Arch, ranging from about 6,000 to 15,000 ft below ground surface. In addition to core samples from several wells in the Frontier Formation along and adjacent to the Moxa Arch, fractures in the Frontier Formation were studied in outcrops along the southern and western margin of the basin. Results of this aspect of our study have been reported elsewhere (Laubach, 1992a, 1992b; Laubach and Lorenz, 1992; Lorenz and Laubach, 1994; Dutton and others, in press).

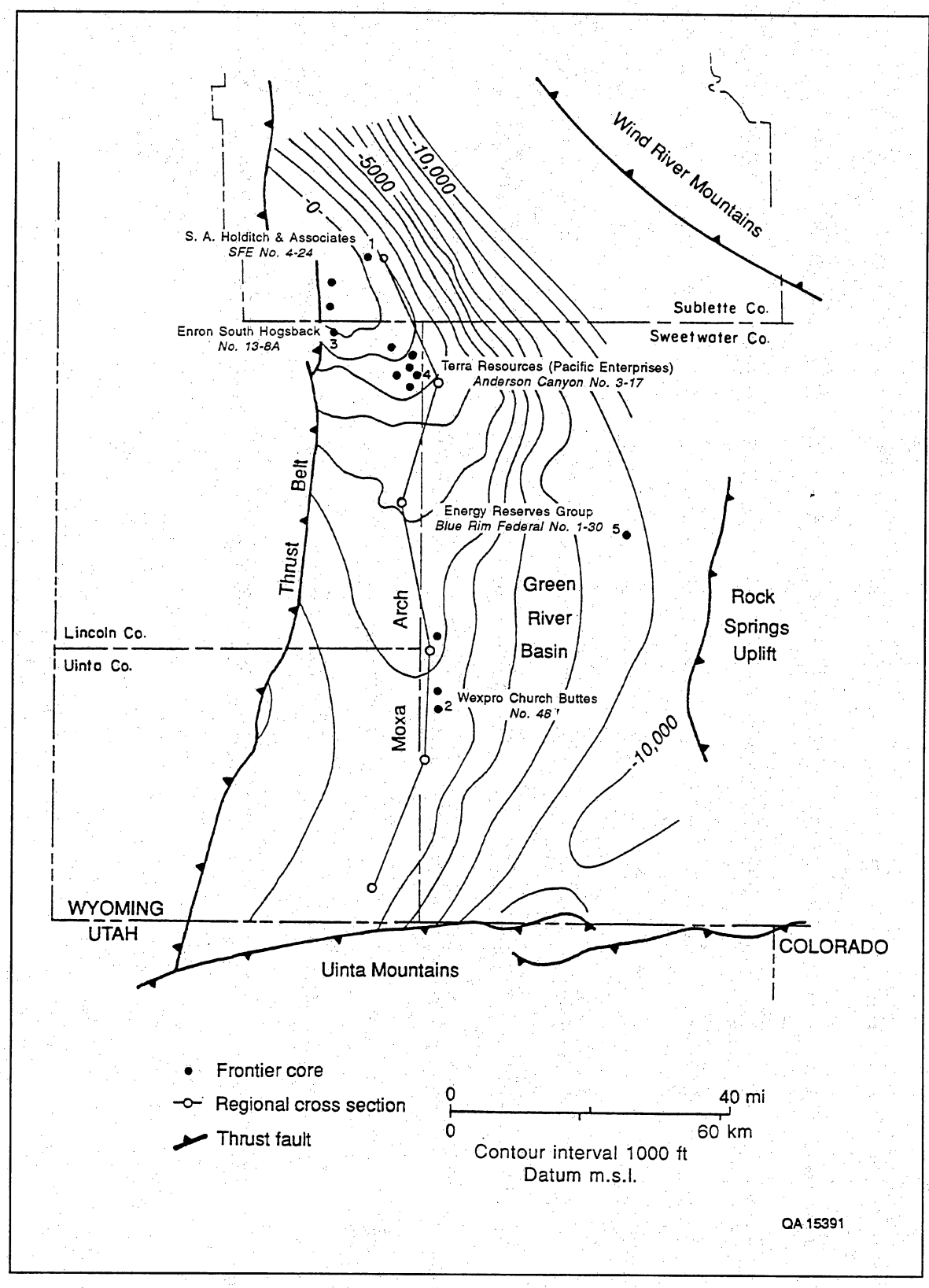

Figure 4. Structural setting of the Frontier Formation, southwestern Wyoming. Structure-contour map on the top of the Second Frontier. Location of wells from which Frontier cores were obtained is also shown. From Dutton and others (in press).

Types of Cement/Fracture Relations

Although such patterns have not previously been described in tight gas sandstones, fracture distributions that systematically vary with rock type are a well-known characteristic of fracture systems in sedimentary rock (Nelson, 1985). This stratigraphic control on fracture occurrence, or *fracture stratigraphy,* reflects the influence that deformation and the boundary conditions of contrasting rock properties and layer thickness exert on fracture growth. At the relatively shallow burial depths where hydrocarbon reservoirs occur, porosity, detrital grain composition and grain size, and cement volume and distribution are all factors that affect a sandstone's susceptibility to fracture. Because porosity is generally low in tight gas sandstones and detrital grain composition is commonly not highly variable within reservoir-facies rocks, cementation stands out as the important variable in governing propensity of sandstones to fracture. Rock properties affected by diagenesis vary in a nonlinear pattern with duration and depth of burial as compaction, dissolution, and cementation progress, but in general older and more deeply buried sandstones are more highly cemented (Dutton and Laubach, 1993).

The importance of diagenesis in governing fracture attributes is by no means restricted to influencing the rock's strength and brittleness. Diagenetic minerals can fill fractures, occluding porosity and altering the shape and connectivity of fluid pathways. Dissolution can also affect minerals that fill fractures, resulting in secondary fracture porosity. Finally, and perhaps most importantly, diagenetic and fracture processes can interact. Such processes can cause particular cement types and fractures to evolve together in predictable ways.

We define three categories of cementation event that can influence the distribution of fractures and fracture attributes in a layered sequence. These categories are distinguished on the basis of the timing of cement precipitation relative to fracture growth. The three categories are:

(1) *prekinematic* cementation, where cement precipitates before fractures open,
(2) *synkinematic* cementation, where cement is precipitated while fracture-opening movement is underway, and
(3) *postkinematic* cementation, where cement is precipitated after fractures form.

This report is the first explicit presentation of criteria for characterizing diagenesis in terms of fracture movement history. Yet the probable widespread applicability of this classification scheme is evident from the limited published information on fracture and diagenesis in other sandstones (for example, Dutton and others, 1993). Identifying the timing of cementation relative to fracture opening movements (kinematics) is the basis for differentiating cement/fracture relations and defining pre-, syn-, and postkinematic cement (fig. 5).

Timing relations between cement precipitation and fracture opening movement are not always clear. Some fractures associated with largely synkinematic cement may develop during only part of a cement-precipitation event, and many sandstones that have complex cementation or fracture histories can potentially contain pre-, syn-, and postkinematic cements, so these distinctions can be ambiguous. Repetitive sequences of authigenic minerals can also be precipitated, and multiple episodes of fracture opening and multiple fracture sets are also probably common. Nevertheless, the distinction of pre-, syn-, and postkinematic cements is useful because these relations can be observed (fig. 6), and the observations lead to predictions about the interrelationship of fracture and diagenesis microstructures and about the properties of macrofractures that often may not be directly observed.

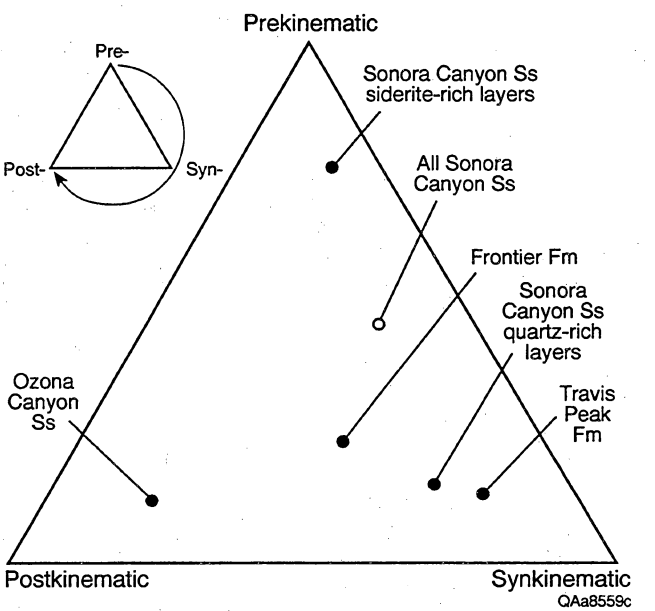

Figure 5. Ternary plot of relative proportions of pre-, syn-, and postkinematic cements in sandstone framework for each of the formations studied: Ozona Canyon Sandstone; Sonora Canyon Sandstone, separated into total Sonora, siderite-rich layers, and quartz-rich layers; Travis Peak Formation; and Frontier Formation. Concept of plot described in text.

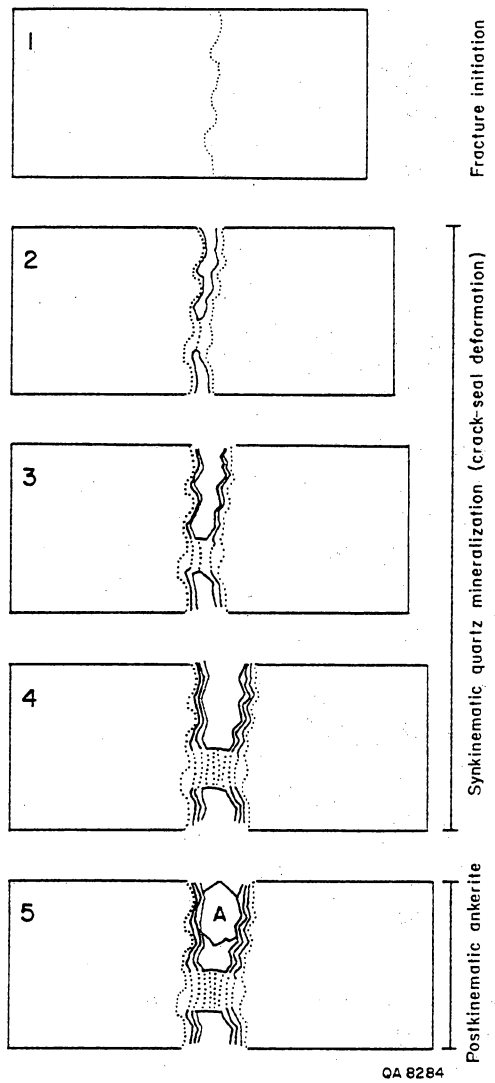

Figure 6. Fracture with synkinematic fracture-lining minerals (here, quartz) and postkinematic fracture-lining minerals (here, ankerite, A). Diagram shows evolution of microstructures within fracture as fracture progressively opens (1 through 5). Dotted lines represent areas where primary fluid inclusions have been trapped by rapid quartz precipitation following (or accompanying) fracture opening (Laubach, 1988b).

The four formations that we studied can be classified based on the volume of pre-, syn-, and postkinematic cement that they contain, as shown in figure 5. The basis for this new classification is the subject of this report and is described in subsequent sections. Each data point in figure 5 represents the relative percentages of pre-, syn-, and postkinematic cements of the sandstone framework of each of the four formations described. Values are normalized to 100 percent and are derived from the sums of the average percentages of each cement phase—categorized as pre-, syn-, or postkinematic with respect to a particular fracture episode on the basis of our analyses of fracture mineralization and cement microstructure—in the formations. In practice, we recommend that this type of information be compiled on a bed-by-bed basis or at least for stratigraphically distinct parts of formations, owing to the dependence of diagenesis on depositional architecture (for example, Dutton and Laubach, 1993). If more than one fracture event is present, diagrams that show the relationship of all cements to each fracture event should be constructed.

In this classification, marked distinctions are evident in cement type for the formations and for parts of formations. Formation character ranges from siderite-rich layers in Sonora Canyon, which are dominantly prekinematic, to Travis Peak sandstones, which have primarily synkinematic cements, to Ozona Canyon sandstones, having extensive postkinematic cement. Normalized percentages of pre-, syn-, and postkinematic cements in the formations are as follows. (1) Ozona Canyon: 12, 18, and 70 percent, (2) Sonora Canyon, siderite-rich layers: 76, 16, and 8 percent, (3) Sonora Canyon, quartz-rich layers: 15, 63, and 22 percent, (4) combined Sonora Canyon: 46, 39, and 15 percent, (5) Travis Peak: 13, 72, and 15 percent, and (6) Frontier Formation: 23, 44, and 33 percent. In addition, there is much variation within formations.

Classification of cement precipitation with respect to fracture opening in turn can be used to help predict fracture attributes. For example, prekinematic cements can create layers with high strength and brittleness that give them a propensity to fracture. Yet, because they precede fracture opening, prekinematic cements cannot fill or line fractures. Thus, in a development situation where reactive minerals (such as certain types of clay mineral) are known to be present as cements, an observation of the timing of fracture relative to emplacement of that authigenic phase could clarify whether that phase is likely to be in fractures and whether precautions are required to protect fractures from reactive fluids. As discussed in the section "Fracture Porosity Preservation," fractures associated with synkinematic cements are more likely to preserve open fracture pore space. Because fracture opening and filling are linked processes for synkinematic fractures, microstructure patterns contain information that can be used to make deductions about typical patterns of fracture porosity, fracture-bridging mineral type (and thus, strength), and fracture roughness.

Synkinematic cements are also associated with microstructures that reflect movement during the time of cementation, as discussed in the section "Using

Microstructure and Test Data to Map Fracture Strike." In other words, small-scale deformation features within or associated with such cements can be used to infer attributes, such as orientation, associated with larger macrofractures. This is the basis for using microstructures to infer macrofracture strike. Postkinematic cements are most likely to fill and block fracture porosity. Diagenetic studies of the degree of postkinematic cement in matrix porosity may therefore be used to monitor the degree to which fracture porosity is occluded, if matrix porosity/fracture porosity relationships can be identified and calibrated.

Identification of Fractured Layers

Measuring rock composition is readily accomplished if cores or geophysical well logs are available. For subsurface beds, identifying fractured layers and fracture stratigraphy is much more difficult. Fracture abundance patterns at the wellbore may provide little valid information, and that information can be misleading. In sandstone reservoirs, measuring fracture abundance is the first challenge to documenting fracture stratigraphy and assessing its relationship to diagenesis. In the Canyon, Travis Peak, and Frontier examples presented here, fractures are predominantly vertical and wellbores are vertical, and it is therefore impossible in most cases to obtain absolute measurements of fracture spacing. Other measures of fracture abundance must be used.

One useful measure of abundance is the total length of fractures in a cored interval normalized to the thickness of the cored rock, called *fracture number.* Fracture occurrence and the vertical dimension or height of fractures relative to the thickness of the cored rock control fracture number. In other words, a single fracture spanning the reference bed thickness and numerous short fractures with cumulative length equal to the reference bed thickness would have identical fracture numbers of 1.0. With extensive sampling through the acquisition of long cores from numerous wells in the same interval, fracture number will give a reproducible estimate of fracture abundance (fig. 7).

Because opening-mode fractures in many gas reservoir cores appear to predominate in sandstone and siltstone rather than in interbedded shale and mudstone and because these coarser grained clastic intervals are the rocks of interest for horizontal drilling, we generally normalize fracture length to the thickness of cored sandstone or siltstone rather than to the length of the entire core. In formations such as the Frontier, where outcrop studies show that some sandstones (such as bioturbated, clay-rich lower shoreface sandstones) have lower fracture abundance than clean upper shoreface sandstone, normalizing core fracture length to clean sandstone thickness is appropriate. In this study, fracture length was also normalized to thickness of compositional subdivisions within sandstones to compare fracture abundance in layers having contrasting primary depositional and diagenetic compositions.

Fracture numbers in reservoir sandstones are generally less than 1.0 in several sandstones that we studied, reflecting the sparse occurrence of fractures in core. In Canyon sandstones, fracture numbers for sandstones ranged from 0, where no fractures are present, to 2.0, where multiple fractures are present. Average fracture numbers for sandstone are about 0.05. In the Travis Peak Formation, fracture numbers range from 0 to 1.5. High fracture numbers reflect short intervals in sandstones where multiple fractures are present. Fracture number is also sensitive to the length of core over which fracture occurrence is normalized. Low fracture numbers are typical of thick cored intervals, whereas very low fracture numbers interspersed with local areas of high fracture number characterize wells where fracture numbers are normalized over short core lengths. Typically Travis Peak fracture numbers for sandstone intervals greater than 100 ft long are much less than 1.

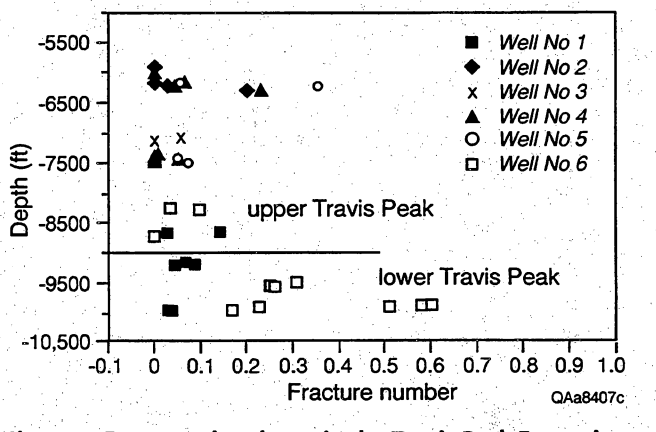

Figure 7. Fracture abundance in the Travis Peak Formation, as shown by fracture number. Well 1, Prairie Mast No. 1-A; Well 2, Mobil Cargill No. 14; Well 3, Werner Sawmill; Well 4, SFE No. 1; Well 5, Arkla Scott No. 5; Well 6, SFE No. 2.

Fracture numbers cannot be converted into fracture spacing measurements; they are a relative measure of the degree of fracturing. It is most suitable to use and compare fracture numbers where extensive core or borehole-imaging log data are available. For the Frontier Formation, fewer cores were available, and these have shorter cored intervals in equivalent stratigraphic units. Natural fractures in these cores are so sparse that fracture numbers are not meaningful measurements for comparison. Alternate approaches used for identifying fracture stratigraphy in the Frontier using outcrop observations are discussed in a later section.

In rocks where distinct zones of cement can be identified within sandstones, fracture numbers can be generated for those zones by using the thickness of the compositionally distinctive zone as the normalization interval. Thin siderite-cemented zones evident in Sonora Canyon Sandstone cores are examples. Fracture numbers for these siderite cemented zones range from 0 to more than 5. For the Sun Dunbar No. 1, the average fracture number for siderite-cemented zones is 0.8. Such high fracture numbers indicate abundant fractures that have cumulative vertical dimensions similar to those of the zones in which they occur.

Abundance patterns shown in figure 7 are representative of the Travis Peak cores in this study. The range of fracture numbers for the relatively more highly fractured lower Travis Peak cores is 0 to 0.6, with an average of 0.3. Fracture number is generally higher in the lower Travis Peak Formation, reflecting greater numbers of fractures in lower Travis Peak sandstones. The SFE No. 1 well, which is representative of the upper Travis Peak, has a fracture number of 0.03 for over 200 ft of core, and the upper Travis Peak in the SFE No. 2 well is 0.025 for more than 100 ft of core. Lower Travis Peak fracture number for the SFE No. 2 well is 0.3. This shows that despite sampling problems inherent in using vertically oriented core to characterize abundance of vertical fractures, differences in fracture abundance can be distinguished in this formation using fracture numbers.

Fracture numbers can also be defined as the total length of fractures in a cored interval normalized to the thickness of a particular geophysical log signature (fig. 8). In the Travis Peak Formation, acoustic log data can be used to distinguish zones within sandstones

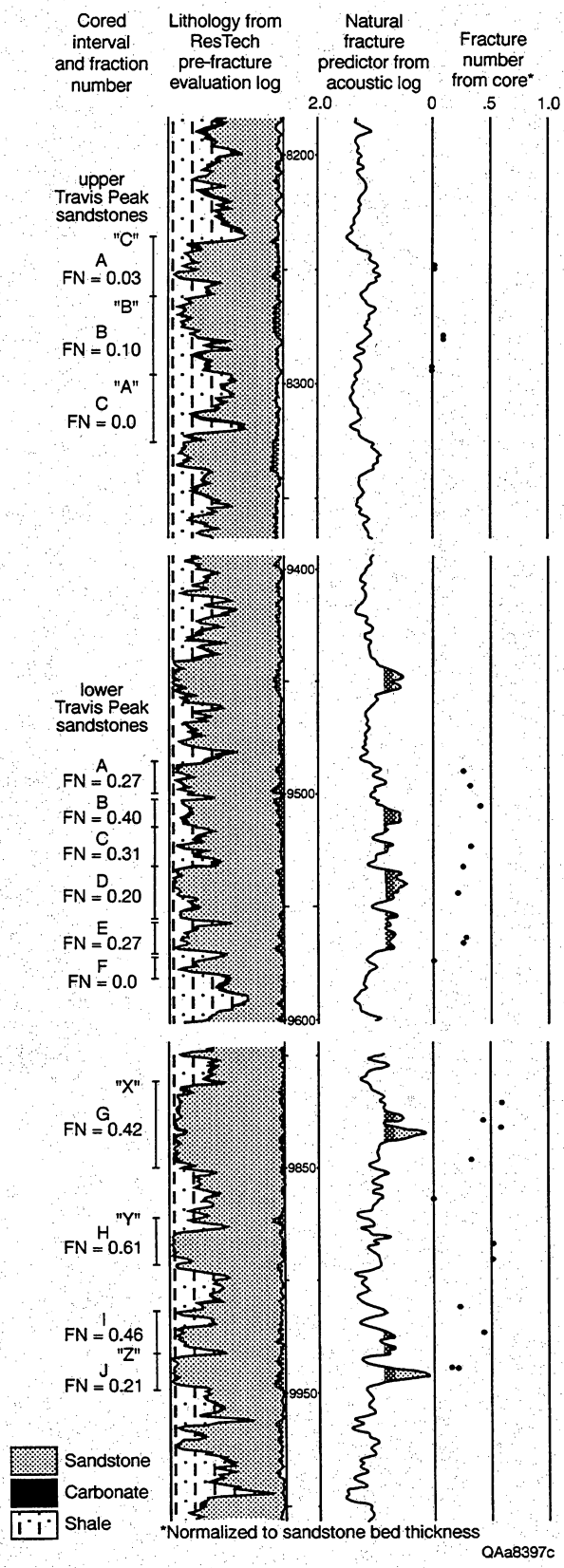

Figure 8. Geophysical well log signatures of fracture-prone beds having synkinematic quartz cement and fracture numbers (FN) from core data, Travis Peak Formation. Holditch SFE No. 2 well. Log intervals where natural fractures are predicted from high sandstone strength indices are highlighted. Fracture numbers in left-hand column are normalized to core length (shown); fracture numbers on right-hand scale are normalized to sandstone bed thickness. Areas of predicted natural fracture are highlighted.

that have distinctive acoustic log signatures. Absolute fracture abundance and fracture numbers are higher for zones having high acoustic velocities, as described in a later section. These anomalies correspond to variations in quartz-cement content.

Application of the fracture number measurement approach to the Travis Peak and Canyon sandstone shows that it is possible to track fracture abundance patterns using currently available vertical core data. What is the character of the fractures encountered in these cores, and what are their relationships to diagenesis?

Observations of Fractures and Associated Diagenesis

Several different types of fracture or fracture-like discontinuities, such as veins, faults, and pressure-solution seams, exist in natural gas sandstone reservoirs, and these features all have different internal structures, characteristic shapes, and associated microstructures. In subvertical opening-mode fractures (veins, joints) the critical internal features are fracture-fill mineralogy, fracture-fill patterns, and fracture roughness. This section describes fracture-fill characteristics and patterns in these fractures as a basis for comparison with diagenetic patterns. These data also illustrate the critical role that fracture mineralization plays in governing fracture porosity preservation.

As will be shown, sequences of cements in sandstones commonly include diagenetic episodes that precede, postdate, and co-occur with fracture opening. Elements of each type of cement are present in each formation. Yet in each formation, certain types of cement—in terms of timing of cementation with respect to fracture opening—are volumetrically dominant.

Dominantly Postkinematic Cement: Ozona Canyon Sandstone

Fractures in Ozona Canyon Sandstone have not previously been described. Fractures in Ozona sandstones are mentioned briefly in Laubach and others (1994, their p. 41–43). Petrographic inspection of 29 thin sections of natural fractures from Ozona Canyon Sandstone cores of the Shell Baggett No. 2-20 (23 samples) and Texaco Kincaid No. D-7 (6 samples) wells enabled detailed analysis of (1) fracture size and shape, (2) petrology of fracture-filling minerals, (3) sequence of mineralization of the fractures, (4) evolution of porosity development in the fractures, and (5) relation of sandstone-framework diagenesis to fracture mineralization. The purposes of this analysis are to describe the mineralogy of Ozona Canyon fractures; to determine the diagenetic controls on fracture mineralization and quality, such as residual porosity/permeability; and to describe the relation between natural fractures and sandstone diagenesis within Ozona Canyon reservoir facies.

Ozona Canyon sandstones illustrate rock and natural fracture attributes dominated by postkinematic cements (fig. 5). We describe this situation first (rather than that of prekinematic cements) because, as an example of a mineral-precipitation event that is not synchronous with fracture opening, postkinematic cementation is perhaps closest to the conventional view of how fractures in the subsurface become filled with minerals. In this view, preexisting fractures are merely large pores that are gradually filled by secondary minerals. For porous sandstone, as is illustrated by the Ozona Canyon, this conventional view can be misleading, even in the case of postkinematic cementation. Mineralization, dissolution, compaction, and other diagenetic events affecting sandstone can also be recorded in fractures. Complex diagenetic sequences are recorded in many fractures.

Fracture Distribution, Size, and Shape

Natural fractures are widespread in Ozona Canyon sandstone cores from the Baggett and Kincaid wells. Most are subvertical, opening-mode fractures that are densely filled with secondary minerals. Fractures in core are typically short (average height approximately 6 cm) and vertically discontinuous (figs. 9 through 12). In thin section, maximum fracture widths ranging from 0.05 to 1.45 mm were documented, and average width is 0.40 mm. Measurements of fractures

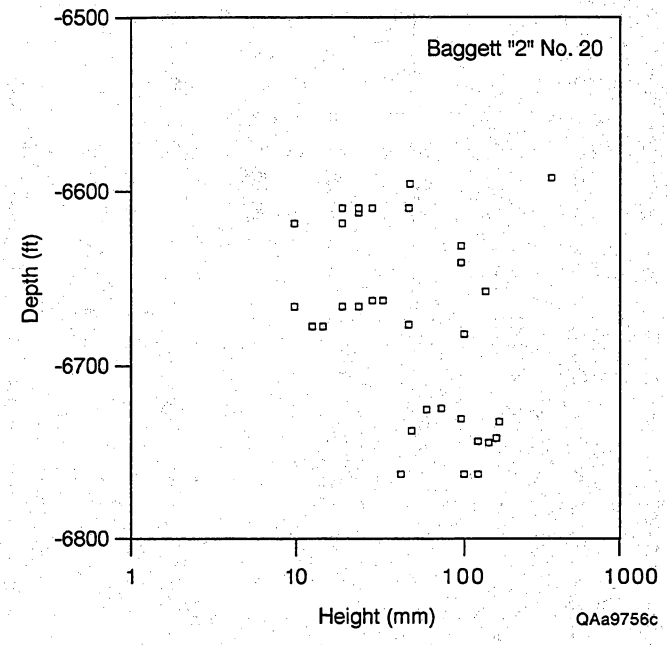

Figure 9. Fracture height versus depth, Baggett "2" No. 20. Ozona Canyon natural fractures.

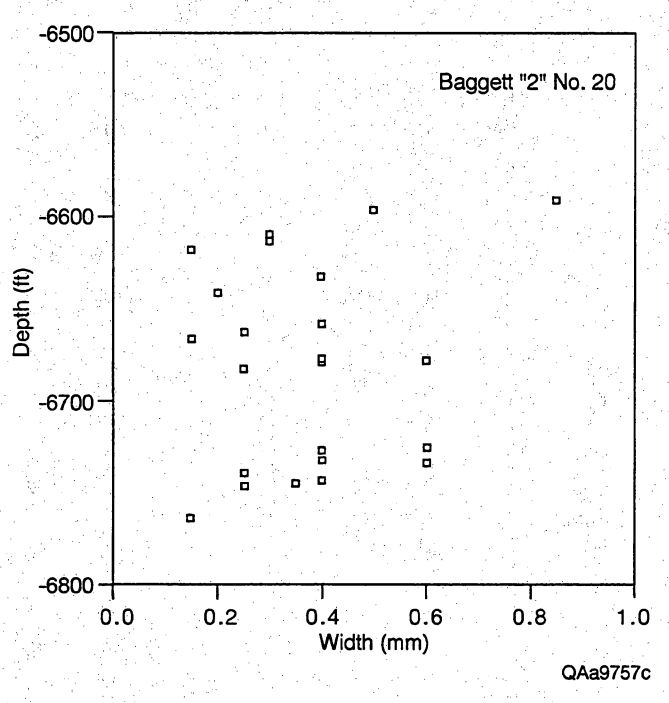

Figure 10. Fracture width versus depth, Baggett "2" No. 20. Ozona Canyon natural fractures.

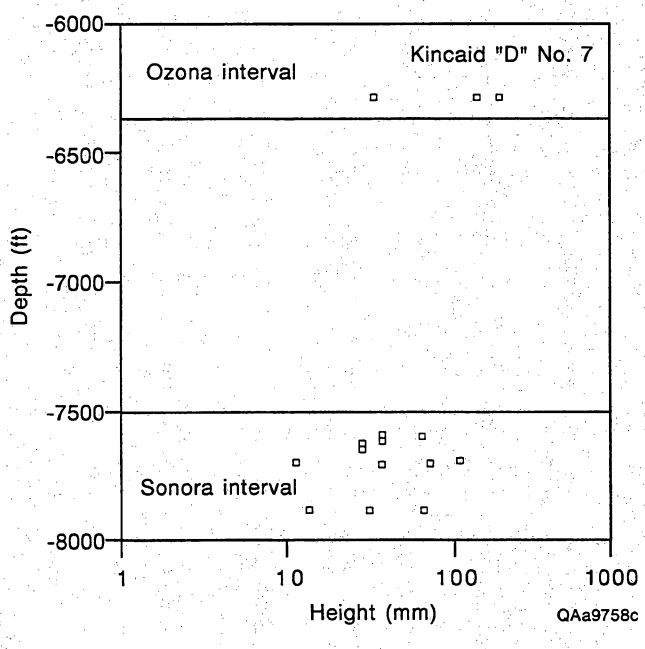

Figure 11. Fracture height versus depth, Kincaid "D" No. 7.

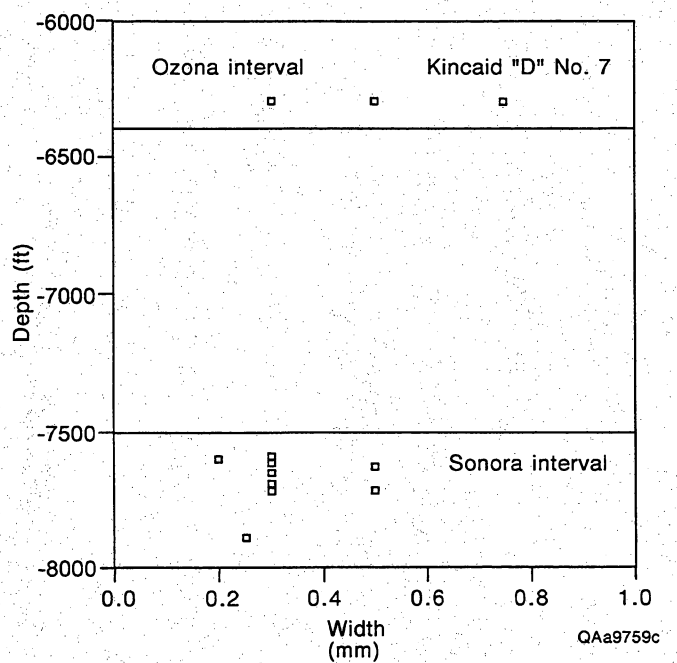

Figure 12. Fracture width versus depth, Kincaid "D" No. 7.

in core made using a binocular microscope and micrometer showed maximum widths ranging from 0.15 to 0.85 mm (figs. 11 and 12). Fractures occur mostly as single fracture strands, with only local branching into very short segments, generally no longer than about 1.5 mm and extending no more than about 0.5 mm away from the primary fracture. In the coarsest sandstone samples, which contain coarse-grained fossil fragments as the dominant framework constituents, as many as five fracture strands are grouped into fracture zones as wide as 0.68 mm. As will be discussed more fully in subsequent sections, most fractures are cut along their lengths by a single, generally mineralized secondary fracture.

The principal control on fracture size (height) in Ozona Canyon sandstones is the scale (vertical spacing) of thin shale beds and laminae because fractures typically terminate at or before reaching these boundaries. In thin section, fractures thin markedly toward shale beds and either end within the sandstone bed or each may extend as one to three thin, discontinuous fractures as much as 0.8 mm into the shale bed before ending. The shale beds do not have throughgoing fractures. Fractures in the cores are typically no taller than the thickness of the sandstone bed that contains them.

Ozona Canyon fractures that were examined in core hand specimen lack the vertical extent and prominent fracture porosity that would mark these features as probable important fluid conduits. On the other hand, the abundance of small fractures observed in the limited sample, combined with the strong bias against intersecting vertical fractures within vertical core, suggests that fractures are common features in Ozona Canyon sandstones.

Observations of this study do not rule out the possibility that there are larger (taller) fractures in the Ozona Canyon Sandstone. The available evidence does not permit us to conclude whether fractures elsewhere in the Ozona trend might be larger, more open, or more interconnected. Moreover, it is not the size (height) of fractures at the wellbore that is important for flow through fracture networks. Extent of interconnected fractures, degree of occlusion of fracture porosity by fracture-filling minerals, and persistence of individual fractures are each more important factors than the vertical extent of the fractures in most reservoir rocks. The limited perspective of the core data does not permit any conclusions regarding lateral (plan view) fracture network connectivity or fracture persistence; however, fracture-porosity occlusion and its diagenetic controls can be addressed with the available core samples.

Mineralized fractures in the core samples, as observed in thin section, occur in two classes characterized by single or multiple fracture strands and other distinctive attributes (table 4). Class I fractures are the more abundant type in the samples studied. They occur as single, isolated strands that average about 0.42 mm in maximum width. Each fracture generally has low sinuosity, moderate to rough walls, and rare visible intercrystalline porosity (fig. 13). Class I fractures are developed in very fine grained to fine-grained Ozona sandstones. In contrast, Class II fractures are fracture zones containing as many as five closely spaced, locally bifurcating strands that average about 0.10 mm in maximum width each (fig. 14). Fracture zones range from 0.49 to 0.68 mm in maximum width. Fracture strands within each zone have moderate to rare high sinuosity, relatively smooth walls, and no visible porosity. Class II fractures occur only in coarse-grained Ozona sandstones, which are typically rich in fossil fragments. Fracture-fill mineral assemblages are similar in the two fracture classes, but textural relations among the minerals in the fracture classes vary (figs. 13 through 24). These aspects are discussed in the next two sections.

Petrology of Fracture-Filling Minerals

Most natural sandstone fractures in the Ozona Canyon Sandstone contain several mineral (fracture cement) phases. The relative abundance and textural relations of these fracture-filling minerals can be used to document timing of fracture filling with respect to diagenetic sequence and to infer the history of porosity/permeability development and destruction within the fractures. Fracture-filling mineral distribution is by far the most important influence on residual (present) fracture porosity.

Although inconspicuous and easily overlooked, thin zones of secondary quartz irregularly line and locally bridge fracture walls (fig. 15). Quartz overgrowths are less common in Class II fractures, in part contributing to the smoother walls of these thinner fractures. The overgrowths are euhedral to subhedral crystals in optical continuity with host quartz framework grains. Crystals are typically aligned with C-crystallographic axis normal to fracture walls. Quartz also forms a grain-bridging cement between quartz framework grains at narrow apertures of primary fractures. Quartz-filled microfractures and parallel transgranular fluid-inclusion planes are developed where fractures thin markedly and extend into sandstone framework grains (at sites of discontinuity of the primary fracture) and also at the margins of primary fractures where microfractures branch off and parallel the primary fractures.

Table 4. Classes of mineralized fractures in Ozona Canyon Sandstone.

Class I	Class II
Single, isolated strands	Multiple, closely spaced strands
Each strand as much as 0.42 mm wide	Each strand as much as 0.10 mm wide
Low sinuosity	Moderate to rare high sinuosity
Moderate to rough walls	Smooth walls
Rare intercrystalline porosity	No visible porosity
Occur in fine sandstones	Occur in coarse sandstones

The most abundant mineral phase in both Class I and II fractures in Ozona sandstones is ankerite. There are two types of ankerite occurrence in the Ozona Canyon fractures. (1) The most common type comprises large (relative to the fracture widths) zones or "bands" of ankerite (0.3 to 1.7 mm long in dimension parallel to fracture) that extend perpendicular to fracture walls and typically fill most of the fracture (fig. 16). Each band displays a different optical orientation relative to adjacent bands. This distinctive banding probably formed by growth of separate ankerite crystals of slightly different optical orientations across and perpendicular to the fracture walls. Siliciclastic framework grains derived from the fracture walls are sporadically distributed in the ankerite. Ankerite is also segmented by well-developed cleavage planes (fig. 17) indicating that an episode of deformation postdates this fracture fill (fig. 18). (2) Small (~0.015 mm), irregular masses ("blebs") of ankerite are encased in both calcite and barite in the fractures (fig. 19). Textural relations suggest that these ankerite masses are remnants that survived an episode of dissolution and replacement of part of the dominant ankerite fracture fill.

Calcite, both ferroan and nonferroan, is the second most abundant fracture-filling mineral. Like ankerite, calcite occurs in two forms in both Ozona Canyon fracture classes. (1) In some fractures, nonferroan and, more rarely, ferroan sparry calcite extends across most or all of each fracture in irregular patches within the predominant ankerite fracture-fill cement and locally contains ankerite dissolution remnants. In rare fractures, calcite is more abundant than ankerite as the primary cement. (2) Nonferroan calcite and rare barite fill thin (0.01 to 0.03 mm wide) secondary fractures that extend within and along the primary fractures in most samples (fig. 20). These secondary fractures crosscut all fracture-fill phases of the primary fractures except quartz. However, the secondary fractures are deflected by, and wrap around, the margins of euhedral quartz overgrowths, evidence that they postdate formation of the overgrowths. Calcite-filled secondary fractures locally cut across—and are aligned with healed microfractures in—quartz framework grains.

In general form and textural relation with other fracture-fill minerals, barite is similar to calcite. Large patches of barite, readily identified as a sulfate in thin section by its very low birefringence and high relief, extend across primary fractures, bridging walls of both fracture classes (fig. 21). In a few samples from both cores, barite is either more abundant than ankerite or roughly as abundant as ankerite in primary fractures. Ankerite dissolution remnants (evenly distributed masses) occur locally within fracture-fill barite. In some samples, regularly spaced tongues of barite extend outward from fracture walls and interband with ankerite, suggesting replacement of dissolved ankerite crystallographic bands (fig. 22). Barite is also a minor component of secondary fracture fills.

Although not a mineral, hydrocarbon residue is nonetheless a prominent fracture-fill phase in Ozona Canyon sandstones. Opaque organic material in primary fractures typically contains finely disseminated pyrite. The organic material is most commonly evenly distributed within ankerite and to a lesser extent in the patchy calcite and barite fracture fill. However, in some samples residual hydrocarbons are concentrated in a single, narrow linear to zigzag-shaped zone in the center of the primary fracture, in a linear zone along a fracture wall, or in both forms extending along most of fracture length (fig. 23). We interpret migration and emplacement of hydrocarbons in the fractures to have occurred along zones of primary permeability. Where organic material is evenly distributed, it fills cleavage partings in primarily ankerite (fig. 24), forming flow paths that have boxwork patterns and dissolution voids in ankerite (fig. 25). In the case of linear and zigzag-shaped organic concentrations, hydrocarbons possibly migrated through nonmineralized secondary fractures within the primary fracture or perhaps through open space between apices of interbanded ankerite crystals that grew vertically relative to fracture walls, forming the observed zigzag pattern.

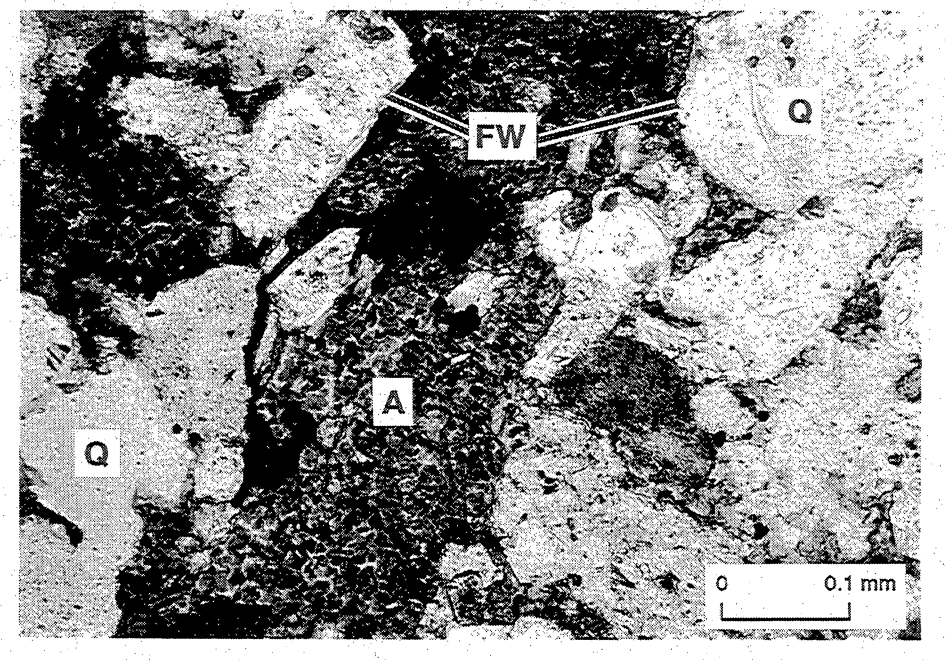

Figure 13. Photomicrograph illustrating attributes of Class I fractures (table 4) of the Ozona Canyon Sandstone, including low sinuosity, moderate to rough walls, and rare intercrystalline porosity (porosity in this fracture largely occluded by ankerite cement [A]). FW indicates fracture walls; Q identifies quartz framework grains.

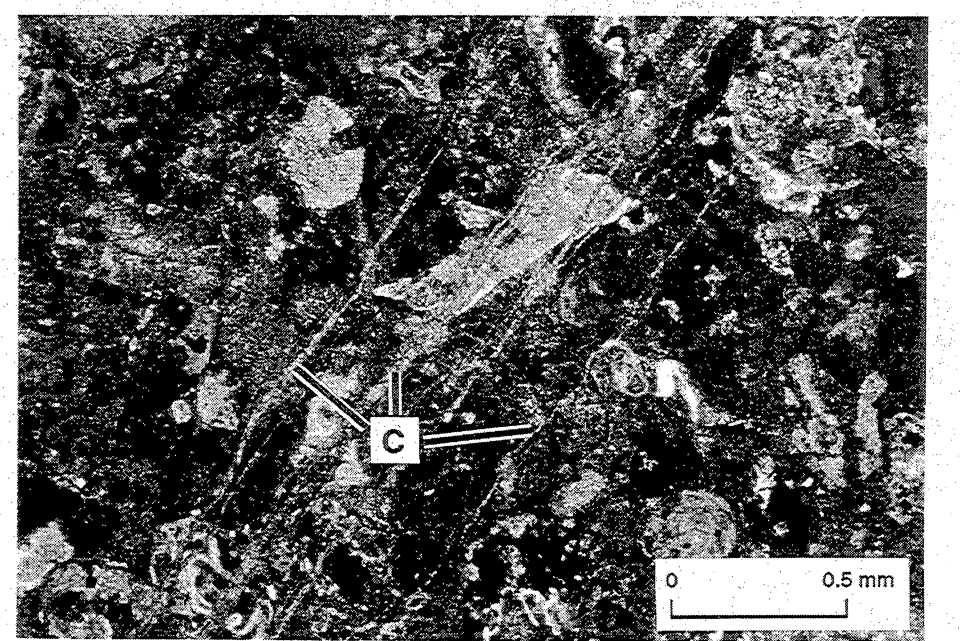

Figure 14. Photomicrograph illustrating attributes of Class II fractures (table 4) of the Ozona Canyon Sandstone, including fracture zone of several strands in a coarse sandstone, moderate sinuosity of each strand, smooth walls, and no visible porosity. Fracture fill is mostly nonferroan calcite (C).

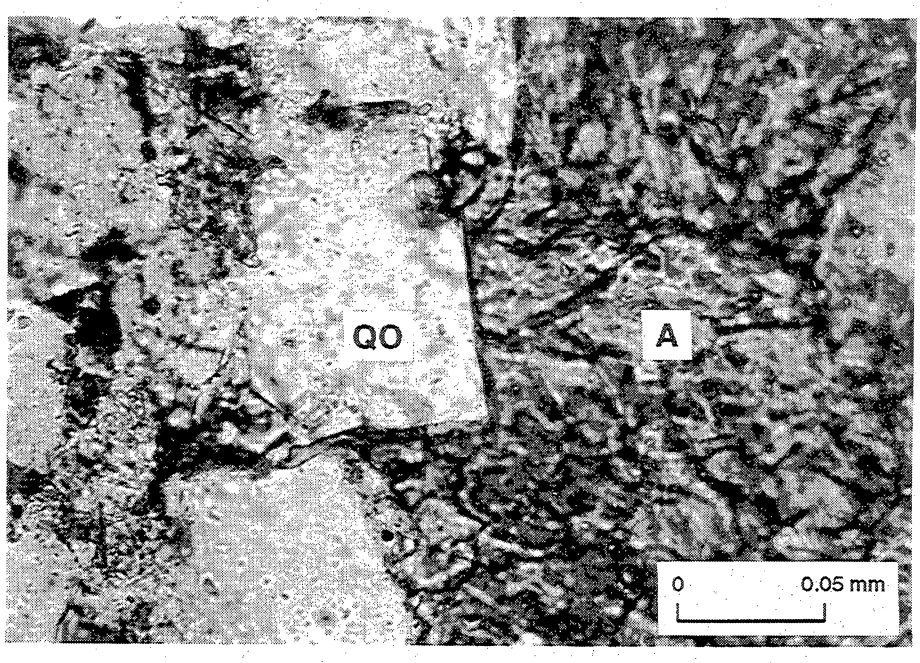

Figure 15. Photomicrograph of euhedral quartz overgrowths (QO) along primary fracture wall in the Ozona Canyon Sandstone. Remainder of fracture fill (right) is ankerite (A).

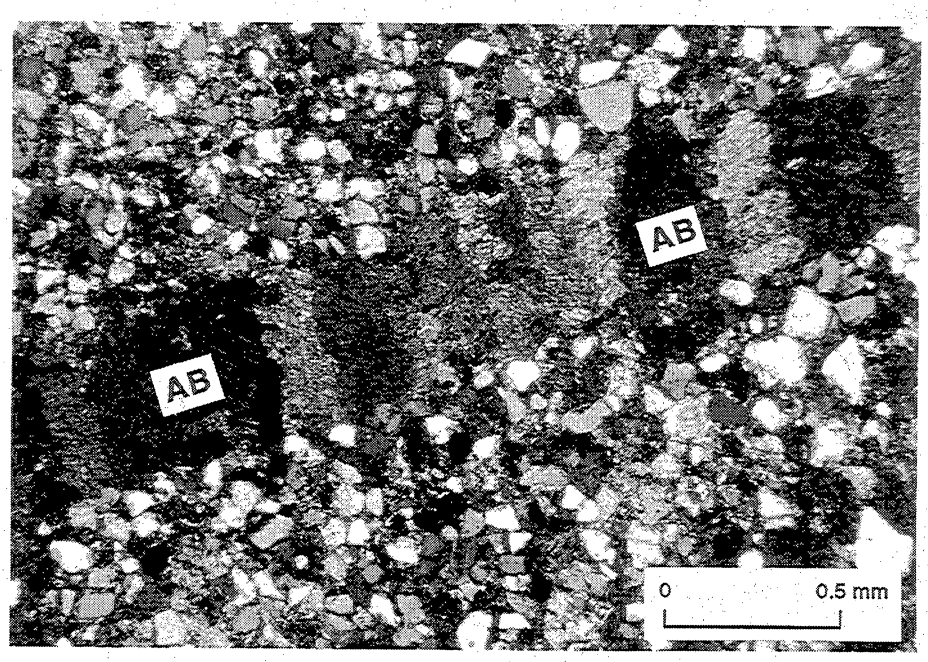

Figure 16. Photomicrograph of distinctive transfracture ankerite bands (AB) in the Ozona Canyon Sandstone. Bands contain variably oriented cleavage sets and represent ankerite crystals of different crystallographic orientations, indicating growth of separate crystals perpendicular to fracture wall.

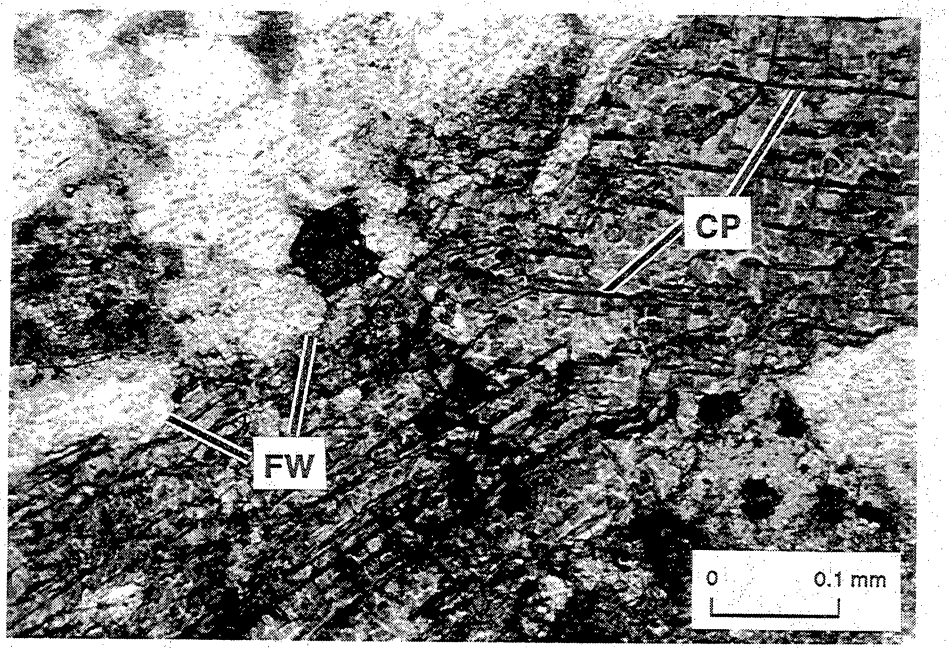

Figure 17. Photomicrograph of well-developed cleavage planes (CP) in ankerite fracture fill in the Ozona Canyon Sandstone, indicating an episode of deformation that postdates ankerite mineralization. FW indicates fracture wall.

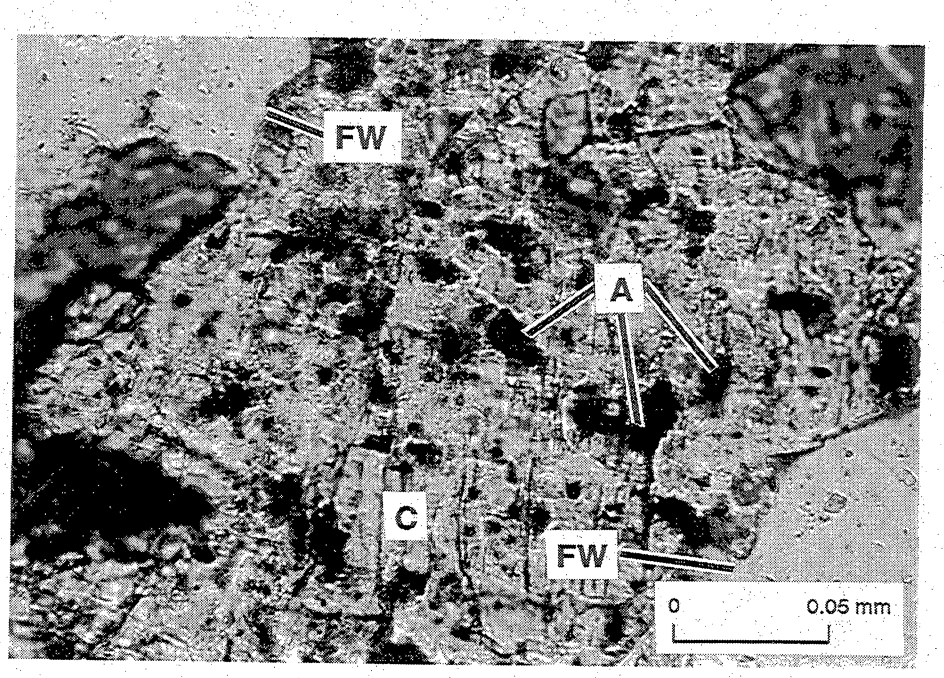

Figure 18. Photomicrograph of replacive nonferroan calcite fracture fill (C) containing dark ankerite blebs (A), which are dissolution remnants. Calcite precipitation was contemporaneous with ankerite dissolution, a prominent diagenetic stage of Ozona Canyon Sandstone (fig. 25, table 5).

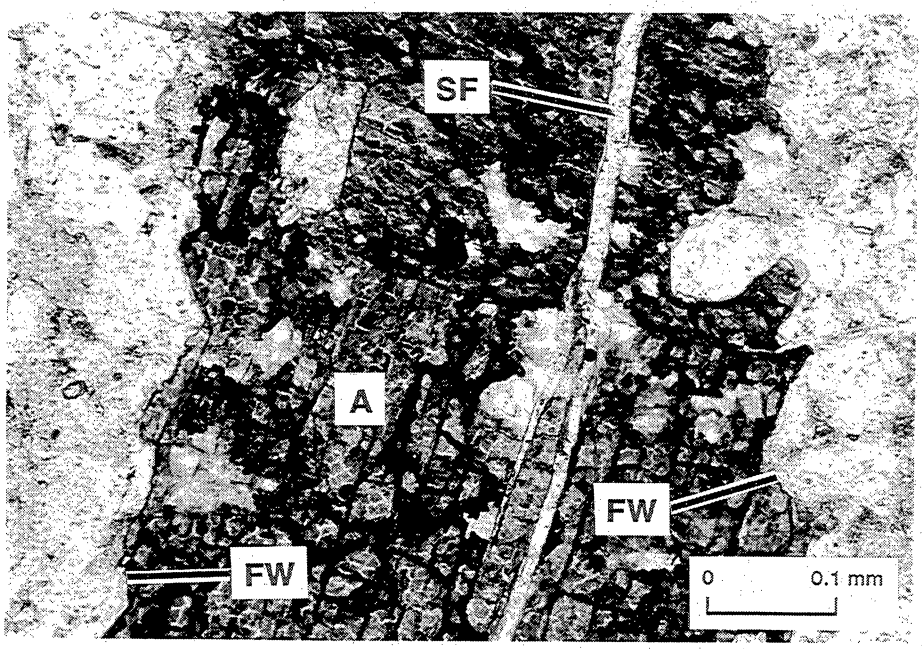

Figure 19. Photomicrograph of calcite-filled secondary fracture (SF) within wider ankerite-filled primary fracture (A) in Ozona Canyon Sandstone. FW indicates fracture walls.

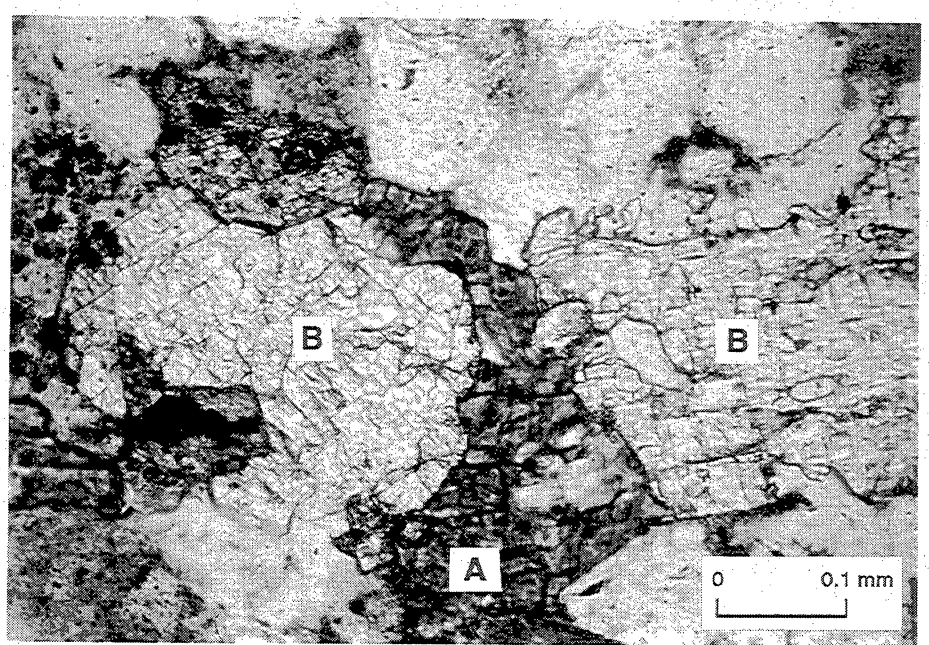

Figure 20. Photomicrograph of barite (B) and ankerite (A) fracture-fill phases in Ozona Canyon Sandstone. Textural relations indicate that barite mineralization postdates ankerite cementation and coincides with an episode of ankerite dissolution.

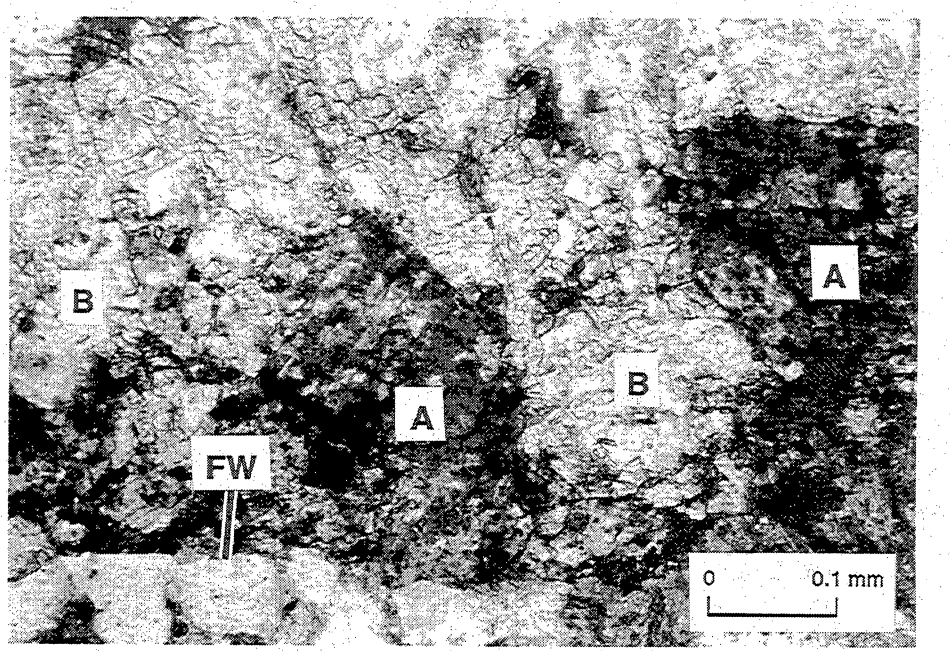

Figure 21. Photomicrograph of replacive barite (B) "tongues" extending into ankerite (A) fracture fill in Ozona Canyon Sandstone. Regular spacing of barite tongues within ankerite and width of tongues that is equal to that of the transfracture ankerite bands indicate that barite is selectively replacing dissolved ankerite crystallographic bands. FW indicates fracture walls.

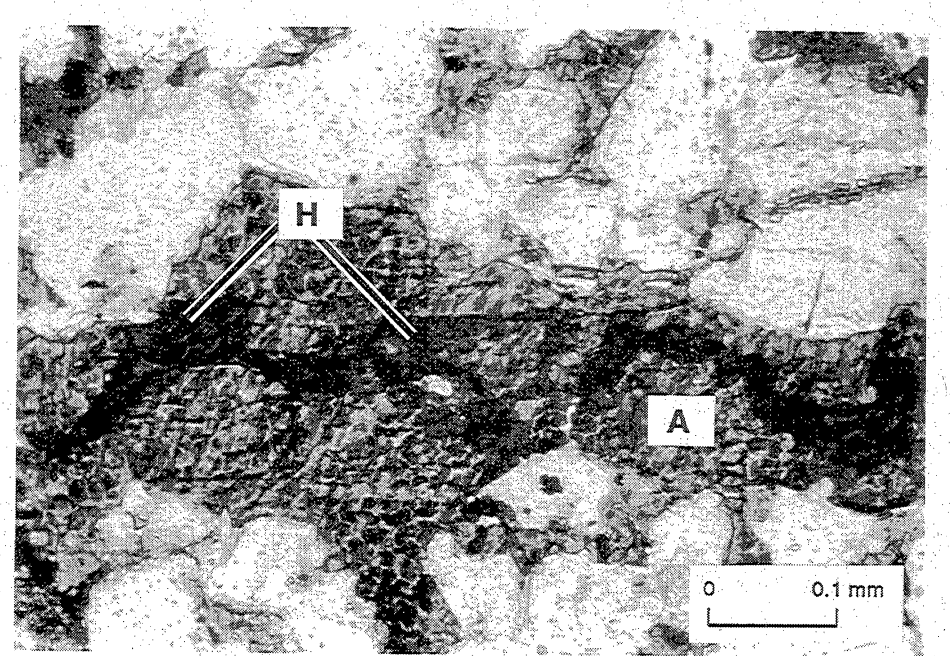

Figure 22. Photomicrograph of zigzag-shaped zone of residual hydrocarbon (bitumen) (H) within ankerite fracture fill (A) of Ozona Canyon Sandstone. Continuous linear zones of hydrocarbon in center of, or against walls of, fractures are also common. Both forms possibly represent hydrocarbon migration through nonmineralized secondary fractures in the primary-fracture fill or, in the zigzag pattern, migration through primary porosity between apices of interbanded ankerite crystals.

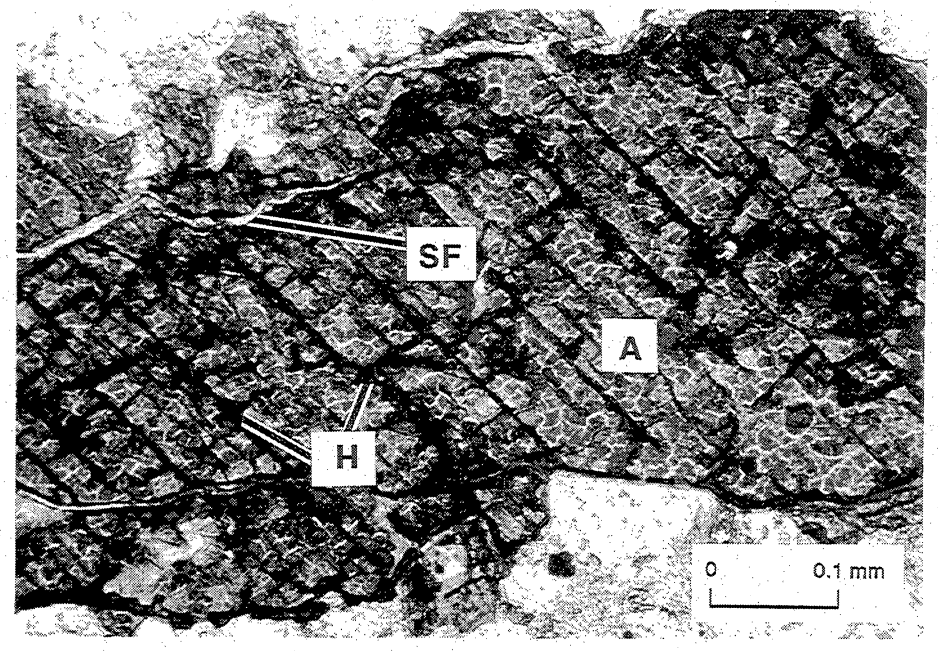

Figure 23. Photomicrograph illustrating hydrocarbon-bearing cleavage partings (H) in ankerite primary-fracture fill (A) in Ozona Canyon Sandstone. Note calcite-filled secondary fracture (SF) cutting through ankerite. Secondary fractures commonly coincide with cleavage segments that are axial parallel with respect to the primary fracture, indicating late-stage fracturing along preexisting planes of weakness.

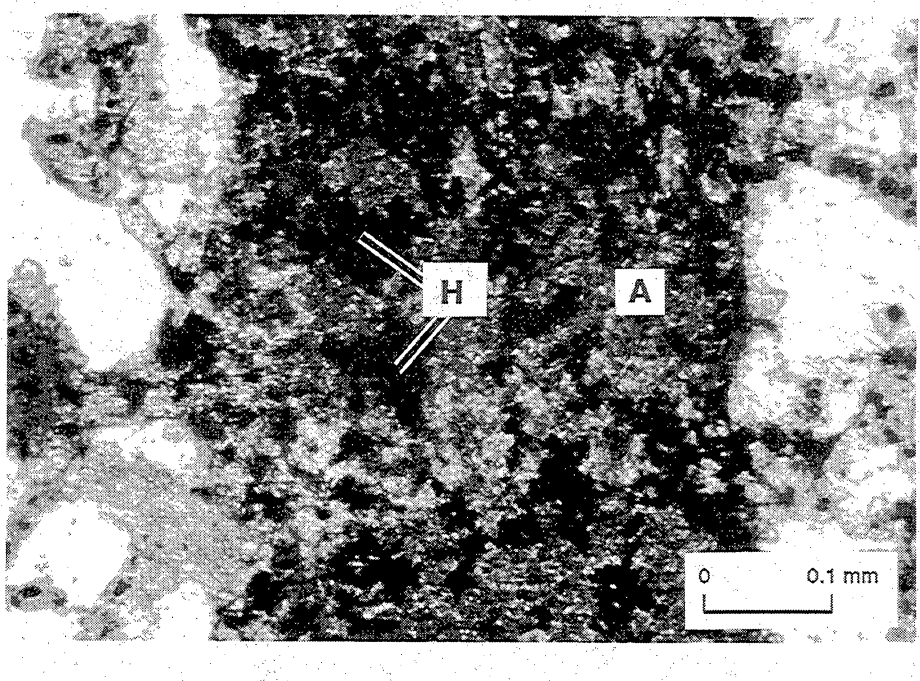

Figure 24. Photomicrograph of residual hydrocarbon (H) occupying dissolution voids (evenly distributed dark spots) within ankerite primary-fracture fill (A) in Ozona Canyon Sandstone. This textural relation indicates that hydrocarbon migration through primary porosity and permeability occurred concurrent with and/or immediately after the ankerite dissolution stage in Ozona diagenetic sequence, well before possible migration after generation of secondary fractures (fig. 25, table 5). Thus, hydrocarbon migration through Ozona sandstones was probably episodic.

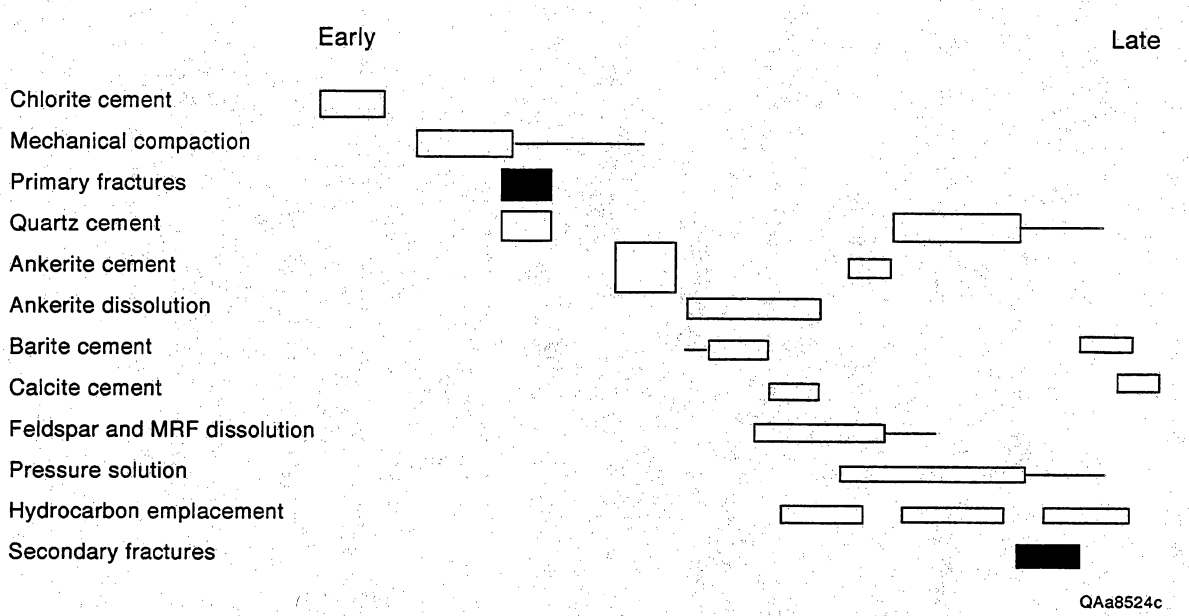

Figure 25. Diagram of composite diagenetic sequence and relative temporal relations of component diagenetic stages of sandstone framework and fracture fill of Ozona Canyon Sandstone. Fracture stages highlighted in black.

Mineralization Sequence of Fractures

From textural relations among fracture-fill mineral phases observed in thin section, the paragenetic sequence of mineralization of Ozona Canyon fractures can be deduced: (1) precipitation of quartz as overgrowths lining fracture walls, as a grain-bridging cement at narrow primary-fracture apertures, and as a cement that fills microfractures; (2) ankerite crystallization; (3) partial dissolution of ankerite cement; (4) barite cementation and replacement of dissolved ankerite (possibly contemporaneous with step 3); (5) nonferroan and minor ferroan calcite mineralization and replacement of dissolved ankerite; (6) hydrocarbon emplacement in cleavage partings, dissolution voids, possible secondary fractures, and intercrystalline pore space in ankerite, and, to a lesser degree, in cleavage partings and possible secondary fractures in calcite and barite; and (7) secondary fracturing within primary fractures and second-phase precipitation of nonferroan calcite and barite in secondary fractures (possibly contemporaneous with step 6).

Because quartz overgrowths line the walls of the primary fractures and because faces of euhedral quartz crystals are in direct contact with ankerite (fig. 24), quartz is inferred to be the first mineral to have precipitated in the Ozona Canyon fractures. Overgrowths are generally not abundant or particularly well developed in most primary fractures of either fracture class. This could mean that the early quartz fracture-filling phase was relatively brief before ankerite mineralization was initiated. Quartz cementation of microfractures and of primary fractures having narrow apertures was probably contemporaneous with overgrowth development, all recording a single early episode of silica mobilization in formation waters. By analogy with similar relations documented in the Travis Peak Formation that are described in the next section, these features indicate that this episode of quartz cement was synkinematic.

The distinctive transfracture banding of ankerite cement (fig. 16) represents mineralization *after* fracture opening and early quartz precipitation. That is, ankerite represents postkinematic mineralization. Ankerite crystallographic bands are single crystals that display no internal cathodoluminescence (CL) variation and that have continuous crystal structure (evident in continuous cleavage planes) across fractures. Moreover, there are no internal variations in the tone of the blue potassium ferricyanide stain within individual bands, and there are no regularly spaced fluid-inclusion planes in the ankerite that could mark inconspicuous fracture and crystallization episodes.

These features indicate that growth of the ankerite crystals occurred in open primary fractures. The uniform composition of crystals may also indicate contemporaneous formation waters having uniform chemistry. Evidence of ankerite crystallization that was contemporaneous with gradual fracture extension, such

as compositional variations, which are shown by CL variation in crystals or stain-color variation, and structural disruption marked by multiple fluid-inclusion planes parallel to crystal edges, is lacking. In this, ankerite fracture fill in the Ozona Canyon resembles postkinematic carbonate (ankerite and calcite) minerals in the Sonora Canyon, Travis Peak, and Frontier Formation fractures described elsewhere in this report.

There is clear textural evidence of an episode of ankerite dissolution and probable contemporaneous precipitation of replacive barite and probable later precipitation of replacive calcite. This evidence includes (1) small (~0.015 mm), irregular ankerite masses "floating" in patches of barite and sparry calcite (fig. 20), (2) tongues of barite extending into and mimicking the transfracture ankerite banding (fig. 21), and (3) crenulate boundaries between ankerite patches and calcite and barite patches within primary fractures.

Hydrocarbon migration through Ozona Canyon fractures may have occurred in several episodes; textural relations indicate that all migration took place after ankerite precipitation. Opaque organic material in fracture fill is well distributed in cleavage partings, dissolution voids, possible secondary fractures within primary fractures, and intercrystalline pores in ankerite. Patchy calcite and barite primary-fracture cements also contain residual hydrocarbons. However, calcite- and barite-filled secondary fractures crosscut ankerite, calcite, barite primary-fracture-fill phases, and also the hydrocarbons. These mineralized secondary fractures do not contain any organic material, although migration of hydrocarbons through these fractures may not have occurred because of early porosity occlusion by mineralization contemporaneous with fracturing.

The presence of linear and zigzag-shaped organic concentrations in primary-fracture fills (fig. 22) suggests that secondary fractures were not mineralized and formed just before or during an episode of hydrocarbon emplacement. These fractures are probably contemporaneous with the mineralized secondary fractures. Open (nonmineralized) secondary fractures within primary fractures occur in one sample from the Kincaid core, indicating that variations in degree of fracture-porosity preservation do exist. Thus, multiple episodes of fracture porosity creation are evident, but some episodes did not involve movement of fracture walls. These events are analogous to development of secondary porosity during diagenesis of the sandstone framework.

Evolution of Fracture Porosity

Enough porosity and permeability in Ozona fractures to allow invasion of formation waters of different solute contents and of hydrocarbons existed in at least four stages in fracture mineralization. First, waters saturated with respect to quartz and ankerite moved through Ozona fractures during and after opening of the fractures, allowing precipitation of quartz and ankerite in fractures and matrix. Quartz and ankerite precipitation probably represents two separate migration events characterized by different water chemistries. Second, partial dissolution of ankerite was caused by introduction of waters undersaturated with respect to ankerite into residual porosity/permeability after nearly total filling of fractures by ankerite.

Replacive barite, but not calcite, probably precipitated from these same waters. A water chemistry that would induce dissolution of ankerite would probably not permit contemporaneous precipitation of the chemically similar calcite phase. However, barite is sufficiently different in chemistry that it probably crystallized from the initial dissolving waters, thus preceding calcite as a fracture-fill phase. Third, hydrocarbons accumulated in primary open cleavage porosity and intercrystalline porosity in fracture-fill ankerite and in cleavage porosity in calcite and barite after partial ankerite dissolution and barite/calcite crystallization.

Finally, the episode of secondary fracturing within the primary fractures created porosity and permeability for (1) second-phase calcite and barite precipitation within mineralized structures, (2) hydrocarbon migration within possible nonmineralized secondary fractures, and (3) fluid flow into currently open secondary fractures. The one sample containing open secondary fractures is from the deepest core from the two wells (882 ft deeper than the next deepest), suggesting that there may be a depth control on degree of secondary fracture mineralization. These relations demonstrate complex postkinematic diagenetic events *controlling* fracture porosity that have an effect on how the size, shape, and geochemical character of fracture porosity evolved.

Controls on Fracture Porosity

The presence of quartz bridges across Ozona fractures suggests that most fracture pore space was created at the time of quartz precipitation. Yet quartz mineralization is not the cause of occluding fracture porosity. Instead, progressive postkinematic carbonate and sulfate precipitation is largely responsible for destroying fracture porosity.

Controls on residual (current) fracture porosity and thus, probably, fracture permeability in Ozona Canyon sandstones include (1) presence of intracrystalline porosity (cleavage partings, microfractures) not already

occluded by residual hydrocarbons (bitumen); (2) dissolution of minor intracrystalline voids in the carbonate fracture-fill minerals; (3) development of minor intercrystalline porosity, primarily between crystal apices in fracture-filling ankerite, not subsequently filled with residual hydrocarbons (bitumen); and (4) presence of open secondary fractures within primary fractures.

Relation of Sandstone Diagenesis to Fracture Mineralization

The Ozona fracture-fill mineral sequence is recognizably part of the overall diagenetic sequence that was independently derived from observations of cement paragenesis in the sandstone matrix. In fact, a useful technical benefit of fracture-mineralization analysis of Ozona Canyon sandstones is that it enables a more precise and comprehensive determination of the paragenetic sequence and deformation history of the sandstones when used with the diagenetic relations observed in unfractured parts of sandstones. Analyses of fracture mineralization and sandstone-framework diagenesis complement each other. Moreover, fracture-mineralization analysis allows direct observations on the controls on residual fracture porosity and permeability.

Discussion of the sandstone-framework diagenesis of the Ozona Canyon Sandstone is presented in Laubach and others (1994). In summary, the primary diagenetic events in the burial history of Ozona Canyon sandstones were, in order of occurrence, (1) growth of chlorite rims on framework grains; (2) compaction (roughly contemporaneous with stage 1) causing deformation of ductile rock fragments; (3) precipitation of quartz overgrowths; (4) precipitation of ankerite and ferroan calcite, which filled pores not occluded by quartz overgrowths, and contemporaneous dissolution of feldspar and metamorphic rock fragments; (5) pressure solution and minor additional silica cementation at quartz-to-quartz grain contacts; and (6) late-stage fracturing.

This sandstone-framework paragenetic sequence is clearly similar to the sequence determined from fractures. However, analysis of sandstone-matrix-framework sequence alone did not identify all elements of the rock paragenetic sequence or relate these features to fracture history. A composite paragenetic sequence (table 5; fig. 25) encapsulates as much of the burial history of the Ozona Canyon as can be observed using petrographic techniques. Sandstone-framework analysis identifies the earliest diagenetic events from the formation's burial history (stages 1 and 2 in table 5), whereas fracture-mineralization analysis details the latest diagenetic events (stages 10 and 11 in table 5). Overlap of the sandstone-framework and fracture diagenetic sequences occurs in their middle range. A basic assumption used in constructing the composite sequence is that cement phases of the sandstone framework are temporally equivalent to the same minerals in the primary fractures. For example, quartz overgrowths on framework grains are assumed to have formed contemporaneously with overgrowths on fracture walls. Cement and vein-fill minerals are locally in crystallographic and optic continuity, and there is no textural evidence to the contrary; therefore, we prefer this interpretation because it requires the least complicated cementation sequence. Where complex multiphase cementation sequences have been observed, petrographic evidence, in the form of reversal of paragenetic sequence, is usually evident. The best documented cases of such repetitive polyphase cement sequences are in rocks that are near faults that acted as intermittent sources of mineralizing fluids (e.g., Burley and others, 1989).

Chlorite precipitation and porosity-occluding deformation of ductile rock fragments mark the early period in the burial history of the Ozona Canyon deposits (table 5). Primary fractures and genetically related microfractures then formed. Quartz cementation in the sandstone framework and fractures during fracture opening further consolidated the Ozona deposits and added to porosity destruction. The precipitation of quartz cement may have embrittled Ozona sands to the point where fracture was possible. Even small amounts of cement deposited near or at grain contacts can impede grain-boundary sliding, making the grain framework more rigid (Yin and Dvorkin, 1994).

Dissolution of ankerite framework cement and fracture fill, feldspar grains, and shaly metamorphic rock fragments probably coincided with precipitation of barite and calcite in middle and deep ranges of burial. Deep burial is also marked by pressure solution at quartz-to-quartz grain contacts, leading to a second minor phase of quartz cementation in the sandstone framework and possibly in microfractures.

Ankerite is postkinematic, and the proportion of matrix porosity occluded by ankerite may be an approximate guide to the extent that fracture porosity is preserved. Ankerite is the most abundant of the postkinematic cements in the sandstone framework, composing an average of 18.4 percent of whole-rock volume. Indeed, the prevalence of ankerite is what distinguishes Ozona Canyon sandstones as dominantly postkinematic in terms of cement volume. Ankerite

Table 5. Composite paragenetic sequence of Ozona Canyon Sandstone.

(1) Growth of chlorite rims on framework grains.
(2) Compaction initiated during shallow burial, causing deformation of ductile rock fragments (roughly contemporaneous with step 1).
(3) Formation of primary fractures and microfractures.
(4) Precipitation of quartz as overgrowths on quartz framework grains and on primary-fracture walls, as a grain-bridging cement at narrow primary-fracture apertures, and as a cement that fills microfractures (possibly contemporaneous with step 3).
(5) Precipitation of ankerite as sandstone-framework cement, filling pores not occluded by quartz overgrowths, and as primary-fracture fill.
(6) Partial dissolution of ankerite in sandstone framework and primary fractures.
(7) Precipitation of barite and replacement of dissolved ankerite in sandstone framework and primary fractures (possibly contemporaneous with step 6).
(8) Precipitation of ferroan calcite and second-phase ankerite in sandstone framework, with contemporaneous dissolution of feldspar grains and shaly metamorphic rock fragments. Precipitation of nonferroan and minor ferroan calcite and replacement of dissolved ankerite in primary fractures.
(9) With deep burial, pressure solution and second-phase quartz cementation at quartz-to-quartz grain contacts in sandstone framework and possibly microfractures.
(10) In sandstone framework and primary fractures, hydrocarbon emplacement in cleavage partings, dissolution voids, possible secondary fractures, and intercrystalline pore space in ankerite, and, to a lesser degree, in cleavage partings and possible secondary fractures in calcite and barite.
(11) Formation of secondary fractures within primary fractures and second-phase precipitation of nonferroan calcite and barite in secondary fractures (possibly contemporaneous with step 10).

occludes an average of about 60 percent of all framework porosity in the Ozona Canyon sandstones. Most fracture porosity, typically as much as 60 to 80 percent, is similarly occluded by ankerite.

Hydrocarbon migration through residual porosity/permeability may have occurred once or several times after precipitation of ankerite (step 5 in table 5); textural relations cannot pinpoint a specific period of migration. Because mineralized secondary fractures within the primary Ozona fractures crosscut ankerite, barite, and calcite cements and hydrocarbon residue, they clearly postdate these fracture-filling phases. However, because hydrocarbons fill apparently nonmineralized secondary fractures in some samples (fig. 24), an episode of hydrocarbon migration may have in part coincided with, or followed, the late-stage fracturing.

Dominantly Prekinematic Diagenesis: Sonora Canyon Siderite Layers

Sonora Canyon sandstones have distinctive zones characterized by differing dominant cement type (Dutton, 1994). These zones of different cement type also have natural fractures that differ in characteristic shape and mineral fill, as well as in time of formation. Here we describe this Sonora Canyon sandstone fracture stratigraphy, and in particular highlight fracture and cement relations in beds cemented dominantly by

the iron carbonate mineral siderite. This is a good example of prekinematic cement and associated fractures.

Fracture Distribution, Size, and Shape

Natural fractures are common in the Sonora Canyon Sandstone in three cores (Phillips Ward "C" No. 11, Enron Oil & Gas Sawyer "A" 144 No. 5, and Sun Oil Company Dunbar No. 1). Sonora Canyon fractures were also observed in the Texaco Kincaid "D" No. 7 core, but they are not included in this description. One hundred ninety-one fractures are present in 842.5 ft of core, with most of the natural fractures confined to sandstones (435 ft of core). A few fractures are evident on Formation Microscanner (FMS) logs, but fractures are short and inconspicuous and therefore easily missed. Calibration of FMS log with core was a useful guide to natural fracture identification.

Core observations and petrographic data show that many fractures have preserved primary fracture porosity but that some fractures are completely filled, as described below. A Repeat Formation Tester (RFT) logging device in the Ward "C" No. 11 well recorded an instant pressure buildup (Laubach and others, 1994) when a test was conducted over a natural fracture at 6,384.7 ft, indicating that the fracture is permeable. Lost circulation has not been widely reported, and most wells are drilled with air, so it is impossible to use instantaneous mud loss while drilling to quantify fracture permeability.

Natural fractures in the Canyon Sandstone are primarily vertical to subvertical opening-mode fractures (figs. 26 through 31). A few fractures have gentle dips (less than 10°), and some moderately to gently dipping fractures having striated surfaces are localized in mudstone beds and probably are laterally discontinuous faults caused by burial and consolidation. The latter fracture type is particularly common in Sun Dunbar No. 1 core in shale and debris-flow intervals with mudstone matrix at depths of 5,810 to 5,811 ft and 6,018 to 6,020 ft, but these fractures are the least likely to influence gas production because they are completely closed. Therefore, description focuses on the vertical and subvertical opening-mode fractures.

Core fracture mapping shows that widths of fractures are generally less than 0.35 mm (fig. 32). Average fracture width is 0.17 mm, and maximum and minimum fracture widths are 0.4 mm and 0.06 mm, respectively. Open fracture porosity is marked by fractures that are lined by faceted crystals. There is little difference between widths of open and filled fractures, and the range of fracture apertures is similar for the three wells. No trends are apparent in fracture width with depth or with stratigraphic position. Although many fractures are completely or nearly completely filled, the amount of fracture fill varies markedly along some fracture traces, and open fractures grade laterally into filled fractures over distances of as little as 1 mm. The pattern of mineral fill in these fractures shows that the assumption commonly made in modeling fluid flow in fractures—namely that fracture porosity can be approximated as a persistent parallel-sided slot—is far from being satisfied in this case.

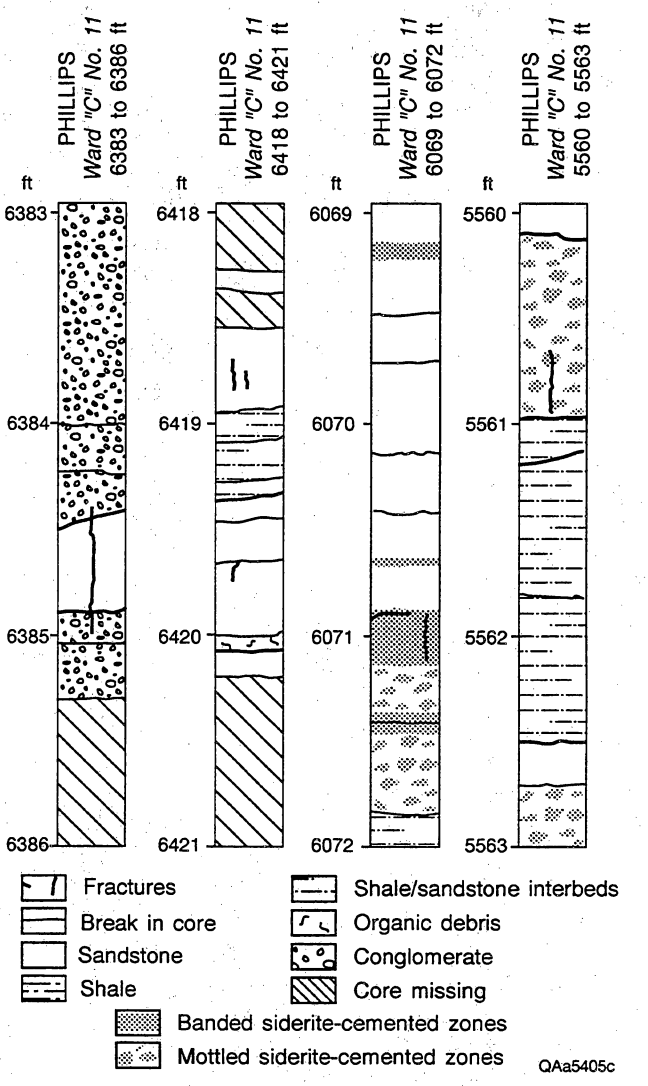

Figure 26. Fractures in Sonora Canyon Sandstone core, Phillips Ward "C" No. 11. Maps show fracture traces, rock types, and location of siderite-cemented zones. A quartz-lined fracture occurs at –6384.5 ft.

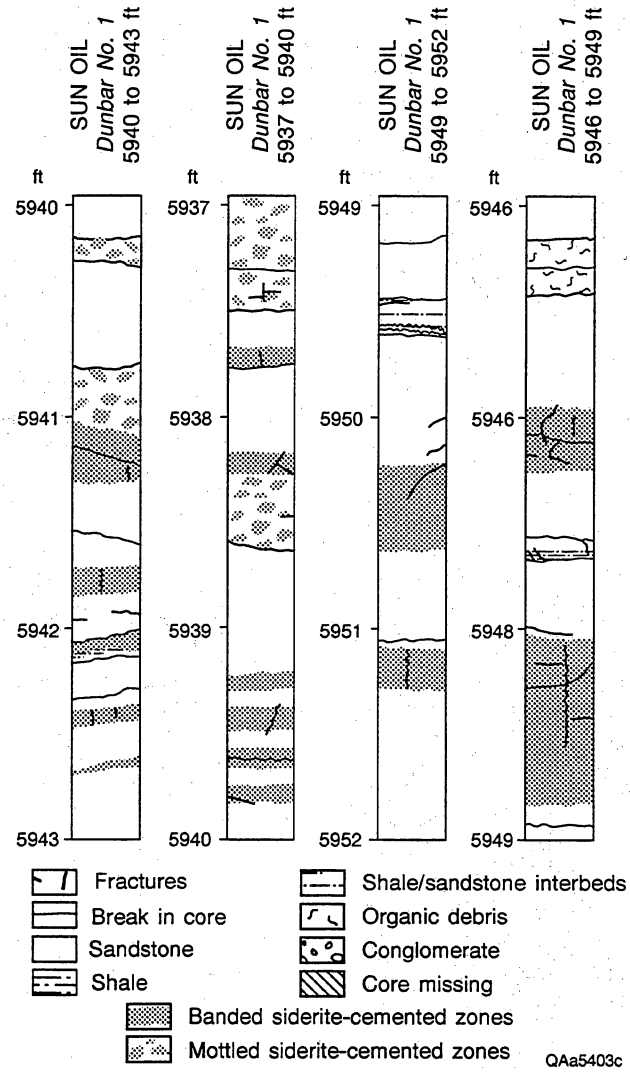

Figure 27. Fractures and siderite layers in Sonora Canyon Sandstone core, Sun Dunbar No. 1. Maps show fracture traces, rock types, and location of siderite-cemented zones. Note fractures localized in siderite layers.

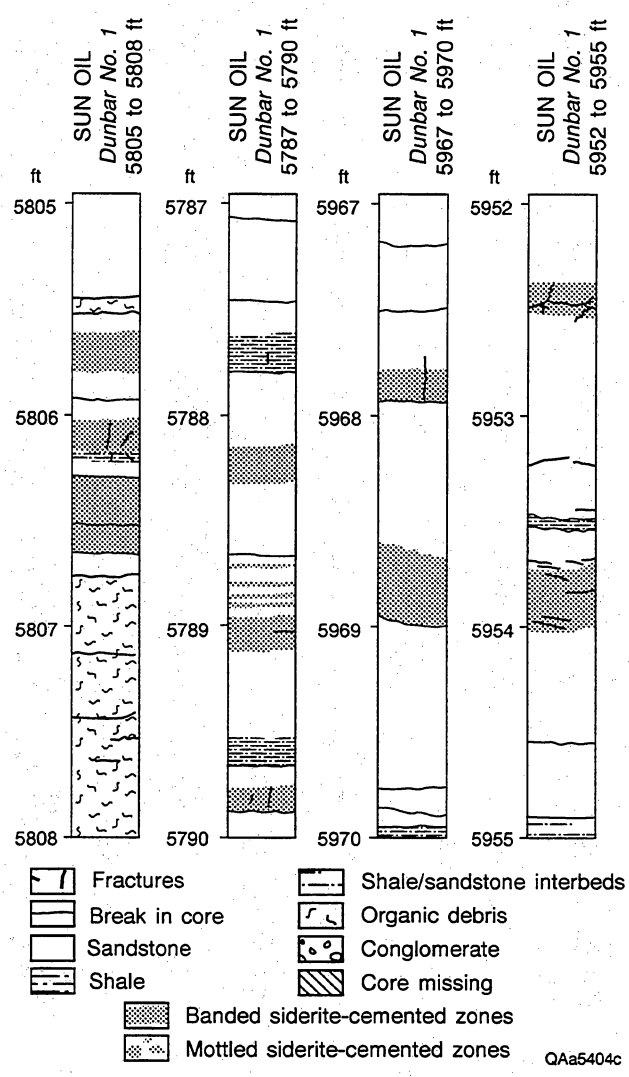

Figure 28. Fractures in Sonora Canyon Sandstone core, Sun Dunbar No. 1. Maps show fracture traces, rock types, and location of siderite-cemented zones. Note that some fractures in siderite layers do not extend across entire layer.

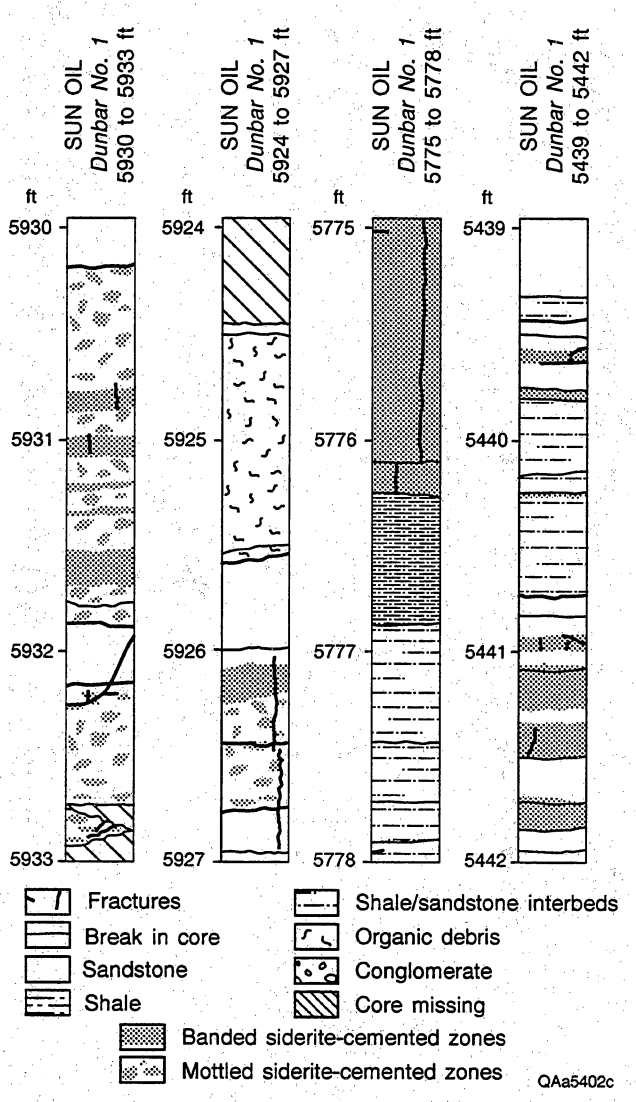

Figure 29. Long fracture in thick siderite layer, Sonora Canyon Sandstone core, Sun Dunbar No. 1. Maps show fracture traces, rock types, and location of siderite-cemented zones.

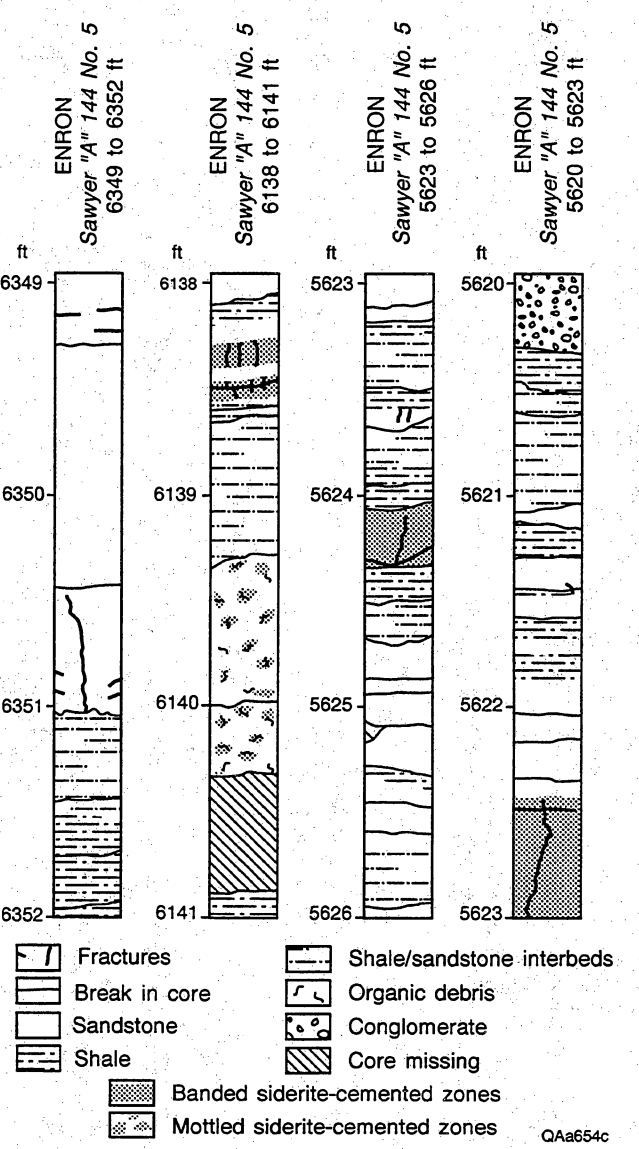

Figure 30. Fractures in Sonora Canyon Sandstone core, Enron Sawyer "A" 144 No. 5. Maps show fracture traces, rock types, and location of siderite-cemented zones.

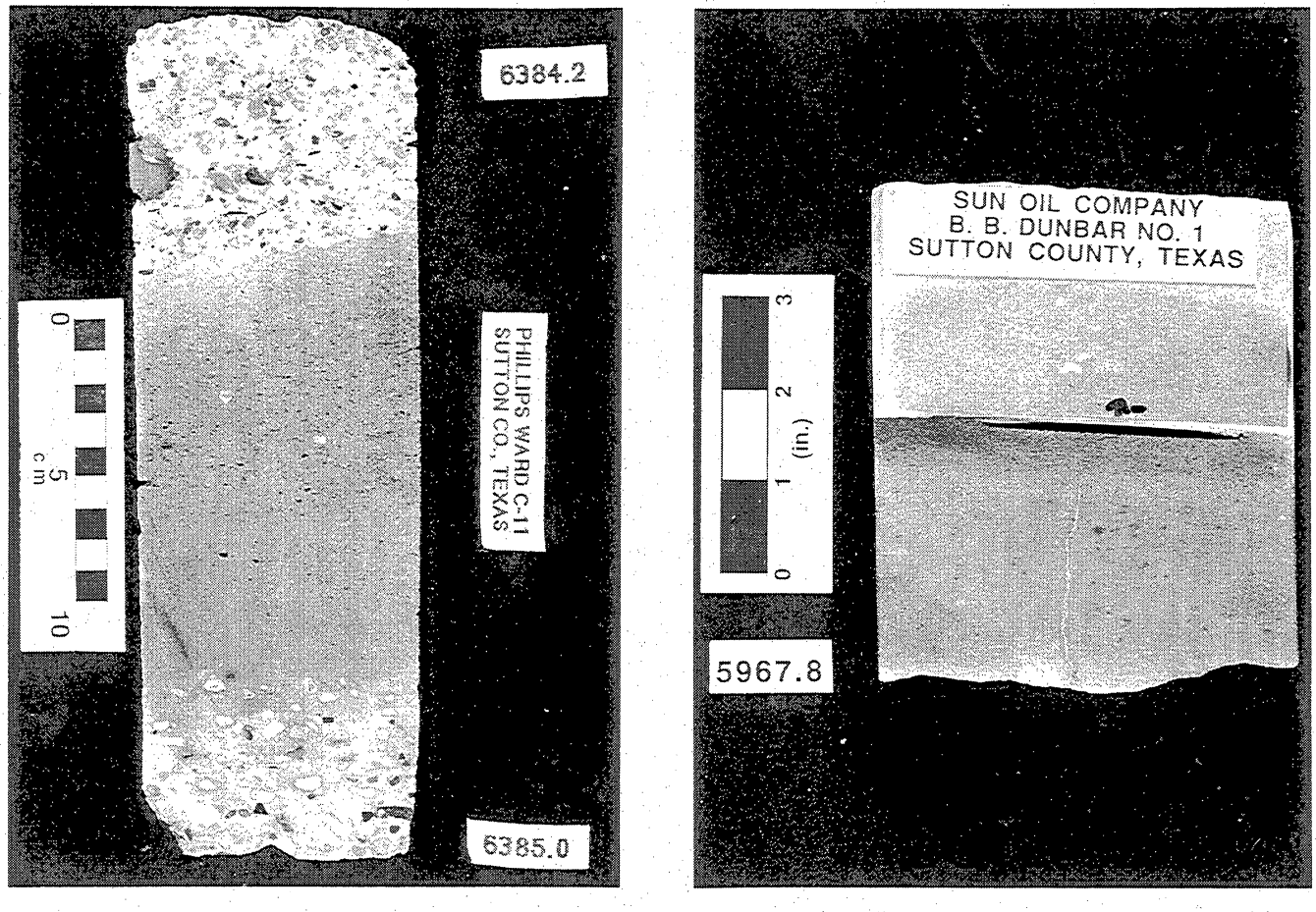

Figure 31. Photograph of fractures in Sonora Canyon core: (a) quartz-lined fracture from 6,384 ft, Phillips Ward "C" No. 11, (b) fracture in siderite layer, 5,967.8 ft, Sun Dunbar No. 1.

In Sonora Canyon sandstones, most natural fractures are short (less than 3 inches tall) and vertically discontinuous, but a few fractures have heights of greater than 1 ft (figs. 33 and 34). The range of fracture heights is similar for all cores, and no trends are evident in fracture height with depth. However, fracture size statistics are dominated by numerous short fractures that are localized in siderite-cement zones. This size data may not be representative of the entire natural fracture population. Categorization of fractures based on their relation to diagenesis provides a way to assess this view.

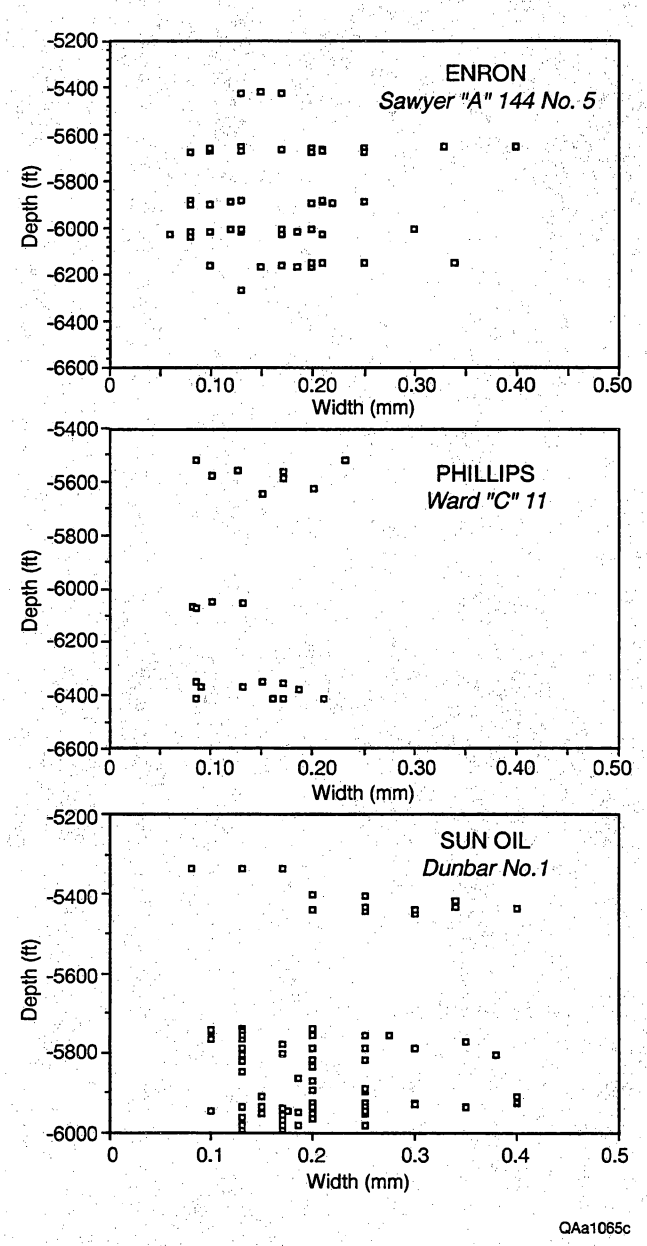

Figure 32. Fracture width versus depth for three Canyon Sandstone wells.

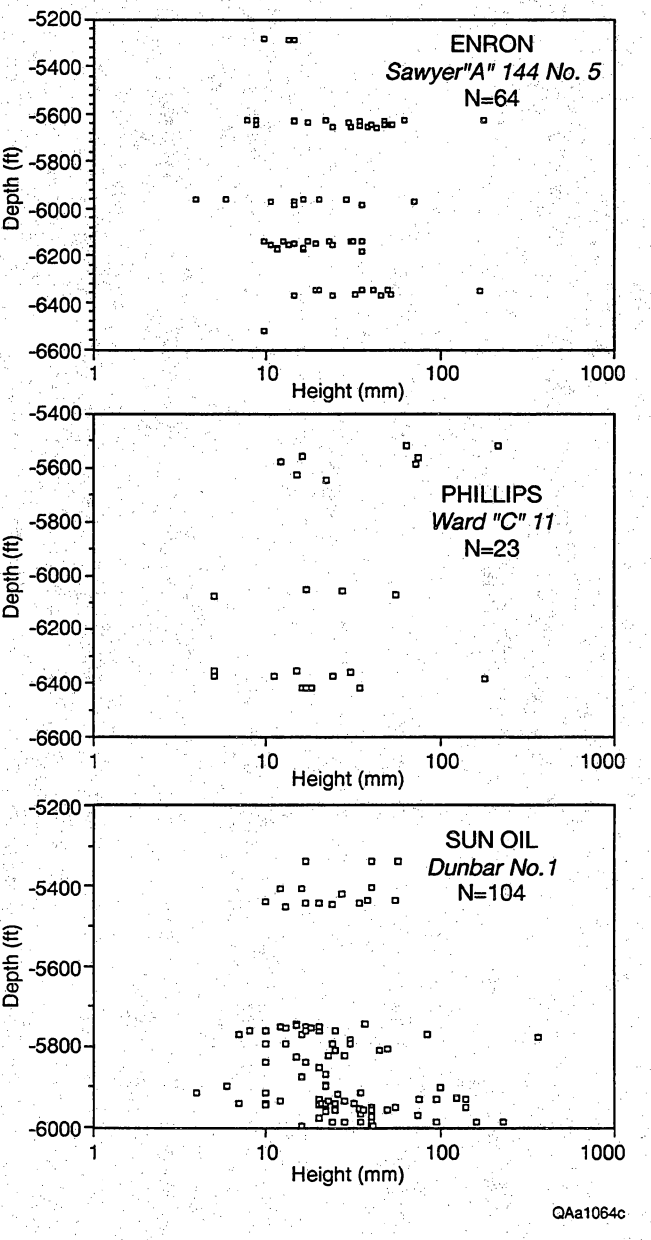

Figure 33. Fracture height versus depth for three Canyon Sandstone wells.

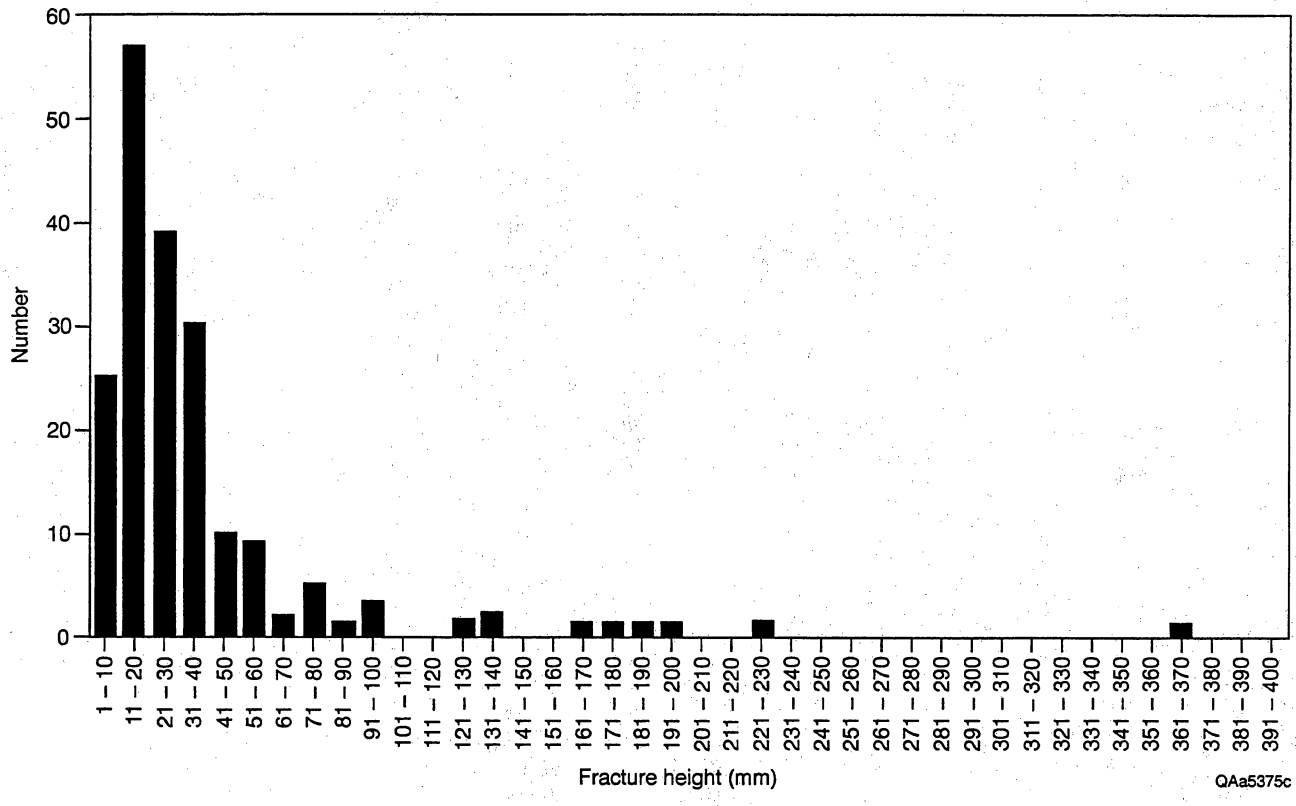

Figure 34. Histogram of fracture heights for fractures in siderite-cemented zones.

Fractures generally end by intersecting shale interbeds or at gradually tapering blind terminations within sandstone. Some fractures are confined to zones of diagenetic alteration, as will be described, and these fractures terminate at or near the abrupt margins of cemented zones. Fractures in sandstone also commonly end at mudstone interbeds. In core, fractures rarely intersect fractures above or below them. These observations, combined with termination of fractures at bed boundaries, suggest that fractures do not form interconnected networks from the top to the base of sandstone beds. According to our core observations, interconnected networks, if they exist at all, are likely to exist only within individual sandstones or parts of sandstones.

Petrology of Fracture-Filling Minerals

The main fracture-filling minerals in the Sonora Canyon sandstones are quartz, calcite, minor ankerite, and the clay mineral dickite (fig. 35). Carbonate minerals (calcite, ankerite) and dickite are the most abundant fracture-filling minerals, but they rarely occur together in the same fracture. Quartz forms a volumetrically minor component and was the first fracture-filling phase to precipitate in some fractures.

Where present, quartz fracture-fill mineralization is typically manifested as a thin (less than 0.5 mm) veneer of euhedral or subhedral overgrowths on broken or intact (more common) quartz grains on fracture walls. Quartz cement that bridges and occludes fracture porosity can be present at any point along fractures, but in Sonora Canyon samples this characteristic is most readily observed near fracture ends. Locally, fracture-filling quartz displays parallel planes of fluid inclusions that are traces of sealed microfractures. Such features result from the process of fracture propagation and sealing during quartz precipitation. Isolated fluid-inclusion planes, representing micron- to millimeter-scale sealed microfractures also occur in parts of the sandstone framework of the Sonora Canyon that are distant from macrofractures (fig. 36). Similar to features in Travis Peak sandstones, these sealed microfractures are more common near large (macroscopic) fractures.

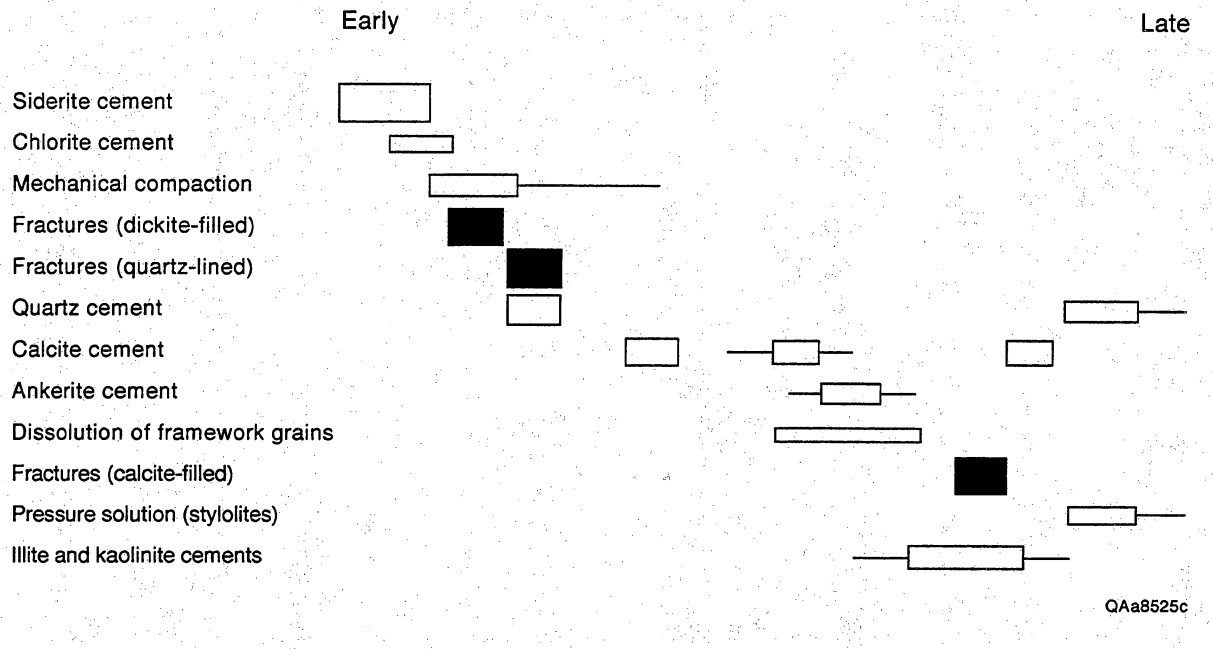

Figure 35. Diagram of composite diagenetic sequence and relative temporal relations of component diagenetic stages of sandstone framework and fracture fill of Sonora Canyon Sandstone. Fracture stages highlighted in black.

Microfracture strikes are in many cases subparallel to macrofracture orientation, as is discussed elsewhere in this report. In fractures where quartz is present, those fractures preserve evidence of fracture opening at the time of quartz precipitation. Thus, at least some quartz cement is synkinematic with respect to some of the fractures.

Calcite in carbonate-lined and -filled fractures typically is sparry and, locally, twinned and fractured. Textural relations of fracture-filling calcite suggest that several phases of carbonate fill may have precipitated in these fractures (figs. 37 and 35). The overall pattern of carbonate precipitation in fractures may not have been uniform throughout the Sonora Canyon, but from the wells in this study the following sequence of events is evident.

(1) The earliest phase of calcite in fractures is found overgrowing fracture-lining quartz. This generation of calcite was precipitated in fractures that did not break (crosscut) quartz cement—we infer that it filled in preexisting open quartz-lined fractures. This calcite is postkinematic.

(2) Locally, calcite precipitated as a pore-lining phase in isolated pores along these fractures after the first generation of calcite fracture fill crystallized. Horizontal stylolites, small fractures, and twin lamellae are evident in a few samples of this generation of fracture-fill carbonate. This represents deformation of preexisting filled fractures. The event includes partial dissolution and replacement of some fracture-filling minerals.

(3) Much of the fracture porosity in the older fracture-lining calcite was filled by a texturally younger phase of carbonate (locally, ankerite). In some cases this younger carbonate generation is associated with short horizontal carbonate-filled fractures emanating from the vertical fractures. These horizontal fracture segments may be indicative of fracturing at shallow depths (possibly less than 1 km) where fractures could open against the load of overlying rock. This could result from uplift and removal of some burial load by erosion, coupled with cooling and contraction of the rock.

A few fractures have only one generation of infilling carbonate that is interpreted to be equivalent to the youngest generation of fracture fill because these fractures crosscut quartz cement (fig. 38). These textural relations suggest that a late episode of fracture growth occurred while carbonate minerals were precipitating in these sandstones.

Layers and patches of siderite-cemented sandstone are interpreted to have formed at shallow depths of burial (Dutton, 1994). Siderite-cemented Sonora Canyon sandstone layers are categorized as either light, medium, or dark, corresponding roughly to increasing

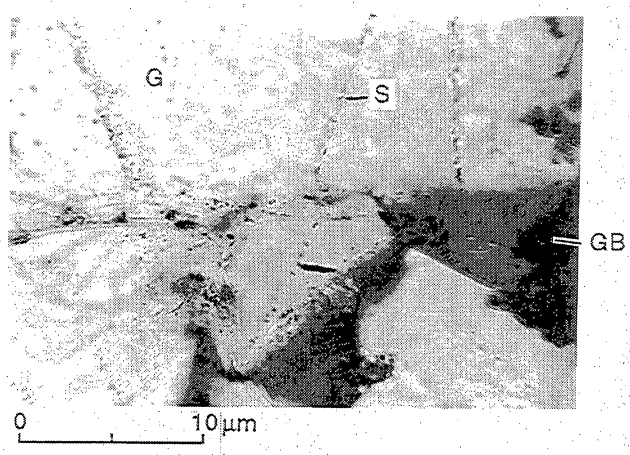

Figure 36. Fluid-inclusion planes (sealed microfractures), Sun Dunbar No. 1, depth 5,335 ft. S, scaled microfracture; G, grain; GB, grain boundary.

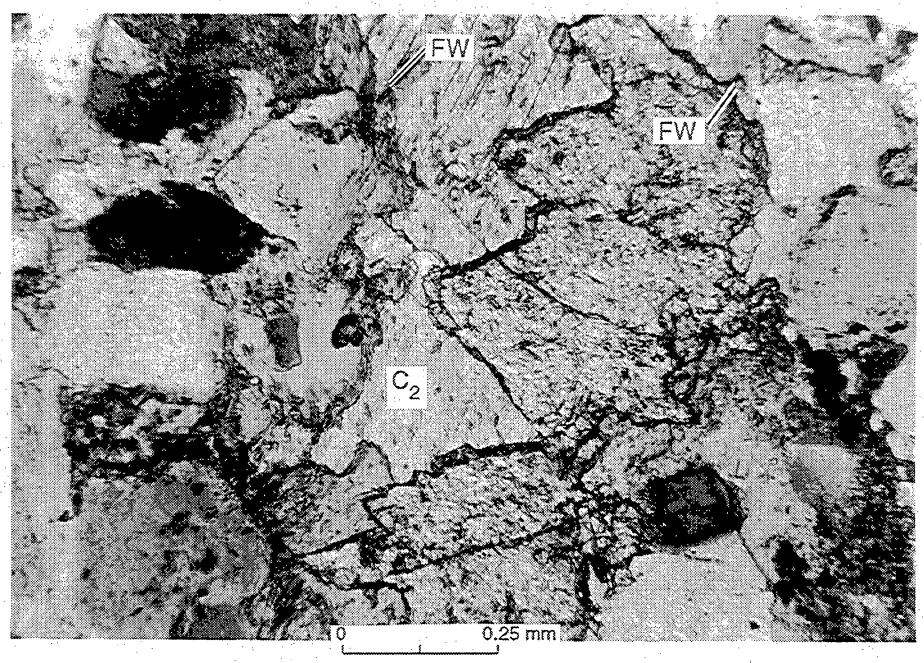

Figure 37. Calcite fracture fill, depth 6,350.8 ft, Enron Sawyer "A" 144 No. 5. Bar = 0.25 mm. Note two generations of carbonate in fracture (C_1 and C_2). FW, fracture walls.

Figure 38. Calcite-filled fracture crosscutting grains and quartz cement, Enron Sawyer "A" 144 No. 5, depth 6,350 ft. Also note later handling-induced fracture (unfilled, dark). Bar = 1 mm. FW, fracture walls.

degree of cementation. Light layers typically have less than 10 percent siderite cement; medium and dark layers range from 10 to 30 percent siderite. There is little variation in fracture shape or mineral fill in layers of differing degree of cementation, but fractures are somewhat more common in the darker layers. In the Dunbar No. 1 core, 77 percent of the fractures are in medium to dark siderite layers, and 78 percent are in layers having a banded appearance and abrupt boundaries. The overall attributes and abundance of fractures in siderite-cemented layers are similar in all three wells, but the Dunbar No. 1 core contains a slightly higher density of fractures than do the other two wells, corresponding to a higher proportion of thin, discrete layers of medium- to dark-colored siderite-cemented layers in this well than in the other two wells, where diffuse, mottled, and light-colored siderite-cemented zones are prevalent.

Mineral fill in fractures in siderite-cemented layers is predominantly dickite (fig. 39), a clay mineral that is a polymorph of kaolinite. Petrogenetic evidence shows that dickite-filled fractures formed later than siderite cement but prior to quartz cement. Dickite typically forms a dense fracture fill with little or no visible fracture macroporosity, but scanning electron microscope images show that fracture microporosity exists within these fractures. In some fractures minor calcite accompanies dickite and textural evidence

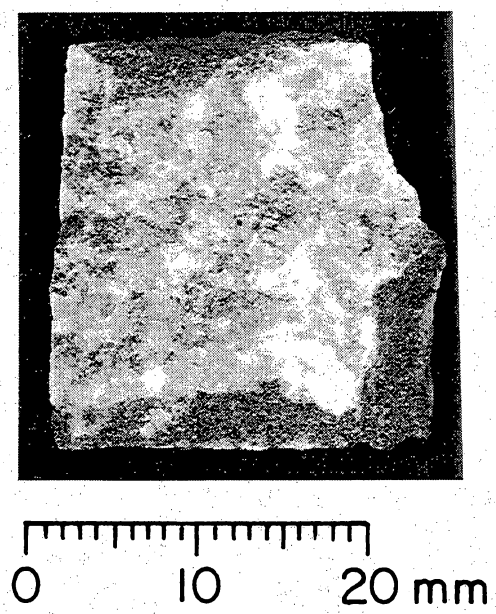

Figure 39. Photograph of natural fracture surface showing clay mineral dickite. Enron Sawyer "A" 144 No. 5, depth 5,644.8 ft.

suggests that the carbonate mineral is younger than dickite. Some fractures in siderite layers in the Ward "C" No. 11 well are largely calcite filled.

Dickite-filled fractures in siderite layers were the first fractures to form, and quartz-filled fractures formed later (fig. 35). This is exemplified by crosscutting relations among fractures. In the Sawyer "A" 144 No. 5 core, a quartz-filled fracture (strike 044°) cuts across a siderite-layer fracture at nearly right angles. Later quartz-lined fractures formed dominantly in rock lacking siderite cement, but quartz does not appear to have been precipitated in fractures having dickite fill, possibly because these fractures were closed (filled) at the time. Petrographic studies show that several generations of fracture-filling calcite exist in Sonora Canyon fractures (fig. 35) and that fracture-filling calcite locally postdates dickite in fractures in siderite layers. Carbonate fracture fill also postdates precipitation of quartz in some fractures. Early calcite fracture fill experienced burial loading and compaction after their formation, manifested by twinned calcite and subhorizontal stylolites.

Fracture Categorization

Opening-mode fractures in Sonora Canyon core can be separated into at least two categories. Fractures in the two classes have contrasting distributions, characteristic sizes, and/or mineral fills (table 6). They also are of different ages and have contrasting patterns of orientation. These categories (classes) represent

Table 6. Summary of Sonora Canyon fracture class attributes.

	Fractures in quartz- and calcite-cemented layers Class I	Fractures in siderite-cemented layers Class II
Height	Many >10 inches tall	10 inches tall (average)
Aspect ratio	Tall and narrow	Short and wide
Visible porosity	Common	Rare
Mineral fill	Quartz; followed by ankerite in some cases. A few fractures lack early quartz.	Clay minerals (dickite); some later calcite
Roughness	Fairly smooth walls	Rough, irregular walls
Occurrence	Cross zones of various cement types	Confined to siderite cemented zones

fractures that have two distinct types of relationship to cementation. In the case of siderite cement, fractures were superimposed on preexisting prekinematic siderite cement. In the case of quartz cement, evidence points to fractures that formed at the time of cementation. In this section we focus on the fractures related to prekinematic cements; synkinematic cementation is discussed in more detail in the section on the Travis Peak Formation.

Fracture Class I in Canyon Sandstone cores comprises quartz- and carbonate-filled fractures that lack dickite and that typically are predominantly in quartz-cemented zones. However, these fractures are not confined to layers that have a particular cement type. Most commonly, these fractures are observed in areas having moderate to extensive quartz and carbonate cement. Marin and others (1993) suggested that fractures in this class can be separated into two classes based on mineral composition of fracture fill, but because of the small number of fractures involved and the variability in mineral diagenesis of the fracture fill, this distinction may not be useful. The distinction may be more representative of differing postkinematic cementation histories for different fractures.

This fracture class exists in all three wells. Unlike fractures within siderite-cemented layers, these fractures cross sandstone containing various cement types. Tall fractures within this class locally cross shale interbeds. These fractures are generally taller and tend to have somewhat greater height-to-width ratios than fractures in siderite-cemented layers. Both carbonate- and quartz-filled fractures are typically smooth-sided with smoothly curved to planar walls, in contrast to rough-walled fractures characteristic of many siderite-cemented layers (table 6). Nevertheless, intragranular fracture pathways characterize these fractures and distinguish them from fractures created by drilling and coring processes and fractures created in laboratory tests of these sandstones (Baek and Laubach, 1994).

Quartz- or carbonate-filled fractures are far less common (n = 48) than those in siderite-cemented layers (n = 116). In the 3 wells there are 40 quartz-filled fractures and 8 carbonate-filled fractures. Quartz-filled fractures range in height from 5 to 230 mm, and calcite-filled fractures range from 11 to 368 mm. This range of measured fracture heights probably underestimates fracture size for these classes of fracture because many do not end within core. From the observation that these fractures end at shale interbeds or at other major changes in rock type (figs. 26 through 30), rather than at boundaries between rock having contrasting cement types, fracture heights for this class of fracture are most likely comparable to sandstone bed thicknesses. Carbonate- or quartz-filled fractures rarely contain both minerals, and where both are present, quartz is the first phase to have precipitated.

Fracture Class II, the class with the most abundant fractures, comprises fractures that exist only in siderite-cemented layers and in isolated patches of siderite cement in sandstones (fig. 29). Fractures in this class cross siderite-cemented zones and typically end abruptly at the edges of siderite-cement layers. The tallest fractures are as tall as the thickest layers of siderite cement. Only rarely do fractures extend beyond boundaries of siderite-cemented layers. Fractures are typically narrow, commonly less than 0.25 mm wide (average 0.17 mm), but short (less than 100 mm tall). Fractures in siderite-cemented layers have a range of height-to-width ratios of 25:1 to more than 2500:1, but most are between 100:1 and 300:1. Locally

fractures have height-to-width ratios of as much as 25:1 where short fractures are exceptionally wide. Fractures of a given height in siderite-cemented layers are commonly wider than fractures of comparable height in other classes.

Fractures in siderite-cemented layers are the most abundant, constituting 116 (61 percent) of the natural fractures documented in Canyon core. Fractures are in 16.5 percent of the siderite-cemented zones in the Dunbar No. 1 core, in 5.3 percent of these zones in Ward "C" No. 11 core, and in 9.7 percent of those zones in Sawyer "A" 144 No. 5 core. Fracture abundance varies with layer thickness; that is, thin layers have greater numbers of fractures. Many thick siderite-cemented layers lack fractures in core. The range of siderite-cemented layer thickness measured from core is 6 mm to more than 1,000 mm. For layers ≤130 mm, the percentage containing at least one fracture is 18.5 percent of siderite-cemented zones in the Dunbar No. 1 core, 11 percent in Ward "C" No. 11 core, and 9.5 percent in Sawyer "A" 144 No. 5 core. Fracture numbers normalized to individual cement layer thickness are often high; where fractures are present, fracture numbers are near 1.0.

Mineralization Sequence of Fractures and Timing of Fracturing

We interpret the dickite-filled fractures to have formed at relatively shallow burial depths. The presence of dickite suggests that fractures formed at depths of more than 1 km (0.6 mi) or that they formed in an area of elevated heat flow. The orientation (strike) of these fractures is highly variable (Laubach and others, 1994), as might be expected for fractures formed at shallow burial depth. Dickite-filled fractures in siderite layers were the first fractures to form, and quartz-filled fractures formed later (fig. 35). This is exemplified by crosscutting relations among fractures. Quartz was not precipitated in fractures having dickite fill, possibly because these fractures were closed (filled) at the time. Several generations of fracture-filling calcite exist in Sonora Canyon fractures (fig. 35). Fracture-filling calcite postdates dickite and precipitation of quartz. Early calcite fracture fill experienced burial loading and compaction, manifested by twinned calcite and subhorizontal stylolites. Some later-stage carbonate precipitated in short horizontal fracture segments that may have formed at shallow burial depths.

Bearing in mind the limited evidence for true ages of fracture formation and the limited oriented fracture data, we suggest that dickite-filled fractures formed shortly after sediment deposition at relatively shallow burial depths (but possibly, based on the presence of dickite, in an area of elevated heat flow). In such a structural setting, the orientation (strike) of these fractures is likely to be highly variable, in agreement with what is known of true fracture strikes and relative strikes of fractures in siderite-cemented layers within continuous core sections.

Quartz-lined fractures developed at greater depths, and if the limited information from oriented fractures is representative, in a tectonic regime of northeast-oriented SHmax. Because several tectonic events in the Paleozoic to Recent history of the region could have caused fractures of this orientation, fracture strike is not diagnostic of the age of fracture growth. Cross-cutting relations among fractures and fracture-filling minerals indicate that calcite-filled fractures may be the youngest fracture set, but internal deformation in vein filling minerals and crosscutting subhorizontal stylolites are evidence that these fractures formed prior to an episode of deep burial. Uplift rather than burial has affected the Canyon since at least the late Tertiary; we infer that these fractures formed in the Cretaceous or earlier. We interpret quartz-filled fractures to have formed in pre-Cretaceous time, possibly initially after Sonora Canyon sandstones reached burial depths of 2 to 3 km (1 to 2 mi).

Porosity Development in Fractures

Porosity in fractures that formed in prekinematic siderite-cemented layers is generally too small to measure. At some time after these fractures formed, various later cement phases began to fill them in. Some porosity survived long enough to be filled with late carbonate cements. Yet despite the generally higher rock framework porosity in siderite-cemented layers, fractures are mainly occluded.

In contrast, primary fracture porosity is preserved along both quartz- and carbonate-filled fractures. Visual inspection of fracture traces on core edges suggests that quartz-lined fractures have the greatest preserved porosity (locally as much as 75 percent). In the Ward "C" No. 11 well, an RFT log recorded an instant pressure buildup when a test was conducted at a depth from which a partly open quartz-lined fracture had been recovered in core (fig. 26), indicating that fracture porosity exists at depth for this fracture class. Petrographic examination shows that parts of quartz-lined fractures are open for distances of several inches, but transitions to filled fracture or areas of disconnected

fracture porosity (on the scale of fractions of an inch) are abrupt.

Sandstone-cement abundance variations between siderite-rich and quartz-rich layers of the Sonora Canyon (fig. 5) reflect the marked difference in timing of fracturing and potential porosity development relative to cementation in the two layers. In the siderite-rich layers, prekinematic siderite is by far the most abundant cement, composing an average of 24.0 percent of whole-rock volume, or 76 percent of all cements. Synkinematic quartz in the quartz-rich layers totals an average of 10.7 percent of whole-rock volume, or 70 percent of all cements. The latter value approximates the percentage of porosity occlusion by quartz fracture-fill in Sonora Canyon fractures, where 70 to 90 percent of fracture porosity is filled with quartz.

Carbonate-filled fractures in the cores are largely filled, and calcite is locally highly twinned, but primary fracture porosity is present locally. This fracture porosity typically does not appear to be connected within the plane of the fracture. We infer that compared to quartz-lined fractures, fractures having extensive carbonate fill are less likely to preserve fracture porosity. The Ozona Canyon example described previously shows that rock-framework cementation patterns can highlight areas where such postkinematic cements are likely to occlude fracture porosity.

Fracture Stratigraphic Units

In this example, early siderite cement likely caused cemented layers to be brittle at an early stage of burial loading, resulting in mechanical properties that cause it to be prone to fracture. As noted previously, core observations confirm that these beds are highly fractured, with fracture spacing about equal to the thickness of individual siderite layers. But fracture-filling dickite suggests that fracture occurred at greater burial depth than siderite precipitation.

Because compaction and authigenic cements subsequently modified the mechanical properties of non-siderite-cemented parts of the sandstone, the mechanical contrast within sandstone caused by siderite cement became less pronounced with time, and later fractures are not concentrated in siderite layers. Data from the Ward "C" No. 11 well suggest that Canyon Sandstone layers having high quartz (10 to 20 percent) and/or siderite (20 to 30 percent) cement volumes have higher static Young's modulus (3.5 to 4 MMpsi) and slightly higher dynamic Young's modulus (7 to 8 MMpsi) (Miller and others, 1991) than rock having lower volumes of these authigenic phases. As described in the next section, fracture toughness measurements give similar results for both siderite- and non-siderite-cemented beds. Thus, these are two separate diagenetic facies in these sandstones that lead to fracture prone rock properties. Yet fracture attributes, and the timing of fracture, differ for the two fracture facies, in part because the timing of diagenesis for the two cements differs.

In the Sonora Canyon example, siderite- or quartz-cemented layer-thickness and observed fracture abundance information can be combined to give an estimate of fracture spacing. The probability of encountering a fracture where the wellbore is perpendicular to bedding and fractures are vertical is equal to the core diameter (4 inches) divided by the median fracture spacing. When fracture spacing is less than or equal to the core diameter, a fracture intersection is certain. If typical spacing in siderite-cemented layers is about the same as layer thickness (6 to 8 inches thick and rarely more than 10 inches), then we should expect to find intersecting fractures in many thin siderite-cemented layers, as is observed.

Where a single joint set is present in mechanically significant beds or in layers of different thickness, the distance between joints in thick beds commonly is greater than that in thin beds. The ratio of bed thickness to joint spacing can vary with a number of factors, including rock properties and length of time that fracture-producing processes have been active, but in thin beds, spacing in many cases is close to, or slightly less than, bed thickness. This may be also true for fractures in siderite-cemented layers (fig. 40). Thus, to a first approximation siderite-cemented-layer or quartz-cemented-layer thickness provides a reasonably accurate estimate of spacing, but direct evidence of a regular relationship between fracture spacing and layer thickness is stronger for siderite-cemented layers because there are many more thin siderite layers, and thus, more fracture/bed thickness observations for this class.

The timing of cementation and fracturing can be used to help interpret the significance of observations of fracture abundance to reservoir properties. Examination of fracture and diagenetic characteristics in Sonora Canyon cores shows that simple fracture abundance patterns can be misleading guides to overall fracture patterns. Siderite cement layers and associated fractures are part of a Sonora Canyon fracture stratigraphy, but fractures in dominantly quartz-cemented intervals also constitute a part of the Sonora Canyon fracture stratigraphy. Fractures in core are observed primarily in layers that have prekinematic siderite cement, but open fractures, though less common in core, are the fractures that tend to preserve fracture porosity. The disparity in fracture abundance may reflect greater average bed thickness and fracture spacing for fractures in quartz-cemented layers. Siderite

layers are thin, and thus fractures in them are more closely spaced and more likely to be sampled. Knowledge of such patterns can be used to evaluate the likely patterns of opening and filled fractures in reservoir rocks, with implications for design of drilling programs (fig. 41).

Many of the fractures in siderite layers are older than quartz cementation and were completely filled at a relatively early stage in the rock's burial. In this case, the position of these fractures in the diagenetic sequence shows that fractures in siderite layers are not likely to be fluid conduits and the cause of high deliverability zones. This is consistent with dense mineral fill in these fractures. On the other hand, diagenetic studies show that siderite layers have higher matrix porosity than adjacent quartz-cemented sandstone and that these siderite-rich zones may be areas of better reservoir quality (Dutton, 1994). Early mineralization and occlusion of fractures in siderite layers suggests that the fractures may be flow barriers. This finding has implications for interpretation of flow heterogeneity and flow anisotropy in the reservoir. Given the evidence that quartz cementation in the Canyon is synkinematic and by analogy with porous synkinematic fractures in the Travis Peak Formation, we predict that the abundance of fractures associated with quartz cementation in the Canyon will increase with increasing degree of quartz cementation.

Quartz cement is synkinematic relative to most fractures in quartz-cemented zones, but it is post–kinematic relative to fractures in siderite-cemented layers. Open fracture porosity in some Canyon quartz-cement zone fractures and the possible synkinematic nature of fracture development suggests that occlusion of fracture porosity by quartz fracture-filling minerals is probably incomplete and that fracture porosity persists in this fracture class. Because structure development is an additional cause of fracture superimposed on fracture-diagenesis relations, additional information such as fault location or bed curvature analysis (Laubach and others, 1992c; Schultz-Ela and Yeh, 1992) should be acquired in these areas to determine the timing of structure development relative to diagenesis and to augment prediction of fracture porosity. Using data from deviated wells may be the best way to test these methods.

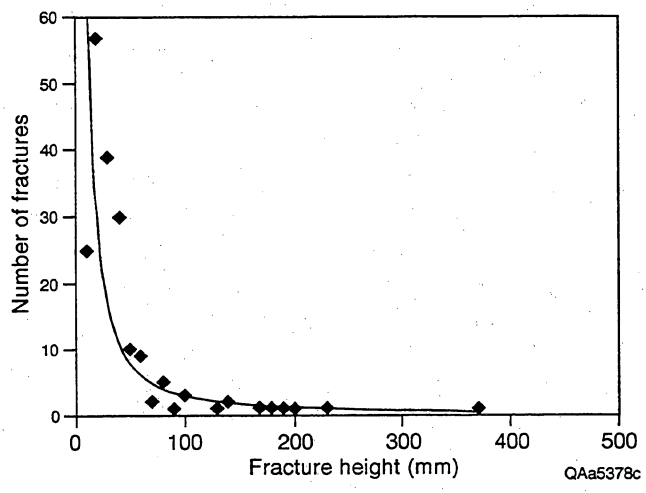

Figure 40. Number of fractures versus fracture height (interpreted to be equal to fracture spacing) and probability of fracture intercept for that fracture spacing and 4-inch-diameter core (solid curve).

Synkinematic Diagenesis: Quartz Cement in the Travis Peak Formation

The Travis Peak Formation is dominated by synkinematic quartz. Core- and log-based studies of fractures in nine wells in East Texas documented fracture type, attitude, abundance, shape, microstructure, and fracture-fill mineralogy and microstructure in the Travis Peak Formation. Some aspects of fracturing and diagenesis in this formation have been reported elsewhere (Laubach, 1989a; Dutton and others, 1991a, 1991b). Data on specific wells and on the relationship of diagenesis and fractures to the overall geology and production aspects of this unit are described in the cited reports. Here we report new interpretations of diagenesis and fractures based on application of cathodoluminescence (CL) imaging technology. We also describe new fracture abundance and fracture shape measurements (table 7) based on extensive detailed core fracture mapping, calculations of fracture depth-of-formation based on fracture shape, and vein mineral isotopic analyses, thermobarometry, and water salinity studies.

The core data base for this formation in selected areas of East Texas is extensive. Parts of several cores were oriented by standard techniques (Nelson and others, 1987) or by comparison with borehole-imaging geophysical logs. The resulting orientations generally have an uncertainty of less than 15° within a given well (appendix 2). Fracture orientation information from this formation is discussed in the section "Using Microstructure and Rock Test Data to Map Fracture Strike." Cement and fracture relations in the Travis Peak are a good example of synkinematic cement.

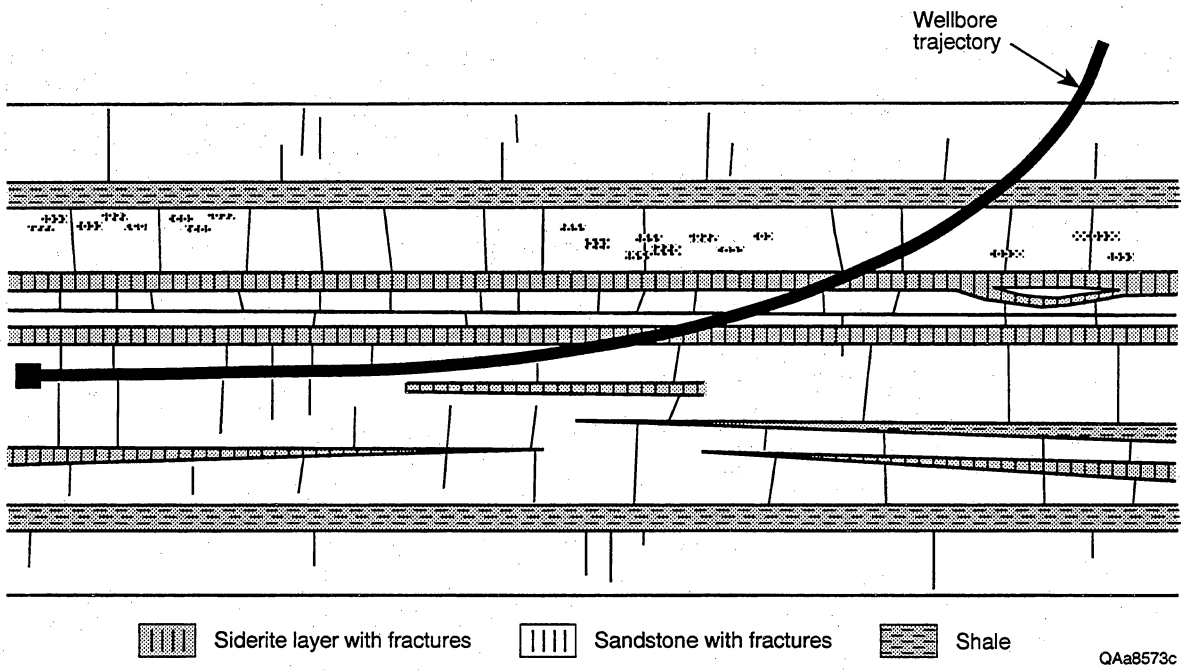

Figure 41. Fracture stratigraphy of Sonora Canyon sandstones. Contrasting fracture types exist in quartz-cemented and siderite-cemented zones. Hypothetical horizontal well bore trajectory is shown. Well is aimed to cross fractures in synkinematic quartz layers, despite low abundance of fractures in these layers in vertical core.

Table 7. Fracture abundance patterns in the Travis Peak Formation.

GRI well name	Level of Travis Peak Formation	Total core (ft)	Sandstone core (ft)	Percent of sandstone core	Total footage of natural fractures per foot of core (FN_1)*	Total footage of natural fractures per foot of sandstone core (FN_2)*
Prairie Mast	Total fm.	199.3	152.9	77	0.104	0.080
A-1	Upper	50.6	37.0	73	0.135	0.071
	Lower	148.7	115.9	78	0.095	0.044
Mobil Cargill	Total fm.	200.7	98.0	49	0.034	0.016
No. 14	Upper	200.7	98.0	49	0.034	0.016
	Lower	—	—	—	0.000	0.000
Marshall	Total fm.	247.0	111.6	45	0.050	0.021
Werner	Upper	247.0	111.6	45	0.050	0.021
Sawmill	Lower	—	—	—	0.000	0.000
Howell	Total fm.	468.5	236.7	51	0.037	0.019
No. 5	Upper	317.5	151.4	48	0.038	0.018
(SFE No. 1)	Lower	151.0	85.3	56	0.035	0.020
Arkla Scott	Total fm.	244.2	113.5	46	0.220	0.067
No. 5	Upper	135.2	40.5	30	0.390	0.078
	Lower	109.0	73.0	67	0.064	0.037
SFE No. 2	Total fm.	359.4	286.2	80	0.227	0.181
	Upper	134.3	97.1	72	0.031	0.022
	Lower	225.1	189.1	84	0.327	0.275

*FN = fracture number

Fracture Morphology and Dimensions

Natural fractures in the Travis Peak Formation can be divided into two major types: (1) mineralized, subvertical, opening-mode fractures and (2) gently dipping faults. Opening-mode fractures occur predominantly in sandstone, whereas faults are present primarily in shale and silty mudstone. Travis Peak opening-mode fractures are commonly filled or partly filled with authigenic minerals such as quartz and carbonate minerals (calcite or ankerite/dolomite) (fig. 42). Small faults in Travis Peak mudstone core result from processes such as soil formation and compaction in the shallow subsurface and probably are not an important reservoir element; these features are not discussed further here. Opening-mode fractures in sandstone, on the other hand, are likely to have a direct effect on reservoir quality because they contain large areas of interconnected porosity.

An important characteristic of many Travis Peak fractures is that they are partly or completely open in core (fig. 42). Petrographic evidence of delicate fracture-lining and -bridging minerals demonstrates that many fractures were also open in the subsurface, including fractures from depths of as much as 9,934 ft. Open fractures are usually lens shaped in cross section and have widths that range from microscopic (<0.05 mm) to 5 mm. Because the mineral fill in fractures is irregularly distributed, open pore networks or channel ways within fractures are curved to anastomosing and have rough walls. Open fractures were sampled from both the upper and lower Travis Peak, but the widest fractures are from the lower Travis Peak in the Holditch SFE No. 2 well. Some of these fractures are also the shortest and least vertically continuous.

Fracture height is the only length dimension of vertical macrofractures that can be measured in vertical Travis Peak core (figs. 43–45). A spectrum of fracture heights is present at any given depth in the Travis Peak, the tallest fractures being as much as 8 ft high. Tall fractures are composed of coplanar segments, ranging in length from inches to tens of inches and commonly arranged in relay and en echelon patterns. In cross section, segments are separated locally from adjacent segments by intact rock. Most fractures do not extend completely across sandstone beds, even where the beds are apparently of homogeneous composition. Instead, they end within beds. Fractures show various styles of termination, including fractures that are truncated by stylolites are locally present in more deeply buried parts of the formation.

Fractures can be subdivided into three categories or classes based on their shape. Class 1 fractures are wide, short fractures that are generally found as isolated features in core (figs. 46 and 47). Their shape is vuglike, and commonly they have triangular to blunt terminations at one (most common) or both ends. These terminations are generally associated with stylolites. These fractures do not have multiple fracture strands. Class 2 fractures are long and relatively thin. They may have a complex geometry consisting of relay and en echelon patterns. These fractures are the longest that are visible in cored intervals. Class 3 fractures

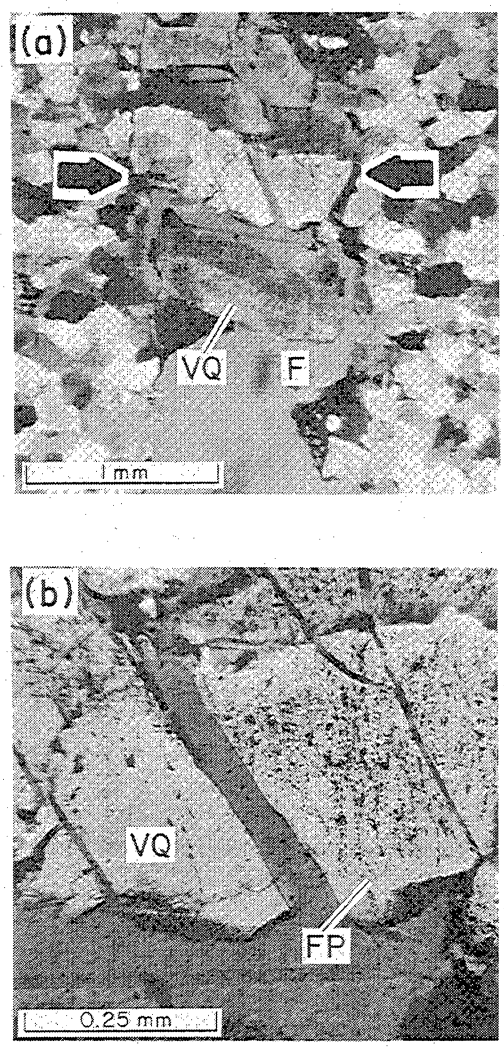

Figure 42. Natural fracture in the Travis Peak Formation, Holditch SFE No. 2 core, depth 9,840 ft. Fracture porosity (F) and fracture-lining quartz (VQ) are shown. Note fluid inclusions and fluid-inclusion-defined planes (FP).

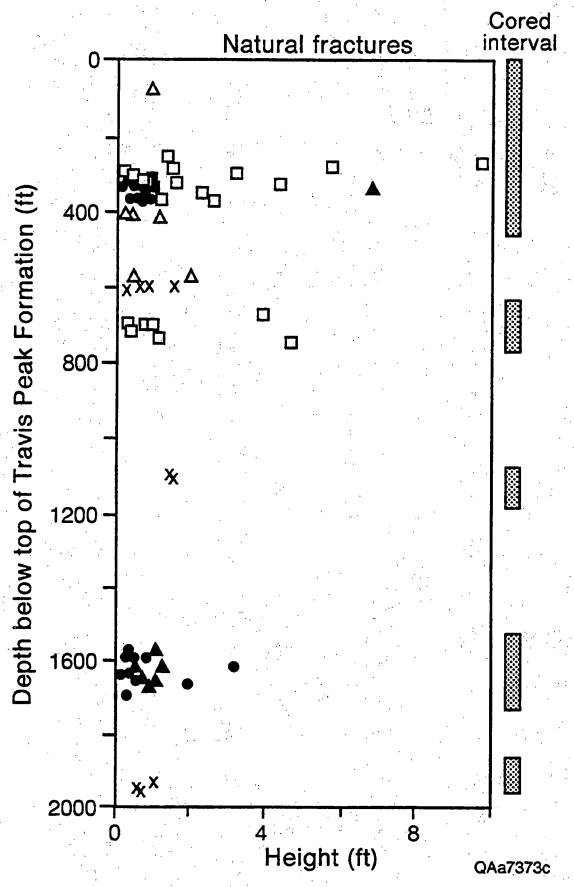

Figure 43. Fracture height in core versus stratigraphic position, Travis Peak Formation. Symbols correspond to wells. Data includes fractures that extend beyond core; truncation sampling bias is therefore present.

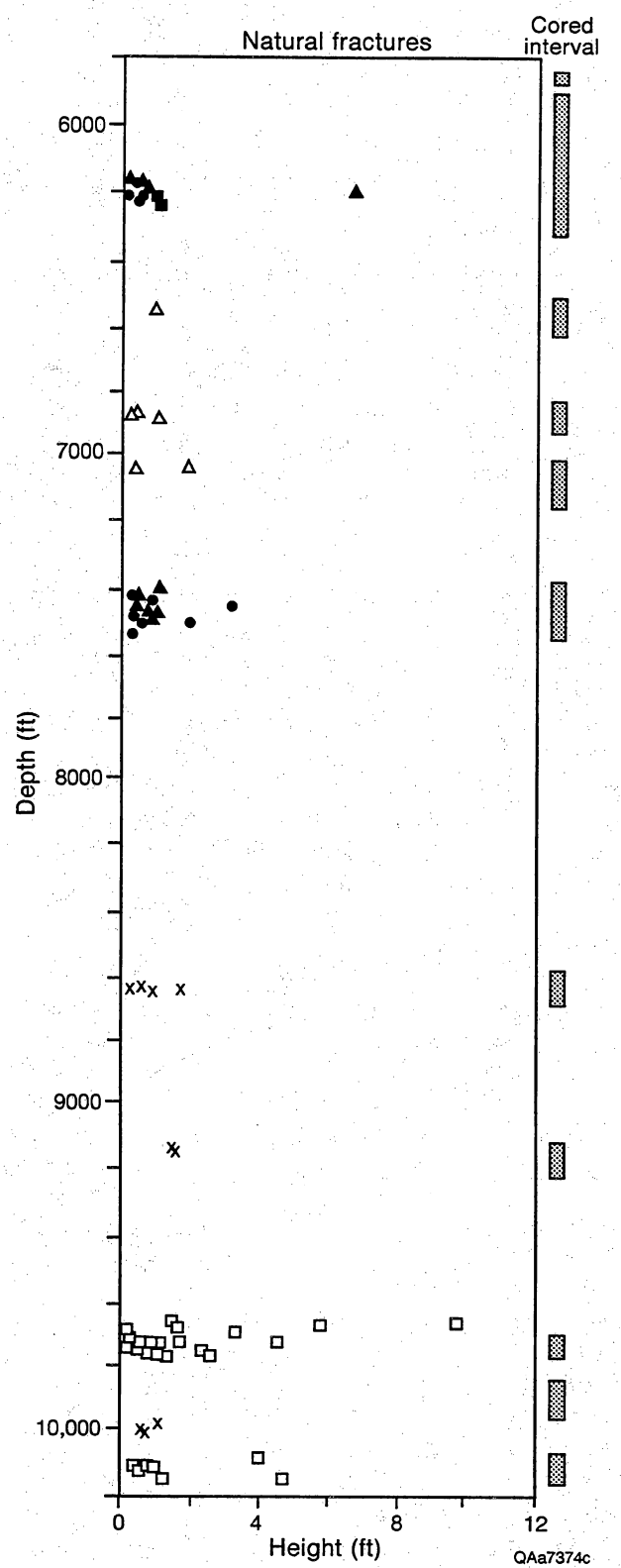

Figure 44. Fracture height in core versus depth, Travis Peak Formation. Symbols as in figure 43.

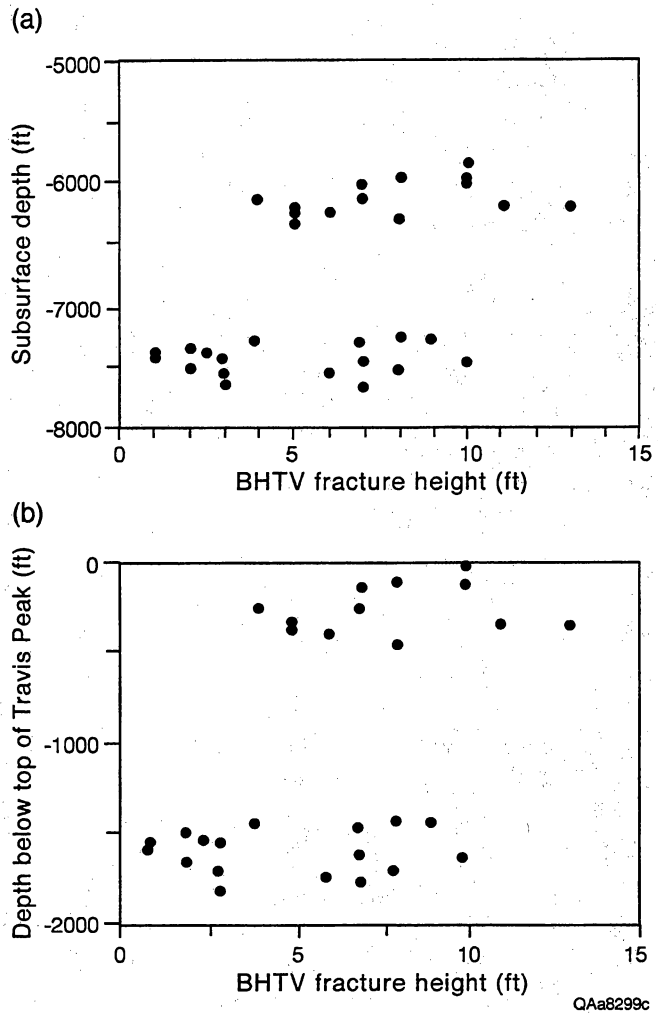

Figure 45. Patterns of fracture height in Travis Peak Formation visible on borehole-televiewer (BHTV) logs.

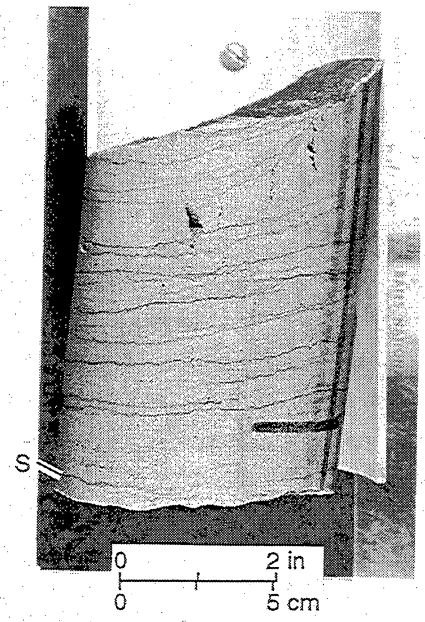

Figure 46. Photograph of a typical Class 1 fracture, Travis Peak Formation, Holditch SFE No. 2 core, depth 9,880.3 ft. Note stylolites (S).

have simple, elliptical shapes, and sharp tapering terminations. Individual segments of complex Class 2 fractures are composed of Class 3 fractures. In fact, these two classes are gradational in their attributes, the main distinction being that the mean length/width ratio is higher for composite Class 2 fractures. For all three classes, the mechanical properties and cement composition of beds containing these fractures is similar, as is the composition of vein-filling quartz. Class 1 fractures, however, are rare in the upper Travis Peak, and are most prevalent in more deeply buried parts of lower Travis Peak sandstones. The complexity of internal structures such as vein-filling texture patterns, crack-seal structures, and distributions of associated microfractures in vein-filling quartz increases from Class 3 fractures, which are the simplest, to Class 1, which are most complex. From this we infer that Class 1 fractures had polyphase opening histories.

Measurements of fracture shapes were derived from core fracture trace mapping. Figures 47 through 50 and tables 8 and 9 show examples of core fracture trace maps. These maps also document open fracture porosity. During mapping, the shape of each fracture was traced onto a transparent overlay, and fracture widths were documented with a binocular microscope with ocular micrometer. By examining fracture widths at a range of distances from the core margin, we could account for some of the most common artifacts that interfere with core fracture-width measurement (fig. 51). Fracture heights in table 9 are only for fractures that have both their upper and lower terminations within the core. Rock properties and fracture dimensions for the three classes are shown in figures 52 through 58. From this information, fracture length/width (or aspect) ratios, and fracture pore volumes were calculated.

If fractures in the Travis Peak Formation are natural hydraulic fractures whose shapes have been preserved from the time of their formation, current *fracture shapes* in these sandstones may reflect equilibrium with the pressure of fluid in the fracture at the depth of formation. Fracture shapes can therefore provide an estimate of the depth of fracture formation that is independent of petrologic indicators. Alternatively, if depth conditions of synkinematic quartz cementation were known, this approach could lead to estimates of

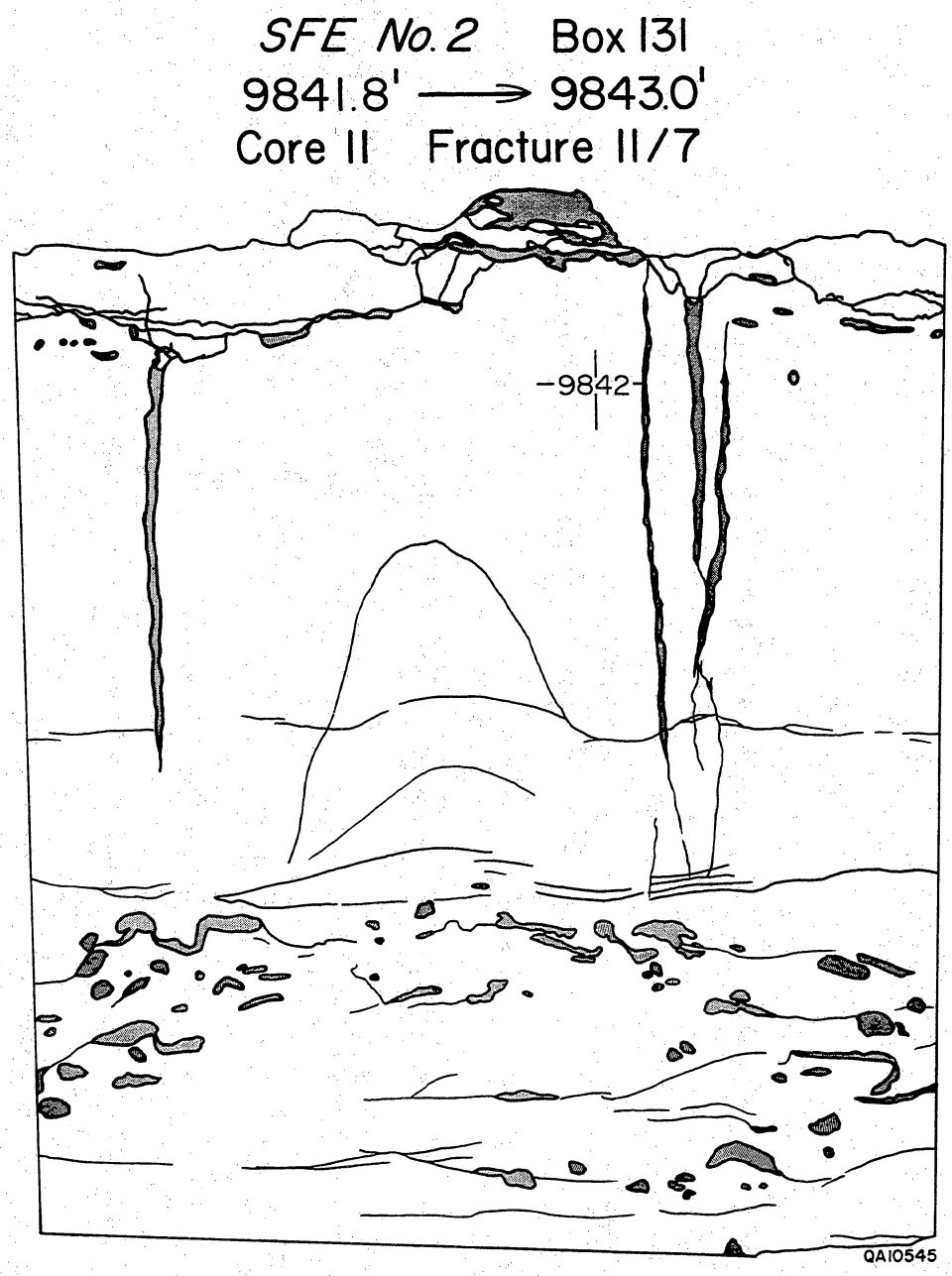

Figure 47. Fracture map, Travis Peak Formation, Holditch SFE No. 2 core, depth 9,842 ft. Map is a tracing of 4-inch-diameter core. These Class 1 fractures have blunt terminations at subhorizontal stylolites.

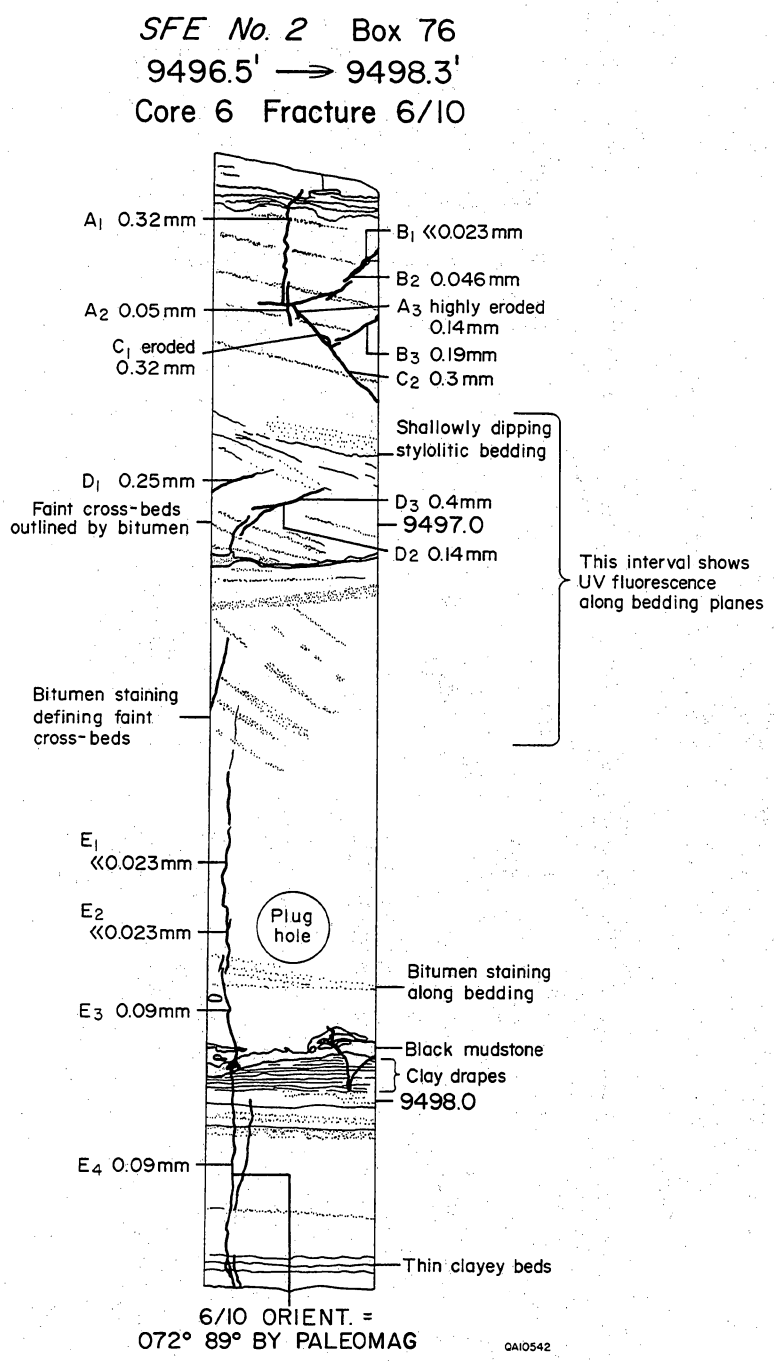

Figure 48. Fracture map, Travis Peak Formation, Holditch SFE No. 2 core, depth 9,496.5–9,498.3 ft. Map shows fracture traces on slabbed core. Numbers mark fracture widths at the points indicated. Core slab diameter is 3 inches.

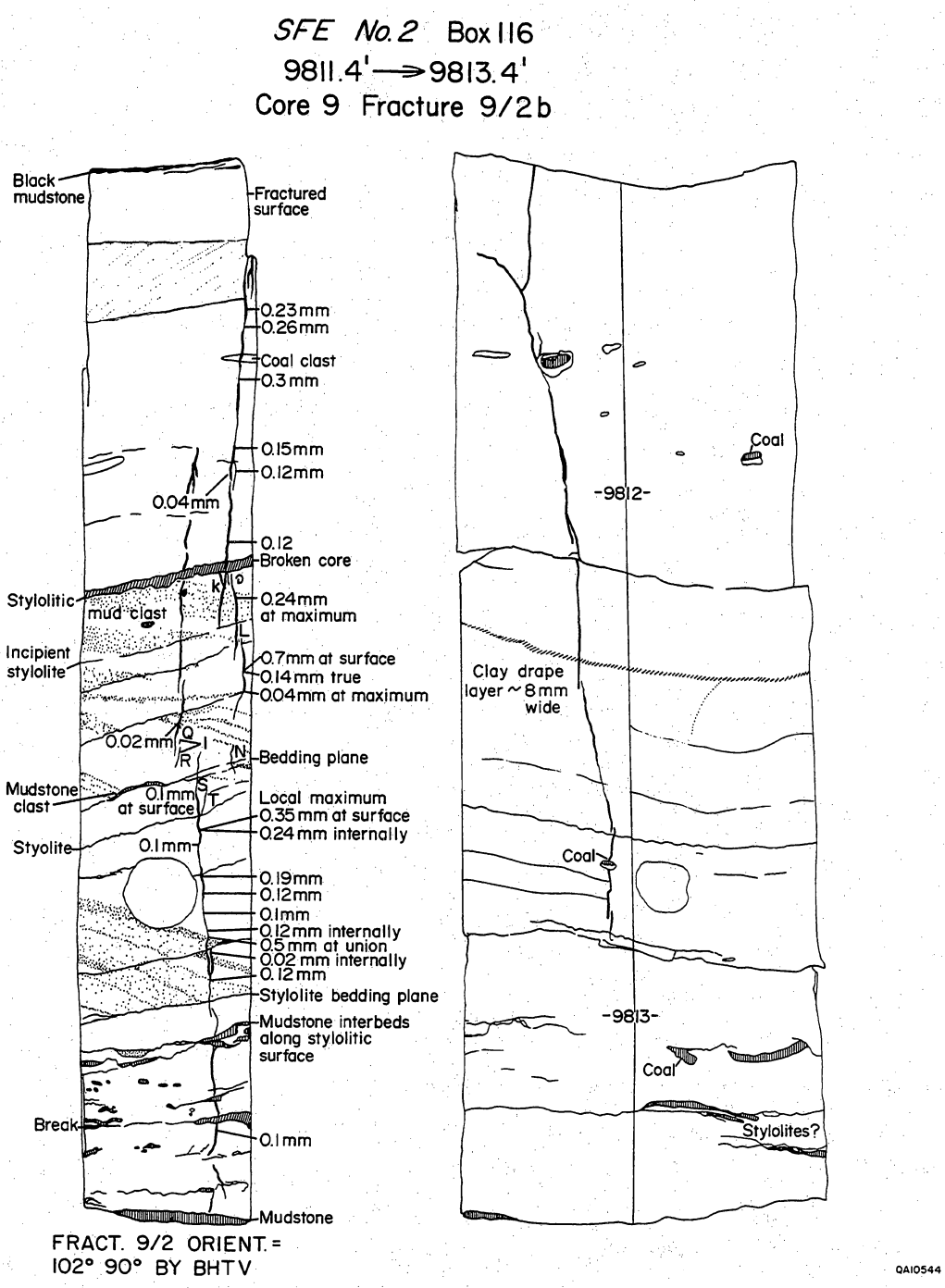

Figure 49. Fracture map, Travis Peak Formation, Holditch SFE No. 2 core, depth 9,811.4–9,813.4 ft. Fracture traces on slabbed core (left) and unwrapped, curved core surface (right). Note fracture widths, stylolites, and coal inclusions. Core slab diameter is 3 inches.

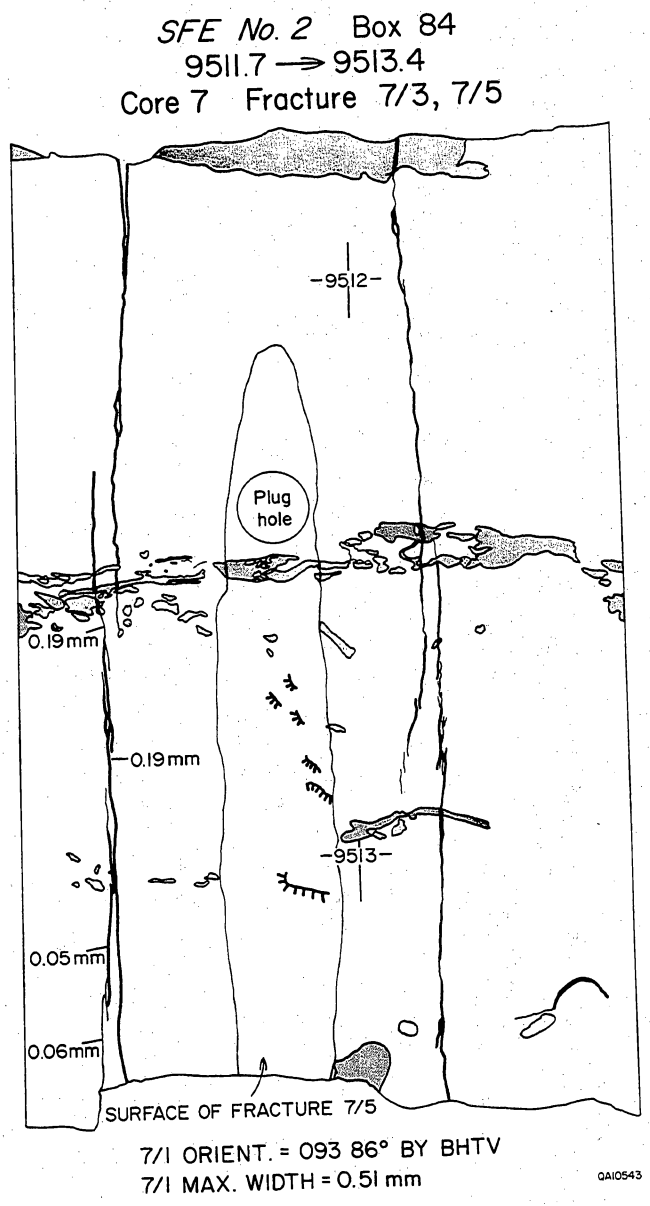

Figure 50. Fracture map, Travis Peak Formation, Holditch SFE No. 2 core, depth 9,511.7–9,513.4 ft. Unwrapped core map, showing Class 2 fractures.

Table 8. Characteristics of three fracture classes, Travis Peak Formation.

Parameter	Class 1	Class 2†	Class 3
Geometry	Wide, short fractures; triangular with blunt terminations, sometimes on only one end; often vuglike; simple geometry, no multiple strands; crack-seal features prevail	Long, thin fractures, longest visible in cored intervals; complex geometries often showing en echelon and relay patterns; usually composed of class 3 segments; crack-seal features locally present	Long, thin fractures shorter than those in class 2; are usually individual segments of class 2 and longer class 3 segments; en echelon and relay geometries
Fracture length (mm)			
maximum	446	3,139	2,440
minimum	150	186	16
mean	**234**	**787**	**149**
Fracture width (mm)			
maximum	5.0	1.1	0.8
minimum	0.7	0.05	0.02
mean	**2.5**	**0.5**	**0.2**
Length/width ratio			
maximum	89.2	2,853.6	3,012
minimum	217.4	3,720.0	800
mean	**94.9**	**1,668**	**764**
Young's modulus (dynamic, from fraclog)*			
maximum	10.1	10.2	10.1
minimum	7.9	8.0	7.1
mean	**9.7**	**8.9**	**8.6**
Poisson's ratio mean (dynamic, from fraclog)*			
maximum	0.21	0.25	0.26
minimum	0.17	0.16	0.16
mean	**0.18**	**0.19**	**0.2**
Calculated fluid pressure (psi)			
maximum	134,843	8,421	28,200
minimum	6,248	727	816
mean	**63,281**	**3,248** †	**9,790**

*fraclog = ResTech Prefracture Stress Evaluation Log

†Fracture class for which pressure calculation assumptions are most likely to be valid

Table 9. Results of fracture-trace mapping and fluid-pressure calculation.

Fracture no.	Depth (ft)	Length (mm)	Width (mm)	E* (Mpsi)	ν* (Fraclog)	Volume (mm^3)	Width/ length	Calculated fluid pressure†
7/1A	–9510	157	0.069	8000000	0.22	1,083.3	0.00043949	1,847.37
7/1B	–9510	99	0.299	8000000	0.22	2,960.1	0.0030202	12,695.26
7/1E	–9510	19	0.092	8000000	0.21	174.8	0.00484211	20,261.97
7/5C	–9510	124	0.391	8900000	0.21	4,848.4	0.00315323	14,679.21
7/5D	–9511.7	155	0.184	8900000	0.21	2,852	0.0011871	5,526.29
7/5F	–9511.7	125	0.046	8900000	0.21	575	0.000368	1,713.15
7/5H	–9511.7	92	0.276	8900000	0.21	2,539.2	0.003	13,965.90
7/5I	–9511.7	70	0.288	8900000	0.21	2,016	0.00411429	19,153.23
7/5J	–9511.7	154	1.38	8900000	0.21	21,252	0.00896104	41,716.31
8/7D	–9549	6	0.161	8300000	0.17	96.6	0.02683333	114,672.36
9/2B	–9809	33	0.046	7800000	0.23	151.8	0.00139394	5,740.01
9/2B	–9809	82	0.29	7800000	0.23	2,378	0.00353659	14,563.07
9/2B	–9809	245	0.46	7800000	0.23	11,270	0.00187755	7,731.44
9/2bB1	–9811.7	350	0.3	8000000	0.2	10,500	0.00085714	3,571.43
9/2bB1	–9811.7	32	0.12	8000000	0.2	384	0.00375	15,625.00
9/2bB1	–9811.7	90	0.24	8000000	0.2	2,160	0.00266667	11,111.11
9/2bB1	–9811.7	73	0.04	8000000	0.2	292	0.00054795	2,283.11
9/2bB1	–9811.7	185	0.12	8000000	0.2	2,220	0.00064865	2,702.70
9/2bB1	–9811.7	100	0.02	8000000	0.2	200	0.0002	833.33
9/2bB1	–9811.7	71	0.24	8000000	0.2	1,704	0.00338028	14,084.51
9/2bB1	–9811.7	30	0.12	8000000	0.2	360	0.004	16,666.67
9/2bB2	–9811.7	100	0.02	8000000	0.2	200	0.0002	833.33
9/2bC1	–9811.7	71	0.24	8000000	0.2	1,704	0.00338028	14,084.51
9/2bC2	–9811.7	30	0.12	8000000	0.2	360	0.004	16,666.67
9/3aA1	–9813.4	96	0.805	8600000	0.24	7,728	0.00838542	38,261.13
9/3aG1	–9813.4	22	0.29	8600000	0.24	638	0.01318182	60,146.24
9/3aG2	–9813.4	23	0.3	8600000	0.24	690	0.01304348	59,515.02
9/3aG4	–9813.4	17	0.115	8600000	0.24	195.5	0.00676471	30,866.12
9/3b1A	–9814.6	65	0.299	8600000	0.24	1,943.5	0.0046	20,988.96
9/3b1B	–9814.6	97	0.391	8600000	0.24	3,792.7	0.00403093	18,392.39
9/3b1C	–9814.6	65	0.414	8600000	0.24	2,691	0.00636923	29,061.64
9/3b1D	–9814.6	38.5	0.322	8600000	0.24	1,239.7	0.00836364	3,8161.75
9/3b3	–9814.6	30	0.368	8600000	0.24	1,104	0.01226667	55,970.57
9/5B	–9815.5	160	0.322	8100000	0.26	5,152	0.0020125	8,741.55
9/5C	–9815.5	62	0.345	8100000	0.26	2,139	0.00556452	24,170.20
9/5D	–9815.5	36	0.07	8100000	0.26	252	0.00194444	8,445.95
9/5F	–9815.5	55	0.184	8100000	0.26	1,012	0.00334545	14,531.41
9/5G	–9815.5	14	0.023	8100000	0.26	32.2	0.00164286	7,135.96
10/1;2D	–9822	61	0.15	8900000	0.25	915	0.00245902	11,672.13
10/1;2E	–9822	114	0.33	8900000	0.25	3,762	0.00289474	13,740.35
10/1;2F	–9822	76	0.07	8900000	0.25	532	0.00092105	4,371.93
10/1;2H	–9822	17	0.11	8900000	0.25	187	0.00647059	30,713.73
10/1;2I	–9822	53	0.07	8900000	0.25	371	0.00132075	6,269.18
10/1;2J	–9822	160	0.23	8900000	0.25	3,680	0.0014375	6,823.33
10/1;2K	–9822	80	0.45	8900000	0.25	3,600	0.005625	26,700.00
10/2B	–9824.5	40	0.45	9000000	0.21	1,800	0.01125	52,960.56

Table 9 (cont.)

Fracture no.	Depth (ft)	Length (mm)	Width (mm)	E* (Mpsi)	ν* (Fraclog)	Volume (mm^3)	Width/ length	Calculated fluid pressure†
10/2C	–9824.5	18	0.11	9000000	0.21	198	0.00611111	28,768.70
10/2D	–9824.5	35.5	0.11	9000000	0.21	390.5	0.00309859	14,586.95
10/2I	–9824.5	87	0.13	9000000	0.21	1,131	0.00149425	7,034.35
10/2K	–9824.5	90	0.2	9000000	0.21	1,800	0.00222222	10,461.35
10/2L	–9824.5	50	0.2	9000000	0.21	1,000	0.004	18,830.42
10/3bE	–9826	50	0.3	9000000	0.21	1,500	0.006	28,245.63
10/3cA	–9826.5	20	0.2	9000000	0.21	400	0.01	47,076.05
10/3cB	–9826.5	40	0.5	9000000	0.21	2,000	0.0125	58,845.07
10/3dC	–9827	40	0.7	9000000	0.21	2,800	0.0175	82,383.09
10/7A	–9832.9	39	0.069	10000000	0.18	269.1	0.00176923	9,142.37
10/7C	–9832.9	18	0.032	10000000	0.18	57.6	0.00177778	9,186.53
11/2A	–9836.3	235	0.2	10100000	0.17	4,700	0.00085106	4,425.78
11/7A	–9841.8	190	5	10100000	0.17	95,000	0.02631579	136,849.69
11/7B	–9841.8	170	0.7	10100000	0.17	11,900	0.00411765	21,412.95
11/7C	–9841.8	150	1	10100000	0.17	15,000	0.00666667	34,668.59
13/4B	–9661.5	43	0.5	8700000	0.2	2,150	0.01162791	52,688.95
13/5A	–9861.5	390	0.11	8700000	0.2	4,290	0.00028205	1,278.04
13/5B	–9861.5	560	0.23	8700000	0.2	12,880	0.00041071	1,861.05
13/8aA	–9869.9	670	0.161	7100000	0.2	10,787	0.0002403	888.60
13/8aC	–9869.9	350	0.069	7100000	0.2	2,415	0.00019714	729.02
13/8aD	–9869.9	400	0.161	7100000	0.2	6,440	0.0004025	1,488.41
13/8aE	–9869.9	200	0.426	7100000	0.2	8,520	0.00213	7,876.56
13/8aF	–9869.9	625	0.092	7100000	0.2	5,750	0.0001472	544.33
13/8aG1	–9869.9	320	0.069	7100000	0.2	2,208	0.00021563	797.36
13/8aG2	–9869.9	185	0.078	7100000	0.2	1,443	0.00042162	1,559.12
13/8aG3	–9869.9	171	0.138	7100000	0.2	2,359.8	0.00080702	2,984.28
13/8aG4	–9869.9	210	0.026	7100000	0.2	546	0.00012381	457.84
13/8aH2	–9869.9	490	0.253	7100000	0.2	12,397	0.00051633	1,909.33
13/8aI	–9869.9	56	0.276	7100000	0.2	1,545.6	0.00492857	18,225.45
13/8aJ	–9869.9	155	0.23	7100000	0.2	3,565	0.00148387	5,487.23
13/8bA	–9871	510	0.038	8900000	0.24	1,938	7.451E–05	351.83
13/8bB	–9871	535	0.024	8900000	0.24	1,284	4.486E–05	211.83
13/8bC	–9871	630	0.024	8900000	0.24	1,512	3.8095E–05	179.89
13/8bE	–9871	870	0.021	8900000	0.24	1,827	2.4138E–05	113.98
13/8bF	–9871	2200	0.014	8900000	0.24	3,080	6.3636E–06	30.05
13/8dC	–9873.5	2100	0.529	8800000	0.23	111,090	0.0002519	1,170.29
13/8dH	–9873.5	1100	0.046	8800000	0.23	5,060	4.1818E–05	194.28
13/8eB	–9876.3	145	0.368	8900000	0.23	5,336	0.00253793	11,924.60
13/8fA	–9877.9	780	0.09	8900000	0.24	7,020	0.00011538	544.84
13/8fB	–9877.9	1740	0.23	8900000	0.24	40,020	0.00013218	624.17
13/8fC	–9877.9	570	0.04	8900000	0.24	2,280	7.0175E–05	331.37
13/8fD	–9877.9	1220	0.32	8900000	0.24	39,040	0.0002623	1,238.55
13/8fE	–9877.9	500	0.02	8900000	0.24	1,000	0.00004	188.88
13/8gB3	–9879.9	75	0.04	8700000	0.25	300	0.00053333	2,474.67
13/8gC1	–9879.9	10	1.25	8700000	0.25	1,250	0.125	580,000.00
13/8gC2	–9879.9	14	2.5	8700000	0.25	3,500	0.17857143	82,8571.43

Table 9 (cont.)

Fracture no.	Depth (ft)	Length (mm)	Width (mm)	E* (Mpsi)	ν* (Fraclog)	Volume (mm^3)	Width/ length	Calculated fluid pressure†
14/19A2	–9911.9	170	0.069	8700000	0.17	1,173	0.00040588	1818.13
14/19D	–9911.9	660	0.092	8700000	0.17	6,072	0.00013939	624.41
14/19F	–9911.9	620	0.069	8700000	0.17	4,278	0.00011129	498.52
14/19;20A	–9913.8	110	1.38	9100000	0.17	15,180	0.01254545	58,780.58
14/19;20B	–9913.8	320	0.092	9100000	0.17	2,944	0.0002875	1,347.05
14/19;20C1	–9913.8	510	0.23	9100000	0.17	11,730	0.00045098	2,113.03
14/19;20C2	–9913.8	1100	0.299	9100000	0.17	32,890	0.00027182	1,273.58
14/19;20D	–9913.8	700	0.138	9100000	0.17	9,660	0.00019714	923.69
14/19;20E	–9913.8	480	0.161	9100000	0.17	7,728	0.00033542	1,571.56
14/19;20F1	–9913.8	1210	0.069	9100000	0.17	8,349	5.7025E–05	267.18
14/19;20F2	–9913.8	350	0.138	9100000	0.17	4,830	0.00039429	1,847.39
14/19;20G1	–9913.8	620	0.069	9100000	0.17	4,278	0.00011129	521.44
14/19;20G2	–9913.8	210	0.069	9100000	0.17	1,449	0.00032857	1,539.49
14/19;20H	–9913.8	460	0.368	9100000	0.17	16,928	0.0008	3,748.33
15/2G	–9918	160	0.046	9200000	0.16	736	0.0002875	1,357.25
15/2Z	–9918	260	0.069	9200000	0.16	1,794	0.00026538	1,252.84
15/2A4	–9918	260	0.414	9200000	0.16	10,764	0.00159231	7,517.05
15/12bD	–9936.9	1600	0.115	8900000	0.22	18,400	7.1875E–05	336.11
15/12bE	–9936.9	1340	0.092	8900000	0.22	12,328	6.8657E–05	321.06
15/12bF	–9936.9	370	0.046	8900000	0.22	1,702	0.00012432	581.38

*Dynamic measurements of E and ν derived from ResTech, Inc.'s Prefracture Stress Evaluation Log (ResTech, Houston, written communication, 1991).

†See table 8; only Class 2 fractures meet the assumption of the pressure calculation: a single episode of fracture opening/filling.

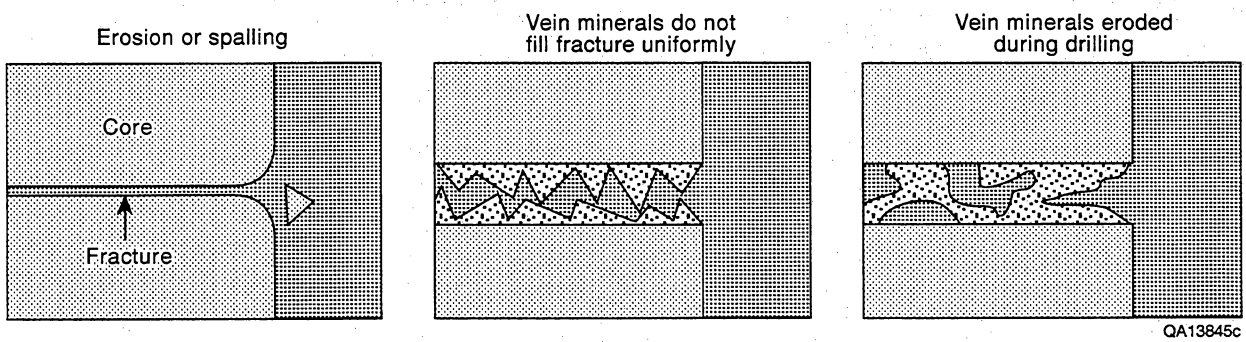

Figure 51. Diagram illustrating potential sources of fracture width measurement error on core samples.

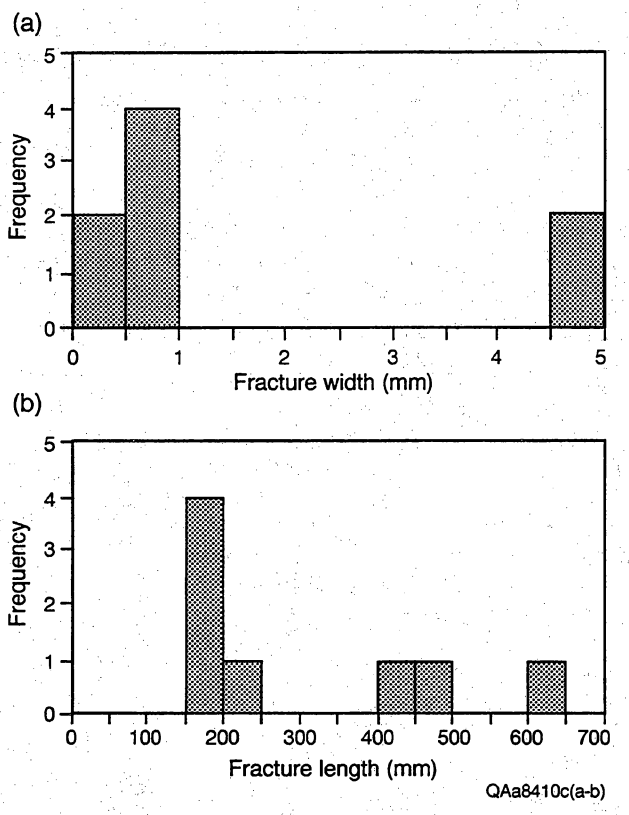

Figure 52. Graph showing fracture Class 1 length and width frequency, Travis Peak Formation. Information only shown for fracture-trace maps where both upper and lower ends of fracture were visible in core.

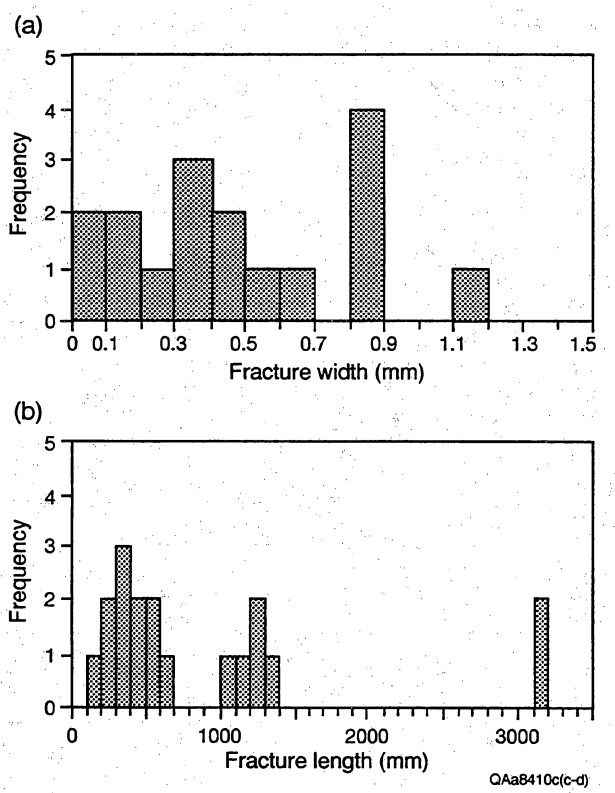

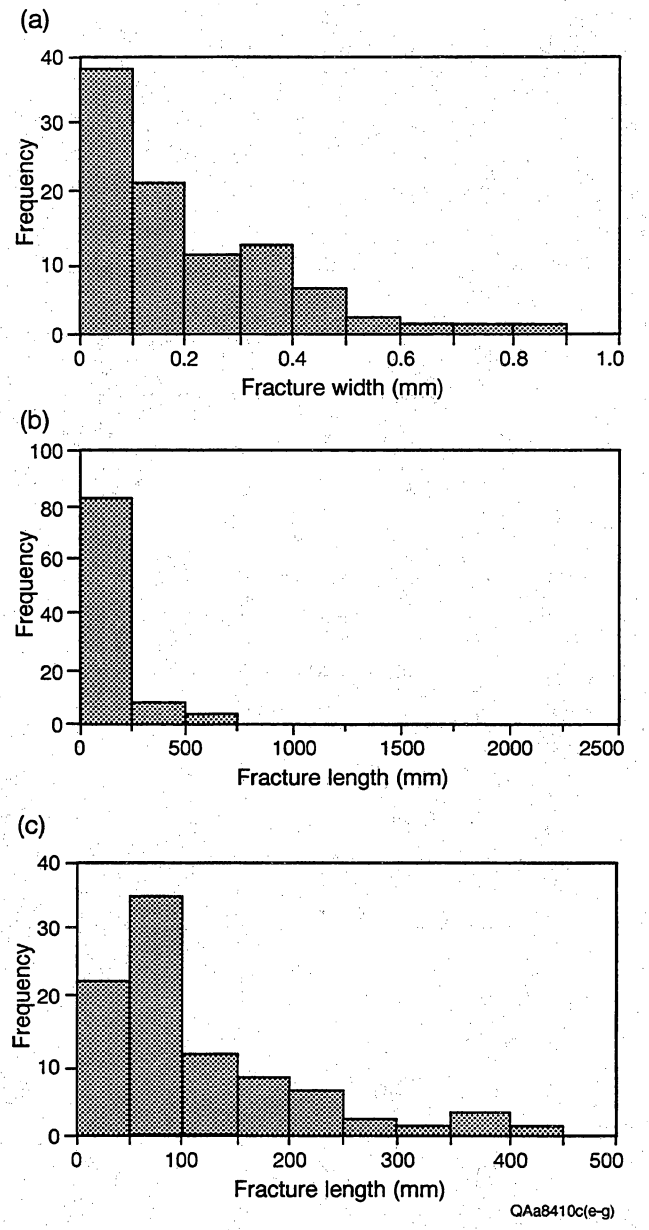

Figure 54. Graph showing Class 3 width and length information, Travis Peak Formation. Information only shown for fracture-trace maps where both upper and lower ends of fracture were visible in core.

◀ Figure 53. Graph showing fracture Class 2 length and width frequency, Travis Peak Formation. Information only shown for fracture-trace maps where both upper and lower ends of fracture were visible in core.

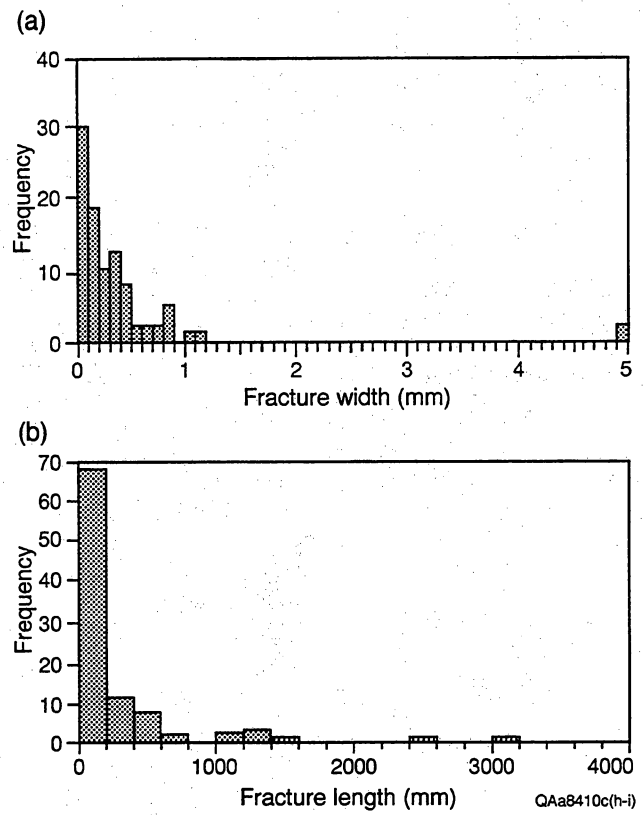

Figure 55. Graph showing combined fracture length and width frequency for all classes, Travis Peak Formation.

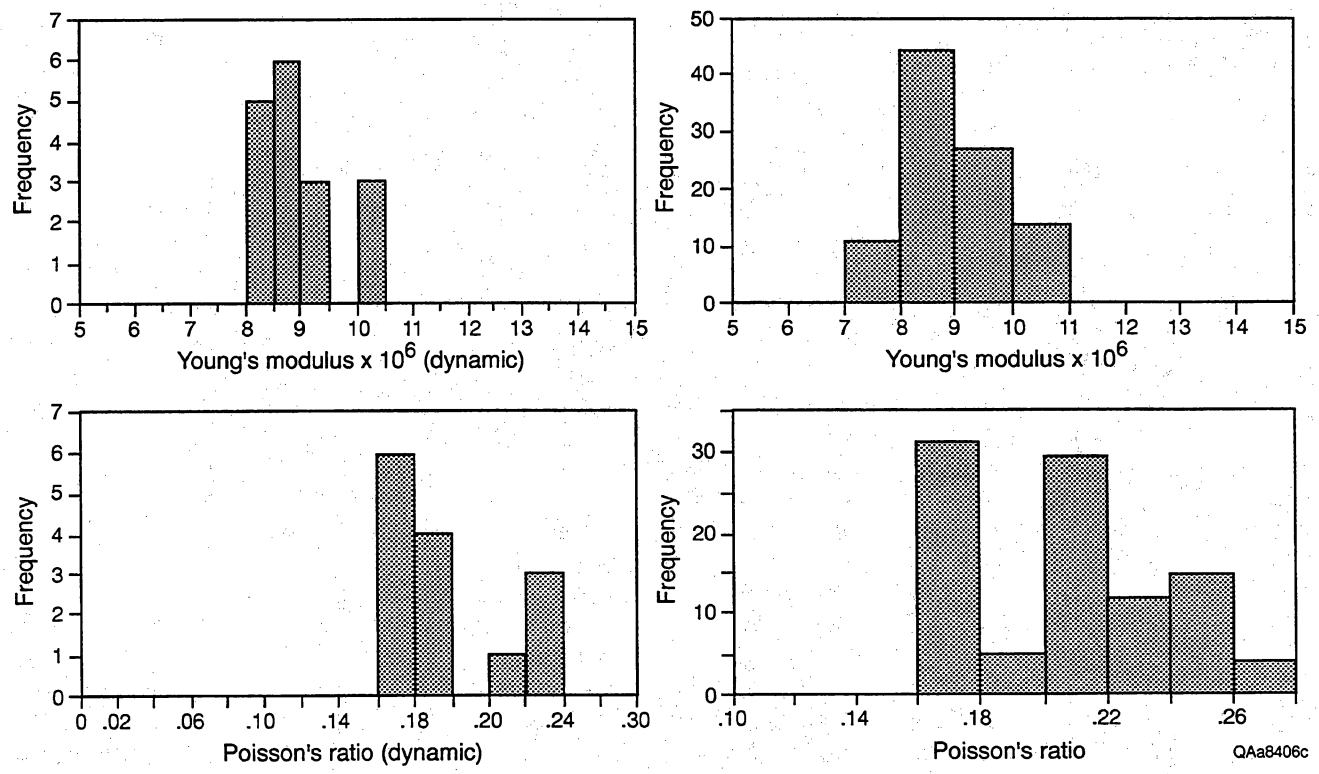

Figure 56. Graph showing mechanical properties for intervals of core having natural fractures, Travis Peak Formation. Dynamic values are derived from ResTech Prefracture Evaluation Log. Other values are static laboratory test results.

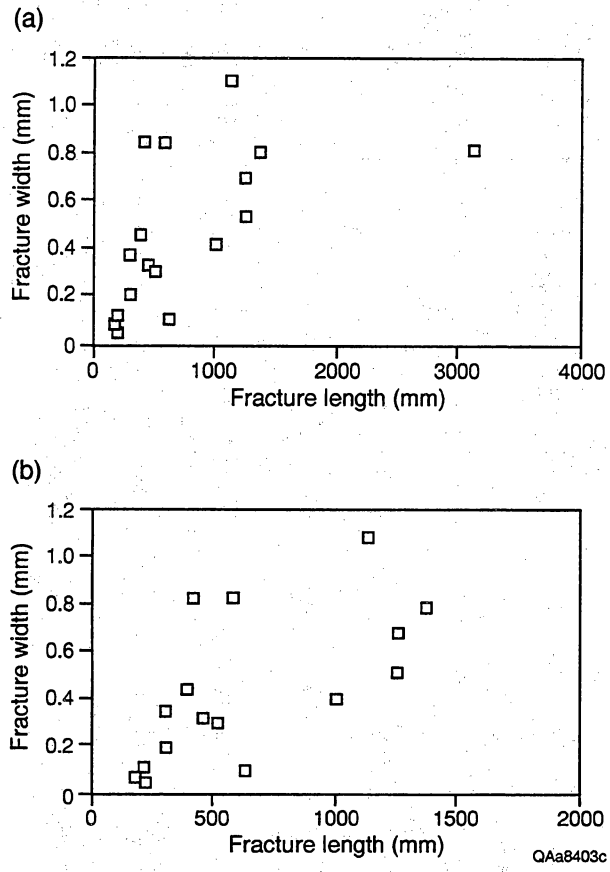

Figure 57. Fracture length-width cross plot, Class 2 fractures, Travis Peak Formation. (a) All complete Class 2 fractures. (b) Detail showing short Class 2 fractures.

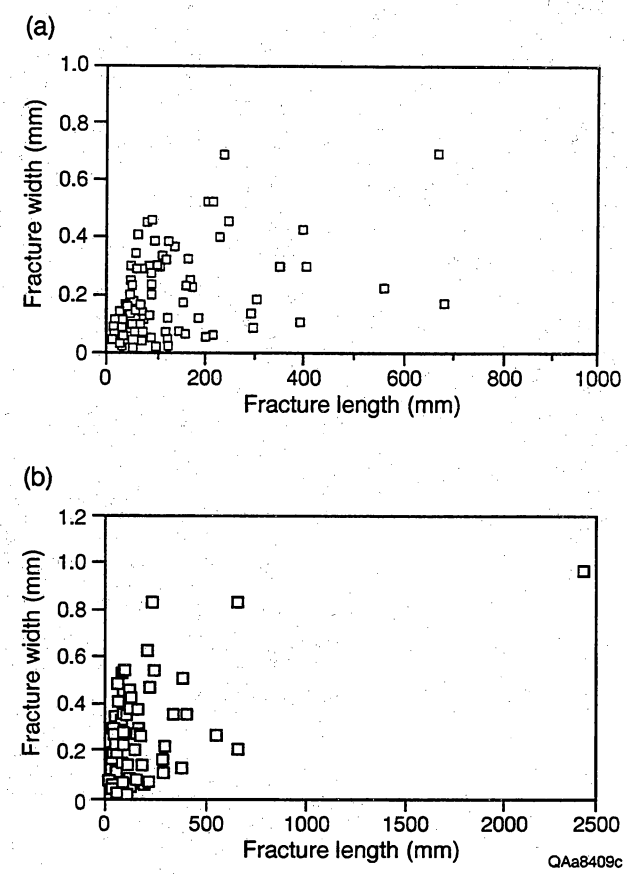

Figure 58. Fracture length-width cross plot, Class 3 fractures, Travis Peak Formation.

typical fracture shapes in a given horizon. A calculation was carried out to test this idea, but the results are ambiguous. Fluid pressure (P_f) was calculated from

$$P_{fluid}\ (P_f) = E/(1-\upsilon^2)(L/W)$$

(Modified from Gudmundsson, 1983), (1)

where E is dynamic Young's modulus derived from sonic logs, L/W is measured length (height)/width ratio, and υ is dynamic Poisson's ratio derived from sonic logs. We assume that current rock properties are substantially similar to those at the time of fracture formation. Because quartz cement is the dominant control on these rock properties, uncertainties resulting from shifts in values due to depth (pressure) variations are probably much smaller than other uncertainties in this approach. Log-derived E and υ values were used in order to match rock-property data from the depth interval where each fracture L/W had been measured.

Table 8 and figure 59 show results of this analysis. Class 1 fractures show unrealistically high calculated pressure values, reflecting the effect of wide, short shapes of these fractures on aspect ratios and calculated pressure. Microstructural observations of these fractures show that their lengths and widths result from a protracted history of opening (and closure), as well as truncation by (or other interaction with) stylolites. Thus they do not meet the criteria of the analysis in that their shape does not reflect pressure at the time of initial formation. This is probably true of many of the Class 2 and 3 fractures as well. Many of these clearly have had multiple opening events, as shown by crack-seal structures and associated crosscutting microfracture sets.

Using Class 2 fractures gives a spread of calculated pressure values that correspond to reasonable fluid pressures for sedimentary basins (fig. 60). Class 2 fractures are the most likely of large fractures to represent single fracture opening events. For samples from SFE No. 2, most of these values fall below hydrostatic at the depths where these fractures are found now (fig. 59). The pressure range and mean are not significantly different for upper end lower parts of the formation. Sealed microfracture shapes give similar results. If the fluid pressure required to promote

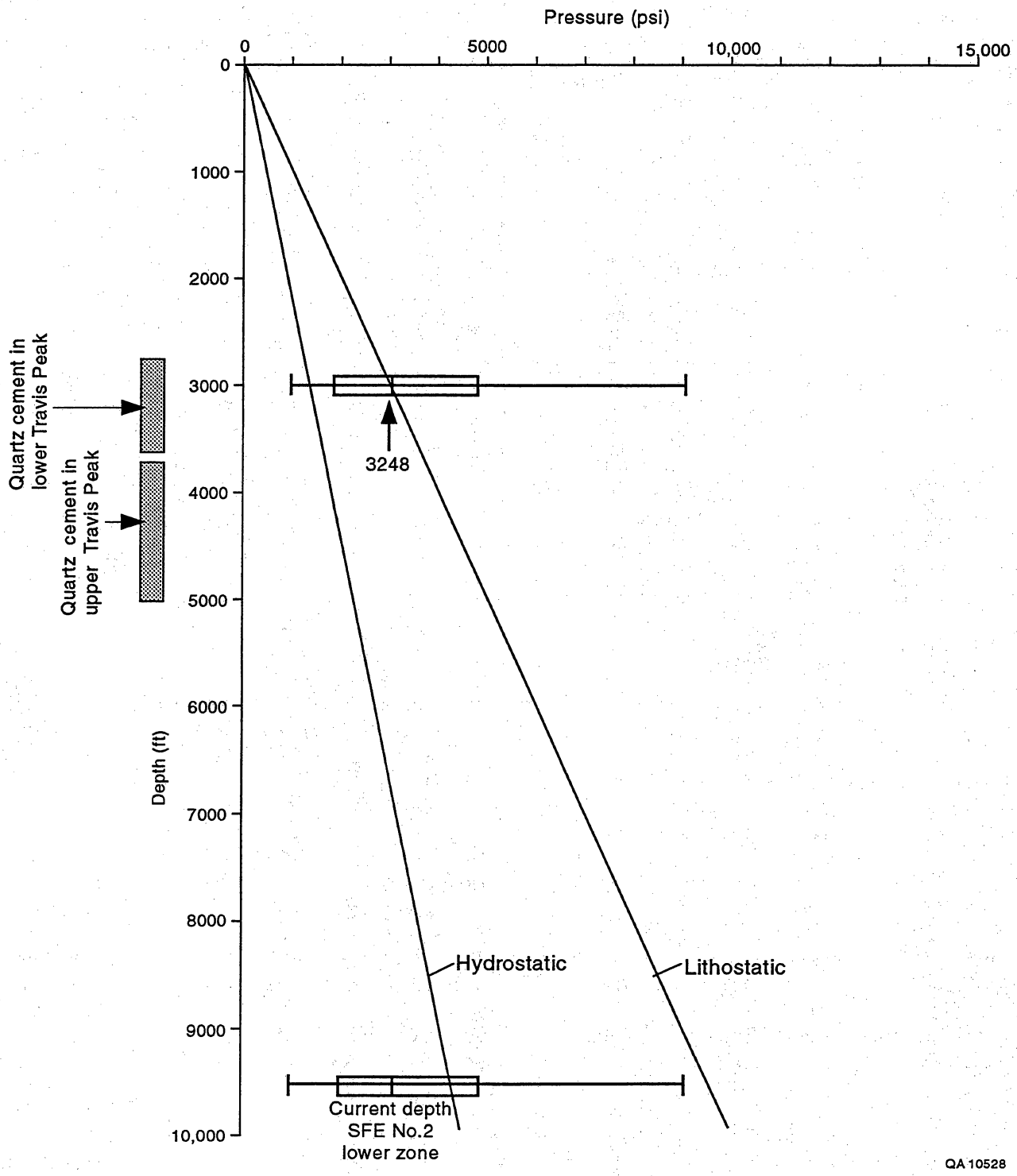

Figure 59. Calculated depth of fracture formation based on natural hydraulic fracture hypothesis. Quartz cement depths are based on one scenario for timing of cementation. See text for explanation.

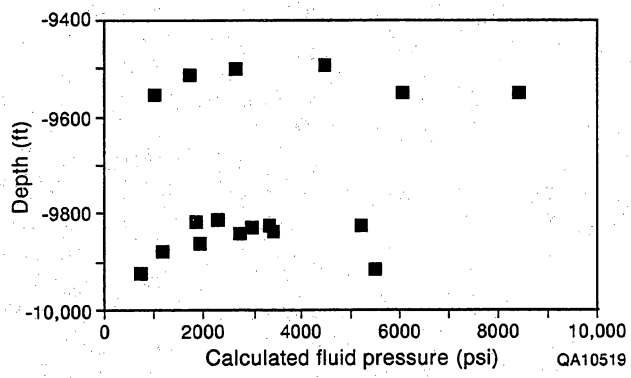

Figure 60. Range of calculated pressures for two depth intervals, Class 2 fractures. See text for discussion.

fractures in the Gulf Coast tectonic setting is some value slightly to moderately above hydrostatic, then these results point to fracture formation at depths between 3,000 and 6,000 ft. This is in the range of current geopressure depths in the Gulf Basin.

Petrology of Fracture-Filling Minerals

Most extension fractures in Travis Peak sandstone are lined by quartz crystals that are in crystallographic continuity with quartz grains in fracture walls. This pattern is identical to that of quartz cement in the sandstone framework. Fracture-filling and fracture-lining quartz occurs as faceted crystals and thin (50 to 100 μm) overgrowths in optical continuity with adjacent quartz grains. Many fractures also contain ankerite/dolomite, calcite, clay minerals, and hydrocarbon residue. Minor amounts of anhydrite are locally present in a few fractures in SFE No. 2 core. The fine-grained clay minerals locally filling fractures are morphologically similar to diagenetic illite elsewhere in the Travis Peak.

Quartz filling or lining fractures is typically manifested as a thin (less than 0.5 mm) veneer of faceted or subhedral growth on broken or intact (more common) grains on fracture walls. Intact quartz bridging and occluding fracture porosity can be present at any point along fractures, but in our samples is most common near fracture ends and in fractures thinner than 0.5 mm. Locally, fracture-filling quartz displays parallel planes of minute fluid-filled cavities that are traces of sealed fractures ("crack-seal" microstructure).

Fracture-filling quartz in the upper Travis Peak contains planes of fluid inclusions that parallel fracture walls and commonly are symmetric about the centerline of the fracture (fig. 61). Scanned CL observations show that the alternation of inclusion planes and clear quartz represents an increment of quartz growth into a partly open fracture with subsequent reopening of the fracture preferentially along the fracture centerline. Locally, wall-rock inclusions are incorporated in these crack-seal zones. Quartz with such banded fluid-inclusion structure is developed discontinuously in fractures. Faceted crystals in fracture pore spaces indicate that fracture sealing was not complete. Euhedral crystals and, locally, fluid-inclusion-rich fracture-filling quartz have rims of fluid-inclusion-poor quartz. The boundary between these two types of quartz is planar to irregular.

In contrast to quartz, ankerite shows no organized fluid-inclusion microstructure. Ankerite typically occurs as single crystals with euhedral to subhedral crystal faces. Internally, ankerite has sparse, thin twin lamellae and rare, narrow, intragranular fractures striking across, rather than parallel to, the main fractures. Ankerite occurs as yellowish-white to yellowish-brown, blocky, rhombohedral crystals having diameters of between 100 μm and 1 mm. Ankerite and, locally, calcite crystals are widely spaced (1 to 5 mm) on some fracture surfaces. Less commonly, ankerite occurs as coalescent masses or completely fills fractures, but generally it is sparse. Matrix porosity is also locally occluded by ankerite. In fact, the style of mineralization and the degree of ankerite development in fractures and in matrix are similar.

The sequence in which fracture-filling minerals precipitated (fig. 62) was established using crosscutting relations, in which a younger phase grows across and covers a crystal face of an older mineral. Quartz precipitated first; it shows euhedral growth faces against both carbonate and clay minerals (fig. 63). Fracture surfaces overgrown by vein-filling quartz are not lined by any other phases, so fractures postdated minor chlorite cements that locally rim quartz grains. Ankerite precipitated after quartz, and is entirely postkinematic. Indeed, there is no microstructural evidence that fractures were ever reactivated after the time of quartz cementation. Locally there is evidence for a second, volumetrically minor episode of quartz precipitation following ankerite crystallization. An episode of clay mineral precipitation postdates the ankerite and late quartz precipitation. Feldspar exposed on fracture surfaces has a pitted or skeletal appearance that indicates partial dissolution, possibly following fracture opening and quartz precipitation.

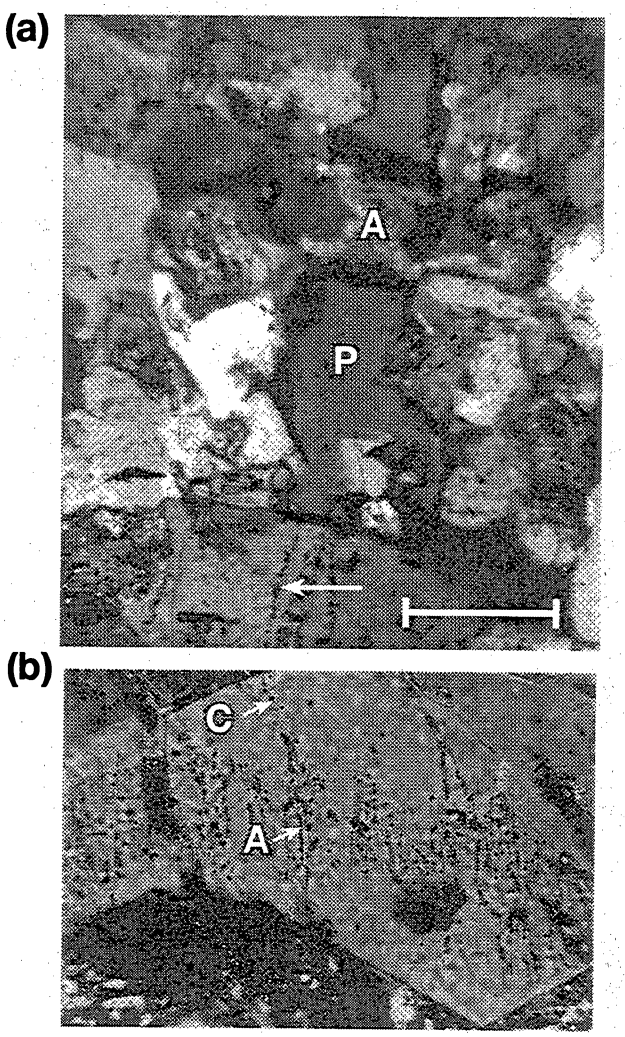

Figure 61. Photomicrographs of fluid inclusions in Travis Peak quartz-filled fractures (vein). (a) Fluid-inclusion planes (arrow), fracture porosity (P), and postkinematic ankerite (A), Holditch Howell No. 5 well. Scale bar = 0.5 mm. (b) Fluid inclusions in fracture-filling quartz, Holditch SFE No. 2. *Type a* and *c* inclusions are indicated. Scale bar = 0.25 mm.

Fluid-Inclusion Microthermometry

Measurements of phase transitions in fluid inclusions as a function of temperature were carried out with a Fluid, Inc., heating/freezing stage. Fluid-inclusion plates consisted of doubly polished, mounted, approximately 250-μm-thick sections. Inclusions were observed through a long-focus objective (Leitz L32), and the maximum magnification used was 512× (16× ocular and 32× objective). Temperatures of homogenization (T_h) and of final melting (T_{fm}) were measured and recorded. Because of the small size of the inclusions and their vapor bubbles and because it is difficult to tell when a bubble has definitely disappeared and the inclusion has homogenized, temperatures were determined by cycling the temperature up a fixed temperature increment from the last temperature at which the bubble was still distinct, and then dropping the temperature. If the bubble returned, the bubble was still present, but it may have been too small to recognize or it may have been hidden within the inclusion walls. If the bubble did not return, it is interpreted to have homogenized. Salinity, expressed in weight percent NaCl equivalent and NaCl molality, was calculated using equations in Potter (1977) and Potter and others (1978).

There are three types of inclusions within the fracture-filling quartz, all of which are either one phase liquid inclusions, or two-phase liquid and vapor phase (L+V) inclusions (table 10). Type A inclusions are small (<5 μm) and closely spaced and give quartz a murky appearance. Type B are small to medium inclusions (3 to 10 μm). They tend to be aligned in planes and to be elongate parallel to those planes. Type C inclusions are isolated primary inclusions that are randomly distributed and of variable but generally large size, ranging from 7 to 26 μm. They are less common than Type A and B inclusions. Type A and Type B inclusions each constituted 30 percent of the data, being the balance Type C inclusions. All of the inclusions in quartz occur in texturally and structurally distinct sets that have contrasting salinity and temperature (figs. 64 and 65 and appendix 3).

Crosscutting relations were used to separate these sets into older and younger generations of inclusions. The first generation, which are Type A inclusions, constitutes planes of inclusions in banded to tabular arrays. Scanning electron microscope observations show that these planes are composed of layers of closely spaced, small (<0.25 μm), equant primary (or "pseudo-secondary") inclusions interspersed with massive quartz layers containing planes of large (0.5 to 10 μm) inclusions with spherical or negative crystal shape (figs. 66 through 70). Homogenization-temperature (T_h) data from these early inclusions suggest that fracture fills formed in the presence of warm (~255° to 285°F) brine of moderate salinity (10 to 15 weight percent NaCl equivalent). These inclusions are interpreted to be synkinematic primary inclusions trapped during opening of fractures. These early-generation inclusions are locally surrounded by rims of relatively fluid-inclusion-free quartz ("clear quartz rims") (figs. 68, 71, and 72), which in turn is locally overlain by postkinematic ankerite or calcite.

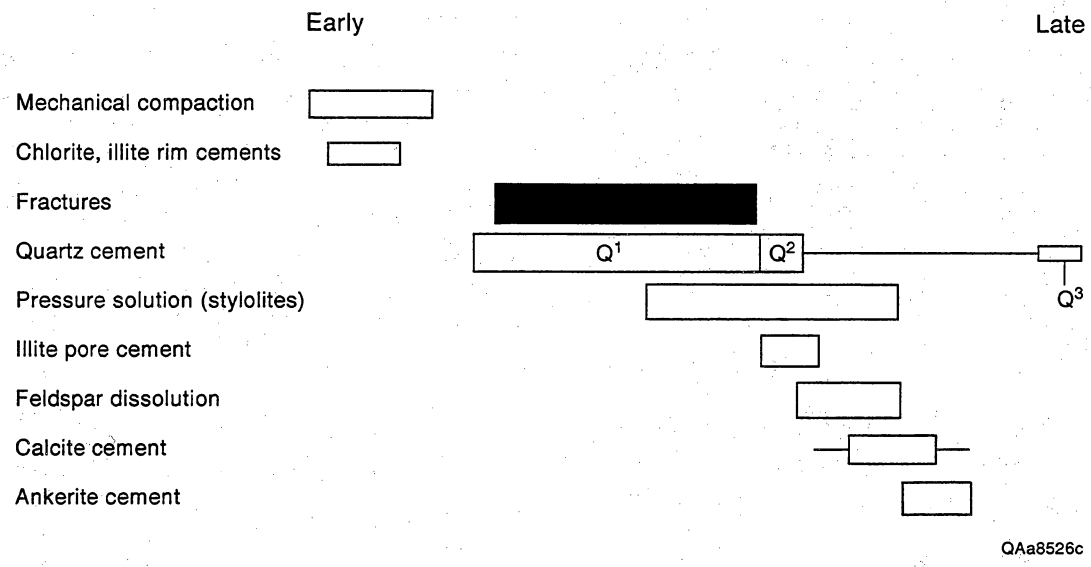

Figure 62. Diagram of composite diagenetic sequence and relative temporal relations of component diagenetic stages of sandstone framework and fracture fill of Travis Peak Formation. Fracture stage highlighted in black.

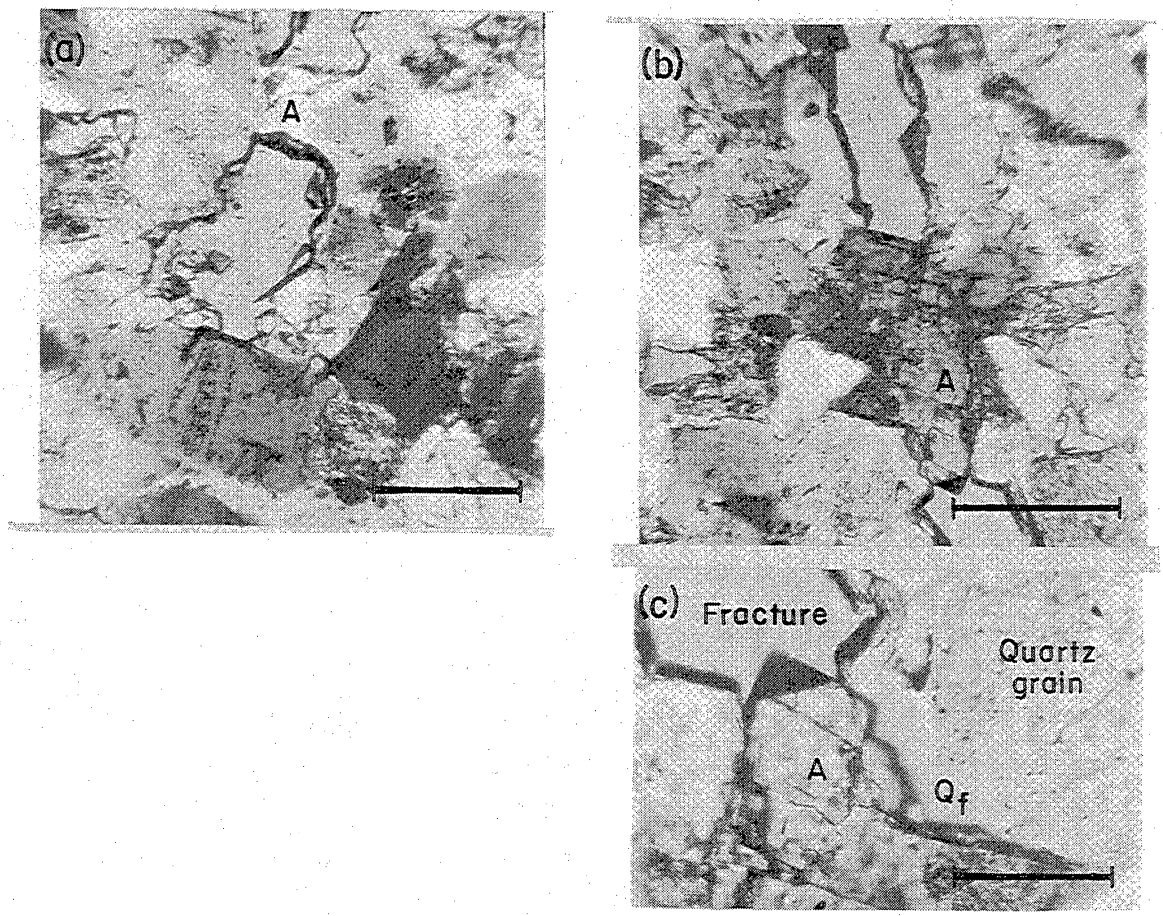

Figure 63. Photomicrograph showing superposition of infilling mineral phases in Travis Peak fracture. Sample is from Holditch Howell No. 5 well. Ankerite (A) postdates quartz (Q). Arrow shows fluid-inclusion-rich quartz. Bar is 0.5 mm.

Table 10. Types of inclusions within fracture-filling quartz.

Characteristic	Type A (Vf_1) Primary	Type B (Vf_2) Primary	Type C (Vf_2?) Primary
Appearance	Closely spaced, small inclusions in dense planar distribution.	More widely spaced distribution of inclusions in planes in otherwise clear quartz.	Randomly scattered inclusions in clear quartz.
	Types A & B crosscut one another. Type C occur within the planes of A & B, as well as in clear quartz.		
Size	Inclusions are small and relatively uniform in size.	Small to medium, with larger inclusions in the same planes.	Small to large inclusions.
Shape	Inclusions of Type B tend to be more elongate (parallel to the plane) and form strings of necked off inclusions. Also, Types B & C may have more angular shapes (but not negative crystal shape), whereas Type A are rounded and locally have negative crystal shape.		
Frequency	High frequency of small inclusions along plane. Spacing of planes is closer than Type B.	Less frequent, more widely spaced along and within the planes than Type A.	Less common, low frequency.
Distribution within crystal	Cross crystal boundaries when in filled veins. Rimmed by clear quartz in isolated patches and crystals of vein quartz.	Planes go beyond the outlines formed by Type A inclusions, and some cross crystal boundaries. Not found in clear quartz that rims isolated, nonbridging quartz crystals.	Random distribution.

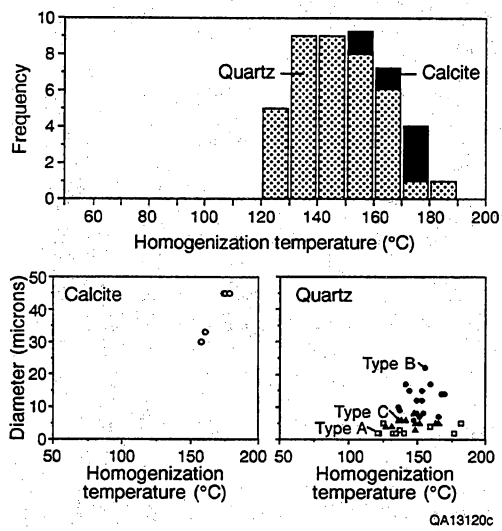

Figure 64. Homogenization temperatures from primary inclusions, synkinematic quartz, and postkinematic calcite. Samples are from Travis Peak fractures, Holditch SFE No. 2 and Prairie Mast No. 1-A wells.

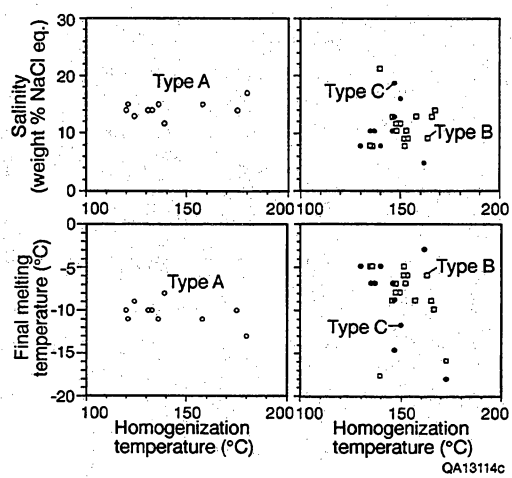

Figure 65. Homogenization temperature versus salinity and final melting temperature. Samples are from Travis Peak quartz veins, Holditch SFE No. 2 and Prairie Mast No. 1-A wells.

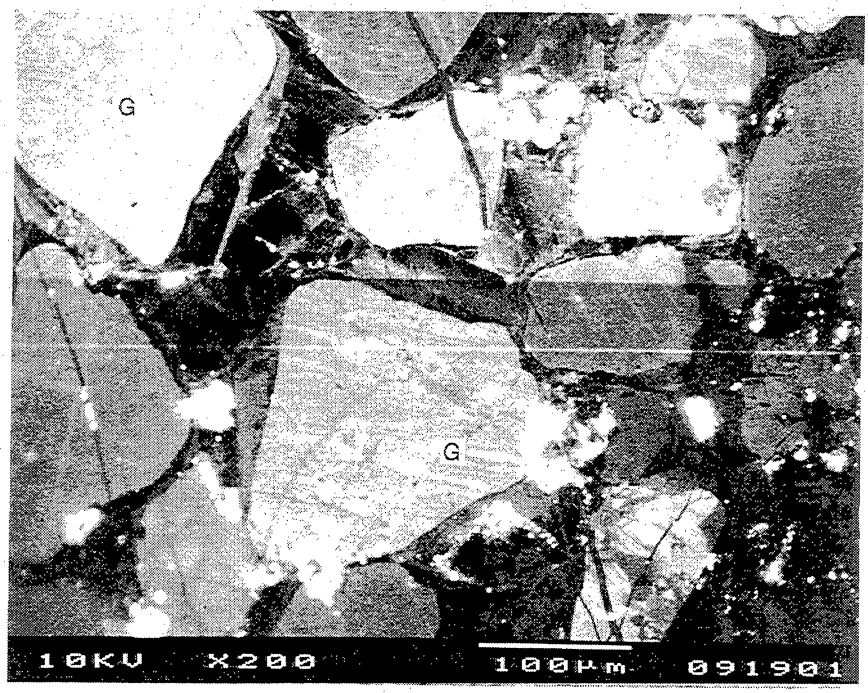

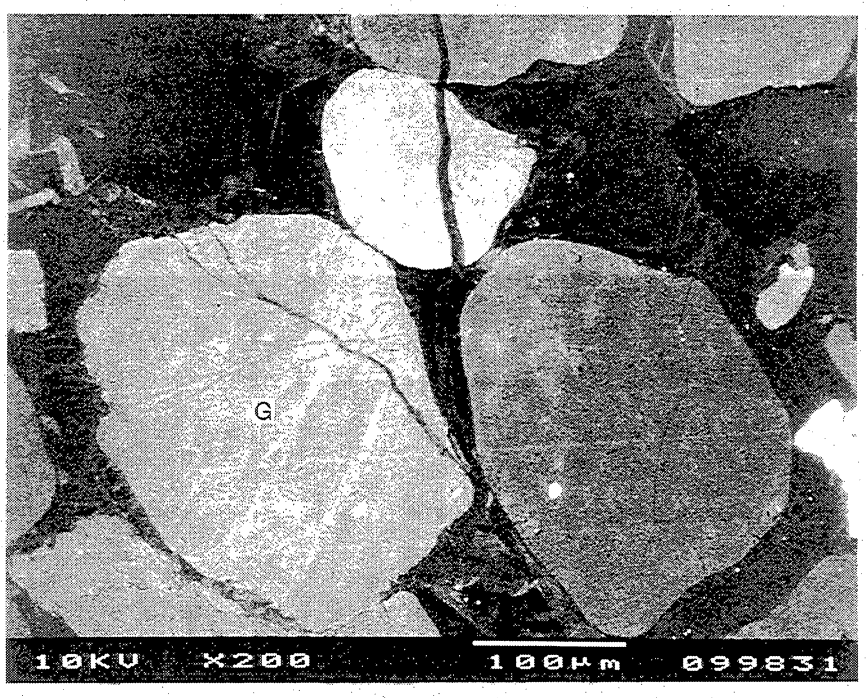

Figure 66. Travis Peak fracture microstructures, Holditch SFE No. 2. Transgranular sealed microfractures. Scanned CL images. Quartz grains (G) have light CL tone, and quartz in cement and filled microfractures has dark CL tone.

(a)

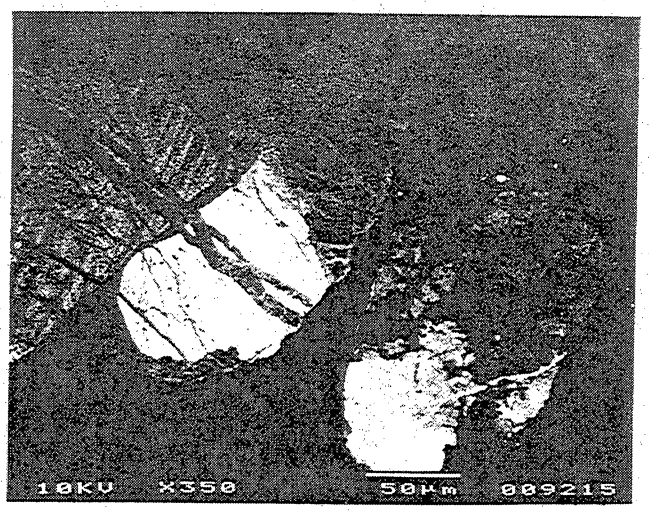

(b)

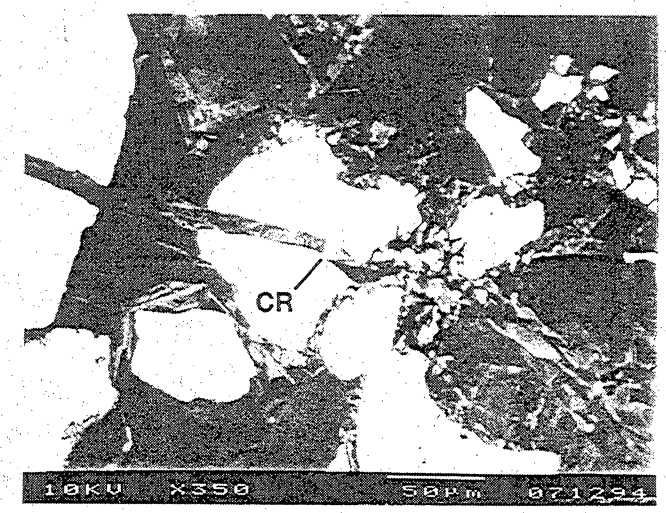

(c)

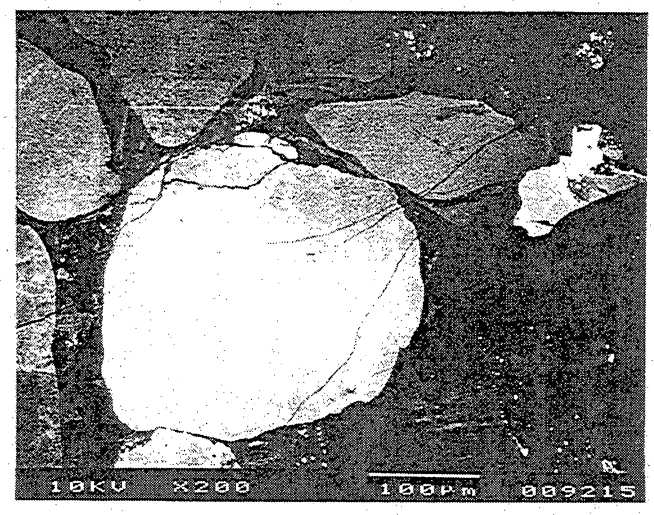

Figure 67. Travis Peak fracture microstructures, Holditch SFE No. 2. Three examples of transgranular microfracture. (a) Note segmented aspect of microvein. (b) Note sharp fracture walls and faceted quartz crystals in microvein (CR). (c) Thin transgranular microfracture. All images show fracture traces in plan view.

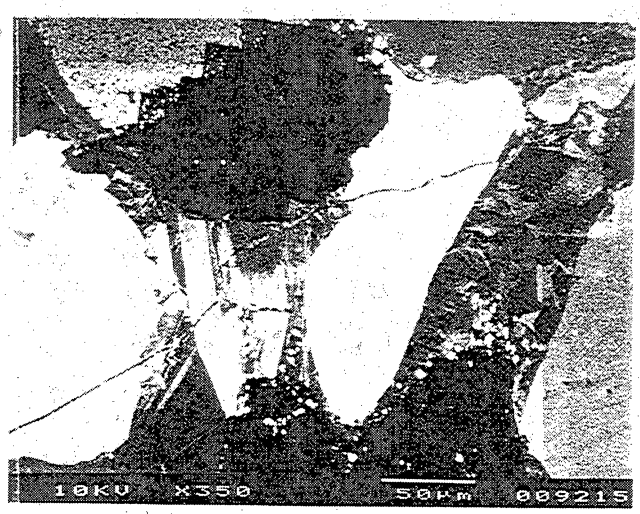

Figure 68. Travis Peak fracture microstructures, Holditch SFE No. 2. Transgranular *Type a+* fracture.

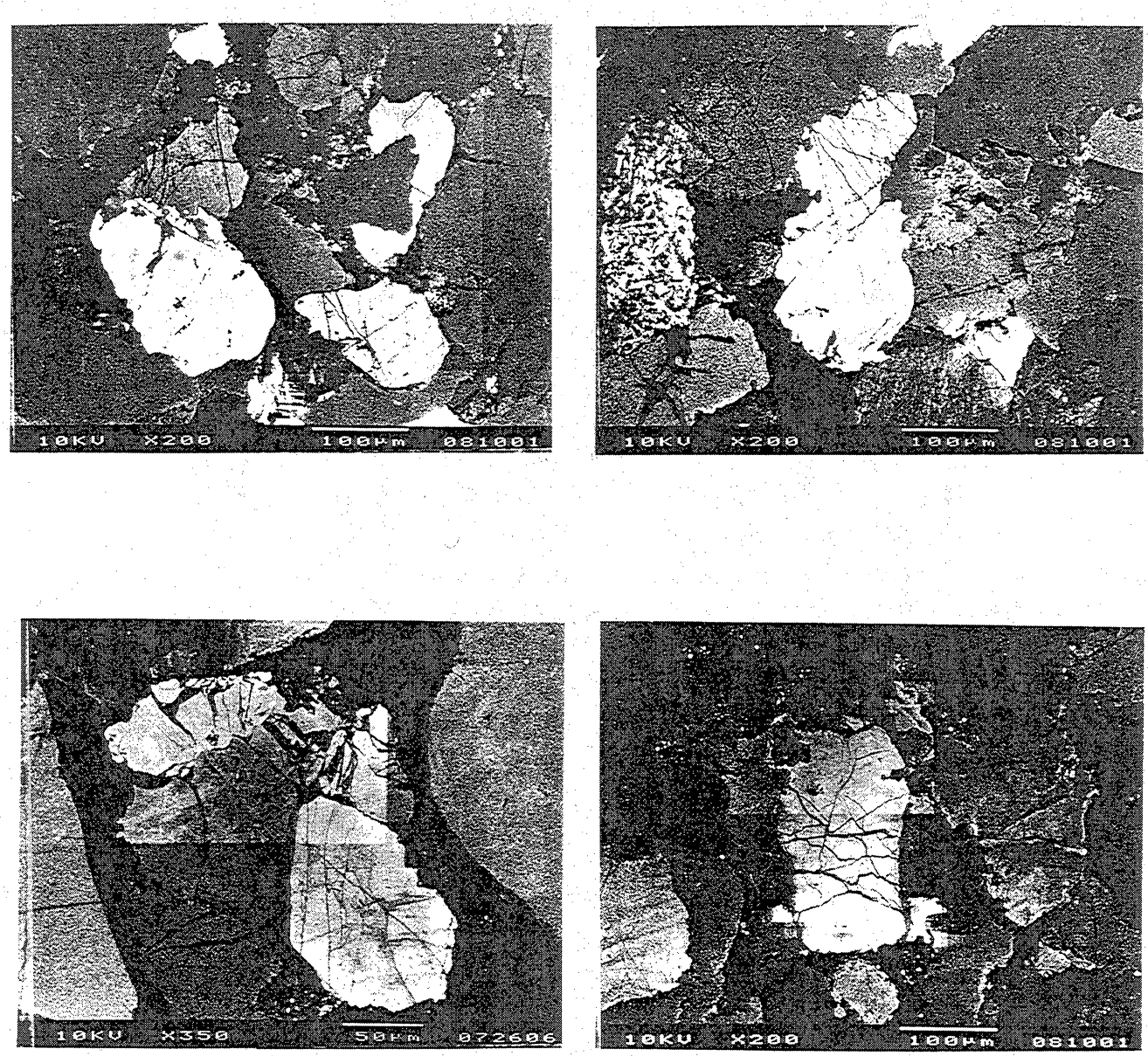

Figure 69. Travis Peak fracture microstructures, Holditch SFE No. 2. Crushed, fractured grains. Plan-view thin sections.

(a)

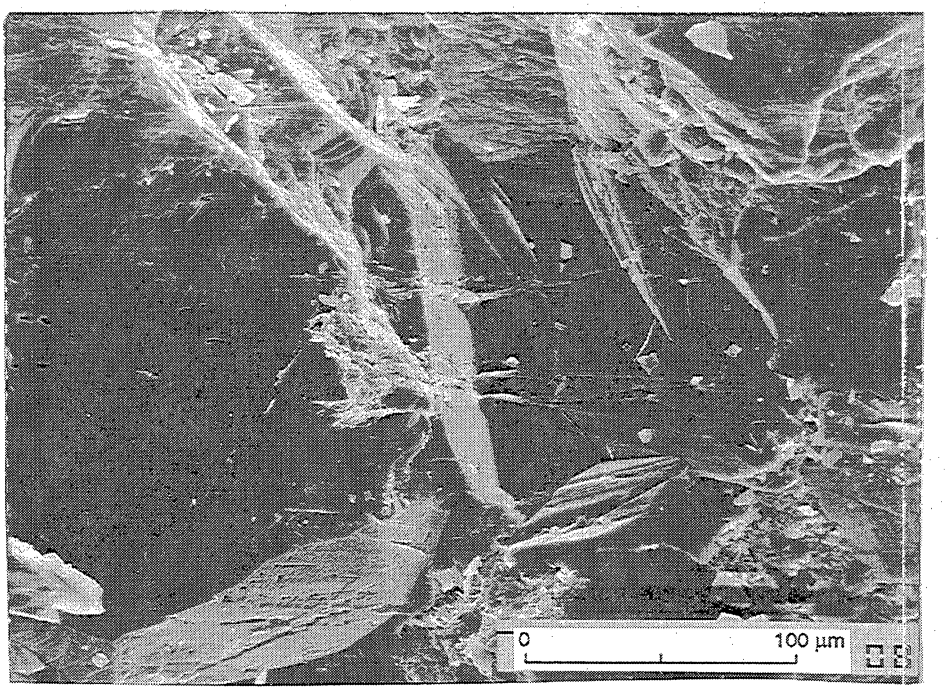

(b)

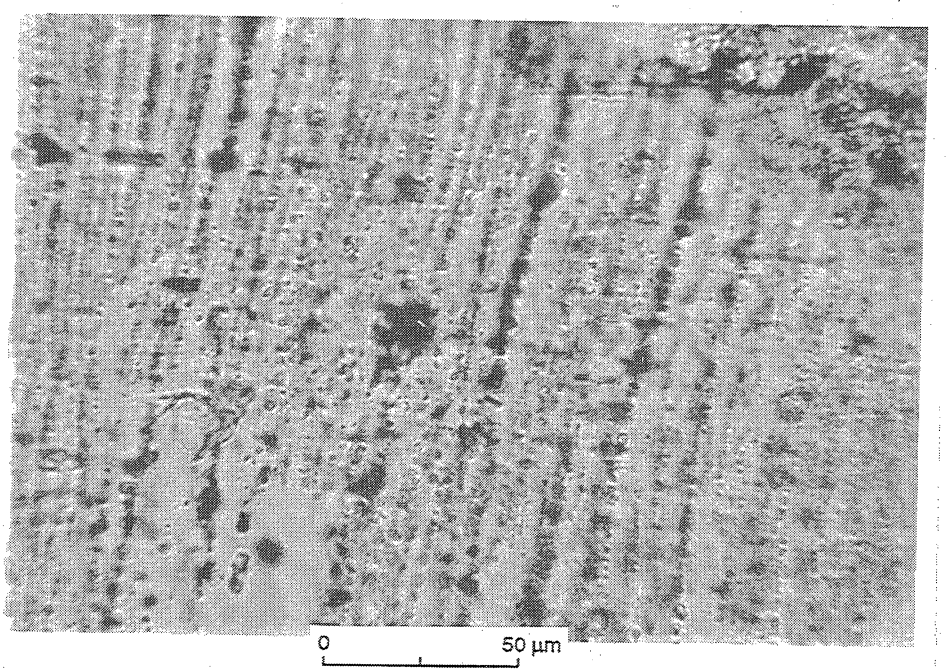

Figure 70. Fluid inclusions in Travis Peak quartz-filled fractures (vein). (a) SEM image of vein quartz. (b) Closely spaced fluid-inclusion plains in vein quartz (photomicrograph).

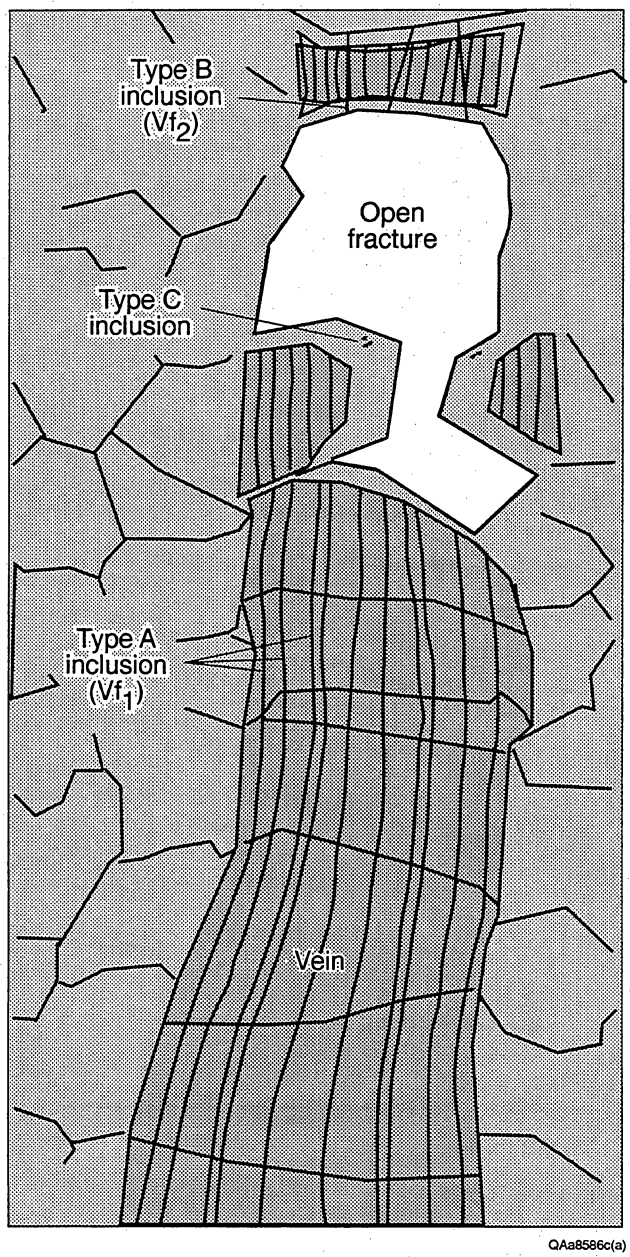

Figure 71. Diagram illustrating typical microstructures in synkinematic quartz-lined fractures showing locations of various fluid inclusion types.

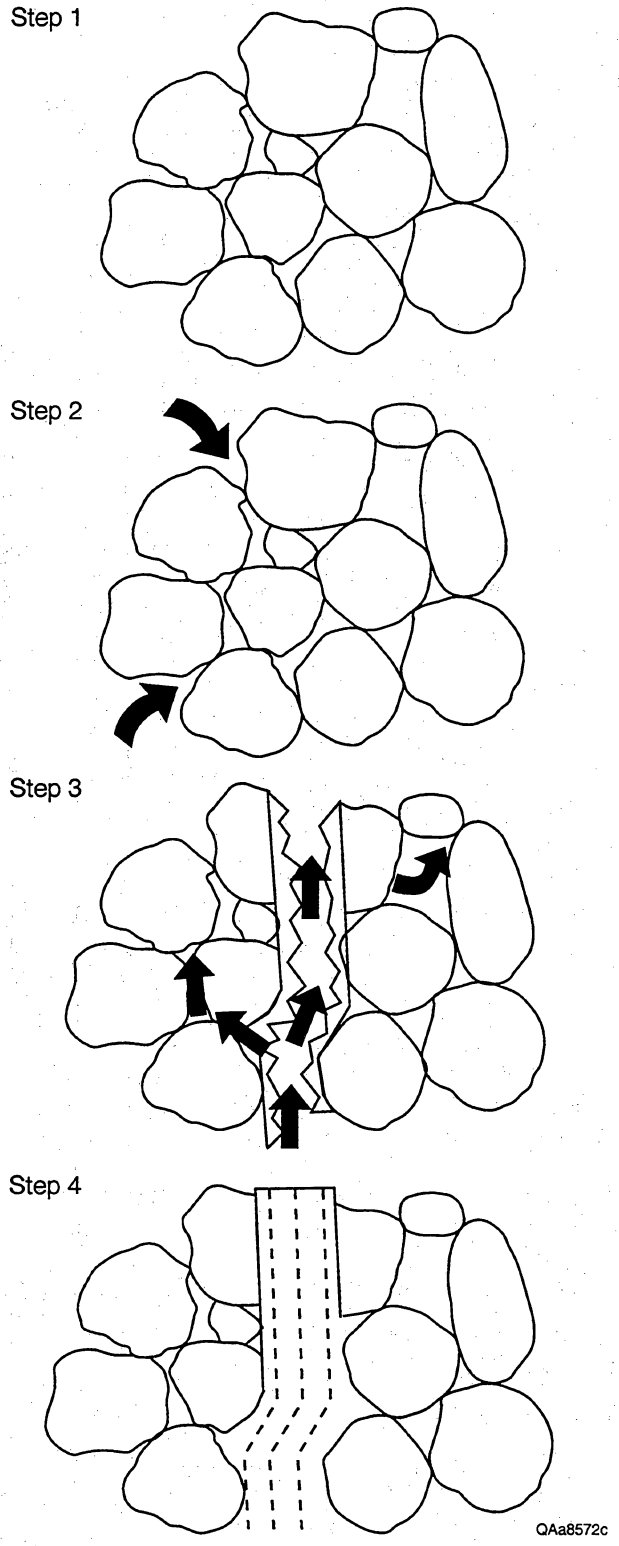

Figure 72. Progressive development of synkinematic cement and associated fractures. Step 1, compaction; Step 2, early cementation locks grains in place; Step 3, fractures form; Step 4, progressive, repeated fracture opening produces vein microstructure. Arrows show hypothetical fluid movements.

Second-generation inclusions (Types B and C) occur in clear quartz rims and in fracture-filling quartz that contains abundant Type A inclusions. Within clear quartz rims these occur as isolated primary inclusions (Type B) and as planes of primary inclusions (Type C) that crosscut both early fluid-inclusion-bearing quartz and postkinematic quartz. Type C planes are subvertical, but they are not parallel or regularly spaced, and they cut across subvertical planes defined by Type A inclusions. Type C inclusions are elongate to irregular, with maximum length ranging from less than 1 μm to greater than 10 μm. Their irregular shape has been interpreted to be evidence of necking and the development of secondary inclusions (Laubach and Boardman, 1989), but cathodoluminescence observations show that this is not the case. All of these inclusions are primary.

For late inclusions, T_h ranges from 250° to 340°F, with a mean of 300°F. Mean salinity is 11 weight percent NaCl equivalent, but values range from 5 to greater than 20 weight percent NaCl equivalent. The temperature range and variable salinity of late inclusions could have been caused by mixing of two fluids of different salinities during trapping, sampling of the same fluid at different times, or variable inclusion distortion and leakage. The trapped fluids are moderately to strongly saline brines containing approximately 133,000 milligrams/kilogram of NaCl, a composition in the range of present-day Travis Peak Formation waters. These patterns suggest that fluids in Travis Peak fractures became more saline as fracturing progressed but that water temperatures did not increase markedly.

Primary calcite inclusions in postkinematic fracture fill have T_h of 315° to 352°F (157 to 178°C), with a mean of 169°C. Textural relations show that calcite precipitated later than quartz, and so these higher temperatures could reflect greater depth of burial during calcite deposition. It is also possible that inclusions in calcite have been deformed. Stretched inclusions would give higher apparent temperatures than undeformed inclusions. Temperatures of final melting lie between –7°C and –12°C, which correspond to salinities from 10.5 to 15 weight percent NaCl.

It is a basic assumption of fluid-inclusion geothermobarometry that the fluid trapped in the inclusion was a single homogeneous phase and that after trapping occurred, the inclusion was a closed system and its volume remained constant (Roedder, 1979). These assumptions are generally thought to be valid (Roedder and Skinner, 1968; Bodnar and Bethke, 1984; Bodnar and others, 1989). There are, however, certain events that may take place that will lead to inaccurate estimates of temperature of homogenization and, in some cases, of final melting temperature used to determine fluid salinity. These include inclusion shape and volume changes (necking, stretching), leakage and decrepitation, and presence of various gas phases within the inclusion.

One environment in which conditions occur favoring stretching or decrepitation is in subsiding basins such as the Gulf Basin, where early-formed diagenetic phases are constantly exposed to temperatures higher than their formation temperature as burial proceeds. If the temperature increase with pressure (depth) is greater than that of the isochore for the inclusions, the internal pressure will be greater than the confining pressure, and stretching or leakage may develop. This may be an important process in fluid inclusions in calcite (Goldstein, 1986; Prezbindowski and Larese, 1987). In fluid inclusions in quartz, no fractures were observed in inclusion walls, and vapor bubbles did not appear to have expanded after homogenization had taken place. Furthermore, bubble sizes within inclusions were of a fairly uniform diameter relative to inclusion diameter. These observations suggest that stretching did not occur in these samples.

Another uncertainty concerns the selection of the Type A inclusions measured. These inclusions are typically less than 5 μm in diameter, and given the optical limitations of the heating/freezing stage we are confident in the accuracy of measurements of inclusions equal to or greater than 2 μm in diameter. Therefore, only the larger inclusions within this group were measured. Some Type A inclusions have negative crystal shape, which is an indication that stretching has occurred, according to Bodnar and others (1989). However, none of these inclusions were suitable to be measured.

The presence of methane in fluid inclusions becomes a problem when pressure corrections are applied. Neglecting its presence results in erroneously high estimates of formation temperature (errors greater than 30°C are possible) (Hanor, 1980). If there has been no leakage or in situ production of CH_4 after the inclusion formed via thermogenesis of organic matter, then T_h will still be a reasonable minimum temperature. Generally pressure is estimated from independent evidence of depth of cover at the time of trapping and P-V-T data on appropriate solutions (Roedder and Bodnar, 1980). Because depth of burial at trapping is one of the unknowns we wished to determine, no pressure corrections were done. There is a distinct possibility that a CO_2 or a gaseous hydrocarbon phase may be present in the inclusions, but no corrections for gas compositions were carried out. If such gasses are present, it will tend to cause overestimation of temperature of homogenization. On the other hand, aqueous phase inclusions containing CH_4 show two distinct episodes of freezing, as the clathrate compound carbon dioxide hydrate ($CO_2 \bullet 5.75\ H_2O$) freezes prior to the rest of the solution (Collins, 1979). This was not seen in our samples.

The estimation of salinity of solutions trapped in fluid inclusions, expressed as equivalent mass percent NaCl, which is deduced by measuring the depression of the freezing temperature of ice by the presence of salts, has some inaccuracy. NaCl may not be the dominant salt in solution, and the presence of dissolved salts other than NaCl will affect the magnitude of freezing-point depression (Roedder, 1962). At present the formation waters in the Travis Peak are Na-Ca-Cl waters. Sodium and chloride were derived from salt dissolution or ingress of subsalt waters, possibly in the Cretaceous (Kreitler and others, unpublished manuscript, 1978).

Isotopic Composition of Fracture-Filling Minerals

Quartz $\delta^{18}O$ compositions of quartz crystals lining fractures were measured on samples that were hand picked from fracture walls (fig. 73). The samples were collected using a fine dental drill while the sample was observed under binocular microscope. Minerals were either gently broken off the fracture surface, or, in the case of acicular crystals, plucked off. With the exception of the sample from 9840 ft in the SFE No. 2 well, where quartz was removed from a densely mineralized, vuggy fracture possibly resulting in contamination of the vug filling quartz with detrital quartz and quartz cement, the purity of fracture-fill samples was very good.

Although cathodoluminescence observations show that it is possible for such high-purity samples to be contaminated with fragments of fractured detrital quartz grains entrained in fracturing-filling quartz (fig. 74), contamination is unlikely to be a general problem for these samples because all of the sample crystals are optically clear and isotopic compositions have a generally narrow range that would be unexpected for variably contaminated samples. Entrained grains are generally a small part of vein-fill quartz, and they are usually concentrated near fracture walls, where they will tend to remain during the type of sampling we used. This does not rule out the possibility that the cement itself has a range of isotopic compositions, however. The cement is zoned, and the zoning patterns are not always simple. Quartz cement average values range between +20‰ (SMOW) at the top of the formation and +24‰ (SMOW) at the base (Dutton and Land, 1988). High-purity fracture-fill quartz samples from two wells have compositions that are bracketed by these two values (table 11).

Results are summarized in table 11. The quartz samples have $\delta^{18}O$ values between 21.5 and 22.9‰ for samples taken from fracture surfaces and $\delta^{18}O$ of 18.3‰ for the sample from the vug-shaped fracture. This latter sample is interpreted to have been contaminated by detrital quartz from the fracture wall.

To analyze each sample, approximately 200 mg of fine ground quartz was needed. Samples were first cleaned using sodium bisulfate for 10 to 15 minutes and then washed with 3N HCL. Then samples were rinsed with distilled water, dried, and then analyzed.

To determine the possible isotopic composition of the water that precipitated fracture-filling quartz, a mean quartz precipitation temperature of 143°C was used. This value was obtained from the mean homogenization temperature of primary inclusions in fractures. A higher homogenization temperature of 151°C may be more appropriate, since this is the mean value for Type C inclusions, which are possibly the inclusions least prone to measurement uncertainty and disruption. Using equations relating temperature, $\delta^{18}O$-water, and $\delta^{18}O$-mineral from Friedman and O'Neil (1977), an interpolated value was obtained of ∂W of +4‰ for the isotopic composition of the water. This value plots with formation waters of Texas and the Gulf Coast (Dutton and Land, 1988) and is more enriched than meteoric water.

Scanned Cathodoluminescence Observations

Scanned cathodoluminescence imaging of fracture-lining quartz shows that this material contains quartz-filled microfractures that are subparallel to the macrofracture walls. Near fracture walls, some detrital grains have been broken and extended by a process of repeated fracturing and authigenic mineral precipitation (fig. 74). Crosscutting relationships of CL-zonation in authigenic quartz show that early-formed fracture-lining cement is subject to numerous episodes of fracturing and sealing (fig. 75).

Scanned CL observations also conclusively show that local pressure solution within sandstones was not the origin of silica for quartz cements. Sand grains are commonly in point contact in areas having extensive quartz cement. On a microscopic scale there is little evidence of conventional pressure solution. However, as Milliken and Dickenson (1994) have shown, dissolution associated with brittle grain comminution may be an important process in local redistribution of material. But it is not volumetrically significant enough to account for the large amount of quartz cement present.

(a)

(b)

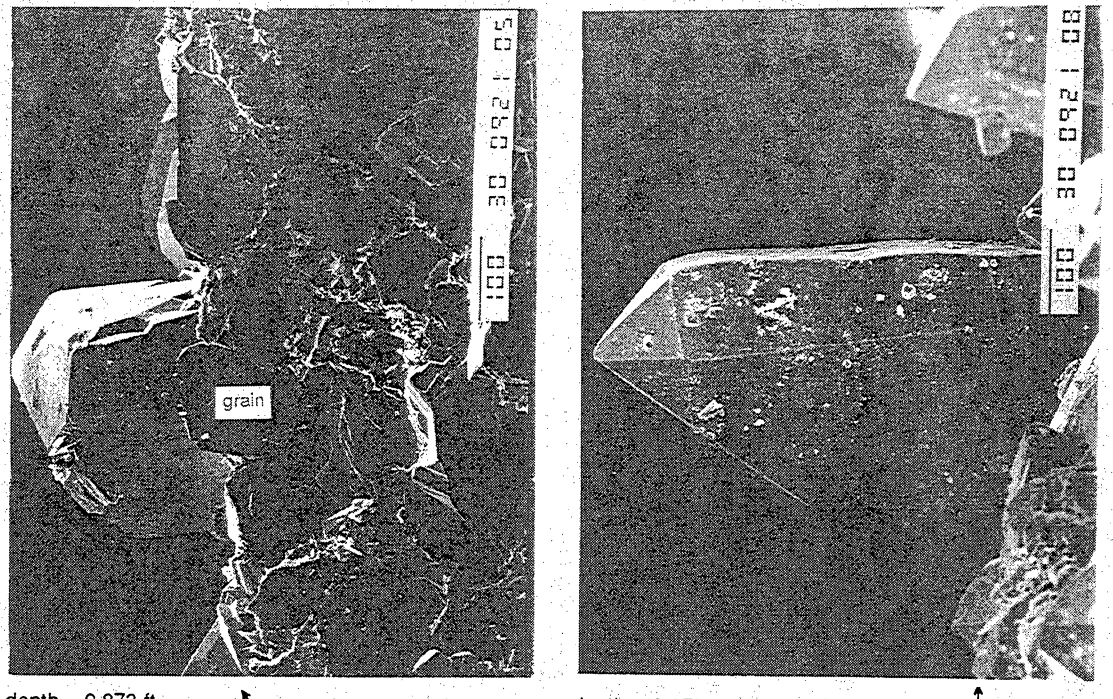

Fracture cross-section: SEM images of fracture - lining quartz facing open fractures

Figure 73. Acicular quartz crystal (q) on fracture wall, Travis Peak Formation. Crystals of this morphology were sampled for oxygen isotope analysis. (a) Note encased quartz grain. (b) Note asymmetry of crystal, with rounded upper surface and sharp, faceted lower faces. Possible geopetal feature reflecting fluid contact within fracture.

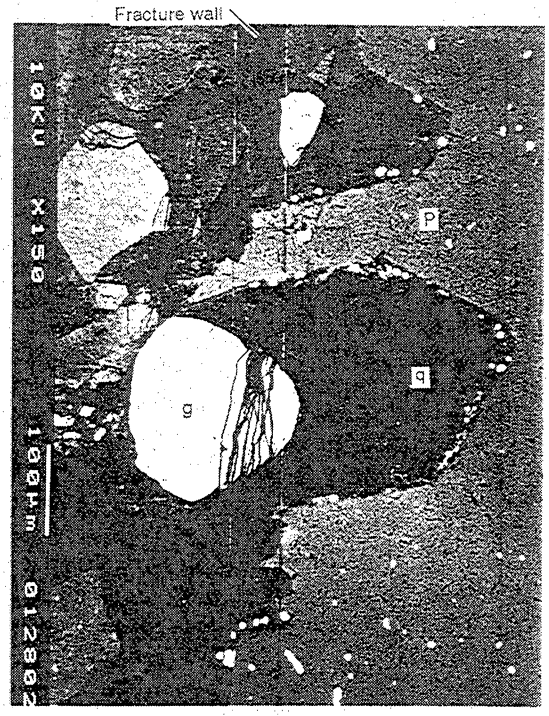

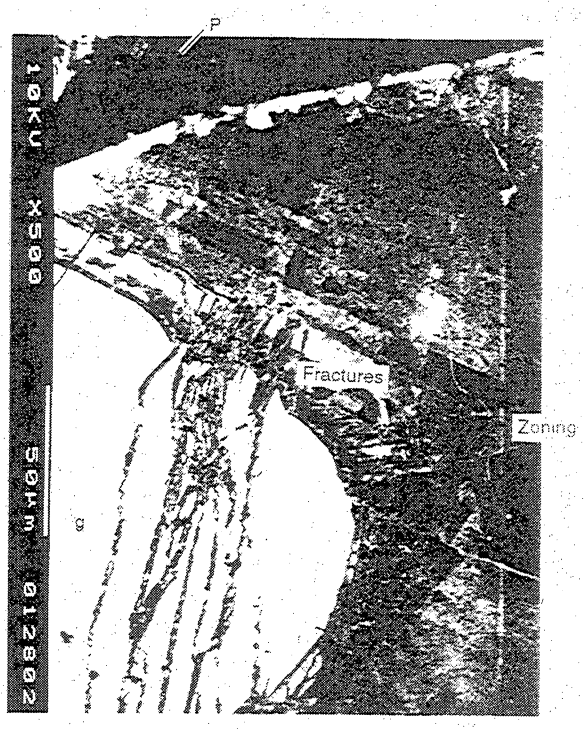

Figure 74. Cathodoluminescence images of quartz lining fracture walls, Travis Peak Formation. Multiple episodes of fracture opening and quartz precipitation are visible. P, porosity in fracture; q, quartz; g, grain. Note fractures and zoning in quartz.

Table 11. Isotopic composition of fracture-filling minerals.

Vein Quartz

Depth (ft)	$\delta^{18}O$	Purity (1=most 5=least)	Fracture type/ generation	Cement generation
–9840.0	18.3	5	Vug (1)	2 and 3
–9871.7	21.8	2	Planar (2)	2
–9873.0	21.5	2	Planar (2)	2
–9873.0	22.9	1	Planar (2)	2
–10,108.0	22.3	1	Planar (2)	2

Vein Carbonate

Well	Depth (ft)	Composition	$\delta^{18}O$	$\delta^{13}C$
SFE No. 2	–9527	Dolomite/ankerite	–11.25	–11.65
HH No. 5	–6242	Dolomite/ankerite	–10.13	–9.14
HH No. 5	–6303	Dolomite/ankerite	–11.33	–9.61
HH No. 5	–7471	Dolomite/ankerite	–10.45	–8.89

Scanned CL images also show that fractures were opening within quartz cement throughout the quartz cementation history. Crosscutting microfractures, and microfractures that extend for different distances out into cement, are common.

Evidence for Synkinematic Cementation

Quartz cement and quartz fracture fill are bracketed by essentially the same paragenetic sequence in matrix porosity and fracture porosity. The paragenetic sequence of fracture-filling minerals matches that of authigenic cements in the Travis Peak Formation (fig. 62). For cements, the sequence consists of (1) quartz precipitation (main stage, Q^1 and late stage Q^2), (2) albitization and orthoclase dissolution, (3) illite and chlorite precipitation, (4) ankerite precipitation, and (5) minor quartz precipitation (Q^3) (Dutton and Land, 1988; Dutton and Diggs, 1990).

In fractures, the main phase of quartz precipitation (synkinematic main phase, Q^1 and late kinematic Q^2) precedes the precipitation of fracture-filling illite, and ankerite and partly dissolved orthoclase grains are visible on fracture surfaces. Small ankerite or ferroan calcite crystals are visible growing on partly dissolved feldspar grains (fig. 67). Minor postkinematic fracture-filling quartz precipitation (Q^3) followed fracture-filling ankerite precipitation (fig. 69), but this episode accounts for less than about 1 percent of the volume of fracture-lining quartz. Postkinematic ankerite in some fracture fills indicates that fractures had ceased to widen prior to ankerite precipitation. Thus, quartz cementation ended at about the time fractures ceased to grow. These textural relationships indicate that sandstone-framework quartz cementation and fracture-filling quartz precipitation were contemporaneous.

This interpretation is verified by scanned CL observations. These observations show that banded planes of Type A inclusions are crack-seal structures in fracture-filling quartz, indicating that quartz precipitated during episodic fracture opening. Precipitation of quartz following fracture opening trapped primary fluid inclusions near fracture surfaces. Relations among quartz cements and fracture-fill quartz show that fracture and cement fill are contemporaneous. Zoning in cements can be traced into fracture-lining quartz. Crosscutting relations of microfractures and cement demonstrate that fractures having identical CL appearance (probably indicating similar composition) grew throughout the cementation sequence (fig. 75). This is consistent with identical $\delta^{18}O$ stable isotope composition of fracture-filling quartz and quartz cement in the rock matrix (see Dutton and others, 1991a, for cement values; table 11). The isotopic composition of carbonate minerals in fractures and in sandstone-framework cement is also similar.

Transgranular microfractures in quartz cement, together with crack-seal structures, are characteristic of synkinematic precipitation of quartz cement. The

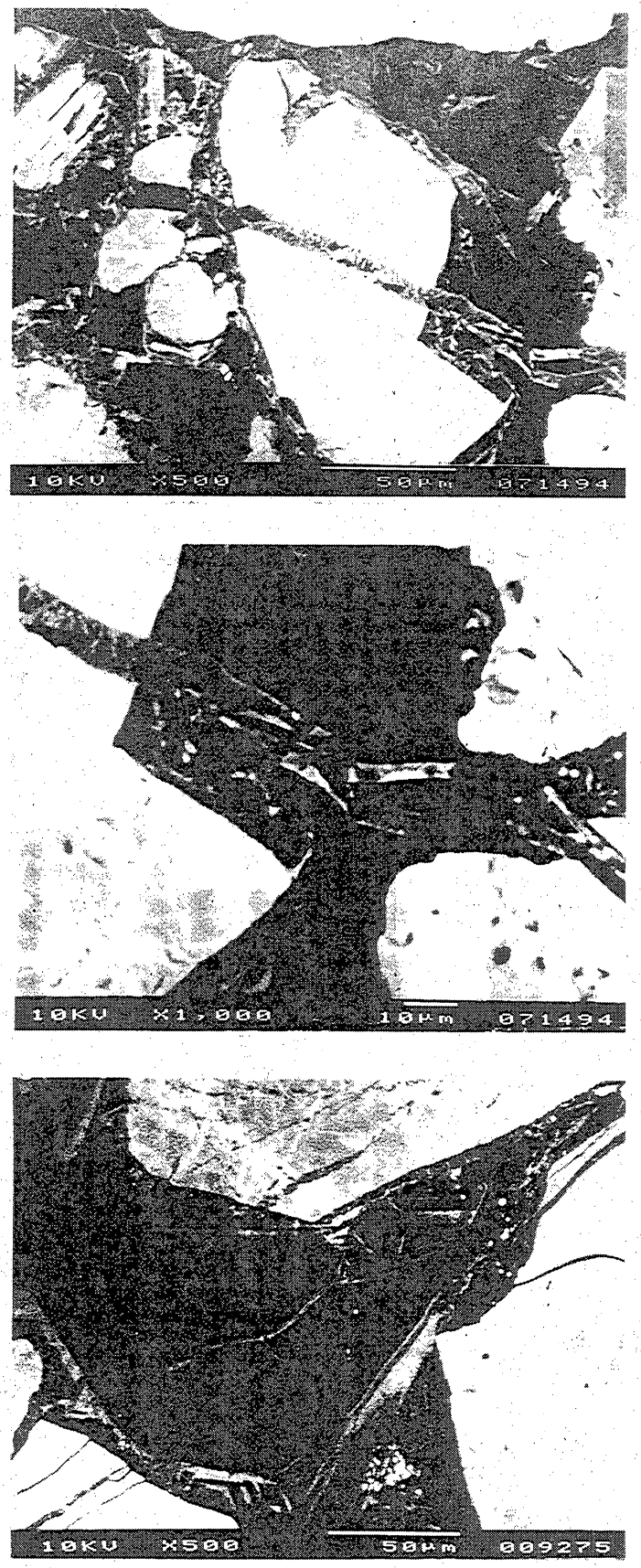

Figure 75. Scanned CL images of sealed microfractures and quartz cement. Prairie Mast No. 1-A, –9,215.2 ft. Plan-view images of fractures. Note sharp sides of fracture within cement.

scanned CL evidence for patterns of fracture growth shows that fractures grew throughout most, if not all, of the period during which quartz cementation was underway. Many of these fractures are not visible without use of optical or scanned CL microscopy. The widespread occurrence of sealed transgranular and transcement microfractures in pore-filling quartz and the large numbers of sealed microfractures that cut across most of the pore-filling quartz-cement stratigraphy suggest that large fractures propagated mainly during the middle and late stages of quartz cementation. This may account for the substantial volume (~75 percent) of fracture porosity preserved in many large Travis Peak fractures.

The crack-seal process during quartz cementation produces a characteristic suite of microstructures in matrix and in veins. These features are best documented in the Travis Peak Formation, but they are also visible in quartz-cemented Canyon and Frontier Formation sandstones. They include, in matrix rocks, quartz-filled aligned microfractures, crushed grains, cemented pores where complex intergrown cement zonation is visible, domains where grains are dominantly in point contact and domains where interpenetrating stylolitic grain contacts are common, and locally, abundant stylolites. In parts of the Frontier Formation, stylolites exist that are subvertical rather than horizontal. Within veins, structures include isolated pillars of inclusion-rich quartz that locally contains entrained wall-rock fragments.

Fracture Abundance

Fractures are widespread in Travis Peak Formation core, particularly in highly indurated, deeply buried parts of the formation in northern Nacogdoches County. They were observed at a range of depths in core or with borehole-imaging logs (Formation Microscanner [FMS], borehole televiewer [BHTV]; Laubach and others, 1990) throughout the geographic area of the study and in all stratigraphic subdivisions of the Travis Peak Formation. The variability and local high density of fracture development are illustrated by two cores from the Holditch SFE No. 2 well in northern Nacogdoches County. Only a few short fractures are present in the core from the shallow interval (fig. 76), but numerous fractures occur in the core from the deeper interval of this well (fig. 77). Significant fracture development is not restricted to deeper parts of the formation, however. Fractures having vertical dimensions of more than 7 ft in the Arkla T. P. Scott No. 5 well in Waskom field are among the longest recovered (Laubach, 1989a, p. 5).

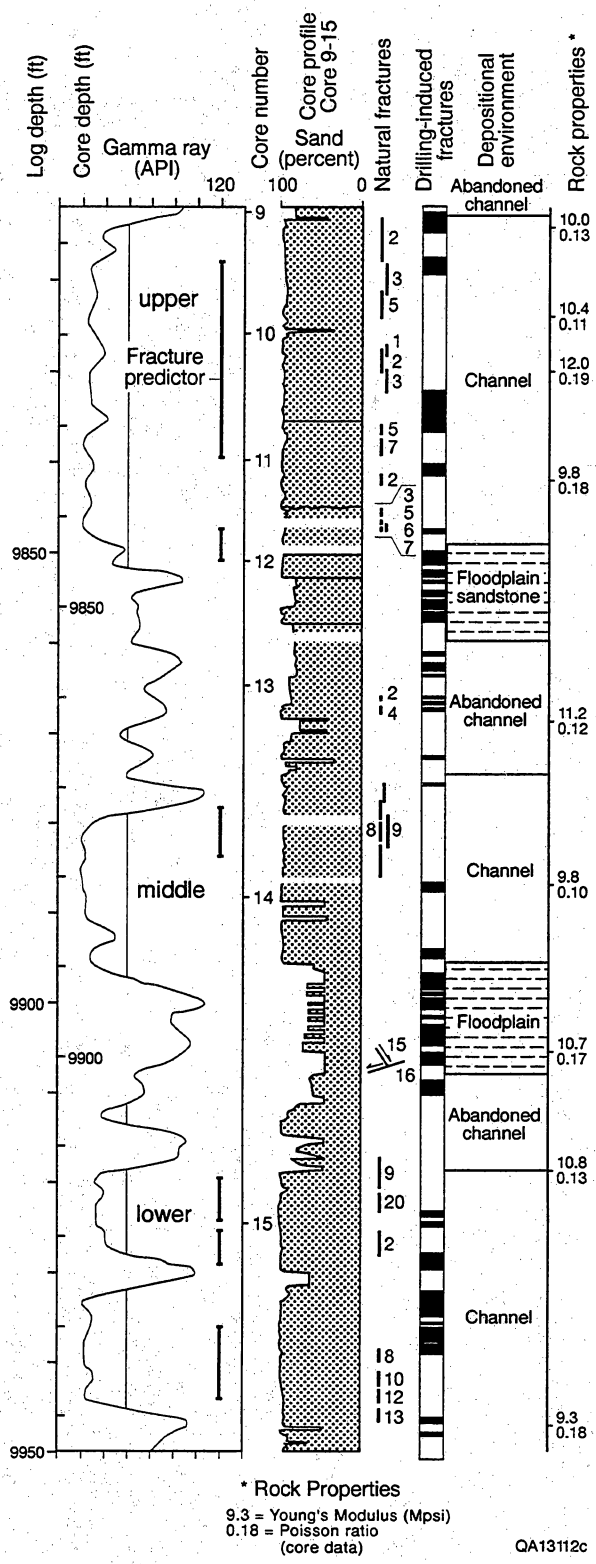

Figure 76. Core gamma-ray log, core profile, fracture distribution, and environmental interpretation, cores 9 through 15, SFE No. 2 well. Static rock-property measurements from core plugs in this interval are also indicated. This core interval contains numerous fractures in lower Travis Peak Formation. Intervals labeled "Fracture predictor" indicate where zones of favorable rock types for natural fracture development were predicted from geophysical log data, as described elsewhere in text.

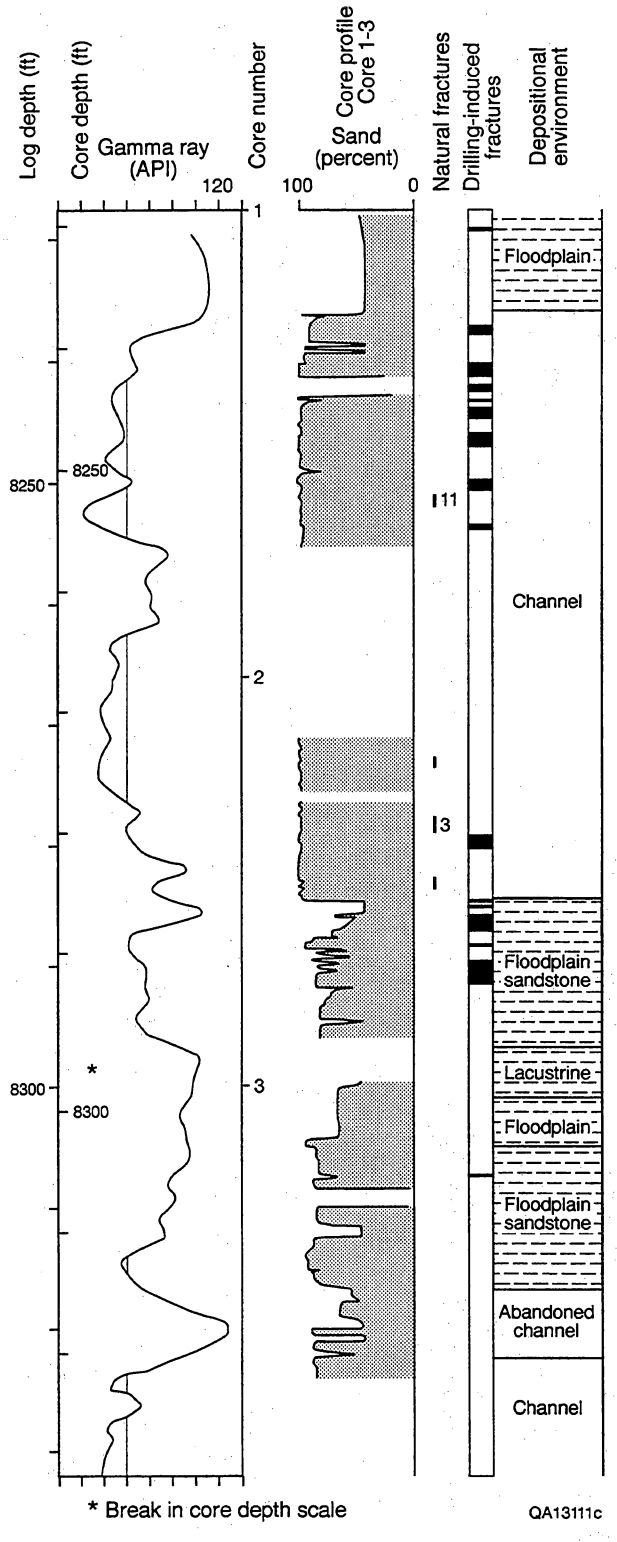

Figure 77. Core gamma-ray log, core profile, fracture distribution, and environmental interpretation, cores 1 through 3, Holditch SFE No. 2 well. Note that few natural fractures occur in this interval.

In common with many other formations, fracture abundance is difficult to quantify with vertical core in the Travis Peak because fracture dip is subparallel to the core axis, and fracture spacing is generally greater than the 4-inch diameter of the core. Abundance measured by fracture number indicates that although fractures in sandstone are more abundant in the lower Travis Peak, fracture numbers are similar (figs. 78 and 79). These fracture numbers were derived by normalizing total length of fractures in a cored interval to the thickness of cored rock. If highly cemented intervals are used for normalization, the number of high fracture number beds is greater in the lower Travis Peak (figs. 8, 76, and 77).

The most highly fractured rocks encountered in this study, which locally had fracture spacing in core of as little as approximately 1 inch, occur in North Appleby field in areas of homoclinal dip far from any fold. Fracture abundance is only modestly higher in fold hinges and none of the study wells was close to mapped faults, so the regional patterns reflect stratigraphic or depth-related shifts in fracture abundance. Generally east- to northeast fracture strikes were interpreted to indicate that most of the observed fractures belong to a single fracture set (Laubach, 1988b), and fracture-abundance measurements at the wellbore do not need to be adjusted to take into account the presence of fractures from multiple sets. This interpretation is supported by the uniform pattern of vein-filling minerals and other petrologic information for Travis Peak fractures that show all fractures to be of the same age relative to the diagenetic sequence.

The increase in quartz cement in clean sandstones with present burial depth has been interpreted to result from an early, relatively uniform episode of quartz cementation, and a later episode that concentrated quartz cement in the deeper sandstones (Dutton and others, 1991a). Extensive quartz cement due to the latter episode is concentrated in sandstones below 8,000 ft. Structurally deeper Travis Peak sandstones are more intensely quartz cemented than are shallower sandstones.

Within deeper and shallower parts of the formation, there is considerable variability in the degree of quartz cementation, and differences in diagenetic history exist between fluvial and paralic sandstones (Dutton and Diggs, 1992). Extensive quartz cementation is reflected in differences in fracture abundance. Fractures are more abundant in the lower Travis Peak and in highly quartz cemented layers within the upper and lower Travis Peak. Beds with high cement volumes tend to have high fracture numbers (fig. 8). Highly quartz-cemented beds also have the greatest number of quartz-filled microfractures.

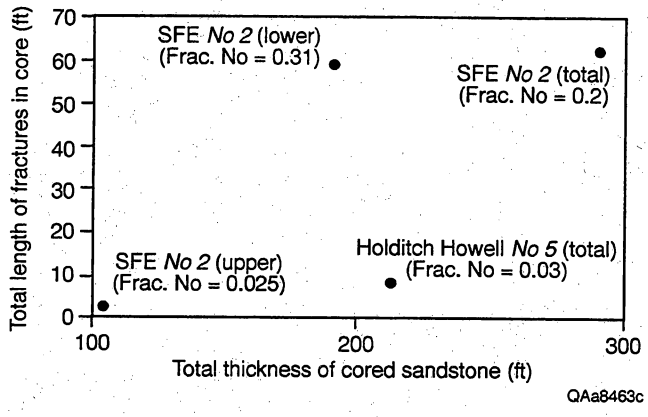

Figure 78. Fracture abundance based on fracture numbers, Travis Peak Formation. Plot shows averages for large stratigraphic intervals.

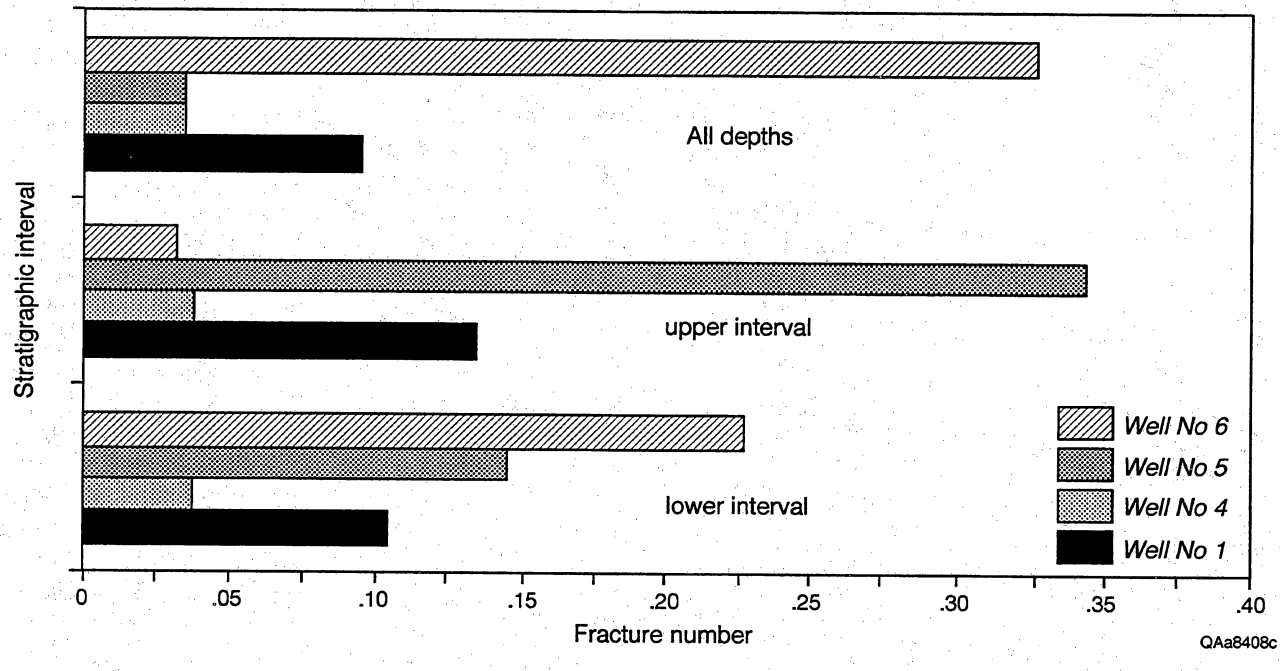

Figure 79. Fracture abundance based on fracture numbers, Travis Peak Formation. Results show averages for upper and lower Travis Peak. See figure 8 for well names.

Mixed Syn- and Postkinematic Cements: Frontier Formation

The Frontier Formation has evidence of both syn- and postkinematic cements. Volumetrically, as illustrated in figure 5, average cement values suggest that the Frontier sandstones have more equal proportions of pre-, syn-, and postkinematic cements than do the other formations described in this report. However, as in the case of the Sonora Canyon, where beds having either pre- or synkinematic cements controlled fracture stratigraphy, variations in diagenesis are masked by average values for the entire formation. These stratigraphic variations in cement type provide critical evidence for augmenting natural fracture analysis.

Diagenesis of Frontier sandstones in the Green River Basin is described by Dutton and others (in press). This study shows that cement patterns vary with facies, depth, and regional setting. Original detrital composition of sandstone plays an important role in diagenesis of these rocks and can cause abrupt shifts in diagenetic attributes. Analysis of vein minerals in Frontier Formation sandstones shows that fracture-filling minerals have a systematic relationship to diagenetic attributes (tables 12 and 13).

Despite the inherent low probability of intersecting vertical fractures with vertical core, 92 fractures were encountered in 1,580 ft of core from 10 Frontier wells (Dutton and others, in press), showing that natural fractures are probably a common reservoir element in this formation. The Frontier provides a useful test of diagenetic predictors of fracture properties because fractures are sparse in core, no doubt a result of wide fracture spacing. Wide fracture spacing is typical of Frontier Formations outcrops along the basin margin (Laubach, 1992c), and homogeneous sandstones in the Frontier Formation are generally thicker than those of the Canyon Sandstone. Moreover, they are not as stiff and brittle as those of the Travis Peak. These latter factors may help account for the lower abundance of fractures in Frontier cores compared to the other two formations. Fractures in five cores from the Frontier Formation were studied to detail fracture distribution and morphology, fracture-fill petrology and mineralization sequence, relation of sandstone-framework diagenesis to fracture mineralization, and controls on fracture porosity (fig. 80).

Fracture Distribution, Size, and Shape

Natural fractures are sparse but persistent features of Frontier Formation cores. They include vertical to subvertical opening-mode fractures and small tectonic faults. Fracture abundance in five cores is illustrated in figure 80, which shows the depth and vertical lengths (height) of fractures in core. From these five wells, 32 vertical or steeply inclined opening-mode fractures and dilatant faults were recovered in approximately 470 ft of sandstone core. Closely spaced fractures in core from depths of 16,130 ft in the Energy Reserves Blue Rim Federal No. 1-30 well suggest that open fractures can occur at great depth in the Green River Basin, distant from major tectonic folds and faults. Mineralized fractures in sandstones occur over a depth range of 7,195 to 16,130 ft in the five wells. The deepest fractures are from 16,130 ft in the Energy Reserves Group Blue Rim Federal No. 1-30 well. The occurrence of a few natural fractures in most cored Frontier Formation wells we studied is qualitative evidence that fractures are widespread in the subsurface of the Green River Basin.

Core from the SFE No. 4-24 well illustrates typical proportions of natural fracture types encountered in these wells. The core contains 3 steeply inclined calcite-lined opening-mode fractures and 22 gently to moderately dipping, striated fractures or small faults. The latter are primarily compaction/dewatering features in mudstones, but several calcite-lined slip surfaces are small tectonic faults (shear fractures). Other fractures include extension fractures (cleat) in coal, and eight vertical, nonmineralized fractures in mudstone that may be either natural or drilling induced. Calcite-filled fractures in one interlaminated sandstone and mudstone interval in the Energy Reserves Group Blue Rim Federal No. 1-30 well have heights of 6 inches, widths of as much as 0.25 mm, and spacing of 0.4 to 1.2 inches. Although this may reflect sampling bias, no consistent difference is apparent in style, number, or height of fractures with depth throughout the area of the Green River Basin where our cores were obtained. Maximum heights of vertical fractures in shallow and deep cores are comparable. The abundance of fractures and the proportion of different fracture types are generally similar for all five wells.

Mineralized opening-mode fractures in Frontier Formation core are typically narrow, commonly <0.25 mm wide, and have lens-shaped cross sections.

Table 12. Frontier Formation fractures and associated cement types.

Well	Depth (ft)	Fracture mineralogy	Fracture type	Lithology	Dominant cement
S. A. Holditch	7,314.4	cc	vein	siltstone	q, cc, minor clay
SFE No. 4	7,330.8	cc	coal cleat	coal	
	7,330.8	cc	coal cleat	coal	
	7,344.6	q	coal cleat	coal	
	7,401.1	q	FIP	fine ss	q, minor cc
	7,403.4	q	FIP	fine ss	q, minor cc
	7,405.9	q	FIP	fine ss	q, minor cc
	7,411.9	q	FIP	very fine ss	q, minor cc
	7,437.8	cc	coal cleat	coal	
	7,437.8	cc	coal cleat	coal	
	7,443.5	cc	vein	mudstone	clay, minor cc
	7,448.6	cc	vein	mudstone	clay, minor cc
	7,629.5	cc	coal cleat	coal	
	7,630.0	q	coal cleat	siltstone	clay, cc
	7,630.4	cc & q	coal cleat	coal	
	7,630.4	cc & q	coal cleat	coal	
	7,469.8	–	open	siltstone	q, cc, clay
Wexpro	12,165.0	q	FIP	fine ss	q
Church Buttes Unit No. 48	12,168.0	q	FIP	fine ss	q
	12,170.0	q	FIP	fine ss	q, minor clay
	12,170.8	q	FIP	fine ss	q, minor clay
	12,169.2	q	FIP	fine ss	q
Blue Rim Federal 1-30	16,131.8	open/cc	vein	siltstone	clay, cc (minor q)
	16,123.1	cc	vein	fine ss	clay, cc (minor q)
	16,122.9	cc	vein	very fine ss	clay, cc (minor q)
	16,131.8	cc	vein	very fine ss	clay, cc (minor q)
	16,067.9	q	FIP	fine ss	q
	16,062.9	q	FIP	fine ss	q
	16,065.7	q	FIP	fine ss	q
	16,053.2	q	FIP	fine ss	q
	16,056.0	q	FIP	fine ss	q
	16,063.5	q	FIP	fine ss	q
	16,070.0	q	FIP	fine ss	q, minor clay
Terra Resources	9,067.5	–	open	siltstone	clay, minor q
Anderson Canyon No. 3-17	9,174.2	–	open	siltstone	clay, minor q
Forrest Oil	13,054.4	q	FIP	fine ss	q, cc
Henry Unit No. 2	13,064.1	q	FIP	fine ss	q, cc (replaces fspar)
	13,028.1	cc	cleat	siltstone	clay, cc
	13,069.0	–	open	very fine ss	q, clay
Enron Oil & Gas	7,261.2	cc	vein	fine ss	q, cc
South Hogsback No. 13-8	7,045.0	q	FIP	fine ss	q
	7,260.0	cc	vein	very fine	clay, minor cc, minor q
	7,268.8	q	FIP	fine ss	q, minor cc

FIP = fluid-inclusion plane; fspar = feldspar; q = quartz; cc = calcite; ss = sandstone; cleat = fracture in coal; open = fracture porosity

Table 13. Summary statistics: number of samples by fracture type and associated matrix cement type.

Well	Fracture type	Associated dominant cement	
	FIP's*	Quartz	Calcite & clays
Holditch SFE No. 4	4	4	0
Wexpro Church Buttes No. 48	5	5	0
Blue Rim Federal 1-30	7	7	0
Anderson Canyon No. 3-17	0	0	0
Forrest Henry Unit No. 2	2	2	0
Enron S. Hogsback No. 13-8	2	2	0
Total (number of samples)	20	20	0
%		100	0
	Veins		
Holditch SFE No. 4	3	1	2
Wexpro Church Buttes No. 48	0	0	0
Blue Rim Federal 1-30	4	0	4
Anderson Canyon No. 3-17	0	0	0
Forrest Henry Unit No. 2	0	0	0
Enron S. Hogsback No. 13-8	2	1	1
Total (number of samples)	9	2	7
%		22	78
	Open Fractures		
Holditch SFE No. 4	1	1	0
Wexpro Church Buttes No. 48	0	0	0
Blue Rim Federal 1-30	0	0	0
Anderson Canyon No. 3-17	2	0	2
Forrest Henry Unit No. 2	1	1	0
Enron S. Hogsback No. 13-8	0	0	0
Total (number of samples)	4	1	2
%		50	50

*FIP's, fluid-inclusion planes (sealed microfractures).

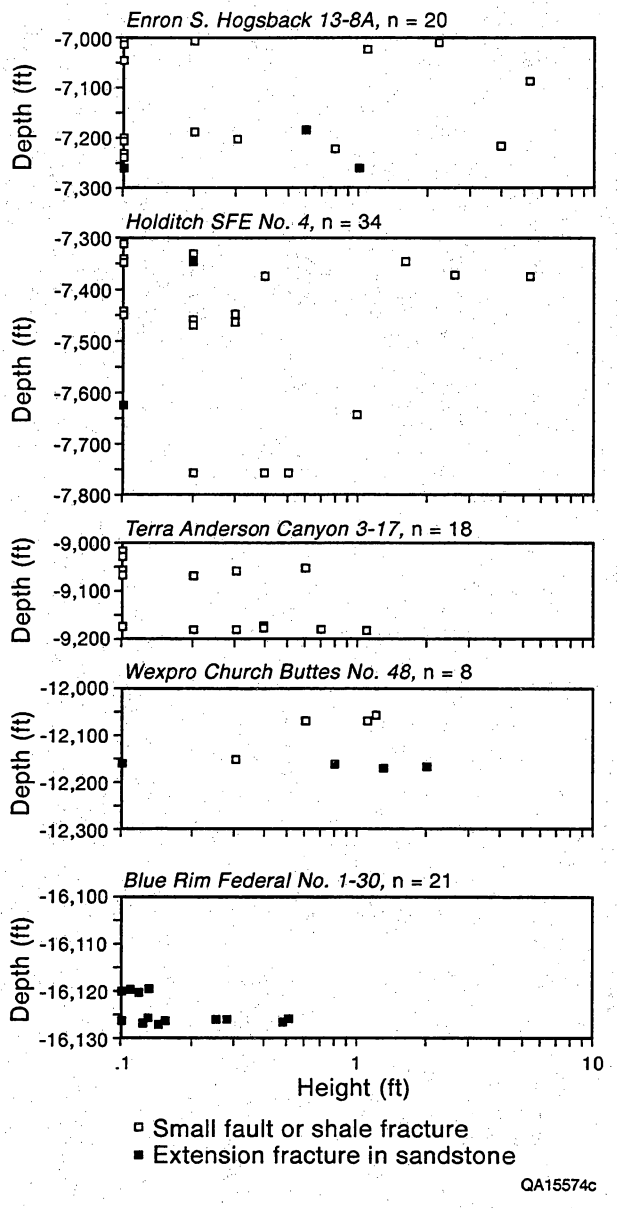

Figure 80. Fractures in core from five Frontier Formation wells, Green River Basin (Laubach, 1991).

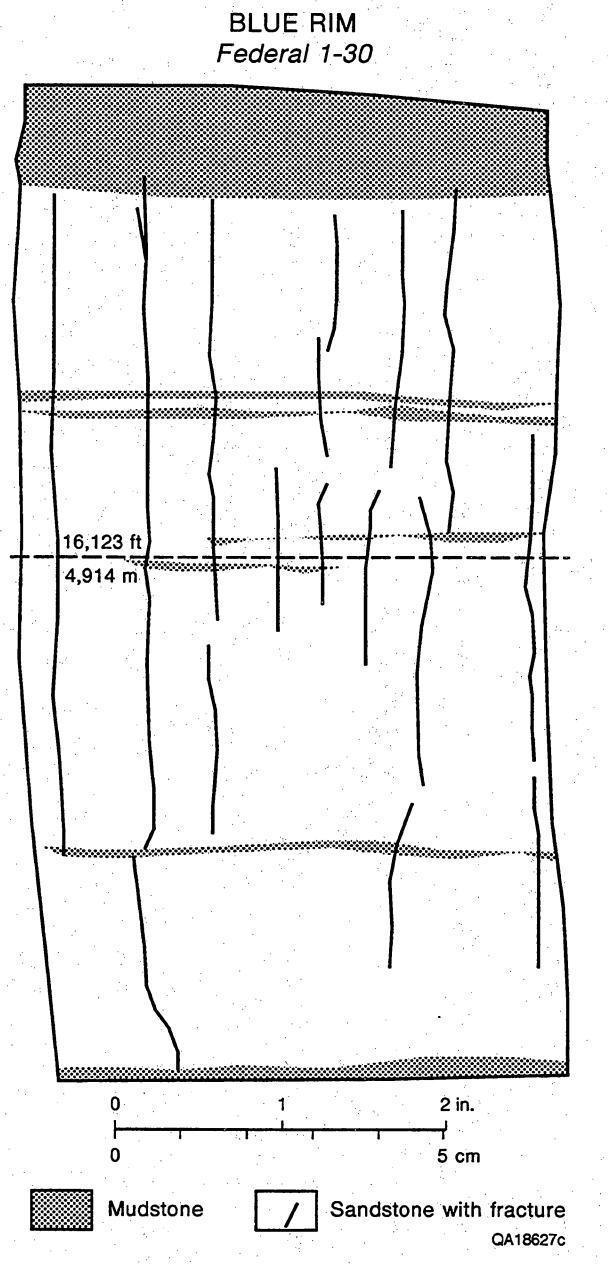

Figure 81. Closely spaced vertical fractures in Frontier Formation core, Blue Rim Federal No. 1-30 well. Core depth 16,123 ft.

Wide fractures are filled or partly filled with minor quartz and calcite. Only a few show evidence, such as euhedral crystals lining fractures, that fractures were open in the subsurface. Vertical fractures are the only type for which meaningful height measurements can be obtained in vertical core. These fractures are short, generally less than 1 ft high. The tallest fracture of this type is about 2 ft high.

Fractures in Frontier Formation core tend to be confined to individual sandstones and generally end by intersecting shale interbeds or at blind terminations within sandstone (fig. 81). Some fractures are also composed of vertically discontinuous fracture strands, suggesting that fractures may not form continuous networks of interconnected fractures from the top to the base of a sandstone. Length (plan-view dimension) and spacing cannot be measured in vertical core, but Frontier Formation outcrop observations, described later, suggest that fracture length is probably much greater than fracture height (>10:1) and that fractures end vertically at bed boundaries. Because of the small number of fractures sampled, it is unlikely that these width and height measurements represent the range of dimensions that exist in the subsurface.

Petrology and Mineralization Sequence of Fractures

The sequence in which vein-filling minerals precipitated (fig. 82) is evident in thin section from overprinting and crosscutting relations. In a few fractures, overlapping relations suggest that quartz precipitated first, followed by calcite. In these fractures only small amounts of quartz are present, forming overgrowths on quartz grains adjacent to fractures. It is conceivable but unlikely that this quartz precipitated as overgrowths before fractures developed, and that fracturing subsequently exposed quartz overgrowths on the fracture walls. In some fractures unfaceted quartz grains occur on fracture walls overgrown with calcite, implying either that locally fracture walls were not entirely coated with quartz or that some fractures were never lined with quartz. Some of these fractures may crosscut quartz cement, but the paragenetic patterns are ambiguous. These relations point to two episodes of fracture. One episode followed or—in view of the presence of sealed microfractures—was contemporaneous with a phase of quartz cementation. The second episode possibly occurred after quartz precipitation, but prior to most (or all) calcite precipitation. From the evidence at hand, more complex fracture-diagenesis timing relations than this cannot be ruled out.

Fractures in core typically are filled or partly filled with calcite, which is commonly massive and blocky. Calcite having slender crystals oriented normal to the fracture surfaces are rare. Locally, euhedral crystal faces are evident, indicating that minerals grew into open-fracture pore space. In some examples, late blocky calcite encloses older, acicular calcite crystals. On the basis of these overprinting relationships and differences in crystal habit and color, at least two generations or episodes of vein-filling calcite can locally be inferred. These mineral habits do not suggest synkinematic mineralization. However, textures such as crack-seal features might not be preserved if fractures opened rapidly relative to crystal growth. Acicular calcite crystals may mark rapid growth into a recently opened fracture. An episode of synkinematic calcite growth (possibly relative to a second fracture-opening event) cannot be discounted.

Timing of the genesis of one fracture relative to feldspar dissolution is evident in crosscutting relations in a calcite-filled vein at 6,912 ft in core from the Mobil Tip Top No. T71X-6G well. Fracture-filling calcite that crosses open secondary pores that formerly contained feldspar grains is evidence that fractures formed, and fracture-fill calcite precipitated, before feldspar dissolution. In this example, the calcite that filled the vein remains after the surrounding feldspar grain was dissolved. Feldspar dissolution following calcite precipitation is a sequence that also occurs in the sandstone framework.

Three samples of predominantly calcite-filled fractures are from oriented intervals. Fracture apertures that range from 0.03 to 5 mm. Calcite is blocky, not fibrous. There is no evidence of a crack-seal mechanism of stepwise opening and mineralization. Calcite-filled fracture strikes range from 048 to 119 degrees. The eastward to northeastward strikes of these fractures are reminiscent of the eastward to northeastward strikes of the younger generation of fractures visible in Frontier outcrops on the western margin of the basin (Laubach, 1992c). No mineralized macrofractures were intersected in the most highly quartz-cemented sandstone core intervals as determined from point count data of Dutton and others (1991a). Instead, mineralized fractures occur in siltstones and mudstones with predominantly clay and calcite cement (tables 12 and 13).

The relationship of fracture mineralogy to diagenesis was studied in 22 thin sections of Frontier sandstones from core of the S. A. Holditch & Associates SFE No. 4-24 well, Chimney Butte field, Sublette County, Wyoming. Fifteen of the samples are from oriented intervals. All samples are oriented parallel to bedding, so that microfracture strikes could be measured. Eight thin sections from quartz-cement-rich intervals were sampled for petrographic microstructural and scanned cathodoluminescence investigation. All eight sections are oriented. Seven of the samples are adjacent to sections point-counted by Dutton and others (1992) and were chosen for their high proportion of quartz framework grains and quartz cement.

In a few samples, fluid-inclusion planes penetrate the quartz cement (table 12), but no transgranular fluid-inclusion planes were observed. Because they cut across cement these transcement fluid-inclusion planes represent postdepositional fractures; they are not inherited features. These observations show that fracturing and quartz precipitation were contemporaneous in these samples. Strikes of fluid-inclusion planes have azimuths that are generally north- to north-northeastward-trending (values range from 199 to 257 degrees; orientation information is described more fully later in this report). The well-clustered azimuths of these microfractures suggest that they are related to a deformation event or events that is of more than grain-scale significance. That is, these microfractures may correspond to a population of macrofractures. Prevalence of quartz-filled microfractures suggests that the observed macrofracture abundance patterns in Frontier core may not be representative of the subsurface fracture population.

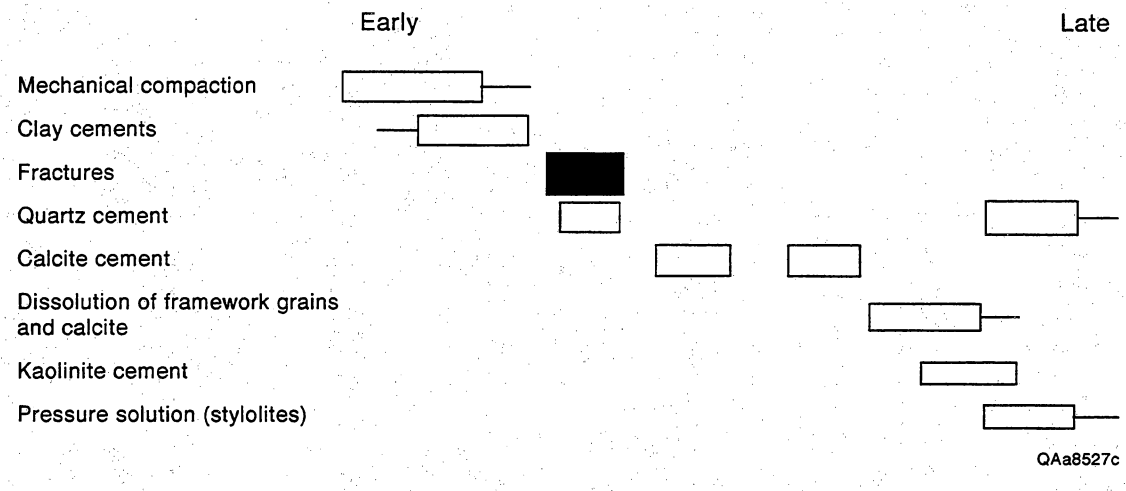

Figure 82. Diagram of composite diagenetic sequence and relative temporal relations of component diagenetic stages of sandstone framework and fracture fill of Frontier Formation. Fracture stage highlighted in black.

Mineralogy of Coal-Inclusion Fractures

Intervals of sandstone containing coalified wood fragments in the Frontier Formation were sampled to characterize mineralogy of fractures in coal inclusions in sandstone. Of seven thin sections from thin coal intervals and inclusions, all but one contain fractures. Coal samples generally have two well-developed, mutually orthogonal sets of vertical opening-mode fractures (such fractures in coal are called cleats). These fracture sets are apparent even in isolated, sub-millimeter-thick seams or inclusions of coal. The fractures end abruptly at the contact between coal and matrix. No mineralized fractures or fluid-inclusion planes were observed in adjacent sandstone beds. In the coal, throughgoing fractures (termed face cleats) generally have a larger aperture and wider spacing than the abutting fractures (butt cleats).

All of the coal cleats sampled are mineralized, with either calcite or quartz or both. Where both calcite and quartz are present in the same vein, lack of clear overprinting relations prevented a sequence of mineralization being established. Vein minerals tend to be blocky in texture, not fibrous. There is no evidence of a crack-seal mechanism of progressive fracture opening and mineralization. In some cases, texture of vein-fill minerals suggests that face cleats were mineralized before abutting cleats were mineralized (figs. 83 and 84). Other intersections of face and butt cleats show coarse-grained calcite infilling both sets, suggesting that they were mineralized simultaneously (fig. 84). Where both quartz and calcite are present in the same thin section, there is no systematic partitioning of minerals between face and butt cleats. These relations suggest that fracture patterns in the coal layers were established before calcite and quartz precipitation. These minerals precipitated as postkinematic fracture fills in preexisting fractures. This is consistent with the conventional interpretation that fractures form in coal at an early stage in burial.

Relation of Sandstone Diagenesis to Fracture Mineralization

Discussion of sandstone-framework diagenesis of the Frontier Formation is presented in Dutton and others (in press). In summary, the major cementation phases of the paragenetic sequence occurred in this order: (1) illite and mixed-layer illite/smectite rims, (2) quartz overgrowths, (3) calcite cement, (4) kaolinite, and (5) additional precipitation of (minor) quartz cement. Early quartz-lined fractures are synkinematic. Later carbonate fracture fills are postkinematic relative to at least some fractures in the formation (fig. 82). However, divergent macrofracture strikes and evidence from Frontier Formation outcrops suggest that at least two separate fracture events affected the formation.

To qualitatively assess the relationship between fracture occurrence, vein mineralogy, and dominant cement type in Frontier Formation cores, 43 thin sections were examined from 6 wells. Samples were taken from intervals where macrofractures had been previously described, highly quartz-cemented intervals,

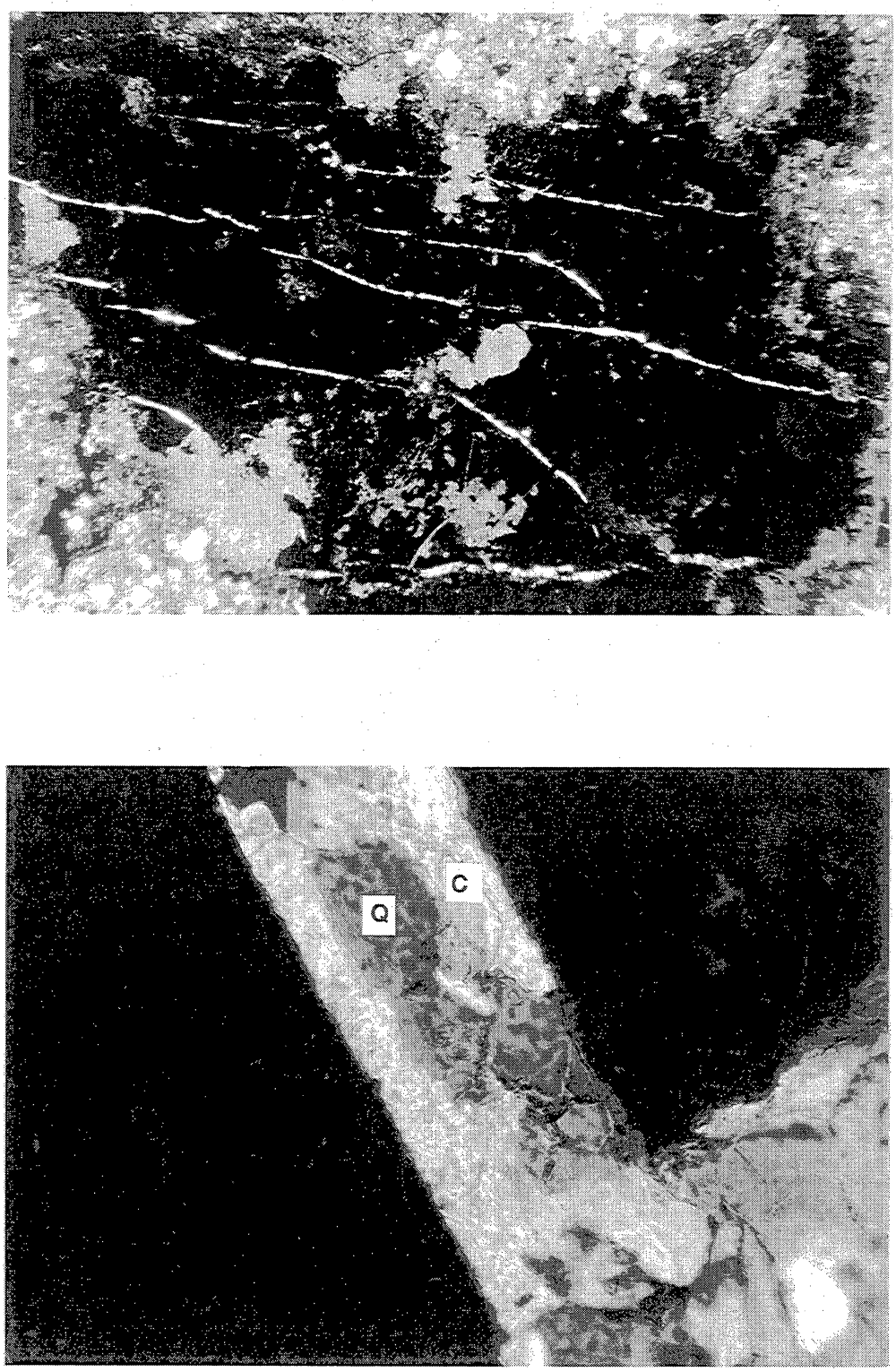

Figure 83. Coal fracture patterns in map view and detail view of fracture mineralogy, Frontier Formation core. SFE No. 4, –7,630 ft. Note uniform strike of fractures in upper image. Note abutting relations among fractures, quartz (Q), and calcite (C) in lower image.

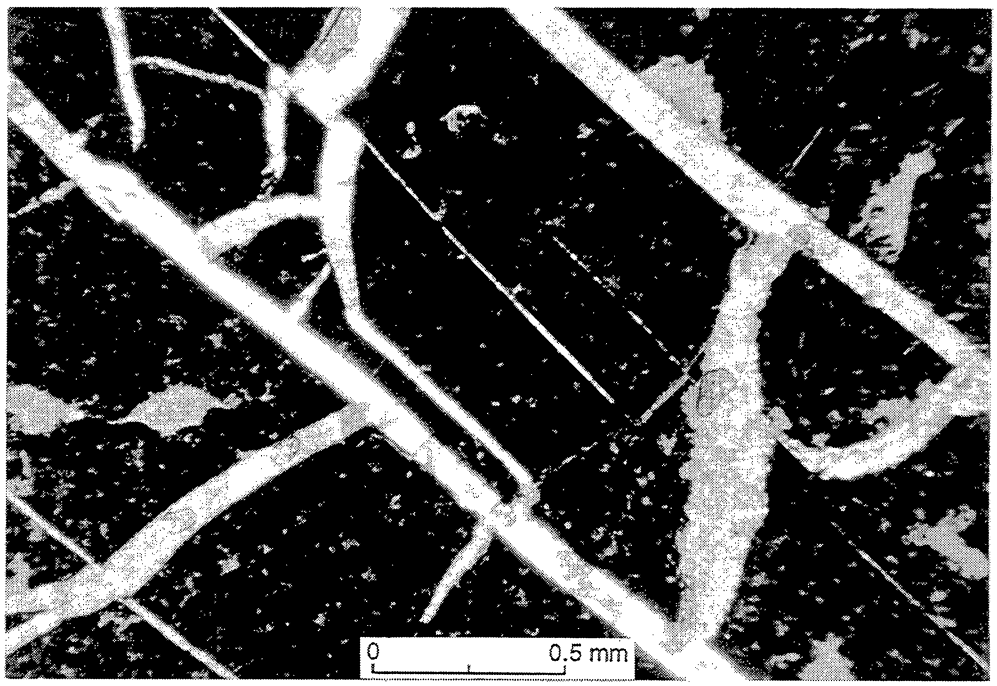

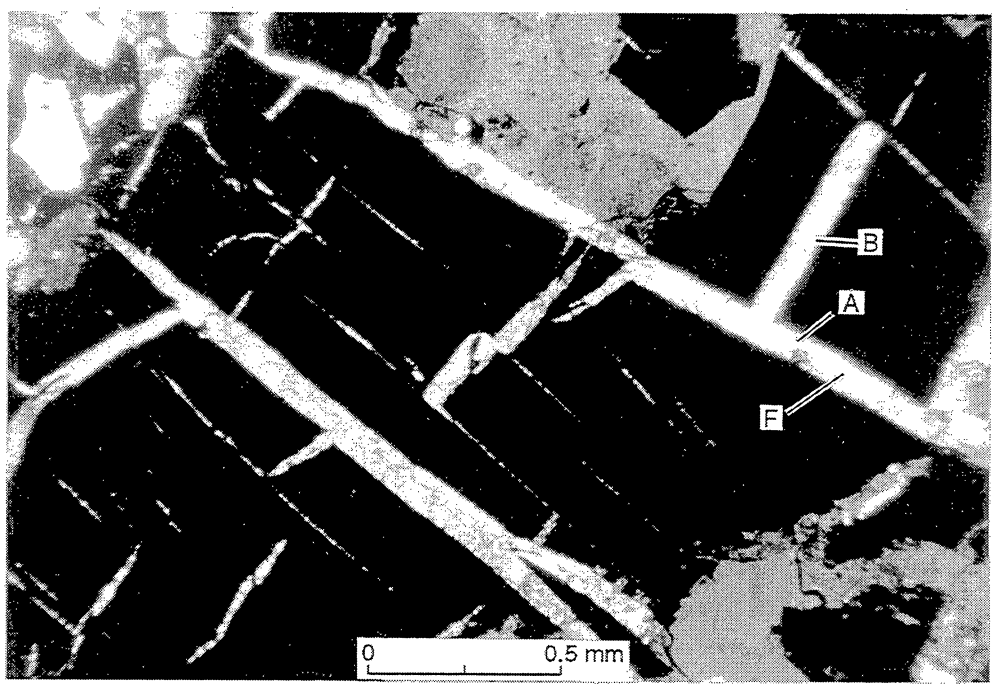

Figure 84. Coal fracture patterns and mineralogy. SFE No. 4, –7,437.8 ft. Plan-view photomicrograph. A, abutting relation of F, face cleat, and B, butt cleat.

and intervals containing coal cleats. Open fractures, open coal cleats, mineralized coal cleats, mineralized veins, and fluid-inclusion planes (FIP's) were found in these samples. The sample depth, mineralogy of vein mineral fill, lithology, and dominant cement type of the rock hosting the fracture were noted for each sample (tables 12 and 13).

Several trends are apparent in tables 12 and 13. All of the macroscopic veins in these samples are calcite-filled. The majority (78 percent) occur in siltstones and fine-grained sandstones that are dominantly clay and calcite cemented. All fluid-inclusion planes (quartz-sealed microfractures) occur in dominantly quartz cemented sandstones. Planar fluid-inclusion planes were found only in quartz grains and quartz cement in these samples. No fluid-inclusion planes were found in samples containing calcite veins. Only four samples contained open fractures—half from quartz-cemented intervals and half from calcite- and clay-cemented intervals. Coal cleats contained either calcite or quartz vein fill, or both. Because the cleats are in coal, sandstone cement type is not listed for these features. However, coal layers and inclusions tend to occur as thin (less than 1 inch thick) layers in siltstones that are dominantly cemented with clay and calcite.

Contrasts in patterns of microfracture occurrence, microfracture orientation (discussed elsewhere in the text), and the diagenetic setting of macrofractures in Frontier Formation cores suggest that sampling bias has affected the type of fracture that predominates in the core collection. The presence of quartz-sealed microfractures suggests that at least one (and possibly two) episodes of synkinematic quartz cementation have affected at least the more deeply buried parts of the formation. In quartz-rich beds that lack substantial postkinematic cement, such fractures are the most likely to be open. Yet, apart from some fractures dominantly filled with postkinematic calcite in the Energy Reserves Group Blue Rim Federal No. 1-30 core and two open fractures in the Terra Anderson Canyon No. 3-17 core, macrofractures with structures that indicate they are contemporaneous with quartz cement are rare. As in the case of the various Sonora Canyon fracture categories, the diagenetic classification of fractures provides a reference point for assessing the clarity of the view of subsurface fractures provided by core.

Controls on Fracture Porosity

Postkinematic carbonate (calcite) precipitates dominate Frontier fractures in core from the Moxa Arch and from outcrop. Fractures from areas east of the Moxa Arch have sparse information on fracture mineralization. However, quartz mineralization along open fractures in some of these cores suggests that synkinematic quartz and open fracture porosity may be more important in these deeper reservoirs than they are in structurally high areas of the arch. If post-kinematic cements are mainly derived from local re-distribution of carbonate, degree of postkinematic fracture occlusion may vary depending on the carbonate composition of the host bed. As described by Dutton and others (in press), the original depositional stratigraphy of the Frontier Formation may play a key role in governing where calcite cement is pervasively developed. Quartz-filled microfractures are also more prevalent in rocks from the deepest wells.

Fracture Stratigraphy from Outcrop Observations

Travis Peak and Canyon examples described in previous sections have beds that localize fractures because they have a particular cement type or particular rock properties resulting from having a critical cement volume. Fracture abundance data can be used to identify these layers. Where vertical core data do not permit effective measurement of macrofracture abundance, as in the Frontier Formation, identification of fracture-prone layers may be possible from observations of outcrop analogs of reservoir rocks. A test of this hypothesis was carried out through examination of the Upper Cretaceous Frontier Formation in the Green River Basin and in outcrops around the margin of the basin. Results of outcrop characterization of fractures have been reported elsewhere (Lorenz and Laubach, 1994; Dutton and others, in press). Outcrop observations can be used to devise a fracture stratigraphy.

Frontier Formation Outcrops

Frontier Formation exposures on the western side of the Green River Basin in southwestern Wyoming are in the limbs of an open, angular-hinged syncline above a thrust fault marking the western Green River Basin and the eastern edge of the Cordilleran overthrust belt. The syncline is a north-trending fault-bend fold produced during eastward transport of the thrust sheet. It contains rocks that were displaced about 8 to 16 km (5 to 10 mi) east of their site of deposition.

Outcrop Fracture Patterns

Most fractures in these exposures are joints or veins oriented normal to bedding. Two prominent fracture sets are evident: north-striking fractures, which formed first, and east-striking fractures, which abutting and crossing relations between fractures show formed later. There are also sets of fractures having other strikes, including a locally prominent northeast-striking set. Beneath veneers of vein-filling quartz (locally) and calcite, plume axes on fracture faces are parallel to bedding (paleohorizontal), consistent with fracture growth in flatlying rocks. In many beds, only north-striking fractures are present, whereas in other beds east-striking fractures are the only fractures present over wide (hundreds of square feet) areas.

Stretching during basin subsidence may account for north-striking fractures, which parallel the depositional axis of the Cretaceous foredeep basin. As the basin subsided, strata were stretched east-west due to lengthening parallel to bedding as the original nearly flat depositional surface adjusted to conform to the asymmetric basin profile. These Frontier Formation outcrops are along the leading eastern edge of the thrust belt. East-striking fractures formed after north-striking fractures when compression related to mountain building was dominant in the foreland, but primarily before local folding and faulting. The convex salient in the foreland basin at this latitude may have accentuated the tendency to form fractures with generally eastward strikes.

Fractures are filled or partly filled with minor quartz, carbonate minerals, and locally, clay minerals. Fracture traces on bedding planes end laterally by intersecting other fractures or by gradually diminishing in width. Fractures end vertically within sandstone beds or at bed boundaries. Because they rarely cross shales between sandstone beds, fracture heights are similar to or less than bed thicknesses, ranging from less than an inch to several feet. Fracture trace lengths, however, can be much greater than fracture heights, with length-to-height ratios greater than 10:1. Although maps of exposures greater than 900 m^2 (2,952 ft) show that fractures with trace lengths of 3 to 30 m (9 to 98 ft) are common, a spectrum of fracture sizes is present, including microfractures normally visible only under the microscope and fractures as long as 830 m (2,722 ft) (Laubach, 1992a). Frontier Formation fractures typically have simple lens shapes and widths ranging from less than 0.2 mm to more than 10 mm.

Attributes of the two fracture sets differ. Fractures formed during burial are uniformly distributed and have a narrow range of trace lengths in beds of a given thickness and composition. Spacing is generally closer in thin beds and beds having extensive early cement. Regionally, north-striking fractures have spacing ranging from inches to several feet, but spacing within a bed is generally uniform. In contrast, the fracture set that formed during regional thrusting has fractures that are clustered into swarms containing fractures ranging widely in length. Swarms of closely spaced fractures are typically simple elongated, lenticular zones having widths that range from inches to more than 48 m (150 ft). Across the margin of a swarm, fracture spacing may change abruptly from feet to inches. Some swarms are separated by rocks having no fractures and others by areas of less closely spaced or less interconnected fractures; swarms are not obviously periodic. These fractures have a wide range of lengths. The loading conditions leading to fracture may be primarily responsible for contrasts in the degree of fracture clustering among fracture sets and for differences in fracture length distributions. The location of fractures, on the other hand, may reflect cementation patterns.

Diagenetic Controls on Frontier Fracture Stratigraphy

In the Frontier Formation, the propensity for a particular fracture set to develop appears to be at least partly controlled by the original composition of the sandstone. Consequently, adjacent beds may contain only one or the other fracture set. Locally, subtle differences in sandstone composition result in drastic shifts in fracture abundance within a fracture set (figs. 85 and 86). This constitutes a type of fracture stratigraphy in which various fracture facies can be recognized. Contrasts in rock composition, including cement composition, and mechanically significant bed thickness can result in abrupt shifts in fracture intensity and dominant fracture orientation.

Lorenz and Laubach (1994) described possible compositional controls on fracture orientation and abundance in these outcrops, and the following summary follows their discussion. Bed thickness, structural position, and depositional environment do not show consistent patterns that could account for the fracture pattern. This leaves petrophysical properties as the probable main control on the susceptibility of the rock to fracture through time.

Petrologic observations suggest that four diagenetic fracture facies can be distinguished within the fracture stratigraphy. Within each group, porosity, grain size, sorting, and depositional environment vary enough that none of these factors alone is likely to account for the differences in fracture orientation. The basic mineralogical composition of the sandstones is similar. Diagenetic sequence, particularly the presence of early quartz cement, appears to be the most important

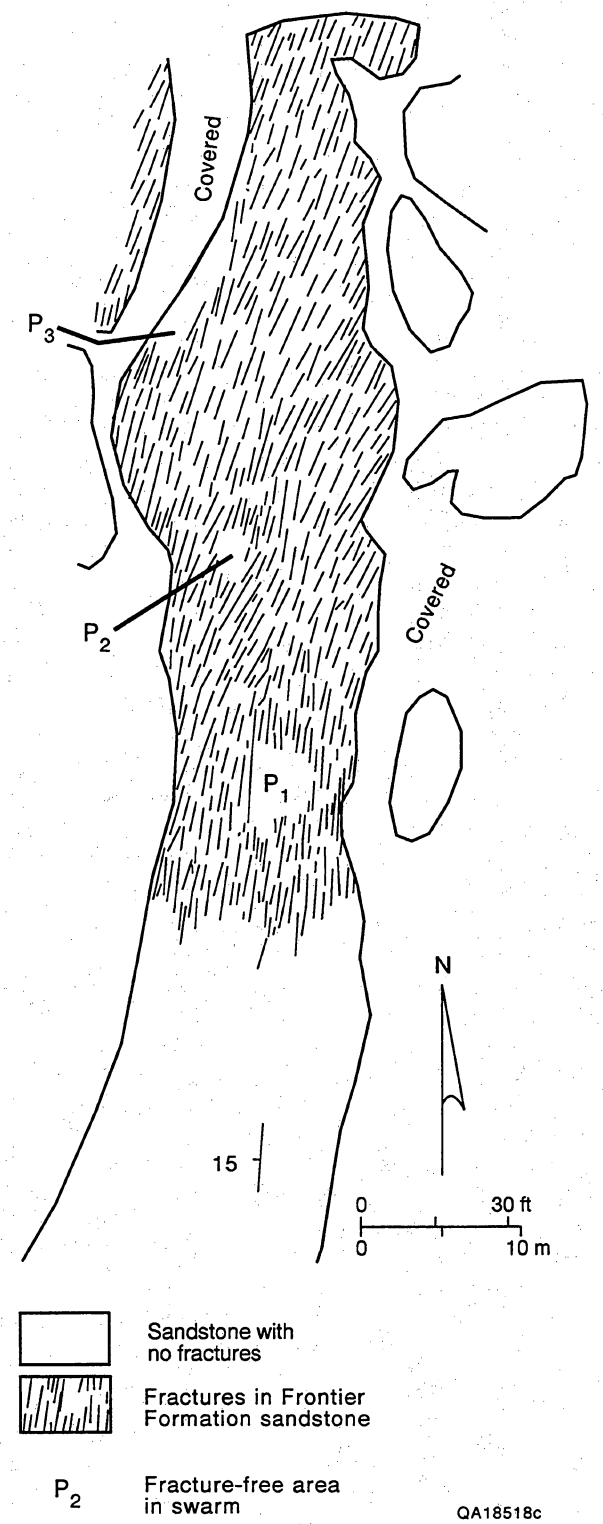

Figure 85. Fracture trace patterns in a bedding-plane outcrop of Frontier Formation sandstone, near Kemmerer, Wyoming (Sec. 36, T23N, R116W). Abrupt shift in fracture abundance corresponds to a slight change in rock composition.

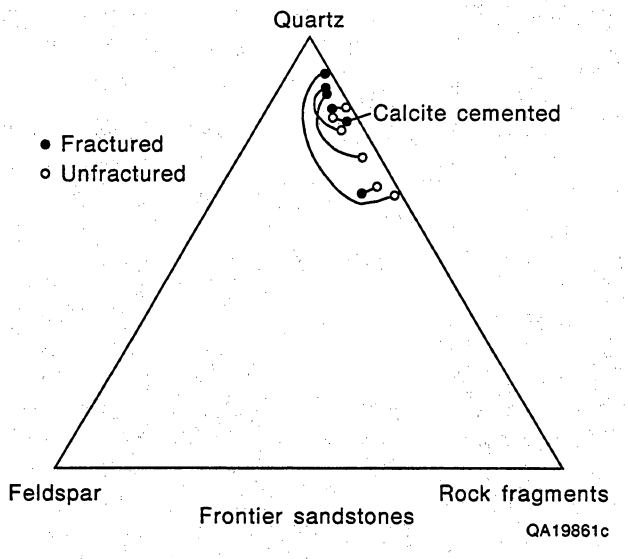

Figure 86. Compositional information from the outcrop of Frontier Formation sandstone, near Kemmerer, Wyoming (Sec. 36, T23N, R116W) shown in figure 85. Lines connecting data points indicate samples within (open circles) and outside (filled circles) the fractured area. Data from S. P. Dutton.

variable. Volume of clay matrix, authigenic clay minerals, and organic components also probably contribute to variability in mechanical properties.

In the study area, beds containing north-striking fractures have evidence of early quartz cement and lack calcite cement. Although surface-related weathering may have affected the outcrop where these samples were obtained, there is no evidence that a later phase of calcite cement ever was present. Fractures may have formed in these rocks during or after quartz cement precipitation caused these sandstones to become brittle. The presence of quartz-filled microfractures suggests that this event may have involved synkinematic quartz cementation that created the higher strength rock properties that caused these beds to be prone to fracture.

The amount of quartz cement necessary to create these fractured beds may have been volumetrically small. In beds having north-striking fractures, fracture abundance locally shifts abruptly within beds (fig. 85). According to petrographic observations from one outcrop, such features may reflect slight differences in quartz cement volume at the time of fracturing. The origin of the contrasts in quartz cement volume may be related to small differences in original sandstone composition. Slightly higher concentrations of unstable chert grains may have led to the development of a rigid grain framework when adjacent parts of the same bed were free to deform without the development of throughgoing fractures. Thus, chert concentrations that are higher than a certain threshold value correspond to abrupt differences in fracture abundance. Disseminated chert grain concentrations are unlikely to have any direct effects on a sandstone's mechanical properties. But at shallow burial depths chert is chemically unstable compared to other siliceous rock fragments. Chert dissolution and silica reprecipitation are likely in chert-rich sandstones, with early precipitation of quartz cement. Even minor amounts of cement could strengthen a sandstone.

Beds with only east- and northeast-striking fractures have little or no early quartz cement but contain abundant calcite cement. Lack of early quartz cement is the reason north-striking fractures did not form in these beds. Lorenz and Laubach (1994) inferred that these beds were poorly cemented and relatively less brittle during the time north-striking fractures formed, but they were cemented with calcite and susceptible to fracture by the time east- and northeast-striking fractures formed.

As indicated by textural contrasts between veins-fill calcite and cement, some calcite cementation was prekinematic with respect to the formation of east-striking fractures. This calcite is postkinematic with respect to north-striking fractures, accounting for calcite after quartz. Postkinematic calcite (possibly a later generation of calcite) also fills east-striking fractures. Beds having both north- and northeast-striking fractures appear have both early quartz and calcite cement. These rocks may represent an intermediate type of fracture-prone stratigraphic element. All of the above fracture facies are localized in clean upper shoreface to marine sandstones. Another fracture facies that is evident in outcrop is lower shoreface sandstones that have a significant proportion of rock fragments, detrital clay, and organic material. These beds generally lack or have few systematically oriented fractures in outcrop.

Comparison with Subsurface Fractures

The fracture-filling mineral sequences in Frontier Formation fractures are consistent with those observed in outcrop, although the number of fractures recovered in core is so small that these conclusions must be tentative. Nevertheless, applying the criterion of cement timing to subsurface fractures and cements shows that examples of cement timing relative to fracture movement similar to those observed in outcrop can be seen in subsurface examples. Petrogenetic evidence suggests that vein-filling minerals are contemporaneous

with early Frontier Formation cements. This strengthens the interpretation, based on other evidence, that the fractures in outcrop are likely to be represented in the subsurface (Laubach and Lorenz, 1992). Indirect tests of rock strength anisotropy may be useful for identifying the outcrop fracture stratigraphy in the subsurface, as described in the sections of this report on rock strength and rock strength anisotropy. These tests show differences in strength anisotropy that in part correspond to differences in volume of quartz cement.

Geologic Controls on Fracture Abundance

In reservoir rocks, the geologic parameters that are generally considered important for controlling fracture abundance include rock composition, bed thickness, and structural history. Generally, all of these parameters will have some effect on observed fracture patterns. The following section of the report discusses rock composition control on fracture abundance and how diagenetic classifications can be used to identify and interpret fractured or fracture-prone layers in sandstone. This is prefaced by the following summary of previous work on compositional controls on fracture abundance. Because other geological controls on fracture abundance must be separated from compositional effects in order to identify fracture-prone layers, these other geological factors are also first briefly reviewed.

Bed Thickness

Bed thickness-fracture intensity correlations need to be accounted for in comparative studies of fracture abundance. Many workers believe that fracture (joint) spacing is proportional to the thickness of the fractured layer. The role of bed thickness in controlling fracture intensity is discussed or reviewed by Price (1966), Hobbs (1967), Sowers (1972), McQuillan (1973), Ladiera and Price (1981), Verbeek and Grout (1984), Nelson (1985), Laubach and Tremain (1991), Narr and Suppe (1991), Rives and others (1992), and National Research Council (1994). Beds, in this usage, are defined by the distributions of fractures (fig. 87). That is, fractured layers are not necessarily equivalent to beds defined by depositional facies or rock composition.

The studies cited above document a tendency for more closely spaced fractures to occur in thinner beds. The relationship is generally best documented for beds that are relatively thin, on the order of a few meters or less. Fracture spacing-bed thickness relations are typically nonlinear, especially when thick beds are considered. Moreover, different fracture sets in a given sandstone can have markedly different fracture spacing (for example, Rives and others, 1992; Lorenz and Laubach, 1994). Fractures may be in swarms rather than in evenly spaced sets (Hodgson, 1961; Dyer, 1983; Laubach, 1991; Laubach and others, 1995). Yet in areas where fractures in thick beds or thick brittle units are distributed in swarms, the spacing of the swarms may still be controlled by the thickness of a thick brittle layer (figs. 88 and 89). However, there is little available information on swarm spacing with which to test this hypothesis.

Subsurface fracture-spacing patterns may differ substantially from those in outcrop. Data from outcrops where surface-related fractures can be identified (Laubach and Tremain, 1994), directionally drilled wells (Lorenz and Hill, 1991), and from tunnels (Nance and others, 1994; Laubach and others, 1995) show that for beds of a given composition and structural history, fracture spacing can be drastically closer or wider than fracture spacing-bed thickness relations derived from outcrop patterns predict. Recent experimental and numerical studies (Wu and Pollard, 1991; Rives and others, 1992) suggest that joint spacing evolves with time, strain magnitude, strain rate, and possibly other factors.

Layer thickness and its influence on fracture abundance is a potentially important cause of differences in fracture abundance observed in core samples both within and among formations. Close fracture spacing may account in part for high fracture abundance in some thin-bedded sandstones where bed thickness is of similar dimension to core diameter, such as fractured siderite-cemented layers in Sonora Canyon sandstones (Marin and others, 1993) and thin-bedded Davis Sandstone (Collins and others, 1992). In the formations in this report, this relationship—and associated sampling bias—may in part explain why thin-bedded Canyon Sandstone core tends to have more fractures than medium-bedded Travis Peak and thick-bedded Frontier sandstones.

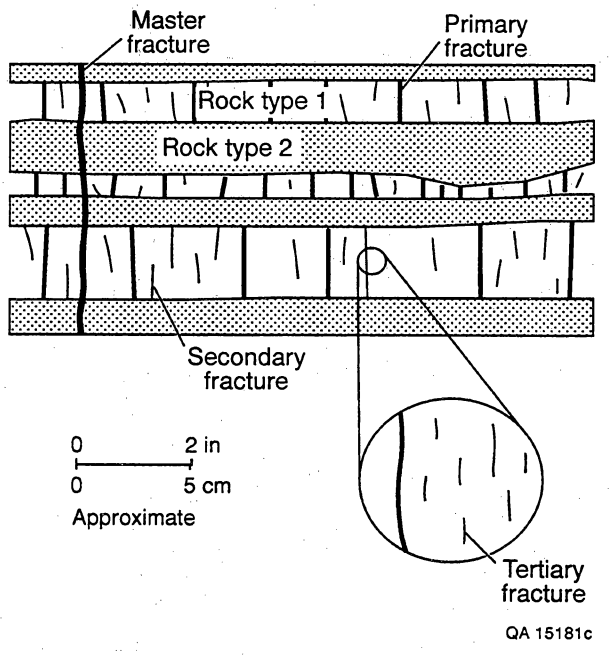

Figure 87. Typical hierarchy of fracture sizes in a sequence of beds having different thicknesses. Secondary and tertiary (i.e., small) fractures are commonly evident in coal beds. They have not been widely documented in sandstone. Many fractures observed in sandstone core are secondary fractures according to this nomenclature. Sealed microfractures are tertiary fractures in this scheme.

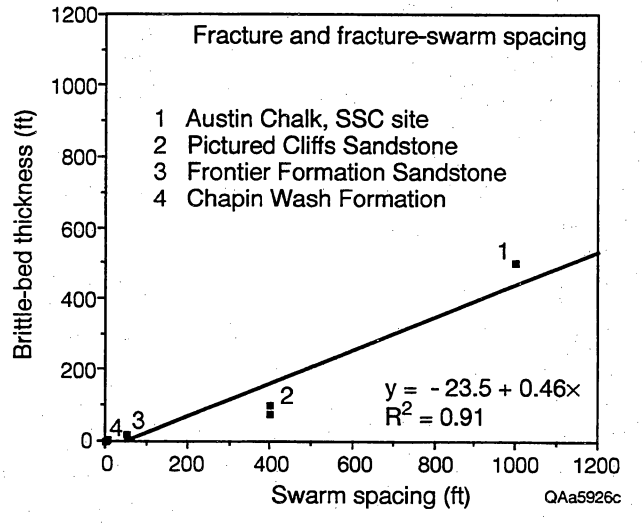

Figure 88. Fracture fracture and fracture-swarm spacing as a function of bed thickness for several units. Swarms in beds or stratigraphic intervals of various thickness.

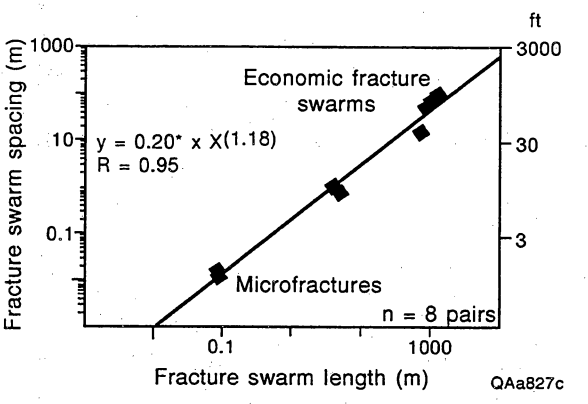

Figure 89. Swarm spacing versus swarm length, bed of uniform thickness, Frontier Formation.

Structural History

Structural position, such as proximity to fold hinges or to fault zones, can be a good predictor of areas of high fracture abundance. For brittle rocks that fail predominantly by fracture, greater strain generally corresponds to an increase in fracture intensity. Methods such as analysis of bed curvature have been used successfully to identify fractured areas (Schultz-Ela and Yeh, 1992). For a given fracture-prone layer, structural position may be key to locating areas where fractures actually occur. Many fractured tight gas sandstones are in areas of relatively flatlying rocks, and in this study we focused on areas where folds and fault zones were not responsible for localizing fractures. Tectonic and burial loading and fluid flow history can affect the timing and mode or regional fracture growth (Engelder, 1985). These processes also have an impact on diagenetic history. In this sense, structural history and diagenesis are linked, and rock diagenetic composition can be directly and indirectly affected by tectonic processes.

Composition

Composition is the main control on the strength and brittleness of sandstone, and variations in rock composition leads to differing strength, brittleness, and susceptibility to fracture. Fracture stratigraphy can be defined by beds having either differing fracture abundance or fracture susceptibility.

For a given bed thickness and structural history, the conventional interpretation is that stronger, more brittle rocks tend to have more abundant fractures (Nelson,

1985). This pattern is most readily apparent in outcrops where near-surface weathering and unloading processes have controlled fracture growth, but observations or fractures in subsurface sandstone also generally support this view. The principal compositional variables that control sandstone strength and brittleness are detrital grain composition, porosity, grain size, and the type and distribution of cement. In general, sandstones with high percentages of brittle constituents, such as quartz, feldspar, and dolomite, will be more prone to fracture (Stearns, 1968; Currie, 1974; Sinclair, 1980). Sandstone with lower porosity tends to have higher strength (Price, 1966; Dunn and others, 1973; Hoshino, 1974), and this relationship is evident in the Travis Peak Formation (Jizba and Nur, 1990; Plumb and others, 1992).

Lower porosity rocks tend to have more numerous fractures than sandstones of higher porosity (Nelson, 1985). In many tight gas sandstones where porosity is generally low, porosity variation commonly has only a slight effect on strength. Decreasing grain size corresponds in some cases to increasing rock strength (Gallagher, 1976) and a tendency to more intense fracture development, but the effect may be slight. Fracture spacing may also depend on elastic properties of rocks, with spacing being closer in stiffer rock of comparable thickness. Fracture development and overall rock-mass deformability can evolve together and interact, as recent boundary element models illustrate (Piscoran and Schultz, 1994). This may be an important consideration where synkinematic cementation has occurred.

Recent tests on synthetic granular material (rock analogs) show that the composition, amount, and location of cement have a primary control equal to that of porosity on evolving mechanical properties (David and others, 1994). As cement volume increases, strength and elastic moduli increase. More highly cemented materials also show more dilatancy and brittleness. Thus, in comparable structural settings, highly cemented sandstones should show a tendency to have more natural fractures than do less cemented sandstones.

However, the distribution of cement can play nearly as important a role as cement volume. Experiments such as those of David and others (1994) show how small amounts of cement can drastically alter rock properties, producing stronger rocks. An example of this effect is the Frontier Formation, where shifts in fracture abundance can be ascribed to small contrasts in cement concentration. The Austin Chalk also provides an example. Corbett and others (1982; see also Collins and others, 1992) showed that different parts of the Austin Chalk have differing strengths and fracture abundance, and that these contrasts appear to correspond to clay-mineral volume in chalk beds. Observations and measurements by one of us of Austin Chalk show, however, that clay-mineral volume may be less important to fracture abundance than clay minerals distribution in the chalk (S. Hovorka and H. Baek, unpublished SEM observations and fracture toughness tests, 1994). In this example, equal volumes of detrital clay in pore spaces are less important for reducing rock strength than authigenic clay that coats individual chalk particles. Similar controls caused by variations in quartz cement distribution on sandstone rock strength properties were observed by Plumb and others (1992) in Travis Peak sandstones.

Cement Types and Fracture Attributes

Diagenesis information can be used to augment fracture interpretation. The preceding examples show how variations in the volume of pre-, syn-, and postkinematic cement can guide expectations about fracture attributes. This classification also helps in assessing the completeness of fracture information derived from cores.

Implications of Prekinematic Cement

Cements that predate all fracturing events are rare in the formations that we studied. In this category are main cements that were precipitated at shallow depths of burial. Siderite-cemented layers and their associated fracture class in Canyon sandstones are a particularly clear example of a fracture stratigraphic unit in a prekinematic cement layer: fractures are localized within layers, they stop at cement-layer boundaries, fracture height increases with increasing layer thickness, and fractures are less abundant in thick siderite-cemented layers than in thin layers, as is expected if there is wider fracture spacing in thick beds. Siderite cement is prekinematic with respect to fractures; there is no siderite in fractures in siderite-cemented layers. Cement composition does not directly indicate the type of mineralization that is in the fracture, except that fracture-filling minerals will not be one of the prefracture cement generations. The minerals in these fractures are part of the postkinematic cement suite. There is no direct microstructural evidence in the prekinematic cement that fractures exist in these layers. Such layers could lack fractures if appropriate structural events fail to occur after cementation.

Although cements form under characteristic burial and geochemical conditions, any cement type can in principle form at any time relative to fractures. Thus, in the case of the Sonora Canyon, areas or intervals with dense siderite cement merely became indurated early in the rock's burial history when conditions leading to fracture did not exist. Diagenetic models can be used to predict the occurrence of siderite cement, and thus to predict fracture occurrence. Because siderite cementation occurred in the shallow subsurface and was influenced by sediment composition, depositional patterns may be useful for predicting where abundant siderite is to be found (Laubach and others, 1994).

Implications of Synkinematic Quartz Cement

The Canyon Sandstones, Travis Peak Formation, and Frontier Formation all contain synkinematic quartz cement. The volume of these cements is highly variable among the units and falls within the various units. In some cases, this cement type is restricted to particular parts of the play. Depth and time of exposure to high temperature burial conditions may be a key control (Dutton, 1994). Many fractures in these beds had significant porosity after synkinematic cementation ceased, despite their occurrence, in some instances, in highly cemented rocks.

If the Travis Peak Formation samples are representative of synkinematic quartz cements, then the origin of cements and fractures in the Travis Peak has widespread implications for where and when such fractures and cement relations will occur. Microstructures in Travis Peak fractures and quartz cements are similar to those of other sandstones with early synkinematic quartz cement, such as parts of the Canyon Sandstone and Frontier Formation. Consideration of other sandstones having quartz cement described by Dutton and others (1993) suggests that these cementation and fracture histories are not unusual. For example, the description of fractures in Mesaverde Group sandstone from the Piceance Basin by Pittman and Sprunt (1986) closely resemble the pattern of the Ozona Canyon sandstones. Photomicrographs presented by Pittman and Sprunt (1986) appear to show early crack-seal-type features in vein quartz. We interpret these features to be possibly indicative of synkinematic quartz in this area.

On the basis of fluid inclusion and isotopic data from fracture-filling quartz and scanned CL evidence that fracture occurred at the same time as the main phase of quartz cementation, we interpret quartz cements in the Travis Peak Formation to have precipitated at depths between 1.6 and 3.2 km (1 and 2 mi). Multiple episodes of quartz cementation may have resulted from changes in burial depth caused by two periods of movement of the Sabine Arch (fig. 90). These depths are consistent with fluid-inclusion thermometry. At these depths expulsion of silica-saturated waters from clay minerals within sandstones and from interbedded shales may have provided sources for quartz cement, consistent with oxygen isotope information.

The source of water and silica for cement is controversial. Scanned CL observations show that silica was not derived mainly from within clean sandstones by pressure-solution processes. Stylolites are widespread in the lower Travis Peak, but they are in part derived from stylolitic bedding planes, and their distribution may ultimately be controlled by both burial depth and stratigraphy. Although the sandstones are all net importers of silica, silica redistribution within sandstones may be reflected in the contrasting textures of sandstones having sutured contacts and/or stylolite zones (local silica sources), microfractured zones (conduits), and point-contact-texture sandstones with highly zoned cements (sinks).

This mechanism implies that sandstones reach a depth and temperature threshold where quartz cementation commences. The Travis Peak example was situated in a tectonic setting of relative structural quiescence at the time of quartz cementation, which suggests that no superposed tectonic events are required to cause fractures to grow in conjunction with the postulated diagenetic threshold. Diagenetically controlled increases in pore-fluid pressure may be sufficient to drive natural hydraulic fractures in this environment. If this is so, synkinematic quartz cementation—and partly open fractures—may be a natural consequence of the thermobarometric history of sandstones in subsiding basins. The degree of fracturing may be predictable from burial history and petrographic evidence of the progress of the quartz diagenesis process, with more highly fractured beds corresponding to areas of advanced cementation. A marker of the diagenesis reaction progress that can in principle be detected on geophysical well logs is the development of stylolites. Both Canyon and Frontier sandstones also have early synkinematic quartz cements and partly open fractures, and for the Frontier Formation at least, length of time exposed to deep burial conditions appears to correspond to increasing degree of quartz cementation (Dutton and others, in press).

The orientation of fractures in such a setting should be aligned with maximum horizontal compressive stress that existed at the time strata reached the depth-and-temperature controlled threshold. Thus, structural

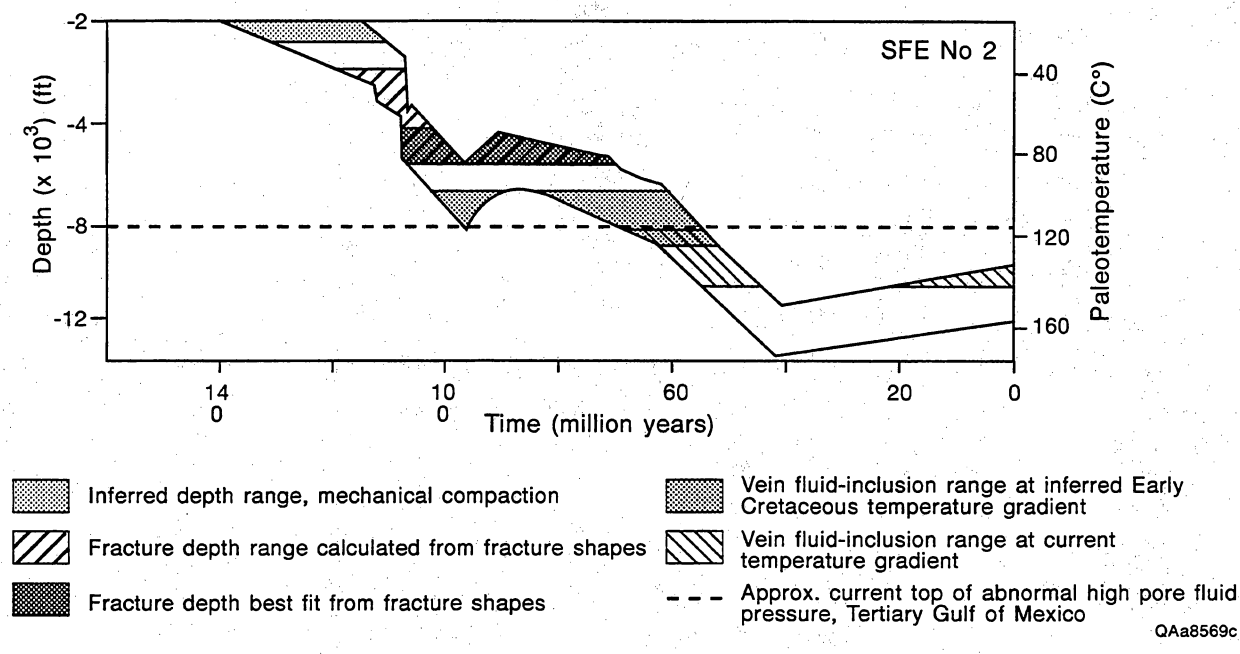

Figure 90. Travis Peak Formation burial history curve, showing timing of various events. In part after Dutton and others (1991a).

models for predicting or modeling fracture development can be greatly refined. Numerical models for the western United States that depict stress trajectories for a particular set of boundary conditions are presented in the report section "Using Microstructure and Test Data to Map Fracture Strike." By comparing the burial history and timing of synkinematic cementation of a particular unit with such regional paleostress models, local fractures patterns can be more accurately predicted. Elsewhere in this report we describe how such predictions of fracture patterns can be verified by new fracture mapping methods.

Implications of Postkinematic Cement

Ozona Canyon and Frontier Formation examples show how extensively postkinematic cements can occlude porosity in both matrix and fractures. Ankerite cement in the Ozona Canyon is the dominant porosity occluding phase in matrix porosity, filling ~60 percent of minus-cement porosity. It is also responsible for filling between 60 and 100 percent of fracture porosity. In contrast, only minor amounts of postkinematic ankerite are developed in most of the Travis Peak Formation, and ankerite within fractures is also sparse. These relations suggest that by assessing the degree of development of postkinematic cement in a given bed or stratigraphic interval, diagenetic analysis can provide direct insight into how likely it is that substantial fracture porosity has survived in a given layer. Maps of high postkinematic cement concentration could be used as guides to areas of poor predicted fracture permeability.

Identifying Fracture-Prone Layers on Geophysical Well Logs

The techniques and technology to directly identify and characterize fractures with borehole-imaging logs, such as acoustic borehole televiewers or pad-type electrical resistivity tools (i.e., Formation Microscanner), are highly advanced, and the use of these tools is described elsewhere (for example, Ekstrom and others, 1986; Fertl, 1990; Laubach and others, 1990). Where fractures intersect the wellbore, or where there is a good chance that they will, as would be expected, for example, in a horizontal well, such imaging logs are ideal for documenting fracture occurrence. Ultimately, such data can be used to construct empirical fracture stratigraphies.

However, it is desirable to know where fracture-prone or fractured layers are *before* drilling horizontal wells. In vertical wellbores that typify many sandstone natural gas plays, the direct measurement approach has a bias against intersecting and sampling vertical fractures, and a large number of wells may need to be logged or cored before fracture abundance patterns become evident. Other, related logging techniques to detect fractures include methods using conventional logs, Stoneley wave reflection, acoustic/full waveform logs, caliper logs, and temperature logs (for example, Aguilera, 1980; Cheung, 1984; Mathieu and others, 1985; Lehne, 1990). None of these methods can identify fracture-prone beds.

A different approach that does not depend on detecting fractures directly is to find log-measured properties that correlate with fracture occurrence or susceptibility to contain fractures. By calibrating logs with core observations, log character can be used to map fracture-prone layers. Thus, a fracture need not be present in the wellbore for the fracture-prone layer to be detected and mapped.

There are at least three ways this approach can be carried out and such layers traced using currently available logging devices. First, a rock type or distinctive rock property that correlates with high fracture abundance can be tracked using conventional gamma-ray, resistivity, density, or other common log type. Second, borehole-imaging logs can be used to image and track small-scale features that are distinctive of naturally fractured or fracture-prone beds. Finally, measurements can be made of rock mechanical properties that are expected to correlate with fracture susceptibility. The first technique is most appropriate where fractured beds have distinctive or unusual composition. An example are iron-rich prekinematic cements in the Sonora Canyon. The use of rock properties alone, particularly where fracture susceptibility is governed by prekinematic cements, is best applied where there is evidence of late-stage deformation to create fractures. Late stage in this case means a deformation event that postdates all volumetrically important porosity-occluding cements. In these areas, the target fractures would all be in beds composed of prekinematic cements.

Conventional Logs and Prekinematic Cement

An example of a distinctive rock property that can be tracked using conventional logs is diagenetic siderite layering in the Sonora Canyon sandstones. Siderite-cemented layers are fractured beds that should be detectable because of the unique, distinctive iron-rich composition of the siderite-cemented layers. Moreover, contrasts in porosity and density between siderite and nonsiderite-cemented zones might make siderite layers distinct on logs such as the formation density (RHOB) log. The photoelectric absorption index (Pe) curve is a sensitive indicator of iron-rich mineralogy, and it is measured simultaneously with apparent bulk density by the Schlumberger litho-density tool (LDT).

A study of North Sea sandstones that have siderite layers shows that this curve responds dramatically to thin beds of sideritic mudstone only 10–15 cm thick that have as little as a few percent siderite (Humphreys and Lott, 1990). Sideritic sandstone layers in Sonora Canyon sandstones have similar dimensions and concentrations of siderite, so detection of the siderite layers in these sandstones is possible in principle. However, Pe curves on logs showed little or no response over wellbore intervals having siderite layers that had been documented in core (fig. 91). Poor wellbore conditions or muds with high barite concentrations can interfere with the Pe curve response, but the Sonora Canyon wells we studied did not contain barite muds, and hole conditions were good. Wireline data are commonly running averages, and it may be that the reason siderite layers were not detected in these wells is that in the Sonora Canyon, siderite layers are too thin to be detected with the tool resolution and logging rates we used. Verification of this approach requires experimentation with logging parameters.

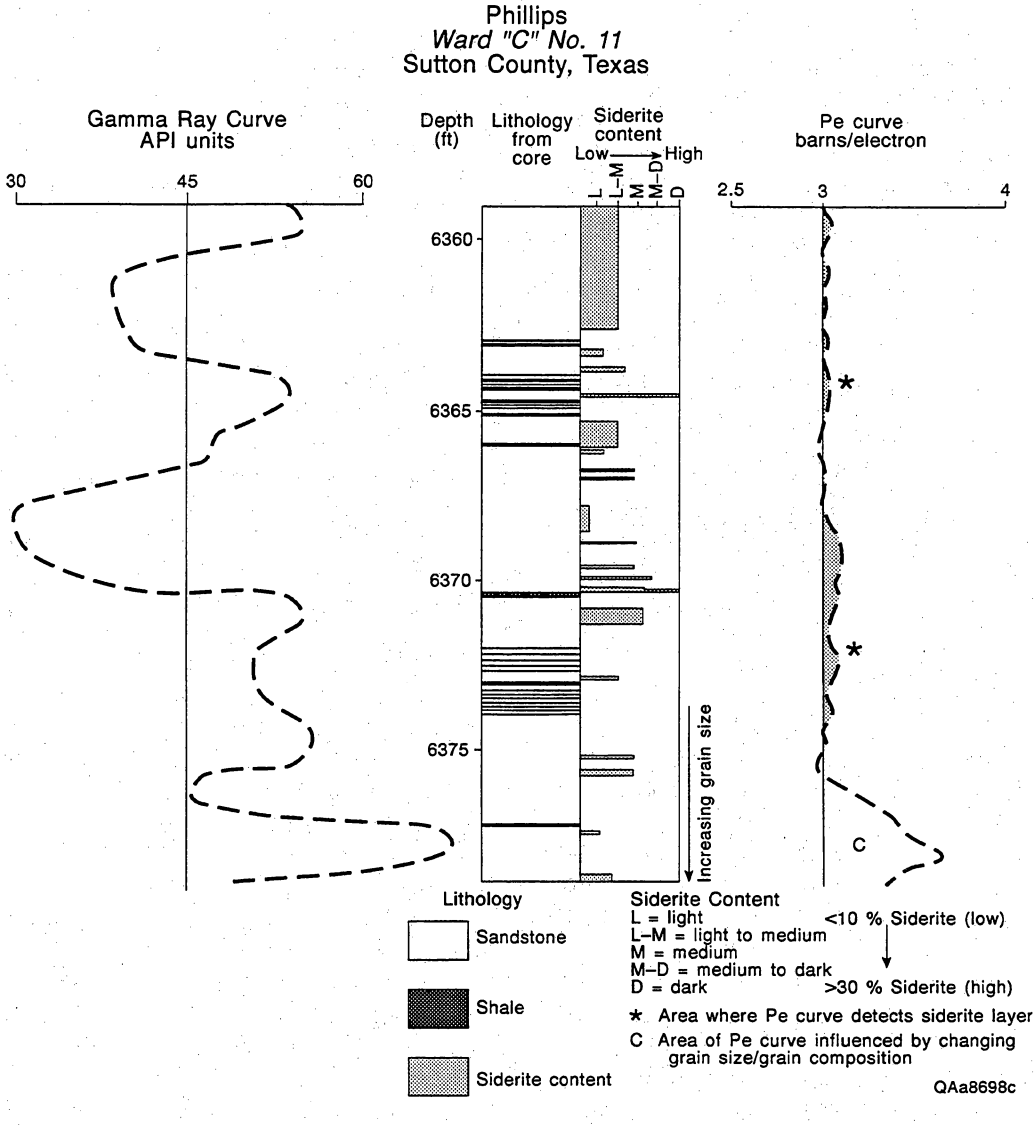

Figure 91. Sonora Canyon sandstone Pe log curve and occurrence of siderite-cemented layers from core data, Phillips Ward "C" No. 11 well. Siderite-cemented layers are not evident on the log.

In summary, we were not able to distinguish siderite layers using density or gamma-ray logs, but there is no reason that properly calibrated or adjusted geochemical logs cannot detect and identify highly siderite-cemented zones. This shows that there is scope for further utilization of detailed mineralogical analysis of logs for detection of mineralogically distinctive fracture-prone beds in the Sonora Canyon and other formations having similar cements. On the other hand, our diagenetic/fracture stratigraphy analysis shows that the siderite-cemented layers may not be the most important fracture stratigraphic unit in the Sonora Canyon. The prime cause of extreme induration in many sandstones is quartz cement, and quartz-cement volume is likely to be the mineralogically distinctive factor in many fracture-prone sandstone beds. For example, as described elsewhere in this report, quartz-cement volume is the most important variable governing point-load strength in the Sonora Canyon and Travis Peak Formation. No currently available logging devices can readily measure quartz-cement content or quantify this critical diagenetic feature.

Imaging Logs

The second approach to tracking fracture-prone layers with logs is to use borehole-imaging logs to detect features (other than fractures themselves) that are distinctive of fracture-prone beds. Thin features such as siderite layers are visible on Formation Microscanner logs. However, borehole-imaging logs may permit mapping of distinctive features in zones that are primarily cemented with quartz. An example of such a feature is the variation in concentration of subhorizontal stylolites in sandstones. Stylolites are sutured to wavy, generally clay-rich seams that result from a combination of dissolution (Tada and Siever, 1989) and fracturing (Milliken, 1994). With current borehole-imaging logs, such features can sometimes be detected and counted, although they are not always readily identified or interpreted as stylolites in the absence of core because they can resemble other types of stratification. Figure 92 shows an example of possible stylolites visible on borehole-imaging logs.

Stylolites are features that are characteristic of some synkinematic quartz-cemented layers, and thus they are an indirect guide to the presence of fractures. However, we found that wellbore images from logs of Canyon and Travis Peak wells could not be effectively used for identification and interpretation of stylolites and stylolite-rich beds because of uncertain stylolite identification. We conclude that currently this is not a practical approach. However, manipulation of images on workstations and calibration of images with core could yield an acceptable level of reliability that would permit stylolite mapping in the wellbore.

Stress Profile Log Suites

A third log approach to fracture susceptibility mapping involves use of combinations of log-derived properties to track rock mechanical properties that correlate with fracture susceptibility. In areas of dense synkinematic quartz cement, such as in the Travis Peak Formation, this approach can be used to highlight thin beds that core analysis shows are also extensively fractured (fig. 8). For example, the log signatures in figure 8 are not responses to the fractures themselves. Instead, they reflect areas of stiff, highly quartz-cemented clean sandstone, and thus they are logs that identify fracture-prone layers. The correspondence of observed fractures and positive log responses in Travis Peak wells is an indication that this approach is valid yet rigorous verification is hampered by fracture sampling bias. This formation is more uniform in its cementation patterns and the character of its fracture stratigraphy than, for example, the Sonora Canyon or Frontier Formation. Analyses of cement patterns, starting with subdivision of the formation based on analyses such as those shown in figure 5, are necessary before log interpretation can be carried out successfully.

Such rock-property logs are based on density and acoustic measurements that are typically compiled from a suite of logs. They also incorporate estimates of formation rock type. These logs were devised in the search for wireline methods to measure in situ stress (Whitehead and others, 1989; Gas Research Institute, 1992), and the construction of these profiles is described in that literature. Log-derived stress profiles require gamma-ray, SP, resistivity, density, neutron, and acoustic logs. Other logs are processed to determine values of porosity, water saturation, and rock type, but the acoustic logs can be processed to obtain values of compressional velocity and shear velocity. These values can be used directly to track beds having high compressional and shear velocities diagnostic of highly quartz-cemented beds. Alternately, these results can be combined with other log information to create derivative logs that highlight rock properties that are known to correlate with fractured beds (figs. 76 and 77), as originally shown by E. Hunt (personal communication, 1993).

Currently it is not possible to accurately and directly measure fracture abundance in areas of the subsurface that are much bigger than the wellbore without using horizontal wells. Most accurate data on subsurface fracture abundance are available where fracture spacing has been measured in horizontal or highly

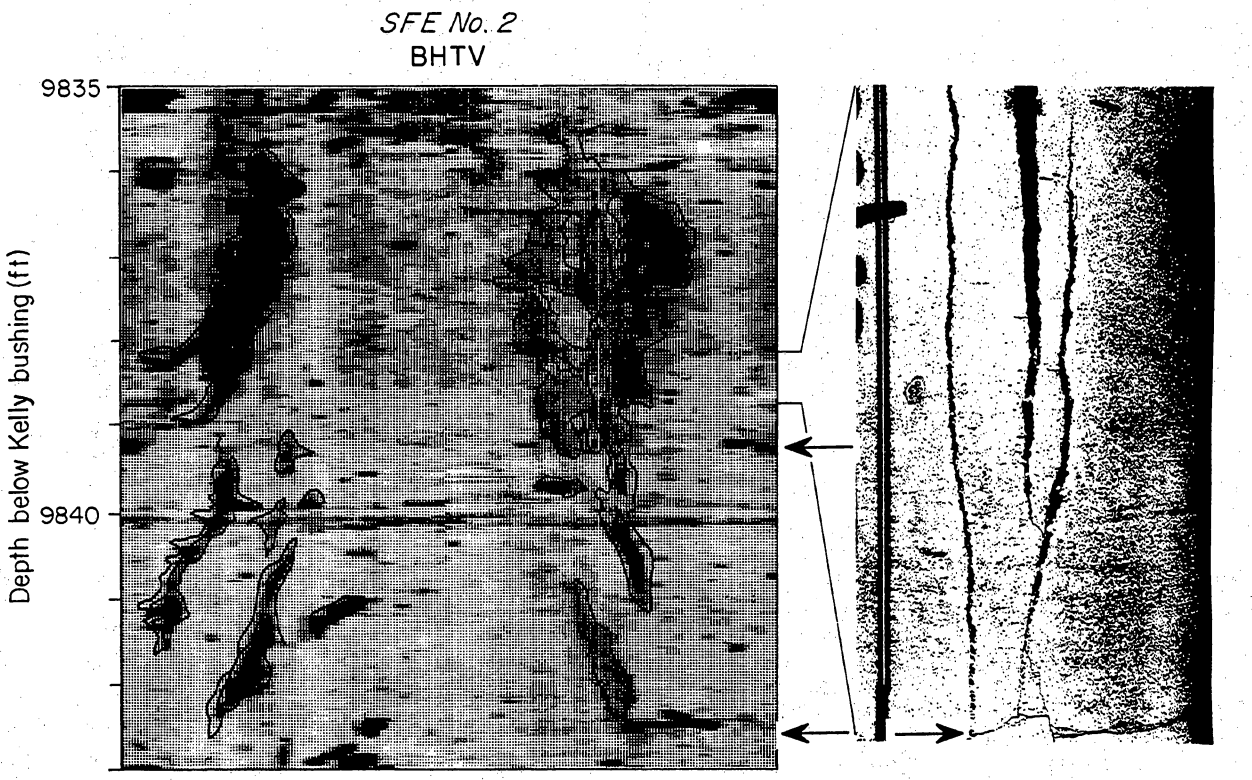

Figure 92. Borehole-televiewer data from a cored interval, SFE No. 2 well, Travis Peak Formation. Fractures and possibly stylolites are visible on the log. Part of the cored interval is shown for comparison.

deviated wells. Yet even in where horizontal wells exist, uncertainty commonly remains concerning overall fracture abundance. For example, in the Austin Chalk play, dominant fracture strikes are to the northeast, and horizontal wells are typically drilled in a direction to intercept these fractures. Yet recently mapped large-diameter tunnels in Austin Chalk show equally abundant northwest-striking fractures (Nance and others, 1994), indicating that overall fracture abundance differs from that seen in northwest-southeast horizontal wells. Finding reservoir fractures in many low-matrix-permeability sandstone gas reservoir rocks is commonly a matter of identifying areas and rock types—fracture-prone layers—that are likely to contain fractures. Because structures such as fold hinges that are likely to localize fractures are subdued or only make up a small part of many plays, finding fractures may depend on identifying fracture-prone beds.

The use of geophysical well logs is one approach to identifying fracture-prone layers. But are the most fracture-prone layers—based on current rock properties—the appropriate ones to find and measure? Diagenetic and fracture relations described in this report suggest that current rock properties may not have any direct relevance as guides to the location of open fractures in reservoirs. Thus, to calibrate wireline detection of *fractured* layers, the diagenetic/fracture history must first be appreciated. The following section illustrates this point using rock tests.

Defining Fracture-Prone Layers with Rock Tests

The approaches described in previous sections seek to identify *fractured beds* based on observed correlations between fracture occurrence and some easily identifiable sandstone attribute, such as original depositional composition or the abundance of a particular cement. If adequate knowledge of fracture abundance can be obtained, this procedure is highly testable and practical. Generally, information on macrofracture occurrence—such as is provided by extensive core and borehole-imaging geophysical logs or wells drilled at a high angle to fracture strike—is lacking, particularly during early stages of development.

Another approach is to distinguish *fracture-prone* beds. This can be accomplished by correlating geophysical well logs with macroscopic fracture occurrence information or with rock properties that are deemed likely to predict fracture occurrence. This can also be carried out using experiments to determine rock parameters such as strength or brittleness that can be used to predict where fractures will be prone to occur. Fracture toughness tests and point-load strength tests are two ways that such information can be acquired. This approach identifies fracture-prone beds. Our results show that if this approach is used without proper appreciation of the timing relations among fracture and diagenesis events, misleading conclusions can be reached regarding the distribution and attributes of fractures.

Tests on Canyon Sandstone

Tests to determine mode I fracture toughness and point-load tensile strength were performed on Sonora and Ozona Canyon sandstone samples. The first step was to evaluate fracture toughness values of different rock (cement) types, aiming to identify factors controlling fracture toughness. Sonora Canyon sandstones have two distinct, common types of cement—quartz and siderite. Brazilian disk fracture toughness tests and petrographic measurements of fracture morphology show that low-porosity sandstone having microstructurally distinct cements can have indistinguishable values of fracture toughness. Mode I fracture toughness values for 30 Canyon Sandstone specimens average 1.77 ± 0.46 MN/m$^{1.5}$ for siderite-cemented zones and 1.72 ± 0.60 MN/m$^{1.5}$ for non-siderite-cemented zones.

Rock Testing Approach to Determining Fracture-Prone Layers

Fracture Toughness Tests

Specimens were taken from 89-mm-diameter sandstone cores, from both siderite- and non-siderite-cemented layers. ISRM (International Society for Rock Mechanics, 1981) suggested that specimen geometries could not be employed in this study because of limited amounts of intact rock materials. Furthermore, the fracture direction induced by the ISRM test methods would be parallel to bedding, an unrepresentative direction for comparing induced and natural fracture morphologies considering that natural fractures are mostly orthogonal to bedding. Experimental procedures and tabulated results are in Baek and others (1994) and Laubach and others (1994).

The mode I fracture toughness values were measured on notched Brazilian disk specimens. This specimen geometry is relatively simple, both in sample preparation and as a starting point for calculation of fracture toughness. A conventional screw-driven type loading frame was used, while both crack-mouth opening displacement and load point displacement were monitored. The Brazilian test was originally developed as an alternative method for measuring Poisson's ratio and elastic modulus of brittle materials (Olszak and others, 1957) and has been adopted for determining tensile strength of rock materials (Bieniawski and Hawkes, 1978). For this test, two diametrically opposite faces of a disk specimen are ground flat on a surface grinder to make loading faces parallel and smooth. An initial notch that serves as a stress raiser is cut through one face of the specimen along the diametrical axis. As shown in figure 93, specimens are diametrically loaded in such a way that the notch remains parallel to the loading line while the load is applied through flat platens. Mode I fracture

toughness is determined from the maximum test load and specimen geometry based on analysis of stress-strain behavior of a circular element under loading. Assuming no significant change in shape of the boundary line of the compressive stress field due to introduction of flat surfaces on top and bottom of the circular element, the expression for evaluating fracture toughness by the notched Brazilian disk specimen is given by Szendi-Horvath (1980)

$$K_{Ic} = 1.264(\sin 2\theta - \theta)\frac{F_{max}\sqrt{a}}{w \cdot t}, \qquad (2)$$

where notations are given in figure 91.

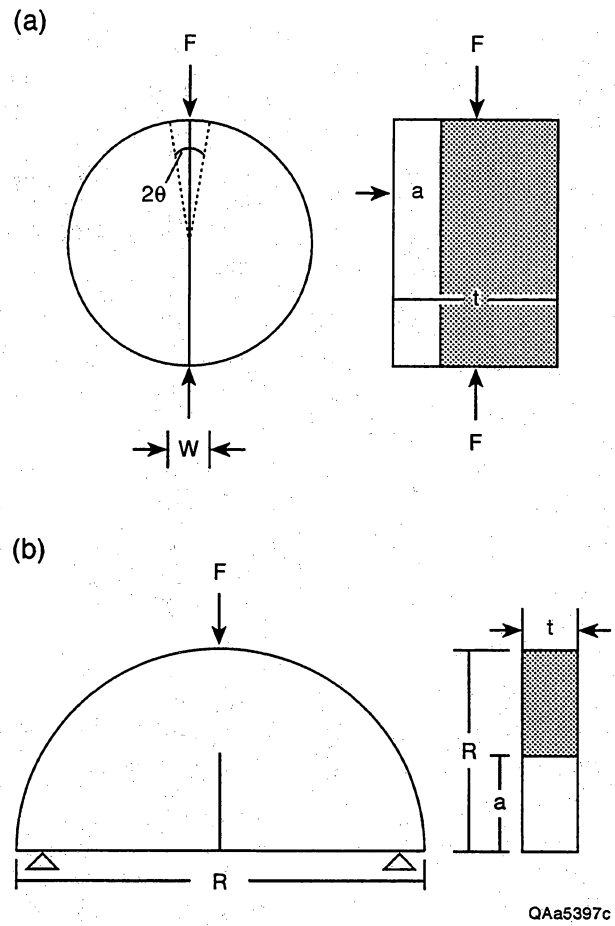

Figure 93. Specimen geometries used for determining fracture toughness in this study. (a) Notched Brazilian disk specimen. (b) Semicircular bend specimen.

Fracture Toughness Test Results

A total of 30 specimens (13 siderite- and 17 nonsiderite-cemented sandstones) were tested, and average fracture toughness values with standard deviations for each lithologic unit are summarized in Baek and Laubach (1994). As shown in their test data compilation, the difference in average fracture toughness values between the two differently cemented rock materials is statistically negligible.

High standard deviations reflect the influence of a variety of compositional variables on fracture toughness. These elements include grain packing, distribution and volume of other cements, and arrangement of soft grains such as clay minerals (fig. 94). As the number of quartz and feldspar detrital grains in direct contact with each other increases, fracture toughness decreases ($r = -0.73$). Poorly sorted, fine-grained sandstones tend to have higher fracture toughness values. An increase in percent quartz corresponds to decreasing fracture toughness ($r = -0.77$). Samples that lack or have very small volumes of clay minerals have a range of fracture toughness values, but for samples having measurable clay mineral contents, increasing clay content corresponds to decreasing fracture toughness ($r = -0.93$; -0.65 if samples lacking clay are included). Differences in volume and distribution of clay particles may account for some variability in fracture toughness values. We found that, for nine samples (all having porosity less than 7 percent), there is no distinct trend in fracture toughness with porosity.

Point-Load Strength Tests

Axial point-load tests involve breaking specimen disks of rock with small, diametrically opposed anvils that approximate point loads. Axial point-load strength is a rapid test method to distinguish rock strength characteristics that may correspond to fracture-prone layers. As described in a later section, direction of sample fracture can reflect strength anisotropy, which in otherwise homogeneous samples may correspond to the strike of natural microfractures or microfractures that exist owing to processes such as differential core expansion that reflect in situ stress directions. In low-permeability sandstone natural gas reservoir rocks, point-load tests are potentially useful supplements to core-based studies of macrofractures.

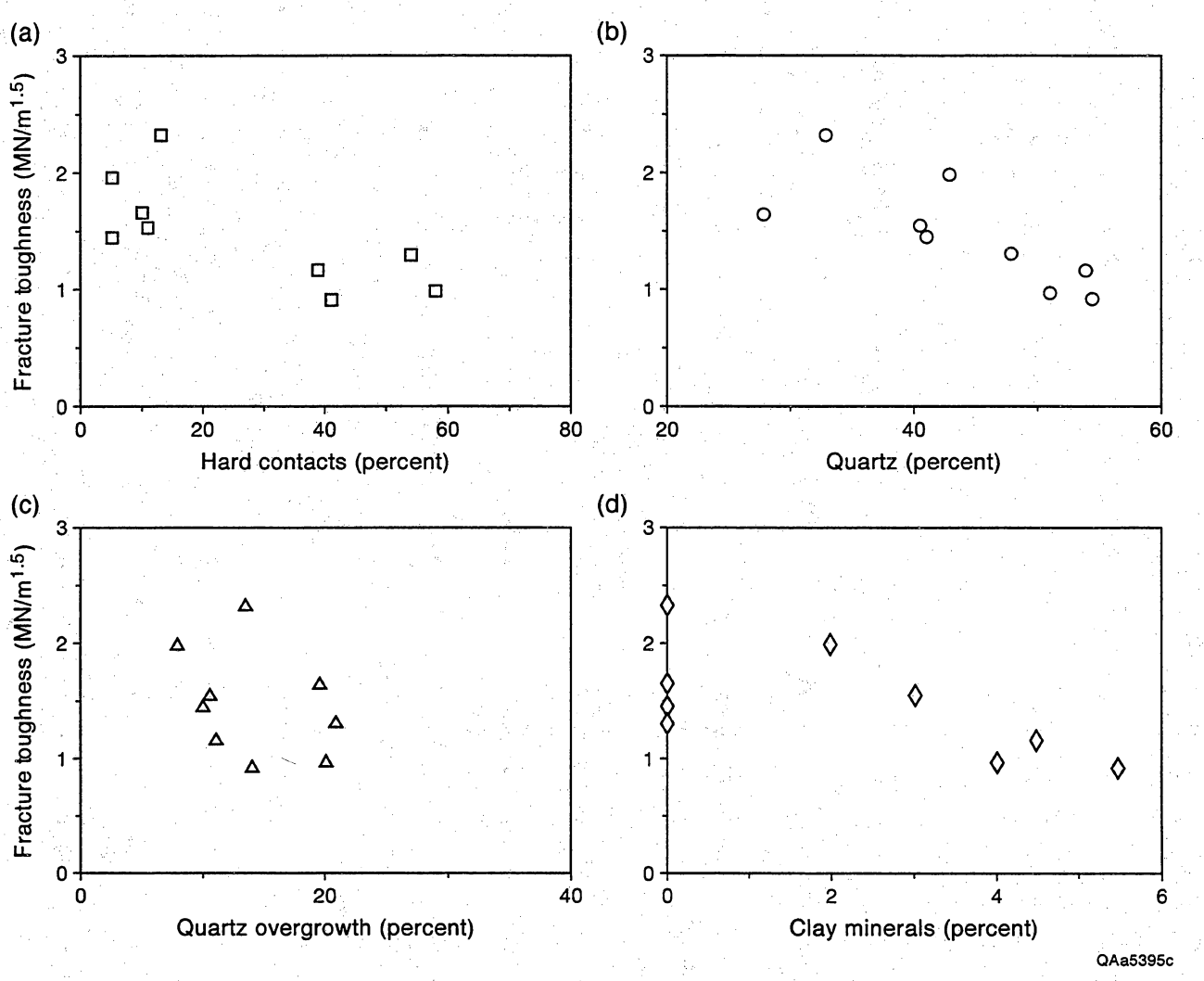

Figure 94. Relationships between fracture toughness and mineralogical composition. (a) Hard contacts (percentage of grains touching counted grain). (b) Percent quartz. (c) Percent quartz overgrowths. (d) Percent clay minerals.

Tests were able to distinguish beds having differing strengths that correspond to different degrees of quartz cementation. Point-load strength test results show that strength increases as the degree of quartz cementation increases (table 14). The point-load strength test is widely used as an index test for the strength classification of rocks. The test measures the point-load strength index of rock, as will be defined.

Point-load test specimens of Canyon Sandstones were obtained from five wells: the Phillips Ward "C" No. 1, Sun Dunbar No. 1, Shell Baggett "2" No. 20, Texaco Kincaid "D" No. 7, and Enron Sawyer "A" 144 No. 5. Test specimens 1 inch in diameter were vertically plugged in homogeneous, clean sandstone intervals. For the Ward and Sawyer wells, specimens were taken within oriented core intervals. For other wells, for which cores are not oriented, specimens were taken at the intervals where well-developed natural fractures are present, and the natural fracture orientation was used as a reference direction.

Two identical 1-inch-diameter plugs of 4-inch length were obtained from each core piece. These plugs were sliced into disk-type test specimens, about 0.5 inch thick. Care was taken to ensure near parallelism of the top and bottom of the disk.

Axial point-load tests on Canyon sandstone specimens were performed using a commercial point-load test machine, in which the load was steadily applied with a hydraulic hand pump (fig. 95). Specimens were perfectly centered on the bottom anvil of the point-loading jig by balancing the specimen on the bottom anvil and visually checking to ensure that it was level. Specimens were not confined laterally, except by a thin electric tape loosely wrapped around

Table 14. Summary of point load strength tests, Canyon Sandstone specimens.

Company	Well	Depth (ft)	Rock type*	No. of specimens	Mean value (MPa)	Standard deviation (Mpa)
Phillips	Ward "C" No. 1	5516.8	A	7	7.28	0.40
		5560.1	A	8	6.47	0.38
		5566.0	B	10	6.37	0.19
		5575.2	A	8	6.15	0.31
		5583.7	A, B	10	6.11	0.88
		5619.9	B	7	6.05	0.21
		5623.8	A	16	5.67	0.34
		6053.8	B	6	7.37	0.33
		6350.0	A	8	7.05	0.34
Sun	Dunbar No. 1	5775.1	C	12	9.18	0.61
		5775.8	C	8	9.66	0.53
		5782.5	A	5	8.31	0.42
		5785.8	A	9	7.05	0.25
		5805.9	A	5	7.04	0.61
		5838.5	A	12	7.77	0.23
		5947.9	A	6	7.21	0.25
Shell	Baggett "2" No. 20	6631.2	C	4	10.09	0.44
		6744.0	D	10	11.18	0.69
		6762.0	C	7	11.31	0.69
Texaco	Kincaid "D" No. 7	6298.8	B	4	7.09	0.08
		7599.4	C	5	11.30	0.48
Enron	Sawyer "A" 144 No. 5	5944.0	A	6	6.92	0.38
		5959.9	A, B	11	6.78	0.39
		5964.7	A, B	5	6.35	0.24
		5966.0	A, B	12	7.13	0.29
		5969.0	B	6	6.65	0.10
		5971.1	B	5	5.68	0.20

*Rock type: A Siderite-cemented samples with local quartz overgrowth
B Heavily quartz-cemented
C Fine-grained, abundant carbonate cement
D Medium-grained, calcite-cemented
All specimens are fine-grained sandstone.

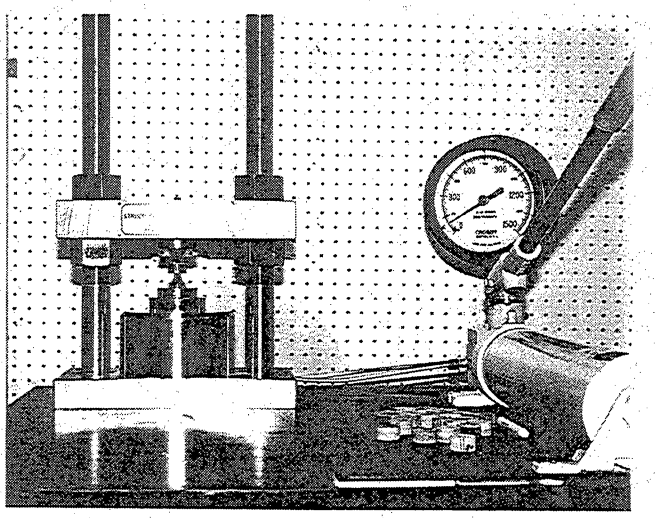

Figure 95. Photograph of point-load strength test rig used for Canyon Sandstone testing.

the specimen. The point-load test outcome on brittle rock material is usually catastrophic failure, and the plastic tape helped to keep broken sample pieces together after the test was completed.

From the maximum test load and specimen dimensions, the specimen width (specimen diameter *W*) and the distance between the anvils (specimen thickness *D*), the Point Load Strength Index I_S is calculated as

$$I_s = P / D_e^2 \quad (3)$$

where D_e, the equivalent core diameter is given by

$$D_e^2 = 4WD / \pi'. \quad (4)$$

In the axial point load test, I_S varies as a function of D_e, so that a size correction must be applied to obtain a unique point-load strength value for the purposes of rock-strength classification. The size-corrected Point Load Strength Index $I_{S(50)}$ of a rock specimen is defined as the value of I_S that would have been measured by a diametrical test with D = 50 mm. The size correction factor F can be obtained from the expression (ISRM, 1981)

$$F = \left(D_e / 50\right)^{0.45} \quad (5)$$

and $I_{s(50)}$ is then calculated as:

$$I_{s(50)} = \left(D_e / 50\right)^{0.45} \cdot I_s \quad (6)$$

The mean value of $I_{s(50)}$ is calculated by deleting the two lowest and highest values from the 10 or more valid tests and calculating the mean value of the remaining values. If significantly fewer specimens are tested, only the highest and lowest values are to be deleted and the mean calculated from those remaining (ISRM, 1981).

A total of 272 Canyon sandstone specimens were tested. Results are summarized in table 14. As shown in this table, measured point-load strength indices have uniform distribution in the various wells, as is implied by their low standard deviations. Specimens fall into four groups according to the main cementing materials they contain. Group A specimens have predominantly siderite cements with local quartz overgrowths. Group B samples are heavily quartz cemented, and fine-grained Group C specimens have abundant carbonate cement. Finally, Group D specimens are mostly medium grained and moderately calcite cemented.

Different cementing materials correspond to differences in measured point-load strength index. Carbonate- or calcite-cemented sandstones from the Baggett "2" No. 20 well exhibited higher values than other specimens. However, because of variable cementing materials for specimens from the same well, no distinct trend in the measured point-load strength index with sample depth could be documented, as shown in figure 96.

Application to Fracture Prediction

Fracture-toughness measurements and point-load strength tests and diagenetic studies of Sonora Canyon Sandstone show that a contrasting cementation histories can lead to sandstones having similar rock properties. Different sandstone layers became susceptible to fracture as episodes of cementation and compaction changed mechanical contrasts among beds. Fracture-toughness data (or any other rock property) alone is not a good guide to occurrence of natural fractures in rock. Diagenetic history, when correlated with structural history, indicates, for example, when changes in rock composition occurred that either promote rock fracture or occlude existing fracture porosity.

Siderite-cemented layers are an example of bed that was preferentially fractured as a result of existence of prekinematic cement. According to Dutton and others (1993), Sonora Canyon sandstone beds that contain more than 10 percent grain-rimming siderite resulted from cementation shortly after deposition of deep-water marine sediments. We interpret siderite-cemented layers to have become strong and stiff as siderite

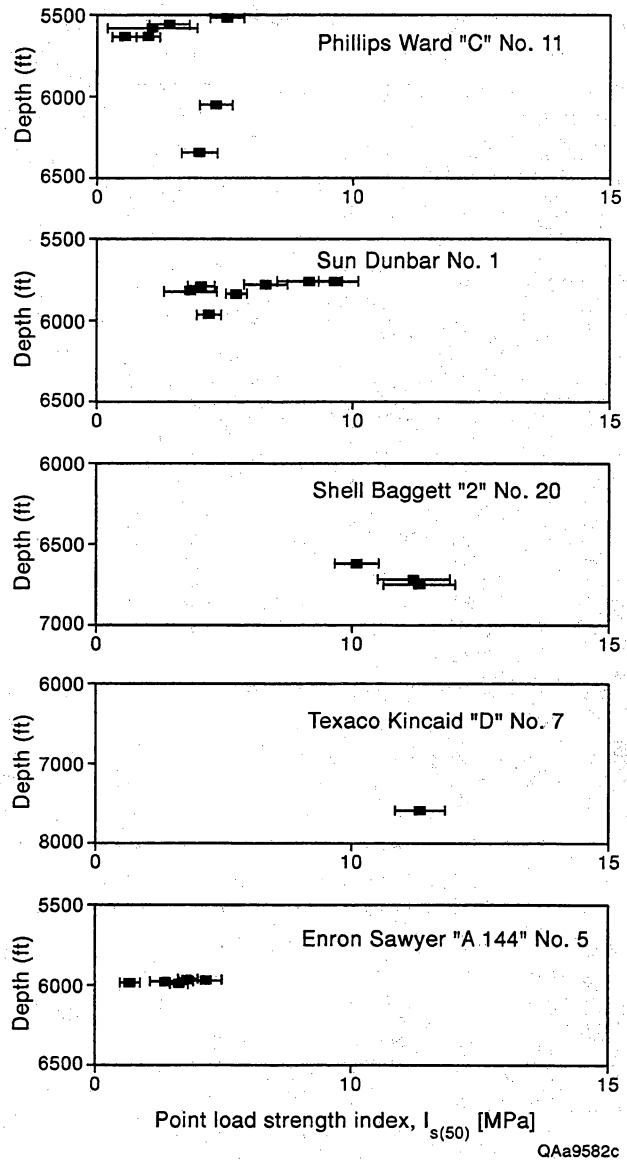

Figure 96. Point-load strength index versus depth for five Canyon Sandstone wells.

cement along grain boundaries resisted grain-rearrangement by grain-boundary sliding. Siderite-cemented layers would have acted as a stiff reinforcement, developing fractures as burial loading continued.

In contrast, noncemented layers could have continued to deform by grain sliding and rearrangement until, later in the sandstone's burial history, quartz cement was preferentially deposited in nonsiderite-cement zones, locking grains in place and increasing fracture toughness to the same level as beds cemented with siderite. Thus, diagenetic contrasts in sandstones undergoing the same burial history can ultimately result in similar *current* properties as measured by fracture toughness tests. Fracture toughness values from tests carried out on rocks representing the end product of such a diagenetic history should not be expected to reflect differences between siderite and nonsiderite-cemented layers that existed when natural fractures formed. These test results may correctly define how *susceptible* beds are now to fracturing, but they are unreliable guides to actual fracture occurrence.

Fracture Porosity Preservation

Syn- and Postkinematic Porosity Preservation

Models of fractures in petroleum reservoir rocks commonly assume that fractures are smooth, parallel-sided, and persistent. Some rock mechanics models of natural fracture permeability incorporate fracture roughness (Pyrak-Nolte and others, 1985), and many recent studies have documented roughness characteristics of barren joints (Brown and Scholz, 1985; Amadei and Illangasekare, 1994, and references therein). In this view of fracture geometry, mismatches between rough fracture surfaces create voids through which fluid can flow, and open channels between asperities can localize flow within the fracture. Patterns of cement distribution within fractures have not been taken into account, probably because no methods to estimate this parameter, apart from direct observations, were available.

However, in natural gas reservoir sandstones, fractures do not typically have smooth barren surfaces (they are also rarely parallel sided and persistent). Instead, fracture surfaces are both mineralized and rough. Locally, they may also have dissolution features in framework grains, cements, or fracture fills along and/or adjacent to fracture surfaces. Mineralization can range from complete filling of the fracture to sporadic isolated crystals on fracture surfaces.

Mineral fillings in fractures have important consequences for flow because they alter flow properties of fractured rock (table 15). In some cases, completely filled fractures can occlude matrix flow, leading to flow anisotropy and compartmentalization. Clay and calcite vein minerals in Sonora Canyon, ankerite in Ozona Canyon, and calcite vein minerals in Frontier Formation sandstones are probably in this category. Mineral fracture fillings may have different permeabilities than those of host rocks, and fracture-cement bridges may prop fractures open, as is probably true of synkinematic quartz in Canyon, Travis Peak, and Frontier examples. As previous sections of this report demonstrate, mineral fracture fills also provide information on the nature of fluids that have flowed in the fractures, progressive history of fracture opening, timing of fracture relative to matrix porosity occlusion and hydrocarbon migration, physical conditions during mineral precipitation, and current fracture aperture patterns.

Descriptions in previous sections show that the distribution of fracture-lining and fracture-filling minerals is the principal control on fracture porosity and fracture-network-porosity continuity. The mineralization patterns we observed of fracture-filling minerals are such that they can be expected to control the way fluid flow occurs in fracture networks and how a fracture responds to changes in fluid-pressure conditions and effective stress. For example, partly open fractures can be fluid conduits, but filled fractures may be flow barriers. We found that the degree of mineral fill can change abruptly along fracture traces. Other than recognizing a general trend of thinner fractures in any given formation to have a greater tendency to be filled, predictions of the pattern of fracture occlusion are not possible in detail based on cement type, depth of burial, or host-rock composition. The timing of cementation relative to fracture opening and the degree of postkinematic cementation in matrix are qualitative predictors of fracture porosity.

Prediction of fracture-porosity patterns can be augmented by determining when volumetrically important cement phases were deposited relative to fracture opening. Postkinematic ankerite occluding fractures and matrix porosity in the Ozona Canyon and porous quartz-lined fractures in the Travis Peak are examples. Fractures in areas of synkinematic quartz cement tend to preserve fracture porosity. Later cementation events (postkinematic cements) can occlude that porosity. In the Ozona Canyon and Travis Peak Formations, postkinematic cement occludes matrix porosity to about the same extent that it fills fracture porosity. Postkinematic cement volume is therefore worth monitoring as a guide to fracture porosity preservation.

Figure 97 illustrates how the relative proportions of syn- and postkinematic fracture-filling minerals and remaining fracture porosity can be represented for a system of fractures. This example is from the Travis Peak Formation, and the increasing proportion of preserved porosity with increasing fracture size is depicted.

Diagenetic Control on Fracture Roughness

In addition to minerals filling fractures, fracture roughness has an effect on fracture porosity. Qualitatively, degree of induration is a well-known control on fracture roughness in sedimentary rocks; fractures tend to break across grains rather than around them in highly indurated rocks, producing smooth fractures. This is true for experimental fractures created in all the sandstones we studied; they tend to be smooth. However, contrary to expectations, many natural fractures in highly indurated sandstones are exceedingly rough. Variable thicknesses of mineral linings on fracture surfaces are one important contributor to fracture roughness, but for these sandstones the minus-fracture fill fracture profiles are also rough. This is true even in the most highly indurated sandstones.

Although fracture growth processes no doubt plays a role, the cause of natural fracture roughness in highly cemented sandstones is mainly related to the interplay of cementation and fracturing. Fractures may be unexpectedly rough because they form before a rock is fully cemented (indurated), or because they form while cementation is in progress (synkinematic cements). In some instances the morphology of fractures propagating through a material can provide evidence of the properties of the rock at the time the fractures grew (Bahat, 1991). Many of the fractures in the three formations we studied grew by cracking along grain boundaries.

These roughness patterns are illustrated by the Sonora Canyon sandstone. Petrographic study of natural and experimentally induced Canyon Sandstone fractures shows that natural fractures are rougher and have broken around sedimentary grains (they have intergranular propagation pathways), whereas experimentally induced fractures predominantly are planar

Table 15. Role of mineral fillings in altering flow properties of fractured rock.

Type of fracture	Effect on flow properties
Completely filled fractures	• No flow occurs in fracture network. • Matrix flow is occluded, with potential for flow anisotropy and compartmentalization. • Mineral fillings may have permeabilities different from those of host rocks.
Partly filled fractures	• Flow channels exist in fracture systems. • Parts of fracture network are isolated. Vein bridges may prop fractures open. • Reactive vein material may interfere with production.

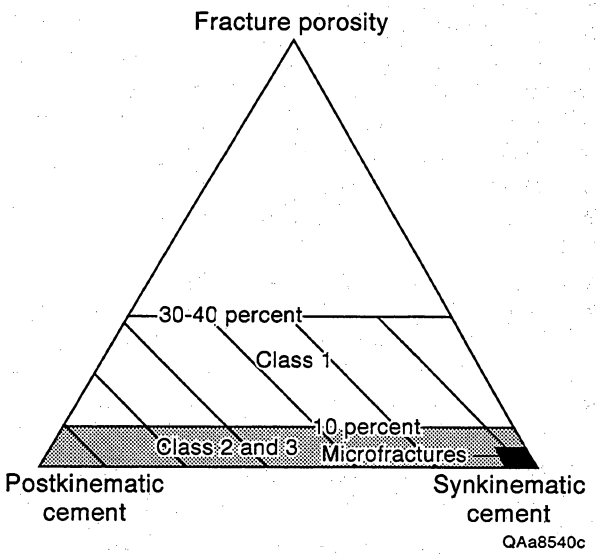

Figure 97. Ternary plot of relative proportions of fracture porosity, synkinematic fracture-filling minerals, and postkinematic fracture-filling minerals. Also shown are areas where different classes of Travis Peak fractures tend to be located. As fracture size increases, fractures associated with synkinematic cement tend to have greater porosity and plot closer to the porosity apex of the diagram. Porosity of large fractures is filled by postkinematic minerals where these cements are prevalent.

and mostly transgranular. Observations of Travis Peak natural fractures also show them to have rough walls for this reason (fig. 98). To illustrate fracture roughness, we profiled several natural fractures that cross various cements by petrographic mapping of crack trajectories and compared them to experimental fractures in the same rocks. Background for these tests is described by Baek and Laubach (1994). Results highlight the importance of timing of fracture propagation relative to cementation as a control on fracture roughness that needs to be considered in modeling and physical testing of fractured samples.

Sample Preparation

Samples containing natural and experimentally induced fractures were carefully cut with a diamond saw blade of 0.71 mm (0.028 inch) thickness. In the case of experimental fractures for which crack propagation had been controlled, thin sections were made from the plane perpendicular to the fracture surface. For natural fractures, the major direction of fracture propagation was assumed to be horizontal, and thin sections were cut in the horizontal plane.

During sample preparation, rock samples containing fractures can easily be broken by vibrations associated

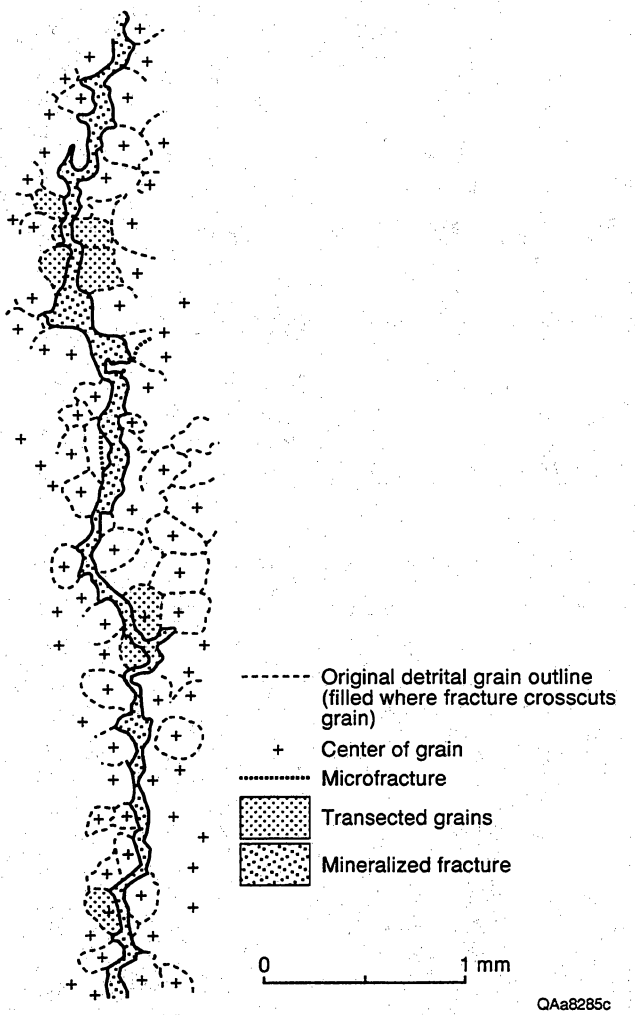

Figure 98. Profile of natural fracture in Travis Peak Formation, showing fracture roughness due to intragranular fracture growth.

with cutting by the rock saw. To avoid creating additional fractures during sample preparation, the samples were hardened prior to cutting with a specially prepared concrete restorer. This material is used for sealing cracks and repairing delaminations in concrete structures. A 4R concrete restorer (1000 ml) from 3M, which contains mainly dicyclpentadienyl methacrylate, was mixed with cumyl hydroperoxide (40 ml). The solution can be hardened by adding a small amount of cobalt or by heating in an oven. After 24 hours of soaking with the solution, each sample was placed in a plastic bag and then put in an 82°C (180°F) oven for 24 hours to promote methacrylate hardening and stabilization of fractures. Hardened samples were then cut with a rock saw and impregnated with a blue-dyed epoxy following standard procedures. Under the microscope, blue epoxy facilitated identification of fracture porosity.

Fracture Characterization

Five thin sections of experimental fractures and an equal number of thin sections of natural fractures were described. A special point-counting procedure was employed to characterize the crack trajectory. Thin sections were advanced with a counting stage along a reference line parallel to the fracture trace in 300-μm intervals. At each interval the character of the fracture section under the crosshair of the microscope was described in terms of the upward or downward deviation of the crack path from the reference line and the type of crack propagation increment in the vicinity. Categories were transgranular crack increment and intergranular crack increment. Transgranular crack increments cross individual grains, whereas intergranular crack increments pass through cement or pore space and commonly curve around boundaries of mineral grains. Other properties noted at each interval were mineralogy, size, shape, and (where appropriate) orientation of grains and cement. The initial notch tip was taken as the starting point for measurement along experimental fractures, and a point toward the center of the core was used as a reference for natural fractures.

A transgranular increment from an experimentally created fracture is illustrated in figure 99. Also visible is grain-rimming siderite cement. Despite numerous poorly bonded, siderite-coated grain contacts, the fracture extends with little deviation across grains. An intergranular increment from a natural fracture is shown in figure 100, an example having angular to subangular quartz grains and thick siderite cement rims and quartz cement. Despite the lack of porosity or other weak pathways, the fracture extends across the sample with numerous deviations from a straight trace.

Quartz cement can have similar mechanical properties as primary quartz grains and should not necessarily be regarded as a "weak" element in resisting crack propagation. Although the join between grains and cement in quartz-cemented sandstones can be relatively weak (for example, mild grinding was used to disaggregate grains and cement for geochemical studies of Travis Peak sandstones; Dutton and Land, 1988), crack pathways between quartz grains and quartz cement are rare in both natural and induced fractures in both the Canyon and Travis Peak sandstones.

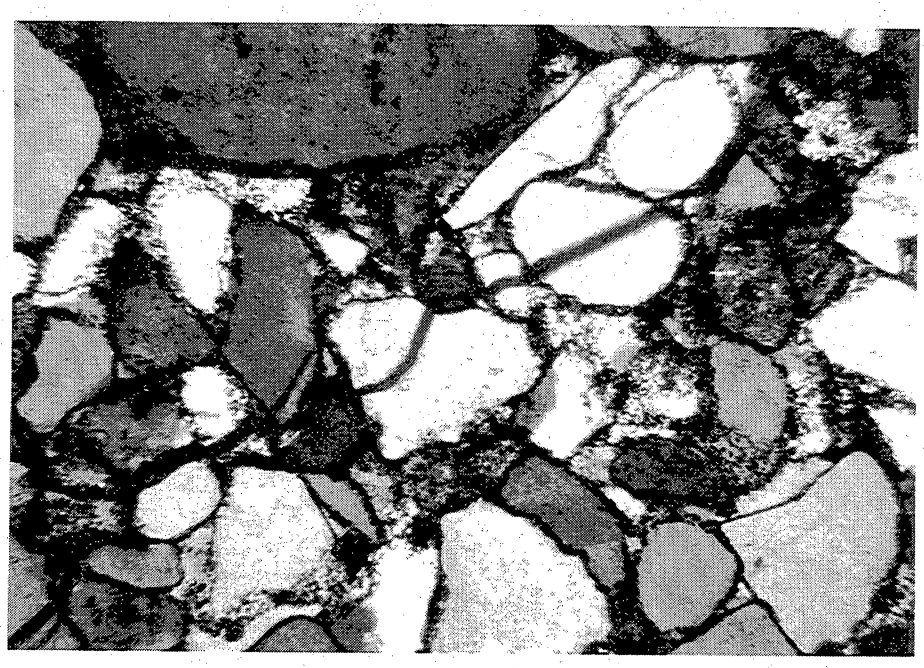

Figure 99. Transgranular crack propagation in a specimen tested for fracture toughness. Cross-polarized light, 77× magnification.

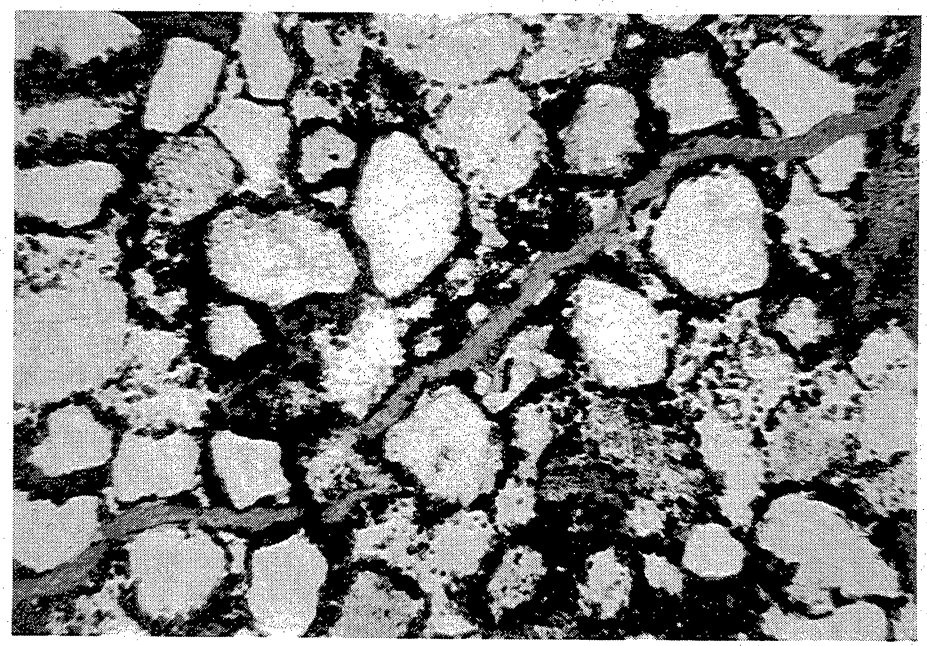

Figure 100. Intergranular crack propagation in a natural fracture sample. Plane-polarized light, 77× magnification.

In this study, for petrographic traverse points near quartz overgrowth cements, the state of adjacent crack increments was used to define the nature of the crack increment. Where cracks propagated through quartz cement that formed a clear boundary between primary quartz grains, the increment was described as an intergranular crack increment. In contrast, if adjacent crack increments were through a zone of secondary quartz, more or less perpendicular to the major opening direction, then a transgranular crack increment was assigned. A schematic description of this procedure is depicted in figure 101. In the point-counting procedure the length of each segment line connecting two adjacent data points sums to the "real" extension length of the crack (fig. 102). For the cracks in this study, deviation from the straight reference line is commonly due to intergranular crack propagation. The crack front takes a less resistant path by extending through weaker but off-line grains or cementing materials. However, large grains of quartz resisted fracture and commonly forced the crack to detour.

Percent fracture length is defined as the ratio of length occupied by a certain crack increment type, either intergranular or transgranular, to total crack length. Hence, final values of percent intergranular and percent transgranular crack propagation sum to 100 percent at the right end of each plot. These graphs show the spatial distribution of two types of propagation behavior along a crack. Percent cumulative length of both intergranular and transgranular crack increments observed in natural fractures plotted versus distance shows that intergranular propagation dominates in natural fractures. Intergranular crack propagation is far more common in these fractures.

For a natural fracture specimen from nonsiderite-cemented sandstone, percent lengths of both intergranular and transgranular crack propagation are similar, and the final percent intergranular propagation length is less than 50 percent. This is only one example, but it is consistent with the interpretation that rims of siderite cement promotes intragranular fracture under natural conditions. Transgranular propagation is dominant among experimental fractures. Overall, a difference between natural and experimental fractures was observed in crack propagation behavior. Cumulative percentages of intergranular and transgranular crack propagation are listed in Laubach and others (1994) in their table 10. In contrast to natural fractures, siderite cement rims are not markedly associated with intragranular cracking in experimental fractures.

Fracture Roughness Profiles

Intergranular crack propagation is dominant in natural fractures, whereas transgranular crack propagation is far more common in experimental fractures. Natural fractures exhibit wavy and rough surface profiles as a result of dominance of intergranular crack propagation. In contrast, experimental fractures show straight and smooth profiles as a result of dominant transgranular crack propagation.

The wall roughness of a rock discontinuity is a potentially important contributor to fracture shear strength, dilatancy, and stiffness, especially in the case of undisplaced and interlocked features. Surface roughness can be described both quantitatively and qualitatively. Qualitative descriptions can be subjective and misleading, so quantitative descriptions should be sought. A semiquantitative description of fracture-wall roughness summarized by the ISRM Commission on Testing Methods (ISRM, 1981). This classification system, originally proposed by Barton and Choubey (1977), was based on observations made primarily in underground openings and on results of simple tests involving direct shear offsets parallel to the plane of the discontinuity. In this scheme the joint roughness coefficient (JRC) has a value from 0 (smooth) to 20 (rough), representing the full range observed in discontinuity joint wall roughness. The JRC of a surface profile is estimated either by visual matching with standard profiles or by back-calculation using peak shear strength and basic friction angle in conjunction with joint-wall compressive strength. The latter approach is obviously impractical, considering that the purpose of the JRC classification is to predict some of these attributes.

Although the JRC classification has been widely used, it may be subjective in practice. Fractal geometry of rock fracture surfaces has also been used in engineering practice (Brown and Scholz, 1985; McWilliams and others, 1990). In this approach, numerical parameters are determined from fractal analyses of digitized surface profiles; drawbacks of this method include the cumbersome data collection requirements. Another quantitative description of roughness profile, related to performance of side resistance in rock socketed piles, was introduced by Lam and Johnston (1985). Their approach is adopted in this study.

Roughness of a fractured surface is described by several statistical terms including maximum asperity

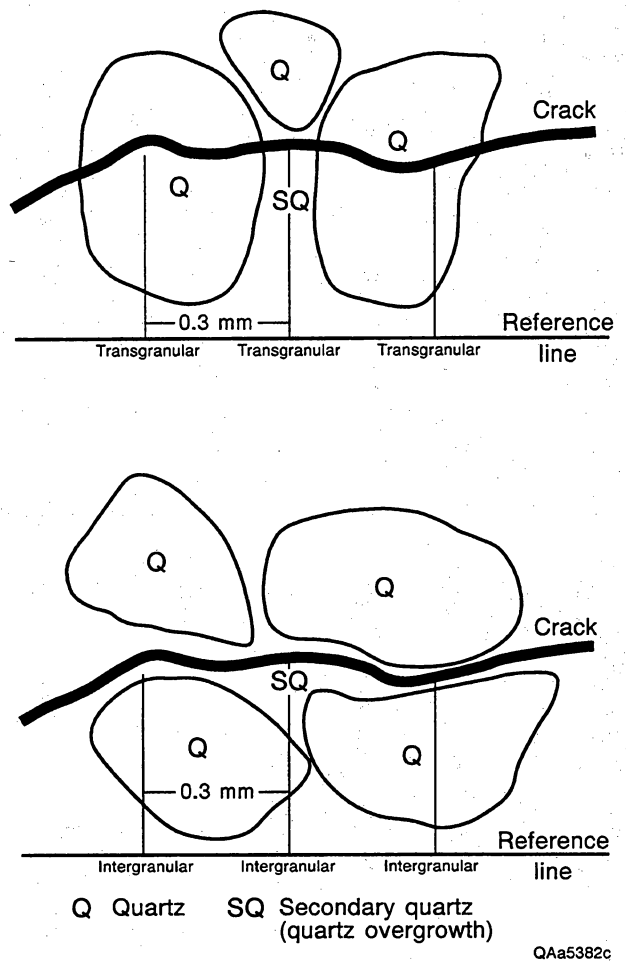

Figure 101. Criteria for counting fracture segment type.

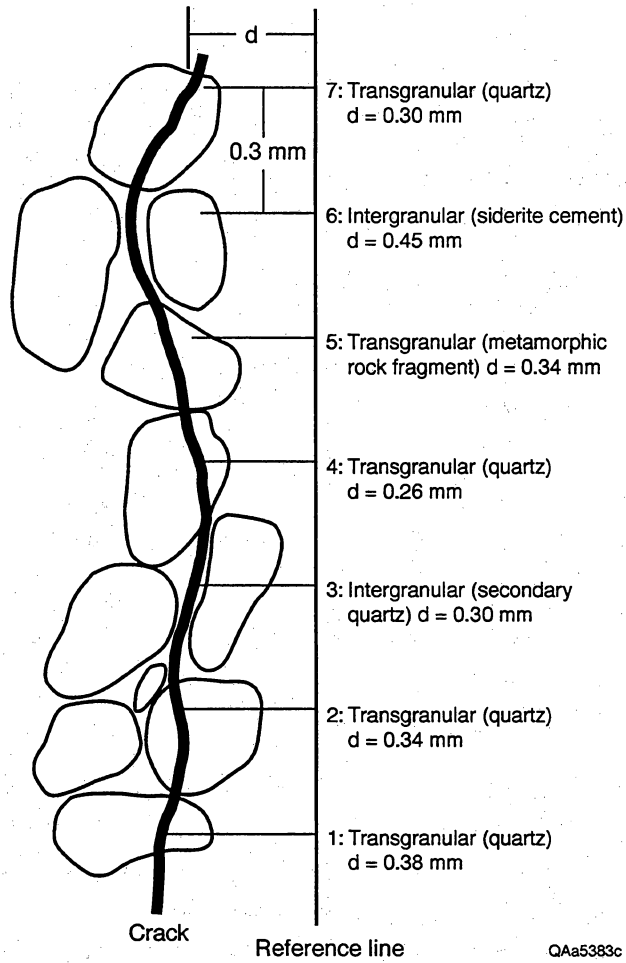

Figure 102. Illustration of point counting procedure for fracture profiles.

height h_{max}, mean asperity height h_{ave}, standard deviation of the heights SD_h, mean asperity angle i_{ave}, and standard deviation of the angles SD_i (fig. 103). Maximum asperity height is the height difference between highest and lowest points on the profile, as shown in the figure. Other terms are calculated by (Lam and Johnston, 1985):

$$h_{ave} = \frac{1}{L}\int_0^L |y|\,dx \tag{7}$$

$$SD_h = \sqrt{\frac{1}{L}\int_0^L \left(|y| - h_{ave}\right)^2 dx} \tag{8}$$

$$i_{ave} = \tan^{-1}\left[\frac{1}{L}\int_0^L \left(\frac{dy}{dx}\right) dx\right] \tag{9}$$

$$SD_i = \tan^{-1}\sqrt{\frac{1}{L}\int_0^L \left(\frac{dy}{dx} - \tan i_{ave}\right)^2 dx} \tag{10}$$

Parameters h_{ave} and SD_h provide an indication of the position of the mean line of profile and deviation of the heights from this mean line, respectively. The parameter i_{ave} indicates average inclination of each segment line, connecting two data points, to the horizontal of the mean line through asperities. In this study, the first and last data points of the crack profile were connected to draw a horizontal reference line,

so that i_{ave} will be zero. Parameters h_{max} and SD_i are the most relevant terms with regard to assessment of shear performance of rough rock joints (Lam and Johnston, 1985). Accordingly, these parameters were used to compare roughness profiles of natural and experimental fractures.

An objective basis for JRC classification can be obtained by applying these numerical parameters to measured data. Standard profiles were digitized using a scanner. Parameters were then calculated; parameters are listed in Laubach and others (1994) in their table 11. The ratio, R, between linear length of a profile, measured by straight-line distance between first and last data points, and real length measured along actual profile represents relative tortuosity of different fracture profiles.

No general relationship between JRC values and statistical parameters of roughness profiles are evident. Most parameters, except SD_i and R, are fluctuating for higher JRC values (Groups 7 to 10). This is because in estimating shear resistance of rock discontinuities the number of asperities is a more important parameter than individual asperity height. Therefore, it is questionable if these statistical parameters apply to JRC profiles in general. However, microscopic profiles of rock fractures are expected have low JRC values, where all statistical parameters are in step with JRC values.

Microscopic roughness profiles of natural fractures in Sonora Canyon sandstones may be roughly described as exhibiting an undulating surface, following descriptive terms for roughness profiles suggested by the ISRM Commission on Testing Methods (ISRM, 1981). Typical roughness profiles and suggested nomenclature are shown in Baek and Laubach (1994, their figure 107). Roughness profiles of experimental fractures are smooth and planar compared to those of natural fractures. However, such a general distinction cannot be documented for all cases.

We expected that experimental fractures with dominant transgranular crack propagation would have lower values of SD_i and R, compared to natural fractures in which wavy and rough intergranular crack propagation was dominant. The parameter SD_i shows a clear distinction between natural and experimental fractures. This reflects rougher surface profiles of natural fractures, since a low SD_i value indicates a smooth and planar surface. However, other statistical parameters, as well as R, do not clearly distinguish between the two fracture types.

Among natural fractures sampled from siderite-cemented sandstones, some specimens have thicker siderite cement. Higher values of SD_i and R of fracture profiles reflect thicker siderite cement. It may be that for each grouping of natural and experimental fractures, siderite-cemented sandstones have higher values of all parameters, that is, rougher surface profiles. This conclusion is consistent with the high percent intergranular crack propagation associated with siderite cementation. All fractures belong to the range of groups 1 to 3 of the JRC classification. However, experimental fractures have much lower SD_i values than that of group 1 profile, whereas other parametric values mostly belong to groups 2 or 3.

Although originally developed for estimating frictional resistance of larger scale surface profiles, statistical parameters of Lam and Johnston (1985) provide a reasonable basis for describing surface roughness of fractures under the microscope. Significantly lower SD_i values of experimental fractures may be interpreted as an indication of smooth and planar profiles caused by transgranular propagation. These observations also point to ways that cement, and the timing of cement precipitation, can govern fracture roughness.

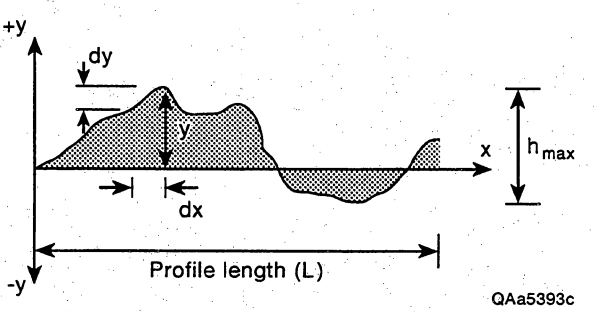

Figure 103. A random surface roughness profile (from Lam and Johnston, 1985).

Using Microstructure and Test Data to Map Fracture Strike

Systematic measurement of fracture strike is exceedingly important for design of drilling programs to exploit natural fractures. Getting fracture-strike information is difficult. Concurrent study of fracture and diagenesis provides breakthroughs in this area. These methods are described in the following section.

Indirect Methods to Determine Macrofracture Orientation

Methods that use indirect approaches to measure the strike of large fractures overcome the sampling bias that is one of the largest hurdles to mapping macrofractures in subsurface sedimentary rocks. In this section we report three approaches to this problem. However, only one of these methods—microfracture mapping using scanned CL imaging—promises to be a revolutionary new source of fracture information, in addition to having widespread applicability and being easy to use.

Other new methods we describe have more limited application or provide data that is difficult to interpret. These methods involve using fractures in coal inclusions in sandstone to track macrofracture strike and using simple rock tests that measure strength anisotropy. The advantage of all of these methods is that in some instances they can provide evidence of fracture strike even in cases where macrofractures have not been intersected by the borehole. Effective use of all of these techniques depends on linking structures that are measured, and factors that control test results, to the diagenetic and kinematic history of the rock.

Mapping Subsurface Fractures with Scanned CL Observations

Justification for Using Scanned CL Imaging

Natural fractures in highly cemented, low-matrix-permeability gas reservoir sandstones can enhance fluid flow and gas deliverability, and they are increasingly viewed as potential targets for directional and horizontal drilling (Finley and others, 1990; Laubach and Marin, 1992; National Research Council, 1994). The orientation, size, and shape of reservoir drainage areas, and the success of drilling, stimulation, and completion operations, also may be influenced or controlled by fractures (Laubach, 1989a). Maps of fracture strike should be basic to exploration and development planning in such rocks. Yet no technology currently available allows *systematic* mapping of natural fracture strike in subsurface sandstones.

There is an obvious reason that such technology is lacking. Few wellbores intersect fractures owing to the nearly vertical inclination and wide spacing that typify large fractures in flatlying sedimentary rocks. Such fractures have an exceedingly low probability of being intersected by vertical wellbores. Fractures that do not intersect the wellbore are not detectable by geophysical logging methods. The same sampling limitations apply, of course, to whole core. Current fracture detection methods commonly do not provide statistically significant data sufficient to map shifts in fracture orientation within a given unit or from one unit to the next.

In this section we describe how bed-by-bed evidence of fracture orientation can be obtained and how subsurface fracture strike can be mapped using core data even where macrofractures are absent in the core. The method is based on evidence that quartz-sealed microfractures are widespread in sandstone, as revealed by petrography and photomultiplier-based imaging of electron beam-induced luminescence (scanned CL). In representative sandstones having synkinematic quartz cement, some microfractures have a preferred orientation that is parallel to that of contemporaneous macrofractures. Using microfracture strikes derived from petrographic observations and scanned cathodoluminescence (CL) images, it is possible to track macrofracture patterns in these sandstones. Because of the small sample volume required to obtain microfracture data, the method is suitable for use with rotary sidewall core samples.

Cathodoluminescence in Quartz

Scanned cathodoluminescence (CL) imaging permits clear distinction between detrital quartz and subse-

quently precipitated authigenic quartz in microfractures at the micron scale (Milliken, 1994). Figures in the following section show scanned CL images that were produced using an Oxford Instruments photomultiplier-based CL detector installed on a JEOL T330A scanning electron microscope. Light collection is carried out with a parabolic mirror inserted approximately 1 mm above the surface of a carbon-coated, epoxy-impregnated polished thin section (fig. 104). An accelerating voltage of 10 KV produced adequate photon emission for examining luminescence variations in detrital, authigenic, and vein-fill quartz.

Although the controls on wavelength and intensity of photon emission from quartz are not fully understood, trace impurities and crystal defects are the most likely factors that affect cathodoluminescence (Marshall, 1988; Walker and Burley, 1991). Regardless of primary controls, it is well established that there is a general tendency for quartz precipitated from aqueous solution at relatively low temperatures to have less intense CL than does quartz crystallized at high temperatures (e.g., Sipple, 1968; Zinkernagel, 1978) and that this CL heterogeneity in quartz persists through a wide range of burial diagenetic conditions before it is ultimately homogenized during low-grade metamorphism (Sprunt and others, 1978).

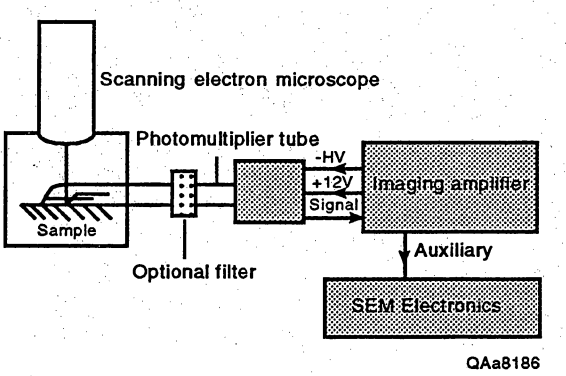

Figure 104. Scanned CL detector arrangement.

Petrographic Methods and Sampling

Microstructures of Ozona and Sonora Canyon, Travis Peak, and Frontier sandstones were studied using standard light microscopy and scanned cathodoluminescence (CL) imaging. Samples were from oriented sandstone intervals, intervals adjacent to macrofractures, intervals in sections of core that are continuous with core that contains macrofractures, and from intervals with various types of cement. Also studied were thin sections from samples that had been used in fracture toughness and axial point-load tests. In addition to these samples, we examined a suite of samples from other tight gas sandstone cores, and from outcrops of sandstones in the Appalachians, Central and West Texas, and various basins in the western United States.

Microfractures

Results from the four formations we studied in detail, as well as our reconnaissance studies of other quartz-cemented sandstones, show that closed microfractures are widespread. Milliken (1994) reported that closed microfractures are common in a separate suite of 12 sandstones. Some closed microfractures are visible with transmitted light microscopy, but scanned CL reveals many more fractures than are visible with conventional petrography, and the fractures are depicted in much greater detail.

Filled or closed microfractures are in some instances visible using standard light microscopy as micron-scale curviplanar arrays of liquid- and/or gas-filled inclusions and mineral precipitates 1 μm to several centimeters in length (figs. 105 and 106). Closed microfractures have long been recognized in igneous and metamorphic rocks (Tuttle, 1949; Sprunt and Nur, 1979; Roedder, 1984). In these rocks, inclusion-decorated planes have been interpreted to be "healed" or "sealed" opening-mode (extensional) microfractures (for example, Tuttle, 1949). Microfractures that have healed evolve from an initial fluid-filled planar crack into fluid-inclusion planes by local-scale diffusive mass transfer and differential solution and deposition driven mainly by surface forces (Lemmlein and Kliya, 1960; Smith and Evans, 1984), whereas sealed microfractures are filled by precipitated material that has been transferred into the fracture from some distance away.

In general, microfractures in buried sedimentary rocks must be measured in samples derived from core because they are too small and offer too little contrast with surrounding rock to be detected with current logging methods. In the future, advanced detectors on drilling systems that can sense features such as microfractures in the wellbore wall might be possible (National Research Council, 1994). Such detectors could possibly evolve from current geochemical logging and electrical fracture-imaging technology. Other indirect methods to detect microfractures may be feasible. A common assumption of geophysics is

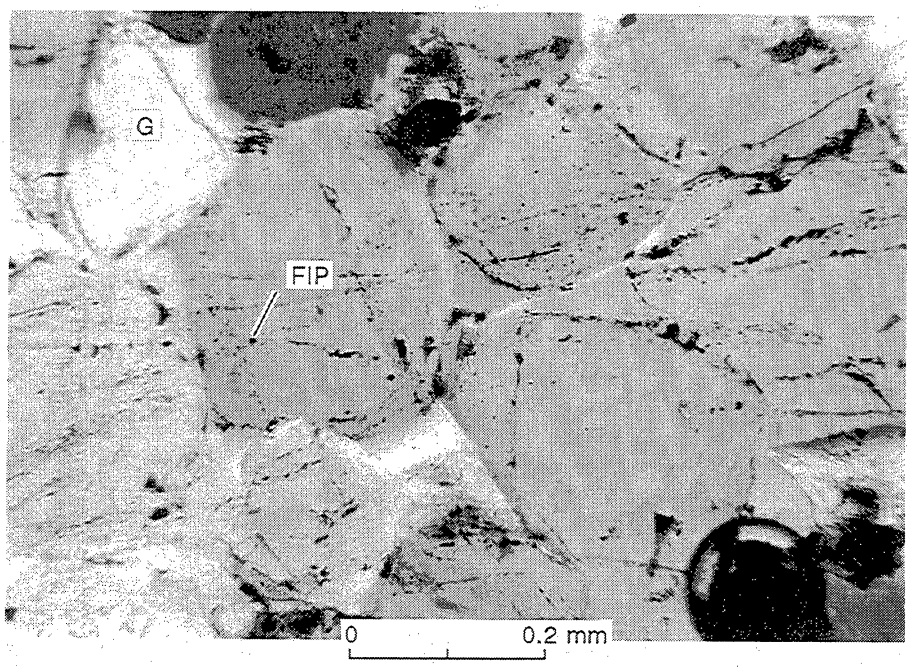

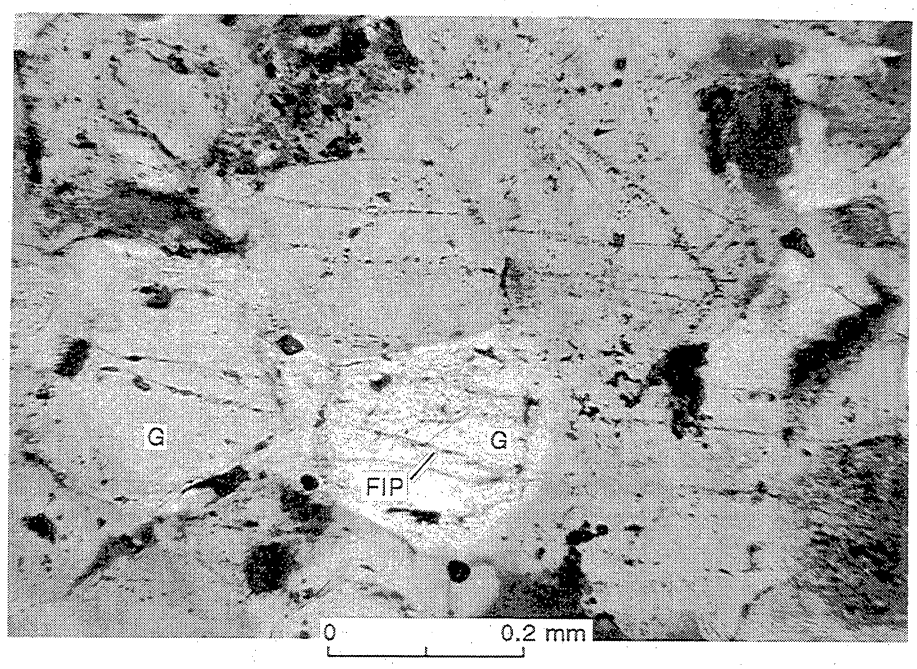

Figure 105. Photomicrographs of fluid-inclusion planes, Travis Peak Formation, Prairie Mast No. 1-A well, depth –9,215.2 ft. G, grain; c, cement; FIP, fluid-inclusion plane (transgranular *Type a+* sealed microfracture). Plan-view thin sections; north is to top of images.

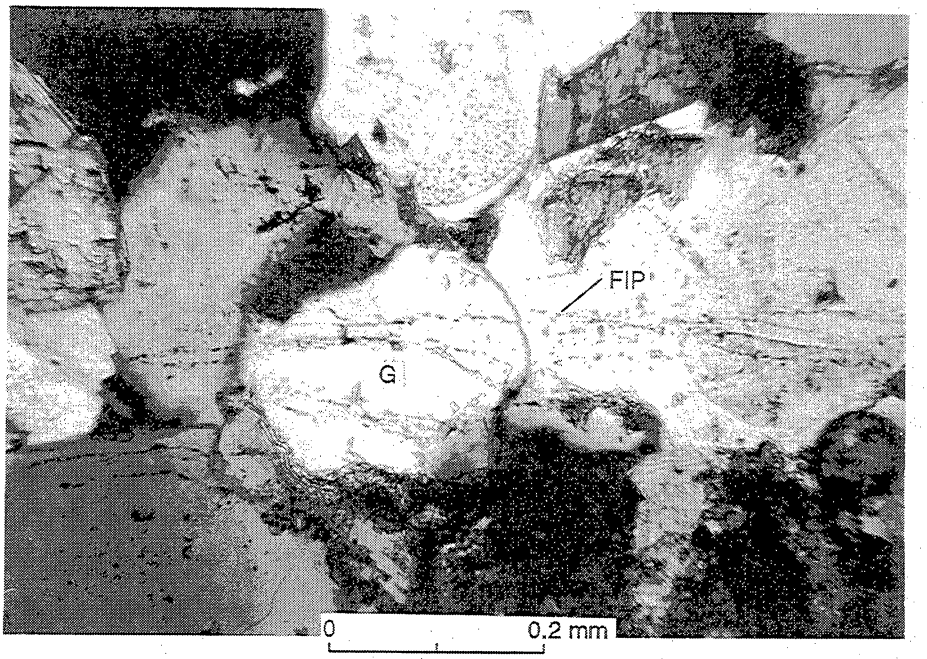

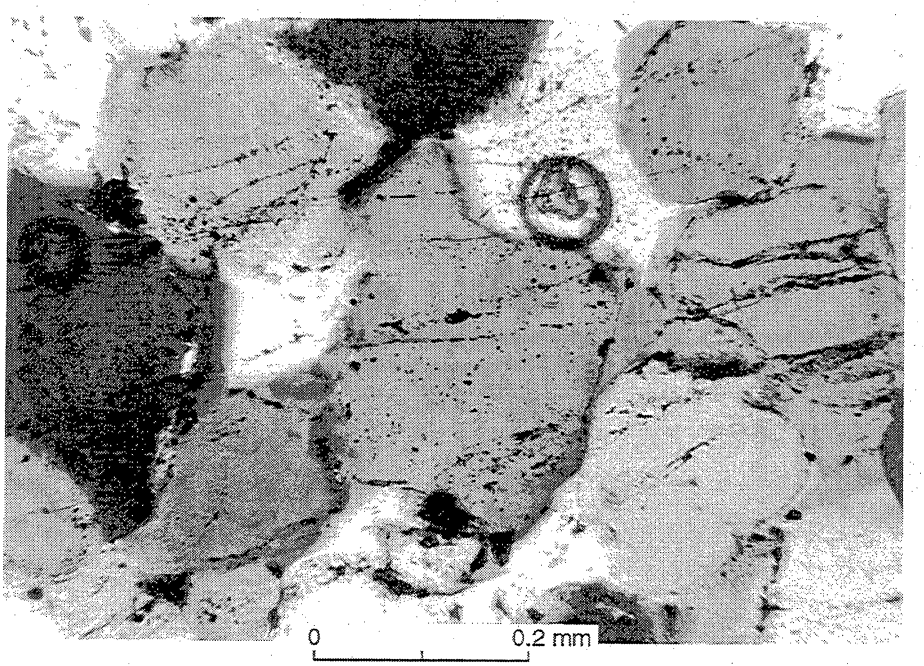

Figure 106. Photomicrographs of fluid-inclusion planes, Travis Peak Formation, Holditch SFE No. 2 well, depth –9,871 ft. Plan-view thin sections; north is to top of image.

that the mechanical behavior of rock in the brittle field is determined by the formation, growth, and coalescence of microcracks. As a result of anisotropy of the stress field at the time of fracture formation, these microcracks show some degree of preferred orientation. Shepherd (1990) postulated that arrays of subvertical fluid-filled microfractures might be detectable by measuring seismic wave anisotropy.

Inherited Microfractures

Fluid-inclusion planes that are inherited from the source rocks of detrital grains are difficult to distinguish with petrographic methods from fractures that are sealed in situ. In metamorphic and igneous rocks, closed microfractures having well-developed preferred orientation are widespread (Tuttle, 1949; Sprunt and Nur, 1979; Kowallis and others, 1987), and the erosion and redeposition of grains derived from such rocks, and from vein quartz, are sources of inherited microfractures in sandstone grains. Closed microfractures are also present in folded and faulted quartzose sedimentary rocks (Dula, 1981; Laubach, 1988a; Onash, 1990; Wu and Groshong, 1991). Inherited microfractures in grains can be identified petrographically and with scanned CL imaging.

Transgranular Fluid-Inclusion Planes

Several types of *postdepositional* fluid-inclusion planes are visible in Canyon, Travis Peak, and Frontier sandstones. Some planes are restricted to detrital grains, whereas other cross grains and adjacent cement or several grains and intervening cement. The latter type, called transgranular fluid-inclusion planes, were used in a petrographic study of the Travis Peak Formation to ensure that inherited filled microfractures were not measured inadvertently. Transgranular fluid-inclusion planes are sealed microfractures that cross more than one grain and that typically cross several grains and intervening cement. In the Travis Peak Formation such fractures may be as much as 3 mm long. They are difficult to identify with transmitted-light microscopy because they are narrow and generally only a few grain diameters long. Moreover, fluid inclusions are sporadically distributed along their traces, so that it is commonly difficult to be sure that the fluid-inclusion plane is continuous across several grains or grains and cement. Although it is sometimes possible to show with petrographic observations that transgranular fluid-inclusion planes are filled with quartz, the quartz in these closed fractures is in optical continuity with host grains or cements. This is the main reason these features are so difficult to see and why it is difficult to identify the attributes of the closed microfractures.

Fluid-inclusion planes visible with conventional microscopy occur as isolated planes that are 1 to 10 μm wide. Grain boundaries are not laterally offset parallel to the traces of planes. Planes are composed of closely to widely spaced, small (less than 10 μm) fluid inclusions that show regular, subspherical to irregular shapes. Some shapes are transitional between tubes and spheres, and locally areas of preserved microfracture porosity are present. Locally, regions of tabular, plate-shaped pores or open microfractures grade laterally into fluid-inclusion planes composed of coplanar cylindrical, spherical, or irregular-shaped inclusions. Fluid inclusions are generally arranged in a single plane, but locally patterns are more complex and include planes composed of multiple fluid-inclusions zones arranged in symmetric patterns about the centerline of the fracture.

The small size of many inclusions in closed microfractures (1 to 5 μm) hinders microthermometric analysis. Many of the inclusions in closed microfractures are composed of a single, colorless, nonfluorescent phase, probably a brine. In all three formations, a few transgranular and transcement fluid-inclusion planes have two-phase, gas+liquid inclusions. In the Travis Peak Formation, a few measurements suggest that the properties of these fluids and their trapping temperatures are similar to those of A-type fluid inclusions in quartz veins.

Transgranular fluid-inclusion planes are generally perpendicular to bedding and are commonly subvertical. Planes cross cement and grains that have different crystallographic orientation with little or no deflection, indicating that there is no crystallographic control of plane orientation. Some planes end at grain-grain contacts and pass through or near grain centers. Other planes cut grains and cements randomly and do not have any specific geometric relation to grain centers or grain-grain contacts.

CL Appearance of Microfractures

Scanned CL images show that microfractures are narrow and have abrupt boundaries marked by changes in CL tone and that fractures have gradually tapering, sharp terminations. Microfractures have smooth, planar walls and CL tone that is identical to that of quartz cement. The CL of thin microfractures is a uniform dark tone, but microfractures that are more than 10 microns thick locally are zoned. Microfractures have a range of widths and lengths. Most of these fractures

are too short or narrow to be detectable by conventional transmitted-light petrography. Many are not associated with fluid inclusions. Examples are shown in figures 107 through 111. Microfractures were examined in polished thin sections, permitting comparison of optical and scanned CL appearance.

Several types of CL microfractures can be distinguished on the basis of the position of the microfracture in the rock and crosscutting relations of fractures and cement. These categories of microfracture are listed in figure 112. *Type a+* microfractures cross several grains and intervening cement. These fractures are generally more than 2 μm wide. This category of microfracture is generally visible with conventional transmitted light microscopy as planes of transgranular fluid inclusions. *Type a* microfractures are similar to *Type a+*, in that they cross several grains and intervening cement, but they are generally thinner than *Type a+* fractures and they are not associated with planes of fluid inclusions that can be distinguished with conventional microscopy.

Type b fractures cross grains and cement, but they do not clearly crosscut more than one grain. *Type c* fractures have a CL appearance that is identical to that of *Type a+* through *b* fractures, but these fractures are restricted to a single grain. Fractures in crushed grains fall into this category, as do other sporadic microfractures within grains. In some instances these fractures emanate from grain-grain point contacts. Locally, in the Travis Peak examples, crosscutting relations show that *Type c* fractures are older than *Type b* fractures. The categories from *Type a+* to *Type c* reflect decreasing certainty that the fractures are truly postdepositional and syndiagenetic (not inherited). The classification also reflects our interpretation of whether the fractures result from deformation that is uniform over the scale of many grains, or if deformation is localized within one or a few grains. Deformation that is uniform over larger areas of sample is more likely to give an accurate view of macrofracture patterns.

Types a+ through *b* are definitely postdepositional features. *Type c* fractures are probably postdepositional, but they are most likely related to local deformation or are too small to interpret accurately. *Type d* fractures represent fractures that have lighter CL tone. These fractures are truncated at grain boundaries and are probably inherited.

Microfracture Abundance

Microfracture types are present in varying proportions in different sandstones and in various parts of the same sandstone. Generally *Type a+* fractures are least common, and *Type b* or *c* fractures are most common. Figure 112 shows varying proportions of microfractures in thin sections from Travis Peak core from the Prairie Mast well. The cause of variation in abundance is probably related in part to sandstone composition, with more quartz-rich samples having more *Type a+* fractures. Coarser, more poorly sorted sandstones also tend to have more *Type a+* and *Type a* fractures than do very fine-grained, well-sorted rocks. *Type a+* and *a* fractures are rare or absent in rocks with clay matrix, abundant clay cement, or more than a few percent calcite cement.

The rock's composition affects abundance measurements in two ways. Fractures are less readily detected in rocks having clay and carbonate minerals because fractures show less contrast and are harder to see when they cross these materials. For example, *Type a* fractures may be incorrectly categorized as *Type c* as a result of the analyst's not being able to track the microfracture across dark-toned clay cement. Conversely, coarse grain size favors identification of fractures because fractures are seen most easily against the background of large, uniform-tone grains. However, the composition of the rock also likely affects how fractures propagate and their abundance. Stronger, more quartz-rich rocks may tend to develop microfractures having significant lateral extent, whereas deformation of rocks composed of large proportions of weak clay and carbonate minerals or feldspar may be by distortion or failure of the weak constituent grains or cement (figs. 113 and 114). Coarse grain size and extensive, strong quartz cement tends to promote transgranular fracture. In contrast, finer-grained rocks or those with weak cements may tend to fracture around grains.

Overall abundance of microfractures is highly variable, and the causes of variation are not yet fully clear. In general, rocks that have been the most deeply buried and that have the most extensive quartz cement have the most sealed microfractures. High *Type a+* fracture abundance, on the order of 10–100 microfractures per centimeter, occurs locally near macrofractures

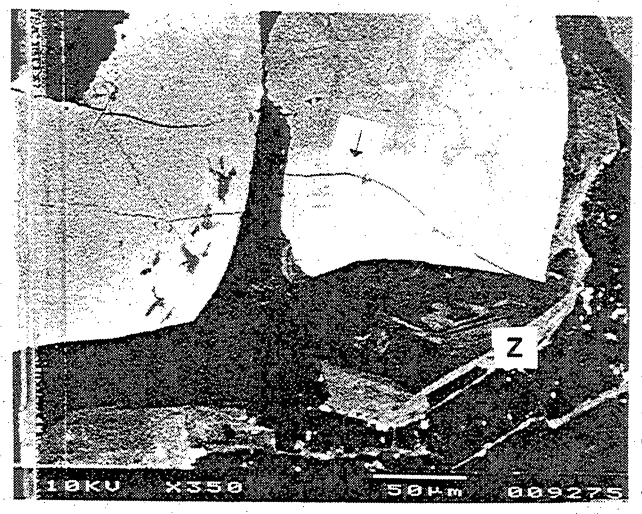

◀ Figure 107. Sealed microfractures revealed by scanned CL imaging, Prairie Mast No. 1-A well, depth –9,215.2 ft. Note cement zoning (Z) and *Type c* microfractures (arrow). Thin section cut parallel to bedding.

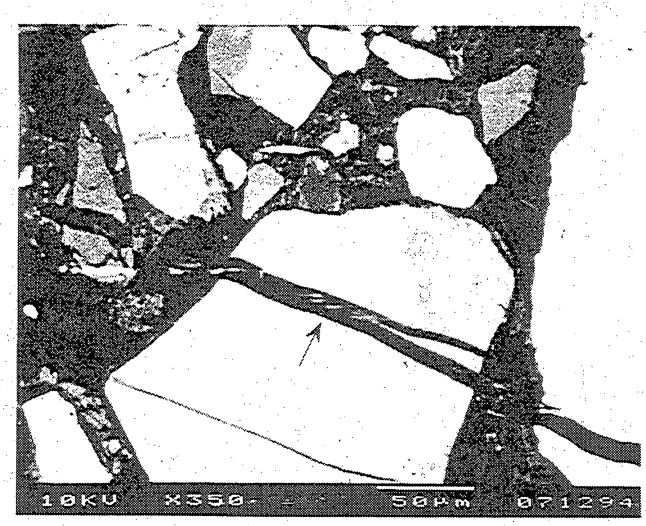

◀ Figure 108. Sealed microfractures revealed by scanned CL imaging, Prairie Mast No. 1-A well, depth –9,966.2 ft. Thin section cut parallel to bedding. Arrow indicates edge of sharp-sided fracture.

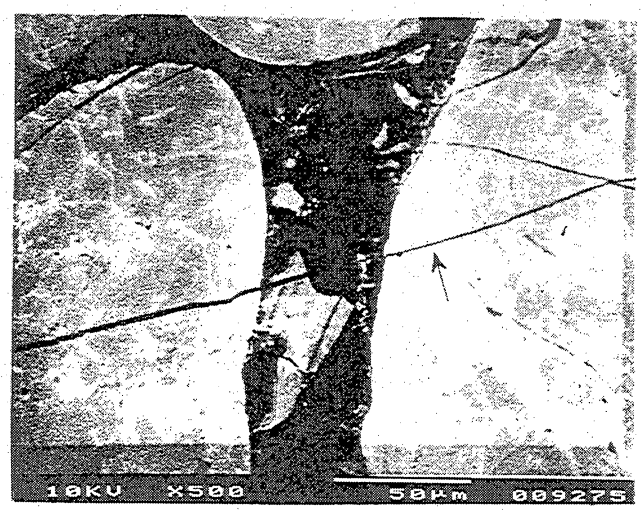

◀ Figure 109. Sealed transgranular microfractures revealed by scanned CL imaging, Prairie Mast No. 1-A well, depth –9,215.2 ft. Thin section cut parallel to bedding. Arrow indicates transgranular *Type a+* microfracture.

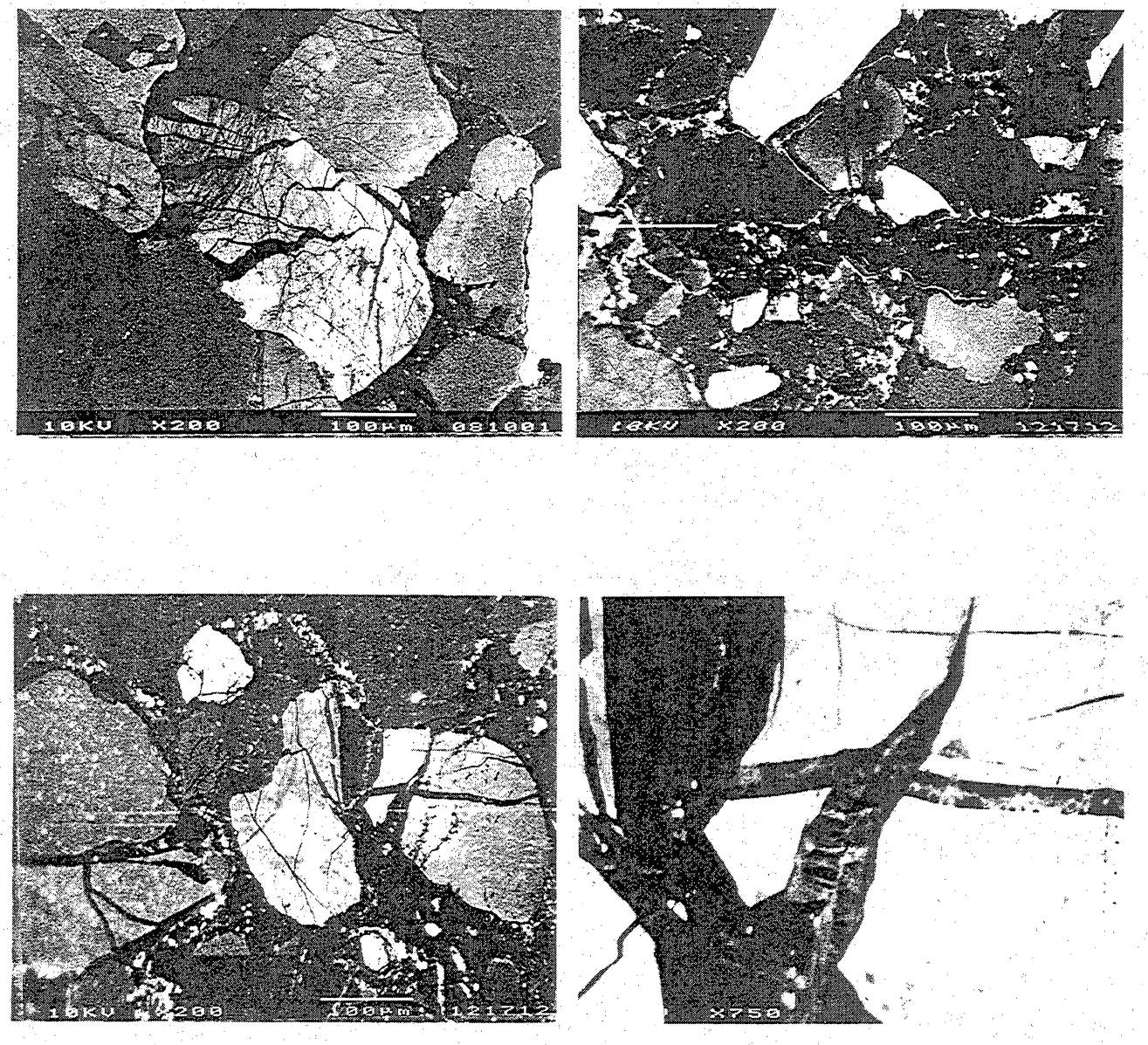

Figure 110. Sealed microfractures revealed by scanned CL imaging. (a) Prairie Mast No. 1-A well, depth –9,214.6 ft. (b) Church Buttes well, –12,170.8 ft, Frontier Formation, sealed microfractures. (c) Same well, showing crosscutting sealed microfractures. (d) Detail of (c). Thin section cut parallel to bedding.

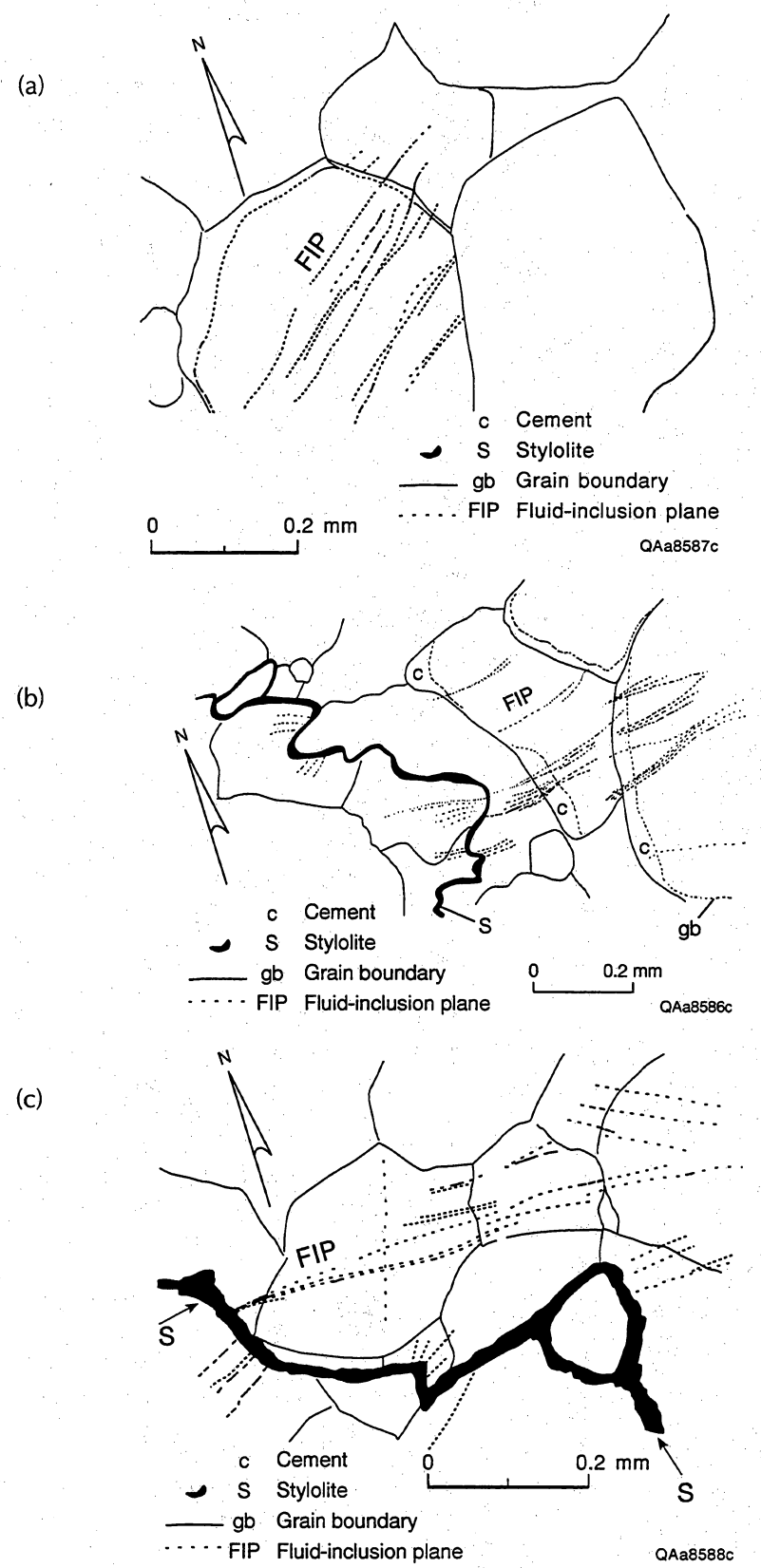

Figure 111. Microfracture patterns in plan view; all thin sections cut parallel to bedding, Frontier Formation. (a) Fluid-inclusion planes (FIP's) cross cement and grain boundary. Wexpro Church Buttes No. 48, depth –12,165.0 ft. (b) Fluid-inclusion planes (FIP's) at a high angle to trace of vertical stylolite(s). Note FIP's cross cement (c) and grain boundary (gb). Wexpro Church Buttes No. 48, –12,165.0 ft. (c) Transgranular FIP at high angle to trace of vertical stylolite (S). Wexpro Church Buttes No. 48, –12,165.0 ft.

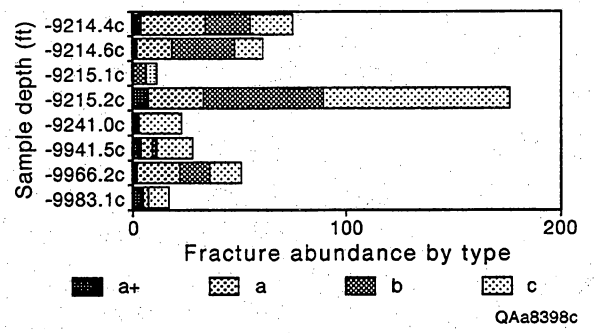

Figure 112. Diagram illustrating abundance (number of fractures) of various types of sealed microfractures. Data from various depths, Prairie Mast No. 1-A well. Microfracture categories are defined in the text.

(fig. 115). The distance over which extensive microfracture abundance occurs is, in some cases, as great as 10 cm. This raises the possibility that microfracture abundance can be used as an indicator of macrofracture proximity. Areas of stylolite development also have locally abundant microfractures and are sites where microfractures should be sought during core sampling. Fractures are commonly located near the teeth of stylolites.

Microfracture Orientation in Three Formations

Transgranular fluid-inclusion planes in sandstone were used to track the strike of macrofractures in East Texas Basin sandstone gas reservoirs (Laubach, 1987, 1989a). Those studies showed that closed microfractures exist in a typical quartz-cemented sandstone—the Travis Peak Formation—even where effects of tectonism are slight and beds are nearly flatlying and undistorted. Our subsequent petrographic and CL studies show that quartz-sealed microfractures with preferred orientation occur in all four formations. In sandstones in these diagenetic environments, fractures are sealed with diagenetic quartz, not healed. We interpret sealed microfractures to be a byproduct of synkinematic cementation.

The significance of the observation that sealed microfractures having preferred orientation exist in formations such as the Travis Peak, Canyon, and Frontier is that these rocks are *not* in areas of intense folding and faulting, yet they locally contain numerous microfractures (fig. 115). The key to rapid and effective detection and characterization of these fractures is scanned CL imaging. Some types of microfracture (*Type a+* and *Type a*) and adjacent macrofractures are generally subparallel where they occur in the same core.

Studies of Ozona and Sonora Canyon, Frontier, and Travis Peak sandstones show that quartz-sealed microfractures are present in all of these sandstones and that the largest microfractures, *Type a+* to *Type b*, have moderate to very strong preferred orientation. Fracture orientation is independent of crystallographic orientations of the mineral grains or grain-grain contact relations. Fracture orientations controlled by grain-grain contacts are visible in all three formations, but these fractures tend to be restricted to individual grains (*Type c*). We interpret these latter microfractures to primarily represent deformation of sandstone at a time when cement was sparse enough for the rock to behave as a granular aggregate. In granular materials microcracks generate tensile stress concentrations in adjacent grains near the crack tip. These stresses, combined with the variable strength of grains, can, in some cases, drive propagation of fractures across adjacent grains, resulting in some early *Type a* fractures having orientations governed by grain-packing arrangements.

Travis Peak Formation Microstructures

In examples from the Travis Peak Formation, orientation information from oriented core over a range of depths from several wells conclusively shows that microfractures are a reliable guide to the strike of nearby macrofractures. These fractures generally have steep dips, similar to those of macrofractures. Fracture dip was measured on the universal stage from 20 sets of 3 orthogonal thin sections from the Travis Peak samples from the SFE No. 1 well, and with smaller sets of orthogonal thin sections from several other wells. Results show that transgranular microfractures have dips that are typically as steep as 80 to 90 degrees (fig. 116).

Microfractures strike parallel to contemporaneous macrofractures, where timing relations are inferred from cement-vein-fill textures. The most compelling examples of this relationship are from the Travis Peak Formation, in part because more macrofractures were recovered from this formation and because long, continuously fitted core intervals exist in this core collection that facilitates comparison. Nevertheless, correspondence in macro- and microfracture strike is also evident for the other two formations. For petrographic studies of microfractures, samples were cut from core containing macrofractures and from oriented core that lacked macrofractures so that fracture strikes could be compared even in cases where the orientation of fractures relative to north was unknown. In the Travis Peak, microfractures and macrofractures from a range of depths in a given well have similar strikes (figs. 117 and 118).

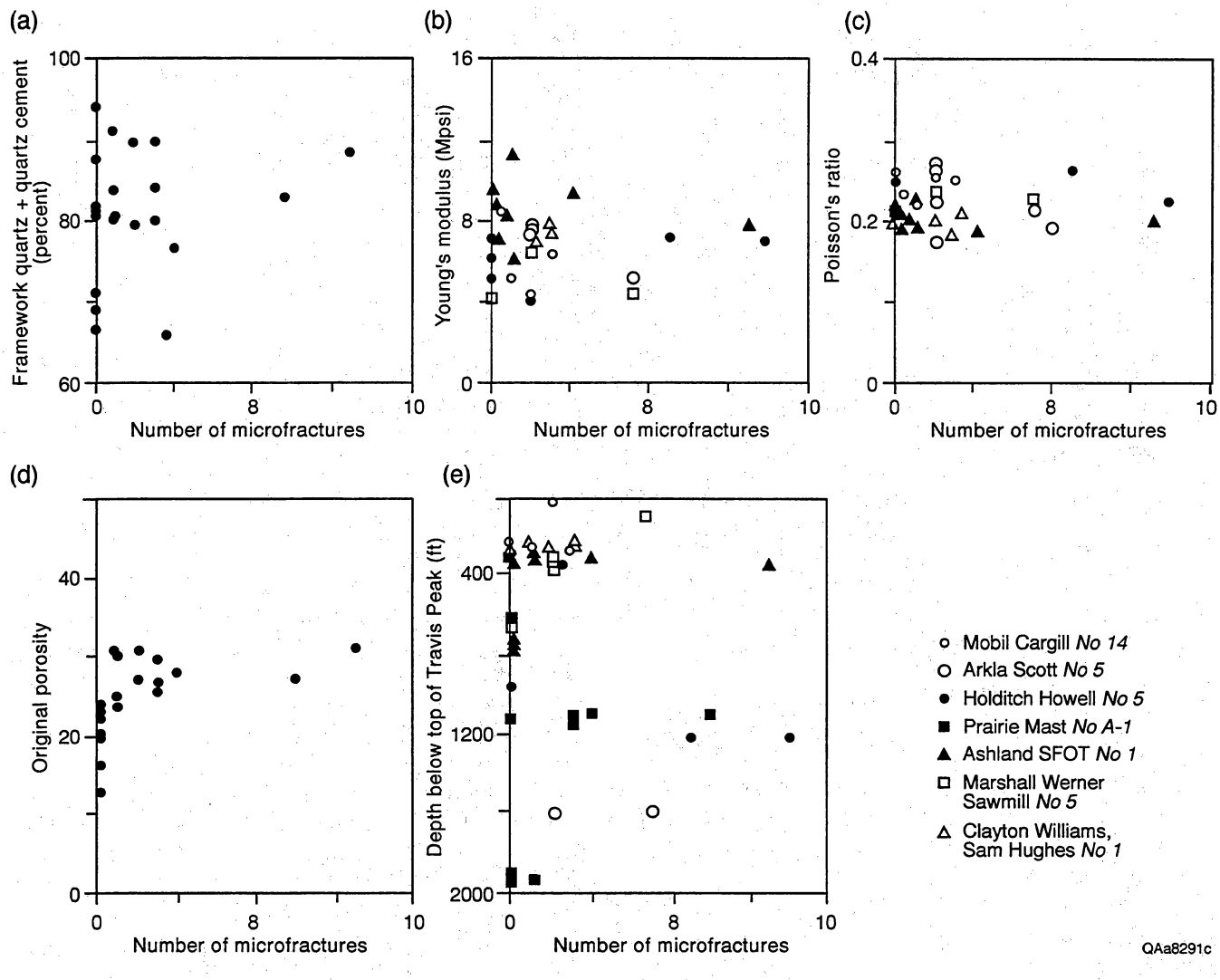

Figure 113. Rock composition and microfracture abundance, *Type a+* microfractures, various Travis Peak Formation wells.

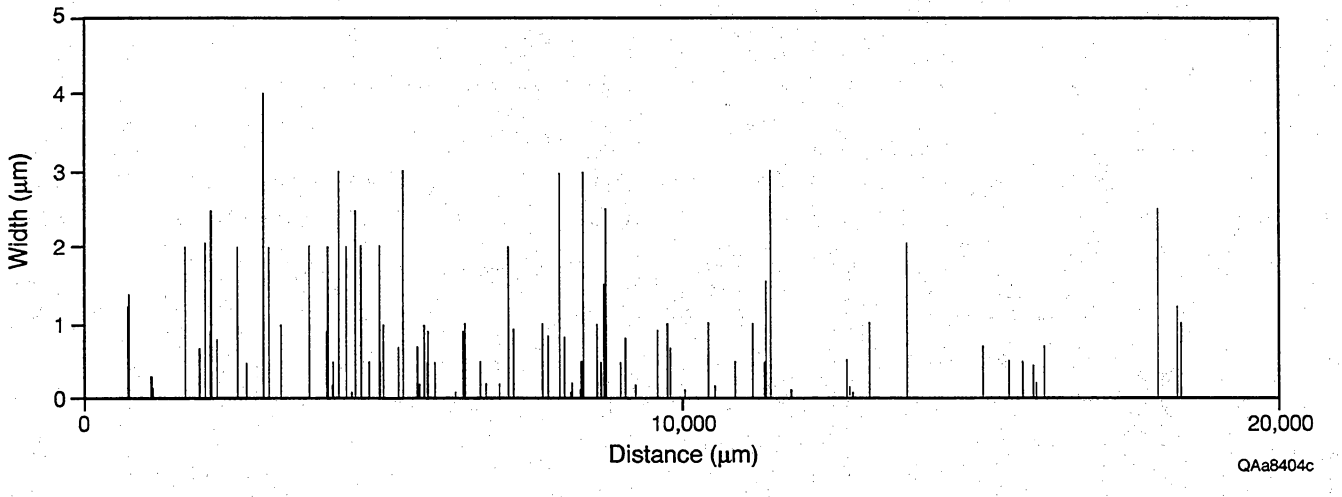

Figure 114. *Type a+* microfracture width versus distance across fracture strike for a highly microfractured sample, Holditch SFE No. 2 well, depth –9,871 ft.

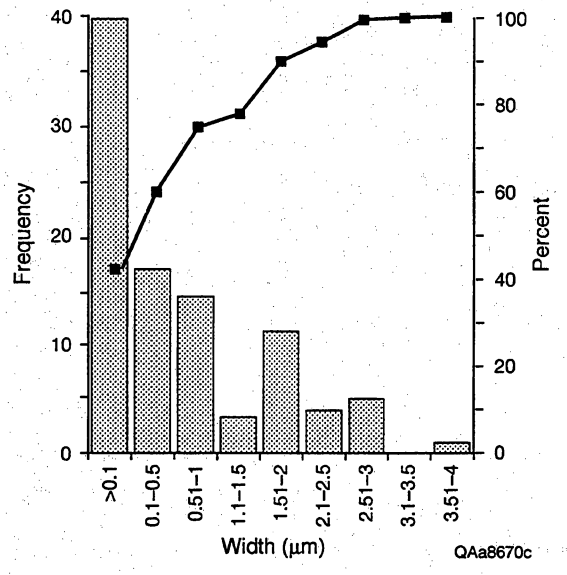

Figure 115. Histogram of sealed microfracture widths. Travis Peak Formation example, SFE No. 2 well, depth –9,871 ft.

Figures 119 and 120 show examples of sealed microfractures in plan view. These specimens from the Travis Peak Formation were cut in a plane parallel to bedding, and the strike of near-vertical fractures can be directly measured from these CL images. In this example, microfracture strike corresponds to that of macrofractures that are present in a continuously fitted section of core, so there is no uncertainty of the relative orientation of macro- and microfractures. The overall strike of Travis Peak fractures from different wells in the East Texas region is also similar (figs. 121, 122, and 123).

Macrofractures in Travis Peak sandstone typically are nearly vertical and strike east-northeast to east, with a range of strikes from 027 to 167 degrees and a mean strike of 081 degrees (fig. 124). Considerable variation in fracture strike is evident from well to well, within a given well, and within any depth interval in a single well. Core orientation results generally have an uncertainty of less than 15 degrees within a given well, so a certain amount of variability in strike may be due to core orientation errors. The range of macrofracture strikes observed in Travis Peak wells in East Texas was interpreted to be the result of some variability in fracture strike with additional scatter resulting from core orientation errors (Laubach, 1989b).

Although these factors must play a role in observed fracture-strike patterns, scanned CL observations show that there are at least two directions of fracture strike that developed sequentially as quartz cement was precipitated. This is consistent with a low-angle intersection between two macrofractures observed in the SFE No. 1 well. With the perspective provided by the scanned CL data, this observation of macrofracture relations can be interpreted as a fortuitous sampling of fractures representing both of the macrofracture sets. It provides information on how two fracture sets that were recognized first with CL observations are interconnected.

Canyon Microstructures

Microfractures in Canyon examples have preferred strike, although the samples we studied all have relatively high dispersion in fracture strike (figs. 125 and 126). Abundance of microfractures is variable; microfractures are mainly concentrated in the most highly quartz-cemented samples.

This type of fracture-strike information can contribute to characterization of regional fracture patterns and to understanding production patterns. Many tight gas sandstones have data sets similar to those of the Sonora Canyon. Given the limited core data and the strike of macrofractures, there is evidence of variability in fracture strike, but lack of sufficient macrofracture orientation data precludes reliable identification of patterns. Laubach and others (1994) and figure 124 summarize natural fracture orientations (strike). In the Ward "C" No. 11 and Sawyer "A" 144 No. 5 wells, some core was oriented by using downhole methods and comparing features in core to oriented borehole images from FMS logs. Fractures in the Ward "C" No. 11 well strike northeastward and northwestward. In the Sawyer "A" 144 No. 5 well, five fractures strike northwestward, two strike northeastward, and one strikes east-northeastward. In this well four fractures visible only on FMS images and interpreted to be natural fractures strike northwestward (mean strike 319 degrees).

This variability is not simply the result of core orientation errors; instead, it reflects real variability in strike from area to area or the presence of multiple fracture sets. A range of natural fracture orientations in Canyon sandstones is confirmed by inspecting fractures in intact sections of core. In the Ward "C" No. 11 well, two fractures in the same core interval differ in strike by 12 degrees (strikes of 244 degrees and 232 degrees). In Sawyer "A" 144 No. 5 core, three fractures in the same core interval have strikes of 006 degrees, 165 degrees, and 074 degrees, indicating that fractures are present that are oriented at nearly right angles. Four oriented fractures in core from this well are in a continuous core interval and have differences in strikes ranging from 12 to 71 degrees. In a single shale layer two fractures in this well have strikes that differ by 30 degrees.

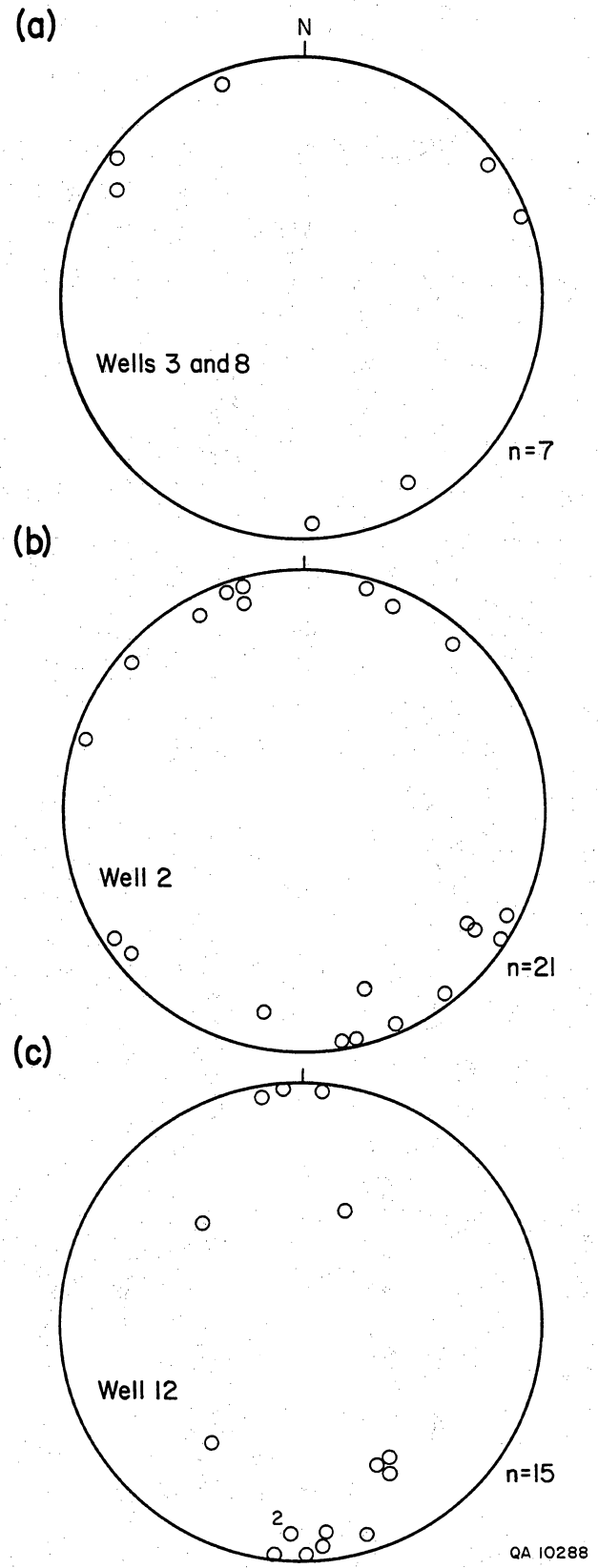

Figure 116. Lower-hemisphere equal-area plot of poles to *Type a+* microfractures, showing generally steep fracture dips. Data from four Travis Peak Formation wells.

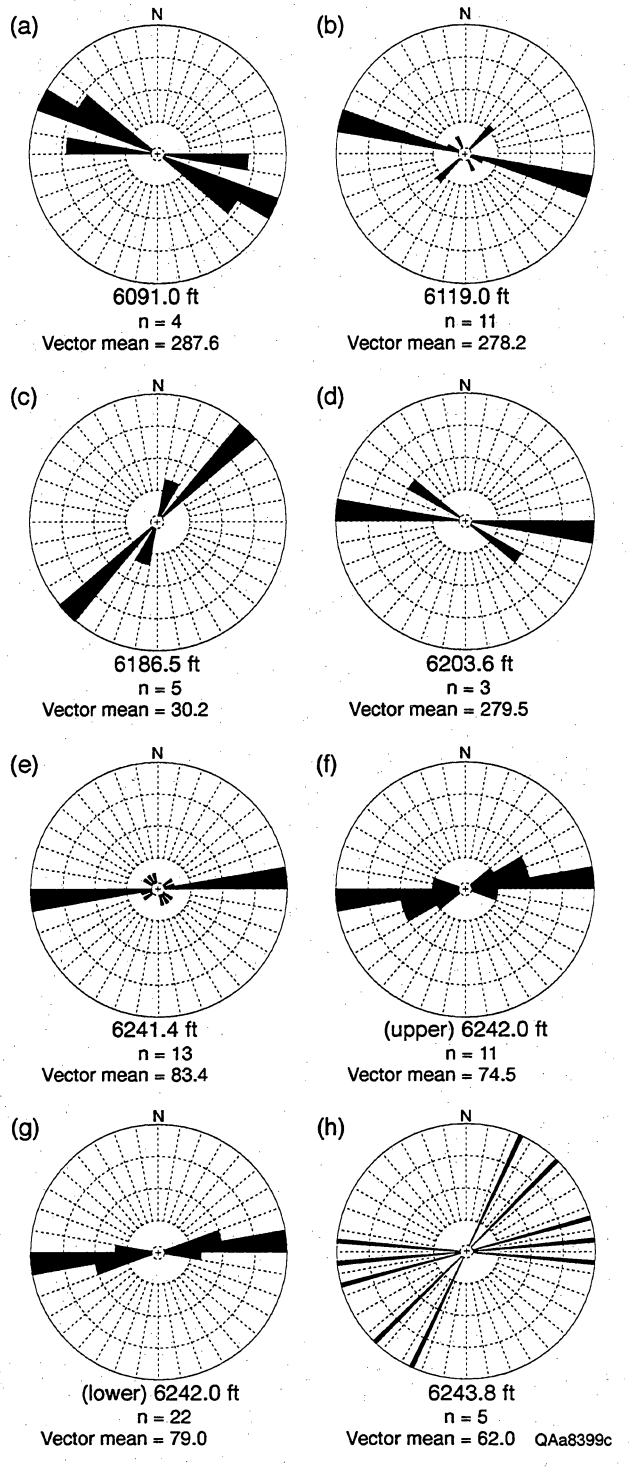

Figure 117. Rose diagrams showing microfracture strike, Holditch Howell No. 5 (SFE No. 1) well, Travis Peak Formation, various depths.

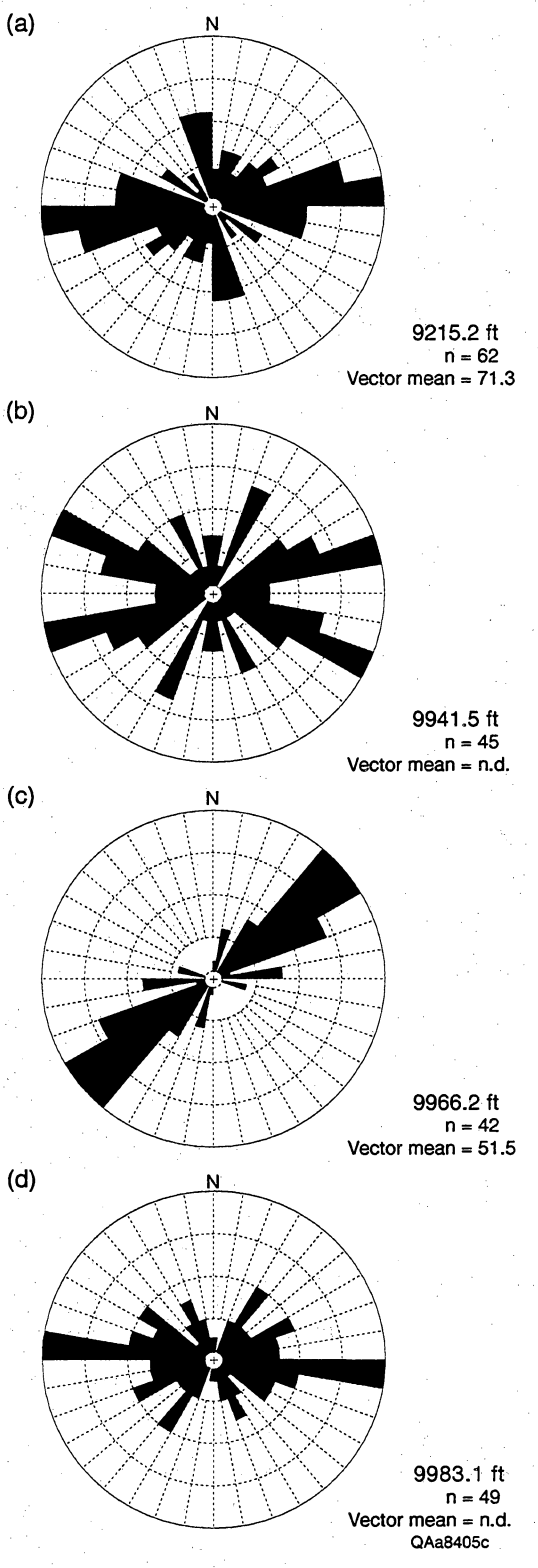

Figure 118. Rose diagrams showing microfracture strike, Prairie Mast No. 1-A well, various depths.

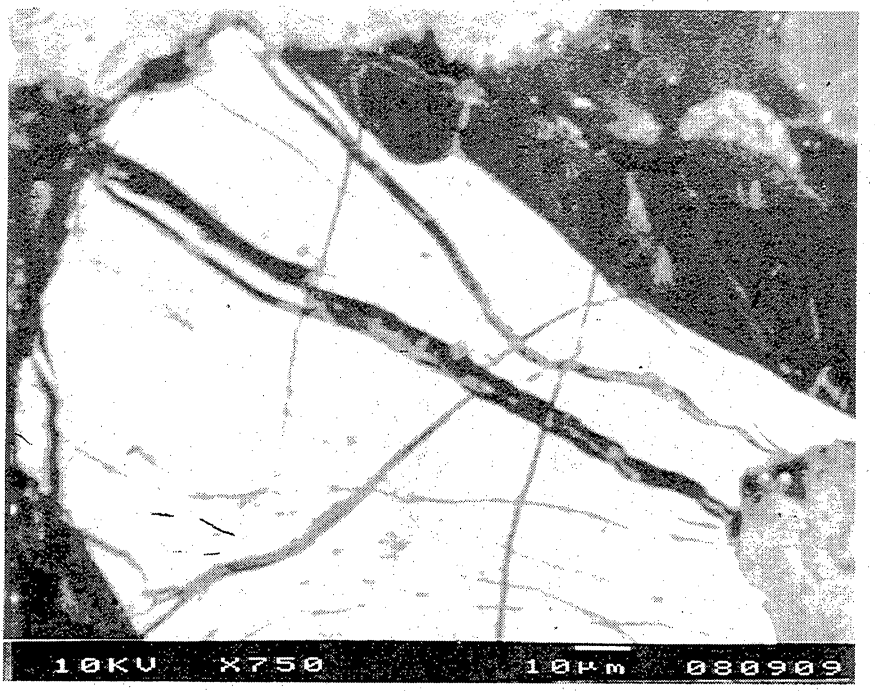

Figure 119. Sealed microfractures revealed by scanned CL imaging, Prairie Mast No. 1-A well, depth –9,214.6 ft.

Lateral intersections of vertical fractures are rarely seen in core. Consequently, evidence is sparse for estimating the relative age of fractures on the basis of abutting and crossing relations. A quartz-lined fracture in the Sawyer "A" 144 No. 5 core (strike 044 degrees) crosscuts an older clay-filled fracture (strike 136 degrees), showing that fractures of more than one age are present. The observed dispersion in fracture strike and evidence of more than one generation of fractures preclude identifying a dominant fracture orientation from the macrofracture data set. Our evidence, however, suggests that sealed microfractures are contemporaneous with northeast-striking quartz-lined macrofractures, and that microfracture data can be used with diagenesis information to unravel controls on fracture porosity in this unit. As described in the following section, point-load strength anisotropy also trends northeastward in some Sonora Canyon sandstones.

Because they strike parallel to SHmax, conventional interpretation of east-northeast or northeast Sonora Canyon fracture strikes in this area is that they would be prone to be open in the subsurface on the basis of subsurface stress conditions. However, if synkinematic quartz-lined fractures formed when Canyon sandstones were exposed to protracted high temperatures at depths of 2.5 to 3 km (1 to 2 mi) early in their burial history, synkinematic fractures could have formed at that time. The strong bridges created by partial quartz cementation could have kept these fractures open during subsequent burial and uplift. A comparison of macrofracture and microfracture strike is shown in figure 127.

Frontier Formation Microstructures

Closed microfractures are evident in the Frontier Formation, but the number of *Type a+* transgranular fractures is sparse compared to the Travis Peak and Canyon sandstones (table 16, appendix 2). This is expected, given the relatively high content of soft components among Frontier Formation grains and cements. These include abundant clay-rich particles, high feldspar content, and locally, extensive carbonate cement. Nevertheless, microfractures are present, and they have distinct preferred orientations (figs. 128 and 129).

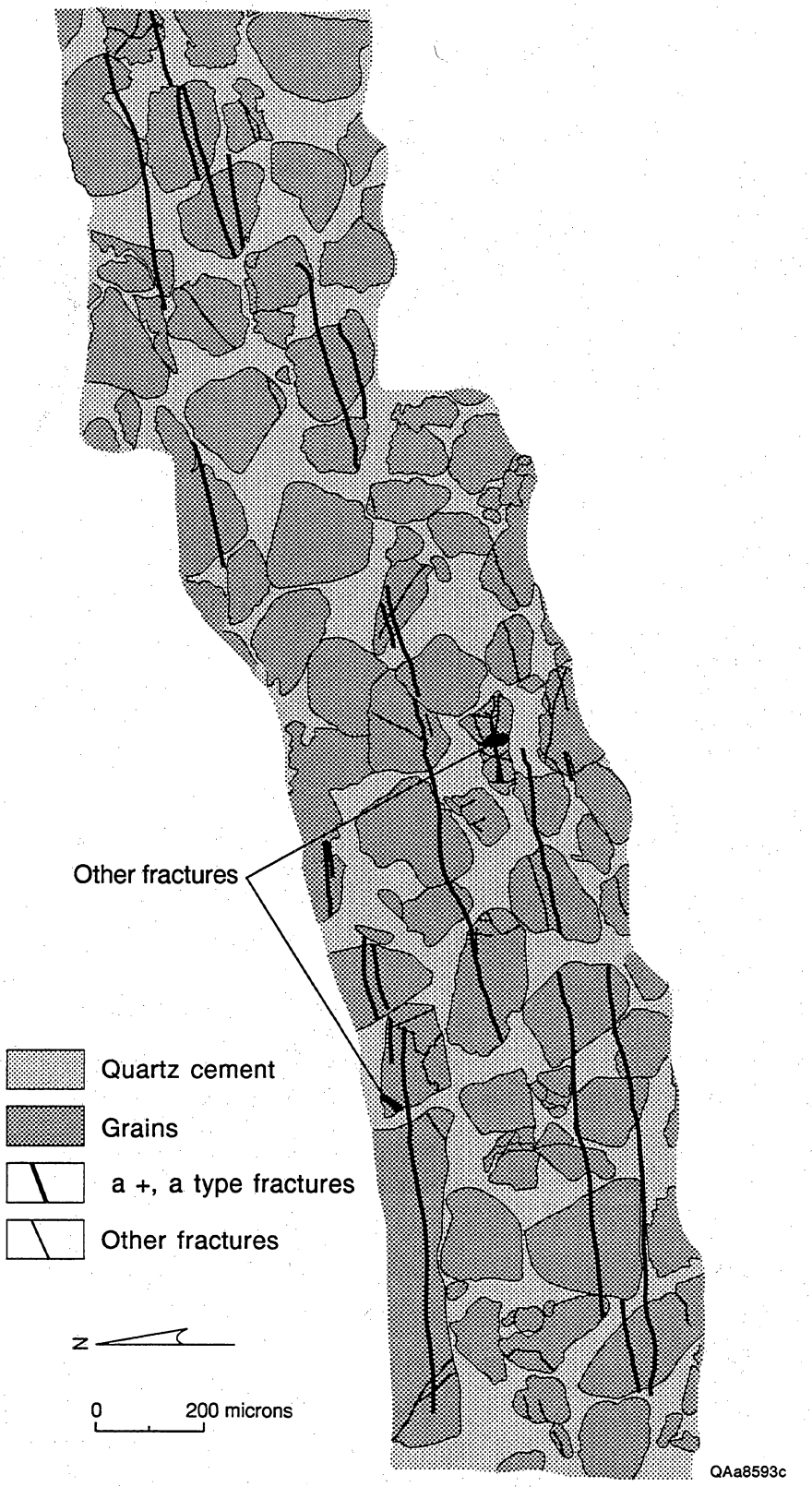

Figure 120. Map of sealed microfracture traces revealed by scanned CL imaging, Holditch SFE No. 2 well, depth –9,871 ft.

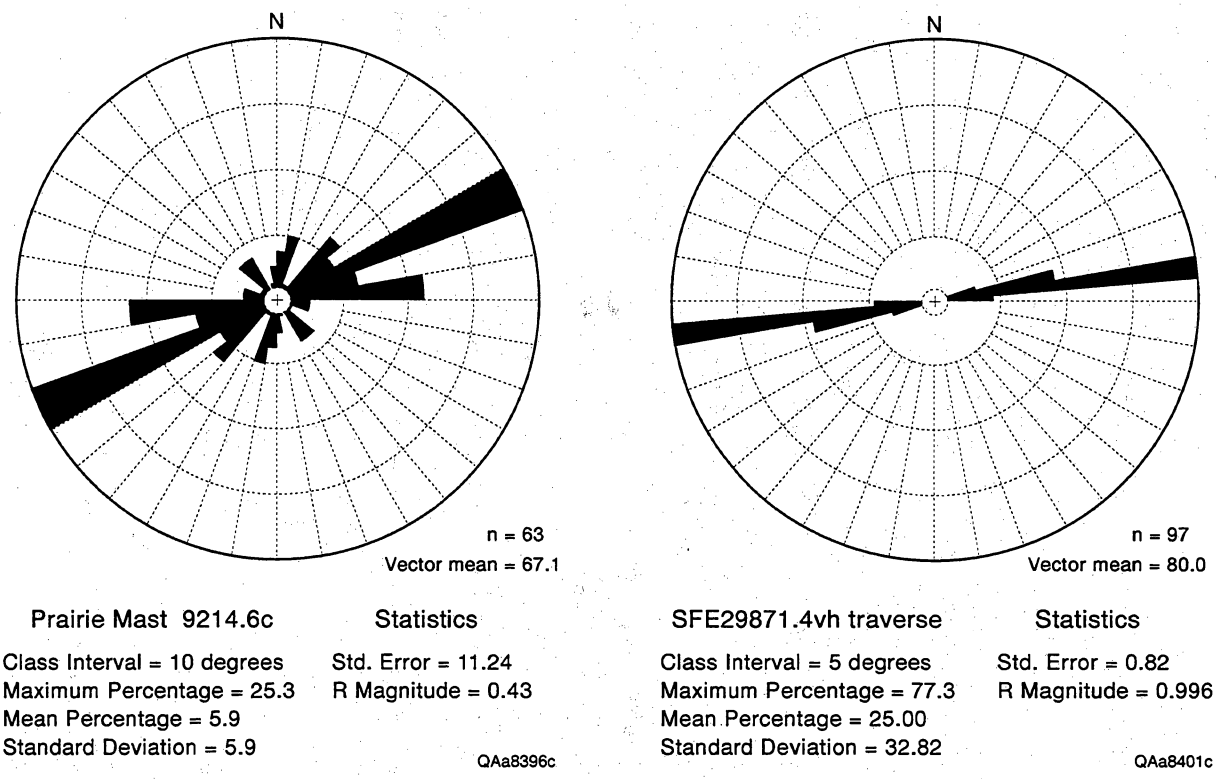

Figure 121. Rose diagrams showing microfracture strikes, Prairie Mast No. 1-A well (a) and Holditch SFE No. 2 well (b). Macrofractures in these wells strike east-northeast.

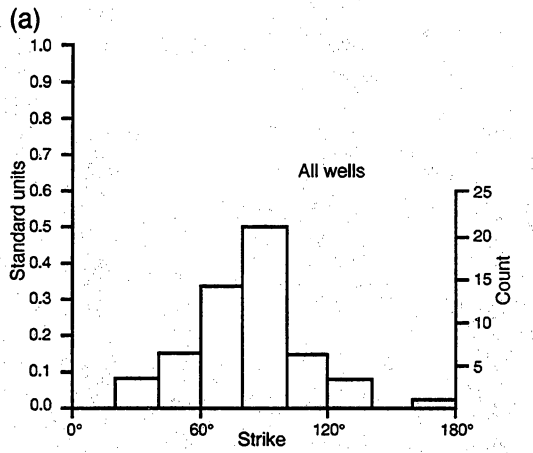

(c)

	Well	Mean Strike	Min.	Max.	Std. dev.	No. of fractures
1	*SFE No. 3* *+	78°	74°	83°	4.6	3
2	*SFE No. 1*	79°	27°	167°	44.8	10
3	*C.W. Sam Hughes No. 1*	85°	46°	130°	30.2	6
4	*SFE No. 2* - all	82°	28°	121°	19.2	34
5	*SFE No. 2* - upper	73°	42°	94°	16.2	13
6	*SFE No. 2* - lower	88°	28°	121°	19.1	21
7	All wells†	81°	27°	167°	26.0	54

*Only fractures oriented with paleomagnetic method are included
†Includes one fracture from *Prairie Mast No. 1-A* well
+ Fractures in Cotton Valley Sandstone

QA13121c

Figure 122. Strikes of natural fractures in Travis Peak sandstones. (a) Histogram showing data from all wells in the study. (b) Box plots of data from the indicated wells and intervals within wells. The center half of the data (from the first to the third quartile) is represented by a rectangle (box), and the median is indicated by a bar. Horizontal lines right and left of the box extend to values that represent 1.5 times the spread from the median to the corresponding edge of the box. Points plotted separately are outliers.

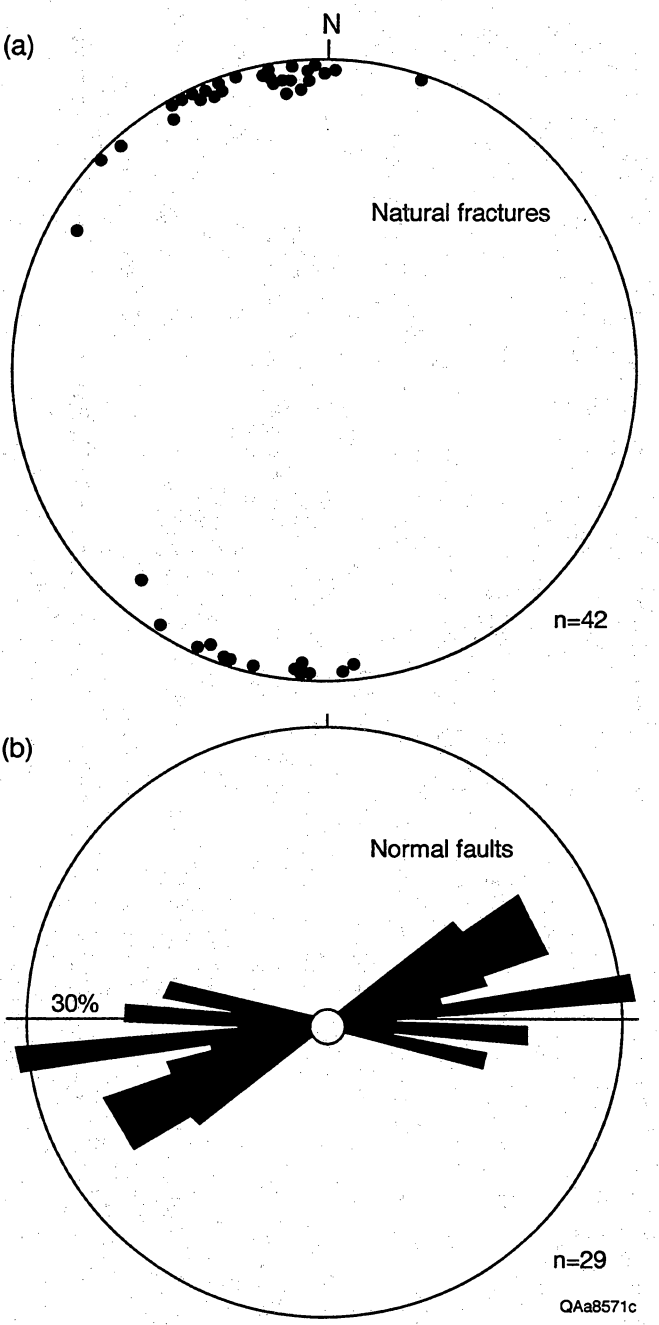

Figure 123. Macrofracture and fault patterns, East Texas. (a) Lower-hemisphere equal-area projection of poles to macrofractures, showing steep dips and east to east-northeast strike. (b) Rose diagram of normal fault strikes in the study area, East Texas. Macrofractures and normal faults have similar strikes in this area.

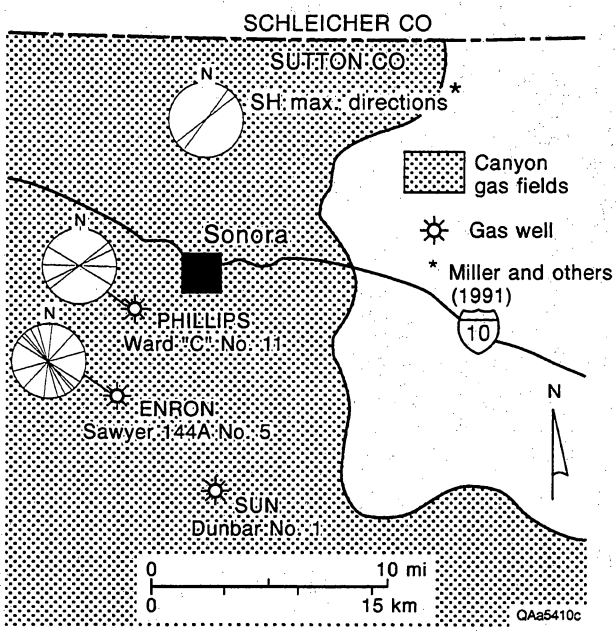

Figure 124. Natural fracture strikes in Phillips Ward "C" No. 11 and Enron Sawyer "A" 144 No. 5 core. Inset shows SHmax direction (from Laubach and others, 1994).

Microfracture strikes are generally northward, consistent with early development of quartz cement during burial of the Frontier. The most abundant microfractures are from the Wexpro Church Buttes and Blue Rim Federal 1-30 cores, both of which are from the deeply buried Frontier Formation.

Other Kinematic Indicators

Microfractures are not the only kinematic indicator that scanned CL imaging reveals. Two other common features that have significance for movement history are grains that have been crushed in a particular direction, and microstylolites (which themselves may largely reflect localized crushing [Milliken, 1994]). These two microstructural features are common in cross sectional views of sandstones, where they attest to vertical compactional shortening of the sandstone. However, these features are also visible in sections cut parallel to bedding, suggesting lateral deformation.

In some cases there is little preference to the orientation of these features in plan view, but in about one-third of the samples we inspected, there are indications of preferred alignment of steeply dipping microstylolites and crushed grains. These alignments indicate deformation of the rock in map view. It is possible that compaction-related deformation produced the appearance of map-view deformation in some of these cases, possibly as the result of out-of-plane movement of individual grains. However, the examples are all kinematically compatible with transgranular microfractures. They are therefore probably another manifestation of the same deformation that produced microfractures.

Best Methods for Applying Scanned CL Technique

The best approach to measuring fracture orientation using microstructure observations and scanned CL imaging depends on the density patterns of sealed microfractures. Currently, too few observations are available to define these density patterns sufficiently to recommend efficient sampling procedures. Thus, the best approaches for efficient and effective sampling and for ensuring the reliability of measurements are unknown. However, our studies show several procedures that can be used to expedite microfracture analysis. These procedures are as follows.

(1) Select samples from clean sandstone in the interval of interest. Samples may be from whole or rotary sidewall cores. Core orientation must be known, so care must be taken in core handling and sample processing (appendix 2). To maximize the probability of finding sealed microfractures of types useful for defining fracture strike, samples should be selected from intervals with some combination of the following attributes: (a) have moderate to extensive quartz cement and medium to coarse grain size or poorly sorted grain size, (b) lack or have low volumes of clay minerals (detrital or cement) and calcite cement, (c) have numerous stylolites, and (d) have high stiffness (high Young's modulus deduced from log measurements or measured in laboratory, reflecting quartz-rich composition—see section on "Identifying Fracture-Prone Layers on Geophysical Well Logs"). This technique is predicted to work best for samples that have been buried to depths greater than 2.5–3 km (1–2 mi).

(2) Prepare polished thin sections. The sections should be cut so that the plane of the thin section is parallel to bedding or a horizontal plane. Core orientation information should be marked, and the thin section should have a grid marked along its edges to ease sample description. If fracture dip information is desired,

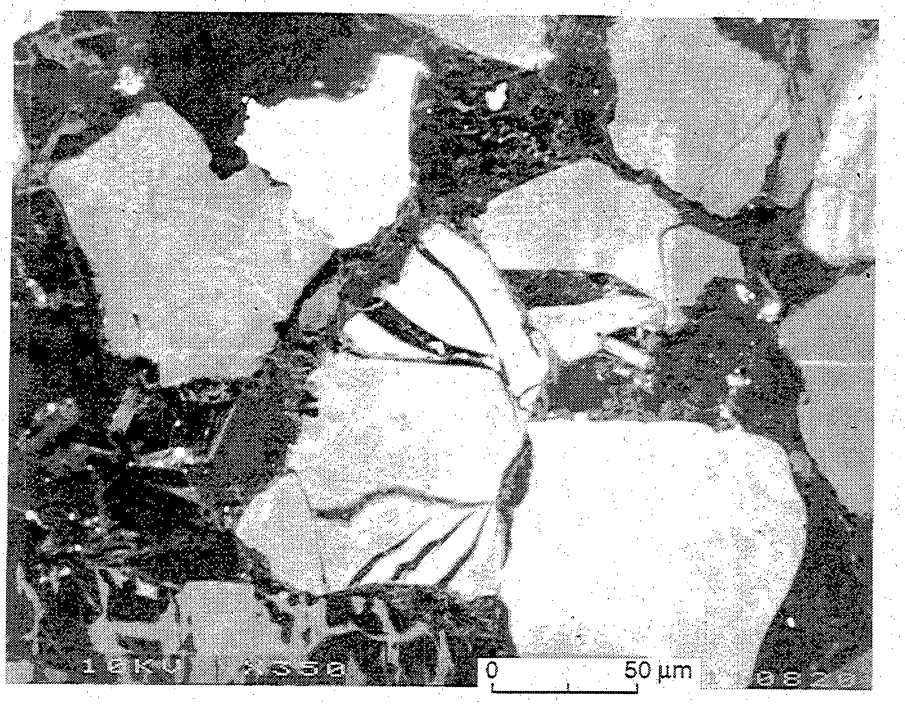

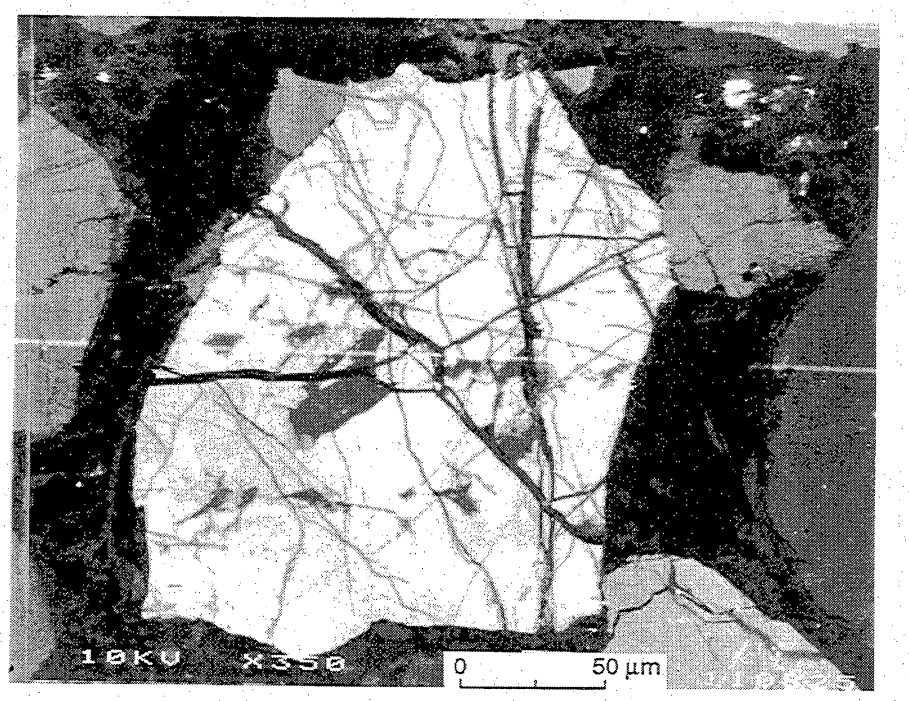

Figure 125. Canyon Sandstone microfractures. Scanned CL images. Note crushed grains, cross-cutting fractures. Sections cut parallel to bedding.

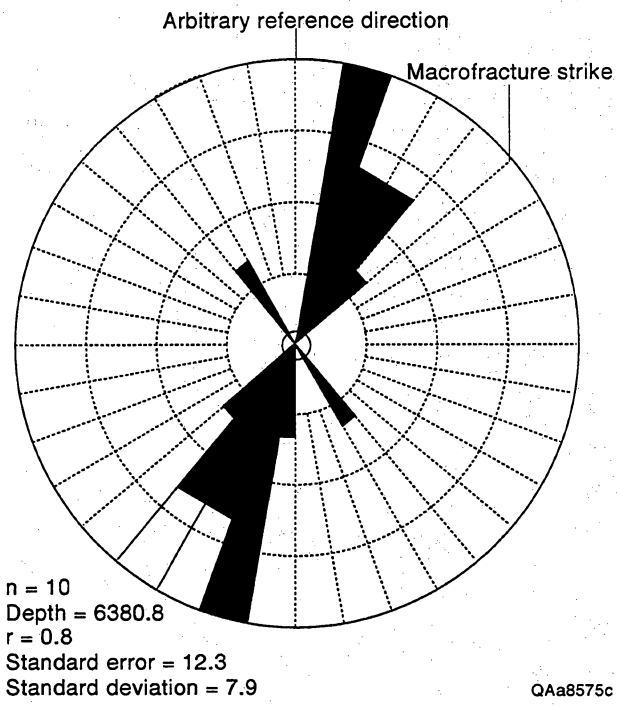

◀ **Figure 126. Rose diagrams showing microfracture strike, Canyon Sandstone.**

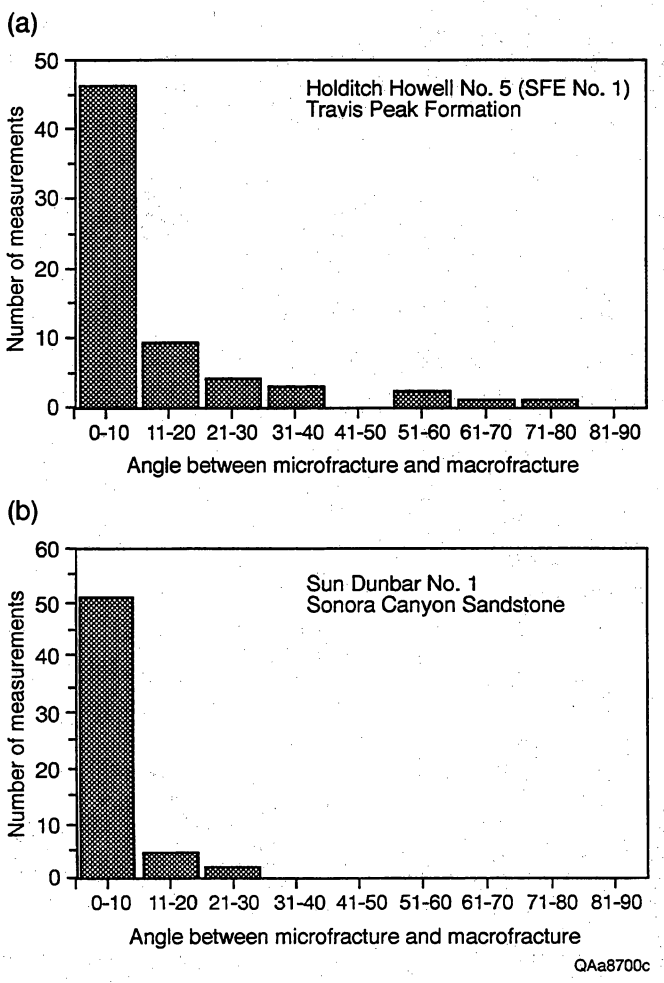

◀ **Figure 127. Diagrams showing microfracture strike relative to macrofracture strike, Travis Peak Formation (a) and Canyon Sandstone (b).**

Table 16. Orientations of Frontier Formation microfractures.

Well	Depth	Relative strike[1]	MOL	True strike	Aperture (mm)[2]	Spacing (mm)[3]	Mineralogy[4]	Type[5]
S. A. Holditch	7314.4	328	331	119	-	-	cc	vein
SFE No. 4	7330.8	83	254	157	0.04	0.84	cc	coal cleat
	7330.8	348	254	62	0.02	0.3	cc	coal cleat
	7344.6	341	-	-	0.00036	0.024	q	coal cleat
	7344.6	291	-	-	0.0036	0.048	q	coal cleat
	7401.1	304	281	45	-	-	q	FIP
	7403.4	336	281	77	-	-	q	FIP
	7403.4	280	281	21	-	-	q	FIP
	7405.9	283	281	24	-	-	q	FIP
	7411.9	274	285	19	-	-	q	FIP
	7437.8	322	337	119	0.04-0.22	1.484	cc	coal cleat
	7437.8	46	337	23	0.04-0.5	1.36	cc	coal cleat
	7443.5	320	88	48	0.03	-	cc	vein
	7443.5	325	88	53	2.7	-	cc	vein
	7448.6	62	31	93	5	-	cc	vein
	7448.6	29	31	60	0.3	-	cc	vein
	7448.6	88	31	119	0.14	-	cc	vein
	7629.5	85	-	-	0.04	0.7	cc	coal cleat
	7629.5	0	-	-	0.04	0.5	cc	coal cleat
	7630.0	76	-	-	0.016	0.4	q	coal cleat
	7630.0	351	-	-	0.004	2.88	q	coal cleat
	7630.4	90	-	-	0.57	1.068	cc & q	coal cleat
	7630.4	0	-	-	0.09	0.45	cc & q	coal cleat
Wexpro	12169.2	87	18	105	-	-	q	FIP
Church	12169.2	88	18	106	-	-	q	FIP
Buttes	12169.2	94	18	112	-	-	q	FIP
No. 48	12169.2	76	18	94	-	-	q	FIP
	12169.2	20	18	38	-	-	q	FIP
	12169.2	54	18	72	-	-	q	FIP
	12169.2	298	18	316	-	-	q	FIP
	12170.8	341	18	359	-	-	q	FIP
	12170.8	80	18	98	-	-	q	FIP
	12170.8	52	18	70	-	-	q	FIP
	12170.8	88	18	106	-	-	q	FIP
	12170.8	63	18	81	-	-	q	FIP
	12170.0	20	18	38	-	-	q	FIP
	12170.0	32	18	50	-	-	q	FIP
	12170.0	326	18	344	-	-	q	FIP
	12170.0	341	18	359	-	-	q	FIP
	12170.0	355	18	373	-	-	q	FIP
	12170.0	333	18	351	-	-	q	FIP
	12170.0	348	18	366	-	-	q	FIP
	12170.0	29	18	47	-	-	q	FIP
	12168.6	8	9	17	-	-	q	FIP
	12168.6	3	9	12	-	-	q	FIP
	12168.6	52	9	61	-	-	q	FIP
	12168.6	4	9	13	-	-	q	FIP

Table 16 (cont.)

Well	Depth	Relative strike[1]	MOL	True strike	Aperture (mm)[2]	Spacing (mm)[3]	Mineralogy[4]	Type[5]
Wexpro	12165.0	303	16	319	-	-	q	FIP
Church	12165.0	300	16	316	-	-	q	FIP
Buttes	12165.0	285	16	301	-	-	q	FIP
No. 48 (cont.)	12165.0	290	16	306	-	-	q	FIP
	12165.0	299	16	315	-	-	q	FIP
	12165.0	286	16	302	-	-	q	FIP
	12165.0	327	16	343	-	-	q	FIP
	12165.0	316	16	332	-	-	q	FIP
	12165.0	330	16	346	-	-	q	FIP
	12165.0	310	16	326	-	-	q	FIP
	12165.0	305	16	321	-	-	q	FIP
	12165.0	325	16	341	-	-	q	FIP
	12165.0	302	16	318	-	-	q	FIP
	12165.0	294	16	310	-	-	q	FIP
Blue Rim	16053.2	93	-	-	-	-	q	FIP
Federal 1-30	16053.2	25	-	-	-	-	q	FIP
	16053.2	73	-	-	-	-	q	FIP
	16056.0	66	-	-	-	-	q	FIP
	16056.0	171	-	-	-	-	q	FIP
	16056.0	147	-	-	-	-	q	FIP
	16056.0	83	-	-	-	-	q	FIP
	16062.9	72	-	-	-	-	q	FIP
	16062.9	71	-	-	-	-	q	FIP
	16062.9	105	-	-	-	-	q	FIP
	16062.9	33	-	-	-	-	q	FIP
	16062.9	143	-	-	-	-	q	FIP
	16063.5	35	-	-	-	-	q	FIP
	16063.5	72	-	-	-	-	q	FIP
	16063.5	122	-	-	-	-	q	FIP
	16065.7	163	-	-	-	-	q	FIP
	16065.7	172	-	-	-	-	q	FIP
	16065.7	159	-	-	-	-	q	FIP
	16065.7	18	-	-	-	-	q	FIP
	16065.7	130	-	-	-	-	q	FIP
	16065.7	22	-	-	-	-	q	FIP
	16067.9	159	-	-	-	-	q	FIP
	16067.9	84	-	-	-	-	q	FIP
	16070.0	48	-	-	-	-	q	FIP
	16070.0	56	-	-	-	-	q	FIP
	16070.0	45	-	-	-	-	q	FIP
	16070.0	81	-	-	-	-	q	FIP
	16070.0	43	-	-	-	-	q	FIP
	16070.0	68	-	-	-	-	q	FIP

[1] Strike relative to MOL; MOL = master orientation line
[2] Aperture not measured for open fractures
[3] Spacing measured only for fracture sets
[4] cc = carbonate cement; q = quartz
[5] FIP = fluid-inclusion plane

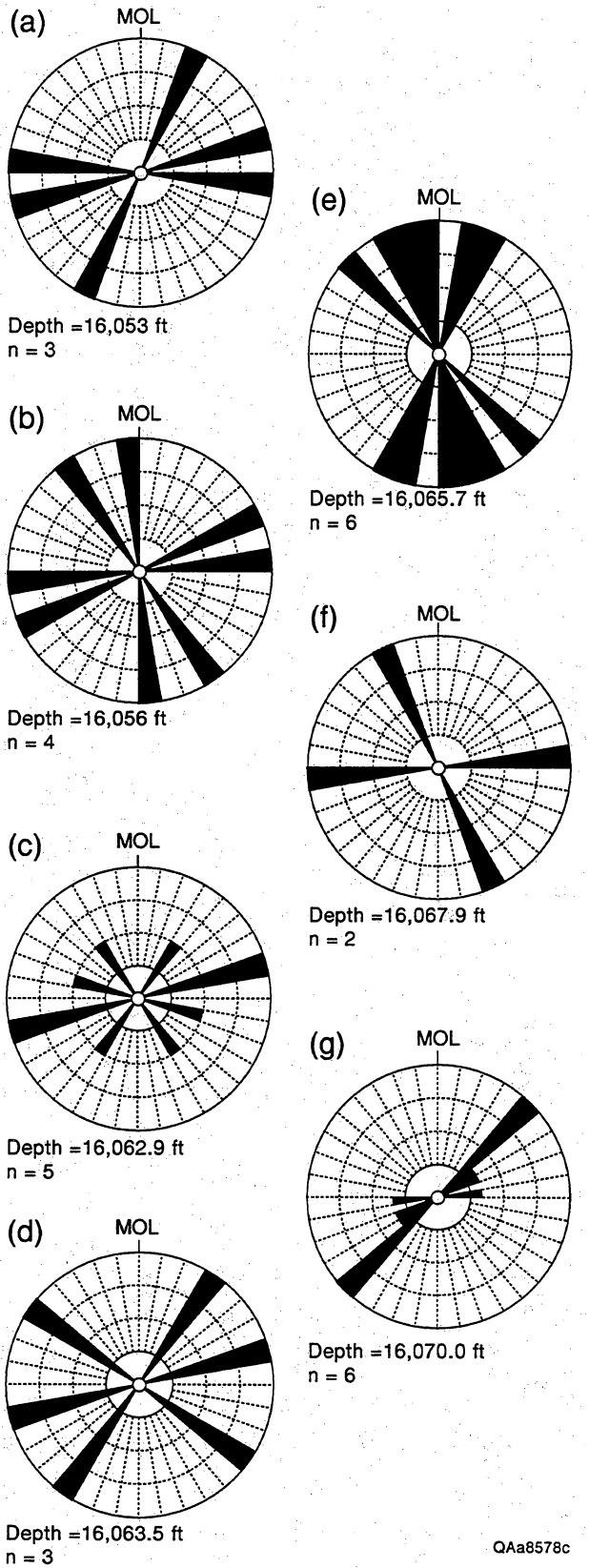

Figure 128. Diagrams showing microfracture strike, Frontier Formation. Blue Rim Federal 1-30. Strikes of fluid-inclusion planes relative to reference orientation line (MOL) at various depths (unoriented core).

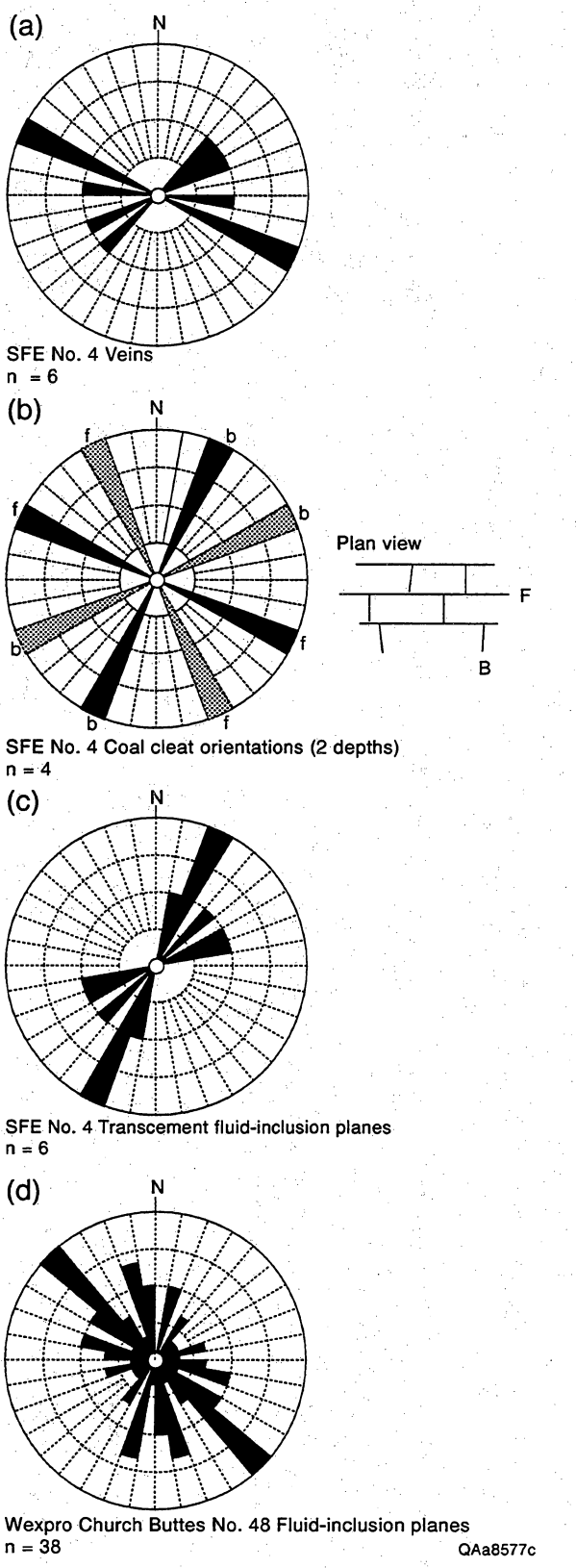

Figure 129. Rose diagrams showing microfracture strike, Frontier Formation. F, face cleat; B, butt cleat. Fracture in inset in (b) illustrates plan-view patterns of fracture traces that define face and butt cleat.

or if there are other indications that fractures do not have steep dips, three mutually orthogonal thin sections should be prepared for U-stage petrographic analysis. In general, our results suggest that this is not necessary for industrial applications because populations of microfractures having steep dips are common.

(3) Carry out a petrographic survey of the specimen to identify obvious *Type a+* transgranular fluid-inclusion planes. Mark their location on the thin section and record location on a sample map. Petrographic analysis is a rapid method for distinguishing the context of microfracture occurrence (such as cement volume and grain composition). It also permits rapid, relatively low-magnification viewing of specimens. Conventional transmitted-light microscopy, however, generally needs to be carried out at or near the highest magnification available on typical petrographic microscopes (60× to 100×) in order to detect fluid-inclusion planes. Conventional compositional and diagenesis studies can be carried out during this step in the analysis procedure.

(4) Prepare samples and carry out photomultiplier-based imaging of electron-beam-induced luminescence (CL). This imaging method reveals microfractures more readily than petrographic methods and speeds data collection. The use of a systematic approach is highly recommended for documenting fractures during CL analysis. Figure 130 shows a data collection form. The most reliable, efficient, and statistically sound methods for applying the method and the best sample selection and preparation methods probably vary with formation, fracture density patterns, and other factors. We currently do not know whether this approach and these sampling techniques apply equally well to all types of tight gas sandstones. Modifications are likely to be required on a case-by-case basis.

Recommendations: Mapping Fractures with Scanned CL Imaging

Determining the orientation of natural fractures in sandstone core that lacks visible macroscopic fractures is not the impossible task that it first appears. Microscopic natural fractures can be recognized and measured, and strike of these microfractures is a reliable guide to the orientation of large fractures formed during the same diagenetic episode. Photomultiplier-based imaging of electron-beam-induced luminescence reveals microfractures more readily than petrographic methods and speeds data collection. For fracturing associated with synkinematic quartz cementation, petrographic and scanned CL evidence provides, for the first time, a capability to systematically map natural fractures in subsurface sandstones that is not subject to the sampling bias and lack of data that plague macrofracture-based studies. Formerly, no methods allowed systematic measurement of fracture orientations on a bed-by-bed basis. Consequently, the variability of fracture patterns that exist in the subsurface have not been adequately measured or documented. Basic natural fracture information in most low-permeability sandstone plays is currently exceedingly sparse (appendix 1).

The ability to measure and map fractures with dense spatial control enables the explorationist or development geologist to improve fracture maps in areas of sparse data. This can lead to better appreciation of the location of fractured areas and better targeting of fractures for directional drilling. Thus, a superior appreciation is attained of patterns of fracture strike and location of fractured areas, helping to narrow the possible fracture patterns in a given area. It can also verify fracture genesis model predictions and hence lead to better forecasting of fracture patterns.

Benefits of the application of this approach include lowered well costs and more accurate and certain targeting of natural fractures (fig. 131). The risk associated with inadequate characterization of fracture strike is clear. Fractures could be overlooked or missed, or—just as importantly—their discovery could be too expensive to justify the search. Effective definition of subsurface fracture patterns requires the high-resolution maps of fracture strike that scanned CL imaging allows.

Fracture Strikes from Fractured Coal Inclusions in Sandstone

In sandstone having dominant cements other than quartz, and in areas where clay matrix and other soft grains or cements are prevalent in sandstone, other methods for indirectly obtaining fracture strike from core information may be needed. Using fractures in coal that occurs within sandstones (coal inclusions) is one technique. Another, described in the section "Strength Anisotropy Tests" uses rock tests to find microfracture fabrics.

Thin Section Number TP2 9870.8 Formation Travis Peak Date Described 12/5/94 Page 3
Analyst SL/SC Well Holditch SFE No. 2

Descriptors

1: Transgranular? (more than 2 grains? How many?)
2: Crushed Grain? (radiating fractures?)
3: Dominant Fracture? Curved fracture?
4: Thickness?
5: Crosscutting relation?
6: Photo? Other? 7. Stylolite? Trend & Axis

Measure "a" fractures length & width

vh = sample from viewing half of core

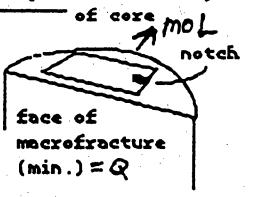

MOL = ____ az
Macro? y
See orientation diagram & core photos

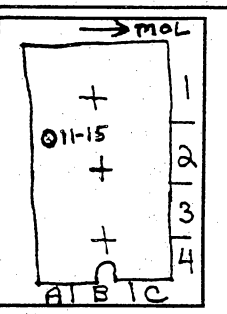

Thin Section Map

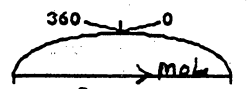

Other notes: t.s. is part of set
t.s. ref. direction mol = E

Categories

a—transgran or trans cement a+ —crosses several grains; a- only crosses cement
b—possibly crosses cement G- quartz grain
c—restricted to grain, but has dark fill that may indicate post-dp frac. Give explanation.
d—Definitely inherited; e.—Unknown origin, see description.

Label & describe each fracture

Q- cement, qtz overgrowths
H- highly luminescent areas
D - dark area in image. Poor resolution

Y= X=

Location on t.s. & grn number	Category a—b—c—d	Strike Apparent — True	Description & Sketch
A-2			~~Length/Width~~
11	a+	321	11 - transgranular through 3 grains and cement
12	b	314	12-13 may be same frac. cont. acr. cemnt - but image too dk to confm
13	b	314	
14	c	344	14 - Frac. fill and cement same tone (dk)
15a	c	304	15 - Fracs. radiate from a point grain-grain Contact
$15b_1$	c	352	
$15b_2$	c	32	

Pos. same frac.

Photo number

Scale b:

TP2 9870.8
#11-15

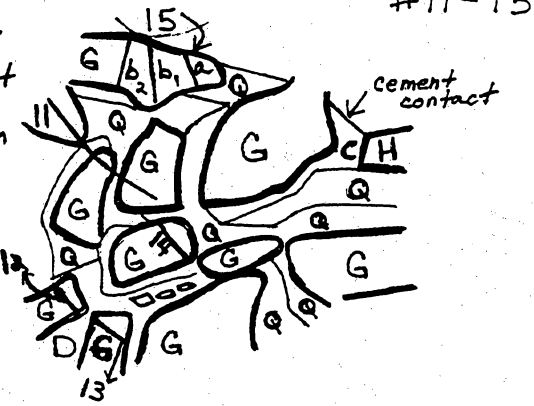

Fracture	thickness	length (approx.)
11	2.5 µm	200 µm
12	2.0 µm	63 µm
13	2.0 µm	60 µm
14	<2 to 2.5 µm	100 µm
15a	3 µm	50 µm
$15b_1$	2 µm	50 µm
$15b_2$	<2 µm	58 µm

Figure 130. Data form for scanned CL microfracture description and mapping.

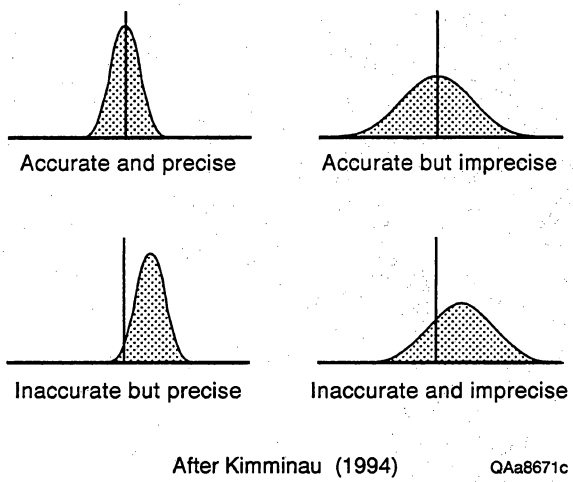

Figure 131. Accuracy and precision in fracture-strike determination. Vertical line represents macrofracture strike; curves show hypothetical microfracture data. After Kimminau (1994).

Coal Inclusion Fractures

Thin coal layers and coalified fragments of organic material (largely coalified wood) are common features in Cretaceous fluvial to shallow marine sandstones in the western United States. In conventional core, most of these coal inclusions in sandstone resemble thin layers (less than 2 inches [5 cm] thick), but these fractures are most likely compacted, coalified wood having very limited lateral dimensions (no more than a few feet), rather than actual coal layers. If fractures in these layers can be related to diagenetic sequence through petrogenetic analysis procedures, then these fractures have the potential to be used to indicate the strike of widely spaced, less frequently sampled macrofractures in sandstone.

The orientation, abutment relationships, and mineralization of coal fractures (cleats) in coalified inclusions in sandstone are not necessarily the same as those of macrofractures in sandstone, since coal may experience fracturing under conditions that differ from those that create fractures in sandstone. Yet by observing mineralization sequences in coaly layers and coalified wood and comparing them to known macrofracture and diagenetic mineral relations, it is possible to place some coal fractures within the diagenetic sequence and to relate them to macrofractures in sandstone. Studies of fractures in coal beds show that they locally parallel fractures in sandstone (Laubach and Tremain, 1994, and references therein).

Figure 132 shows calcite-mineralized coal fractures from the Travis Peak Formation. Similar features are visible in Frontier Formation sandstones, where quartz and two generations of calcite are present in fractures (fig. 133). Coal layers and coalified wood are not apparent in Canyon Sandstones, which represent a deeper water depositional setting where such features are rare or absent.

The key to interpreting fracture strikes in small coal layers in sandstone lies in relating coal fracture-fill mineralogy to diagenetic sequence and—where possible—fracture-fill sequence in sandstone fractures. The fracture-fill patterns in Frontier Sandstones were described in an earlier section. The paragenesis of minerals in the coal fractures is ambiguous, but the types of relationships that are visible, such as cross-cutting and overprinting patterns among vein-fill minerals, suggest that linking coal fracturing events to diagenetic events is feasible.

Oriented thin sections from Frontier Formation Sandstones show that coal fractures in sandstone are easily recognizable and that the fractures have diagenetic mineral sequences that resemble those of the host sandstone. Aperture, spacing, and orientations of the fractures in the coal were measured and oriented with respect to north where core orientation was successful (table 16, appendix 2). Core sections with thin coal layers are less susceptible to failure of core-orientation methods than are sandstones having macrofractures. This is because small (less than 2.5 cm [1 inch] thick) coaly intervals within sandstone generally do not cause core breakup unless they extend completely across the core. Consequently, the proportion of fractures successfully oriented is higher for fractures in coal inclusions than that of fractures in sandstone. Fractures in thick coal seams, on the other hand, are not necessarily more easily oriented than fractures in sandstone.

The limited information on coal fracture patterns we obtained from one Frontier Formation well is not sufficient to confirm that small coalified features in sandstone give reliable and consistent strikes that match sandstone-fracture patterns. Outcrop study of coal-fracture patterns within coal seams in the Frontier Formation on the western side of the Green River Basin found northward- and eastward-trending face-cleat strikes in coal beds in different parts of the coal-bearing section of the formation. These patterns resemble the orientations of fractures in nearby sandstones. Coal fractures in Travis Peak cores have similar strikes to macrofractures in host sandstones.

The information derived from using fractures in entrained coal within sandstone can be readily compared to regional coal-fracture patterns and

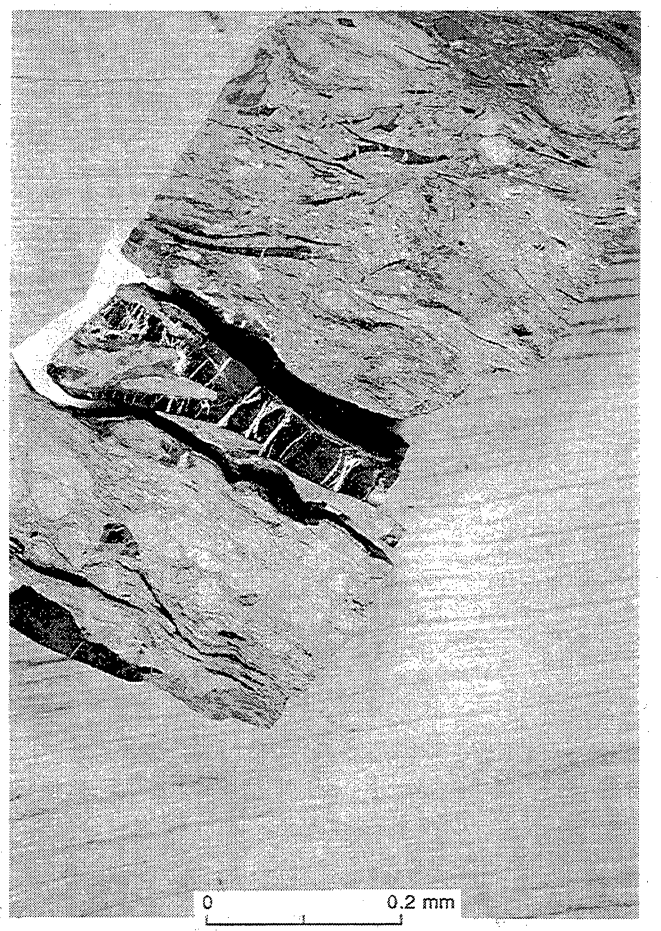

Figure 132. Coal fractures in Travis Peak Formation, Holditch Howell No. 5 (SFE No. 1) well, depth –6,600 ft. Fractures are filled with calcite.

models. Observations of fractures in coal in the western United States show that these fractures have regular patterns over wide areas. Coal-fracture observations for coal seams are currently the only coherent self-consistent fracture data sets available to test regional fracture models. Thus, fractures in sandstone coal inclusions are the features most directly comparable to the only systematic observational data set on fractures in these reservoir intervals, and they are most readily comparable to numerical models designed to predict fracture patterns.

Numerical Models of Fracture Strike

Coal fracture patterns have recently been compiled for the western United States (Laubach and others, 1992a, 1994). As part of our study of fractures in sandstone, a finite-element model incorporating realistic rheologies was used to simulate stresses and strains in a wide region of the western United States where fracture patterns are of interest (D. Schultz-Ela, unpublished numerical models, 1993). Owing to lack of appropriate data sets from sandstones, such patterns must be compared to coal-fracture data sets.

The numerical models were developed using the software GEOSIM-2D, which can simulate large strains for a variety of rheologies, including elastic and elasto-plastic with frictional yield. The models we used are elastic, with 2,285 elements. They have free-slip boundaries parallel and perpendicular to the overall thrust front (in some realizations, boundaries were fixed). Figures 134 and 135 show the overall geometry of the model and representative model results. In this example, a 0.6-mi (1-km) displacement (shortening) has been applied perpendicular to the thrust front. The model has elastic properties in the low range for

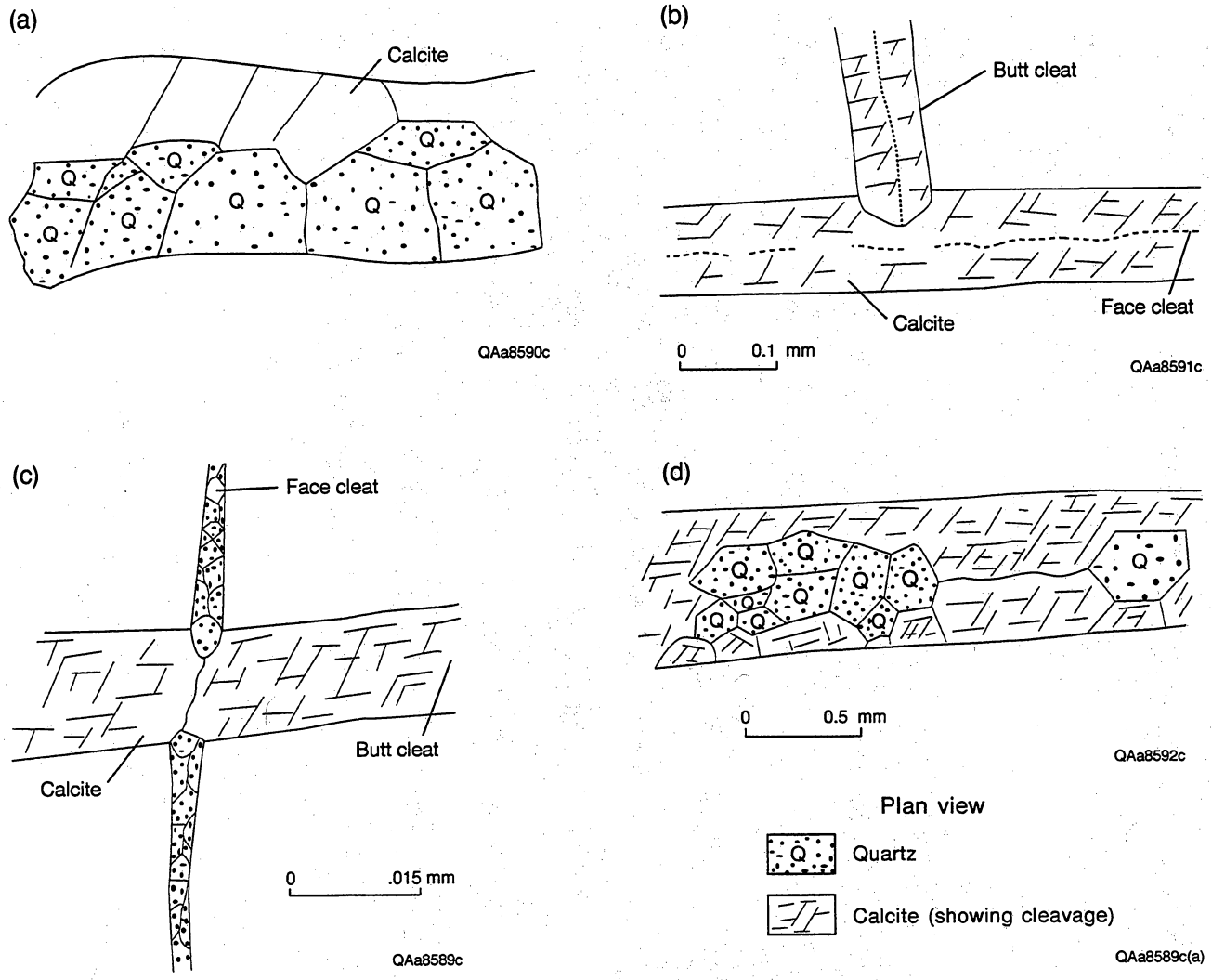

Figure 133. Coal fractures in Frontier Formation, SFE No. 4 well. Diagrams illustrate textural relations among fracture-filling minerals and abutting relations among fractures (as seen in plan view). (a) Quartz and calcite are present; mineral precipitation sequence is ambiguous. Holditch SFE No. 4, –7,630.4 ft. (b) Abutting relations in calcite-filled fracture. Mineral growth from walls is nonfibrous, possibly postkinematic. Textures indicate face cleat was filled before abutting cleat opened. Holditch SFE No. 4, –7,437.8 ft. (c) Face cleat is quartz filled; butt cleat has calcite. Face cleat opened and filled before abutting fracture formed. Holditch SFE No. 4, –7,437.8 ft. (d) Quartz and calcite are present; textures suggest calcite preceded quartz. Neither mineral is fibrous, and both may be postkinematic. Holditch SFE No. 4, –7,630.4 ft.

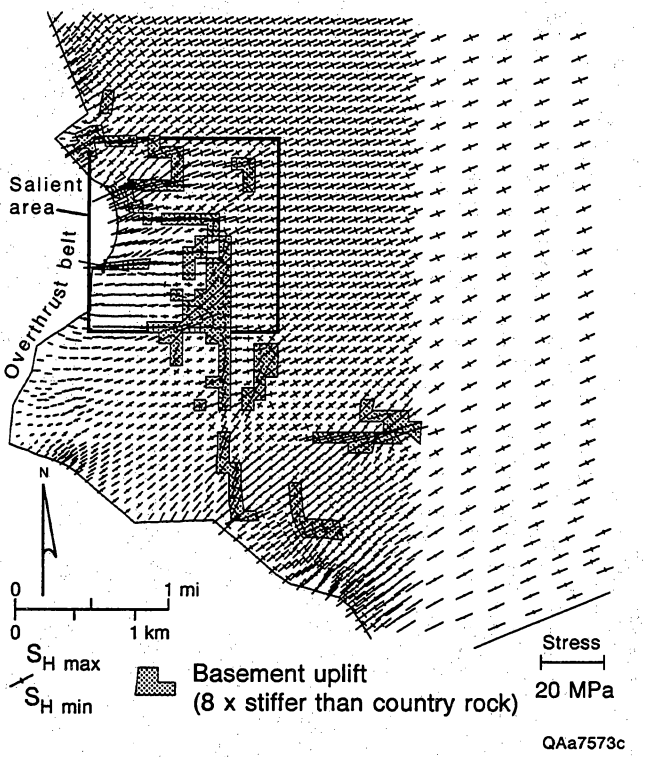

Figure 134. Numerical model of deformation in western United States, Late Cretaceous–early Tertiary. Long and short crossed lines show maximum and minimum horizontal compressive stress, respectively. Short, thick lines represent measured fracture (face-cleat) strike in Cretaceous and Tertiary coal beds. See text for explanation. Model by D. D. Schultz-Ela, 1994.

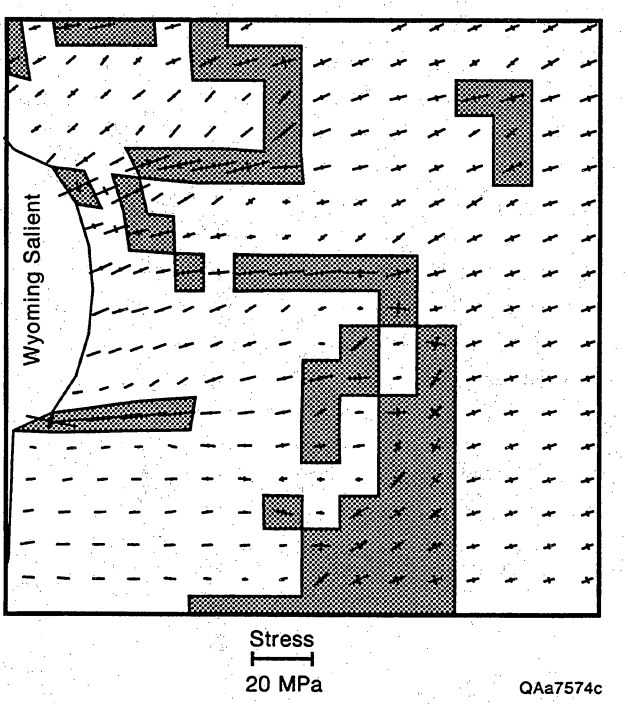

Figure 135. Stress trajectories near Wyoming salient of overthrust belt. Detail of previous figure (labeled "salient area").

sandstone and shale, except (in this example) for more rigid elastic blocks that have properties in the middle range for igneous rocks. These rigid inclusions are about eight times stiffer than surrounding rock, and they are designed to simulate foreland basement structures.

Maximum horizontal stress axes are shown with lines having length proportional to stress magnitude. Assuming that maximum horizontal stress directions predict the strike of opening-mode fractures at the time of their formation, this model depicts the tectonic situation in which fracture formation may have occurred for Cretaceous coal (and somewhat later) for sandstone. Such fractures may have formed during subsidence, burial, and tectonic loading of the foreland in the Late Cretaceous and early Tertiary, during deformation in the Cordilleran thrust belt. In the model shown in figures 134 and 135, which features simplified basement uplifts, stress axes swing toward parallelism with elongate basement blocks, as these features act as stress guides. Local perturbations of stress patterns are evident near uplifts, especially those having long north-south dimensions. Stress magnitudes are locally lower within basins surrounded by uplifts, as basement blocks act as strong "beams" shielding enclosed areas. Locally high differential stresses are associated with the Uinta Uplift and a few other foreland basement structures.

Coal-fracture patterns match the model closely in some areas, but elsewhere there is wide divergence from predictions. This is partly due to the simplified nature of the numerical model and to the assumptions built into it (for example, that basement uplifts can be approximated by stiff elastic blocks in an elastic medium). The observed fractures depicted for comparison also may not be exactly the same age as the deformation that is being depicted. The fractures shown here are face cleats in Cretaceous and Tertiary coals. On the basis of crossing and abutting relations, face cleats are defined (Laubach and others, 1992a) as being the oldest fractures in a coal layer. Although for a given coal layer the face cleat will be the oldest fracture present (based on this definition), it is unlikely that face cleats in many different coal beds, and particularly coal beds of different ages and burial history, will be the same age. The flexibility of numerical modeling procedures permits the observed coal fracture patterns to be matched more closely than is shown in this example, but doing so would be misleading. The main limitation to building and verifying a useful predictive numerical model of regional fracture patterns is a reliable sandstone fracture-strike data set against which model predictions can be tested.

Results of coal-fracture mapping and numerical modeling show that in slightly structured foreland areas adjacent to orogenic belts, fracture patterns may have relatively uniform patterns over wide areas (Laubach and others, 1994). Yet fracture patterns also may shift gradually or abruptly. More closely spaced controls on shifts in fracture strike in a few areas show that, on a local scale, dominant coal fracture strikes shift abruptly over distances of a few miles to tens of feet (Laubach, 1991). Although orientation of joints and veins in sandstone may remain constant over large areas (on the order of 5 mi^2), there is good evidence that in some areas fracture strikes shift abruptly within beds, sometimes over distances of as little as a few feet (Laubach, 1992a; Lorenz and Laubach, 1994) or over distances of a few miles (Engelder, 1982; Verbeek and Grout, 1983; Laubach and others, 1991). Joint orientation may also shift vertically from one rock unit to another (Engelder, 1985; Helgeson, 1990; Laubach, 1992a).

Numerical models and maps of coal-fracture strikes show that shifts in fracture orientation should be expected on regional, field, and interwell scales. This illustrative pattern for coal fractures is equally suggestive of the fracture patterns that likely exist in sandstone. A review of the factors that can in principle affect fracture strikes warns that current models should not be expected to accurately pinpoint where such shifts occur on a field or play scale, except in a general way. This follows from the flexibility of the models—model predictions are seldom unique (in many cases several contradictory models can account for the same fracture orientation). This emphasizes the important need for direct measurement of fractures strikes. Areas that have natural fractures where horizontal drilling is applied could be erroneously condemned as unfractured if the well was drilled in an inappropriate direction relative to fracture strike. It is certainly possible that within-field shifts in fracture strike exist that could produce such a drilling result.

One key unknown for prediction of fracture strike is the timing of fracture growth. If this were better known or more accurately predicted, models of paleostress trajectories that are relevant to reservoir intervals could be created. Coal fractures likely form when coal beds reach a particular temperature and burial depth threshold. The timing of coal fracturing—and its tectonic setting—can therefore in principle be deduced from burial history curves and generalized tectonic models. This underlines the significance—for predicting fracture patterns—of recognizing the timing of fracture formation relative to diagenetic events. Distinguishing diagenetically controlled fracture events, such as synkinematic quartz cementation and fracturing, that might be comparable in its regularity to coalification processes and attendant fracturing of coal, could aid development of useful regional fracture

models. If the process of, for example, synkinematic quartz cementation occurs over a narrow, predictable temperature and pressure range (somewhat like a metamorphic isograd), then the tectonic setting of fracture formation could be more closely specified. Results presented in this study are compatible with such an interpretation of fracturing.

Lack of knowledge of subsurface fracture orientations precludes fully testing and verifying predictive models of fracture strike. Thus, current predictive models of fracture strike are not complete solutions to exploration and development needs, but diagenesis and fracture timing information can improve the models' applicability. Clearly, direct measurement and mapping of fractures is the most direct method to guide development drilling and to provide a framework for testing and verifying predictive models.

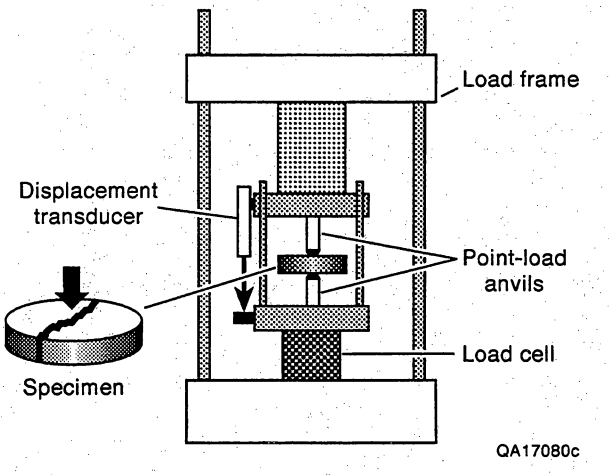

Figure 136. Diagram of apparatus used in axial point-load tests of Frontier and Travis Peak Formation samples.

Strength Anisotropy Tests

Background and Objectives

Our purpose in using this test is to measure strength anisotropy as a possible rapid method to document microfracture fabrics. The stress field produced by axial point loads is axisymmetric, but the induced fracture preferentially aligns along a direction perpendicular to that of the rock's minimum tensile strength. In sedimentary rock that lacks preferred grain orientations, aligned subvertical microfractures are generally the cause of tensile strength anisotropy in the horizontal plane (Reik and Currie, 1974; Lajtai and Alison, 1979). This direction is reflected in the strike of fractures induced by point-load tests, and specimen failure has been inferred to occur along planes defined by microfractures (McWilliams, 1966; Friedman and Bur, 1974). Our results show that this test method works best in rocks having a significant component of compliant grains and cement. These are the rocks for which scanned CL imaging is least effective (because of sparse sealed microfracture density), so these two approaches are potentially complementary.

The axial point-load test consists of loading a small disk of rock to failure with two opposed indenting anvils (fig. 136). The test provides a measure of strength and strength anisotropy. Conventional point-load tests have established procedures and sample sizes and are used to determine compressive strength (Broch and Franklin, 1972). These tests have some similarities to indention hardness tests (cf. Lawn and Wilshaw, 1975), but loads are applied along the central axis of a disk of sample material rather than across the diameter of a cylindrical specimen, and the specimen is loaded to failure.

Point-load tests have been used to identify prevailing microfracture fabric anisotropy (Queen and Rizer, 1990; Clift and others, 1992), and outcrop strength anisotropy studies of sandstone have found unimodal and polymodal induced fracture directions that locally correspond to strikes of macroscopic joints (Lajtai and Alison, 1979). In principle, induced point-load directions could correspond to microfracture anisotropy caused by either current in situ stresses, core deformation, or deformations unrelated to current stresses. Among the advantages of point-load tests is its simplicity. The test uses only a few ounces of test material and a simple test apparatus, and can be conducted in only a few minutes. It can be applied to existing reservoir core material.

Experimental Procedure

Sample Material

Samples used for this study are from oriented core from three typical low-permeability sandstone gas reservoir rocks: the Travis Peak Formation of East Texas, sandstones of the Frontier Formation of the Green River Basin, Wyoming, and the Canyon Sandstone of the Val Verde Basin, Texas. These rocks differ in their depositional, diagenetic, and tectonic history and have contrasting mechanical properties and in situ stress environments. High detrital quartz content and pervasive quartz cement in Travis Peak sandstone correspond to high stiffness and tensile strength, whereas lithic-rich detrital composition and abundant authigenic clay in Frontier Formation sandstones produce relatively

lower moduli and strength. Canyon Sandstone properties range between those of the other two formations.

Samples were taken from seven wells, the Holditch Howell No. 5 well (SFE 1) in Harrison Co., Texas; the Holditch SFE No. 2 well in Nacogdoches Co., Texas (Travis Peak), the Holditch SFE No. 4-24 well in Sublette Co., Wyoming (Frontier); Enron Sawyer A-144 No. 5, Phillips Petroleum Ward C-11, Sun Dunbar No. 1 (Sonora Canyon); and Shell Baggett No. 2-20 and Texaco Kincaid No. D-7 (Ozona Canyon). Dutton and others (1991, 1992) and Laubach and others (1994) summarize the geology and describe the setting of the wells. Detrital composition of Travis Peak and Frontier samples is summarized in figure 137, and representative elastic properties are summarized in table 17; representative properties of the Canyon Sandstone are summarized by Laubach and others (1994). A limited number of tests were carried out on Frontier Formation outcrop samples.

Sonora Canyon Sandstones have a range of natural fracture strikes, but too few fractures have been measured to confirm that dominant directions or multiple fracture sets exist. Maximum horizontal stress trends northeastward (Laubach and others, 1994). The Travis Peak Formation is characterized by east-northeast-striking macrofractures (Laubach, 1989a). Wellbore breakout directions, the strike of drilling-induced fractures, and the growth directions of remotely monitored hydraulic fractures all indicate east-northeast-trending SHmax (Laubach and Monson, 1988). The Frontier Formation was deposited in a foreland basin subjected to tectonic shortening in the Late Cretaceous and early Tertiary. Natural fracture strikes in the subsurface are poorly known, but fractures in outcrops on the western basin margin have been interpreted to be representative of the subsurface. Fracture sets in these rocks strike predominantly northward, northeastward, and eastward (Laubach, 1992a; Laubach and Lorenz, 1992). Efforts to measure in situ stress directions in the Frontier Formation along the Moxa Arch have proven problematic; both eastward and northward directions have been observed (Laubach and others, 1992b). We interpret SHmax to trend northward in the vicinity of the Moxa Arch.

Petrographic observations show that none of the test sample material had preferred grain orientations within the bedding plane, so we interpret the preferred strike of induced fractures to reflect the presence of oriented microfractures. Microfractures are visible petrographically in all three formations.

Sample Preparation

Sample selection is critical for point-load testing; we sought homogeneous sandstone and sandy or muddy siltstone samples that lack obvious sedimentary anisotropy. Thin sections cut parallel to bedding were examined to eliminate samples with sedimentary lineations that might cause strength anisotropy. Core was taken from intervals that were oriented by standard orientation techniques, and for comparison of results from different stress-detection methods, from intervals for which methods such as anelastic strain or ultrasonic velocity measurements, hydraulic fracture tests, or wellbore breakout measurements had been carried out. Samples represent a range of dominant compositions and authigenic cements.

All test specimens were taken from vertical plugs from oriented core. For the Frontier and Travis Peak samples, plugs were sliced into approximately 0.33-inch-thick (8.4-mm) disks. Prior to specimen extraction, a centeringhead tool was used to draw a reference line, the master orientation line (MOL), on flat ends of the core specimen to be plugged (fig. 138a). A line was drawn down the side of each plug to indicate the MOL (fig. 138b). This line was used to orient fractures created in the disks. Sufficient plugs from each core piece were taken in order to obtain 20 to 30 disks. Disks were ground flat on each end with a diamond cup wheel on a Hillquist Thin Section machine. (The use of brand names in this report is for information only and does not constitute endorsement by the Bureau or GRI.) After disks were faced, they were approximately 0.25 inch (6.3 mm) thick. Disk thicknesses ranged from 0.09 to 0.44 inches (2.3 to 11.2 mm), but the range 0.25- to 0.33-inch-thick (6.3- to 8.4-mm) disks yielded the most consistent results for Travis Peak and Frontier samples. Disk thickness was measured in four areas (at approximately 0°, 90°, 180°, and 270°) with a micrometer in order to ensure near parallelism of the top and bottom of the disk. The difference in the four measurements was less than 0.002 inch (0.05 mm) for all tests.

Test specimens for the Travis Peak and Frontier tests are disks that are 1 inch (25 mm) in diameter and approximately 0.25 inch (6.3 mm) thick. For these formations, a range of sample thicknesses was used to determine if results were sensitive to sample thickness. Test specimens for the Canyon tests are all 1 inch (2.5 cm) in diameter and 0.5 to 0.6 inches (1.3 cm to 1.5 cm) in thickness, corresponding to standard dimensions for engineering point-load tests.

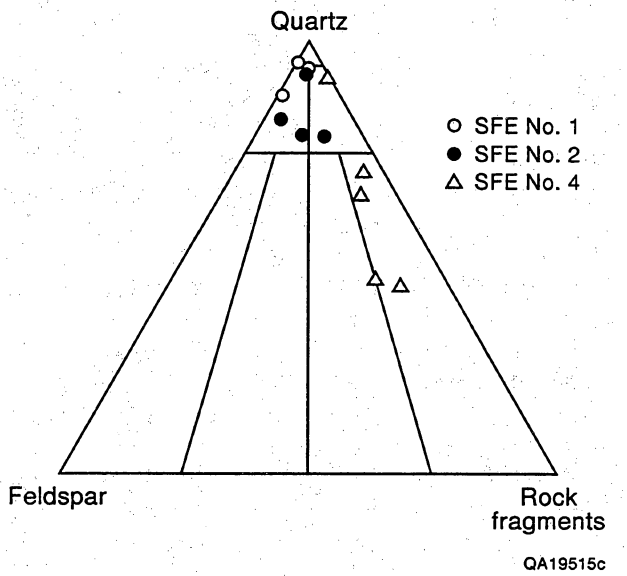

Figure 137. Framework-grain composition in test specimens. Data from Dutton and others (1991, 1992).

Table 17. Orientation statistics for Blue Rim Federal 1-30 well microfractures.

Depth (ft)	Number of microfractures	Vector mean*	Standard error*	R magnitude*
16053.0	3	–	–	–
16056.0	4	–	–	–
16062.9	5	79.8	46	0.38
16036.5	3	–	–	–
16065.7	6	354.3	20.6	0.68
16067.9	2	–	–	–
16070.0	6	56.4	11.2	0.89

*Statistics were not tabulated for N<5.

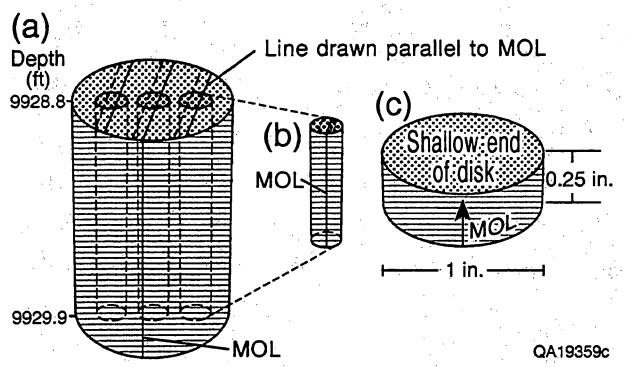

Figure 138. Core sampling and disk orientation procedure. (a) Locations of sample plugs in 4-inch diameter core. (b) Reference line (MOL) marked on 1-inch-diameter plug. (c) Disk with MOL and "up" direction indicated.

Test Apparatus and Procedure

The test apparatus is shown schematically in figure 136. An axisymmetric point load was applied to the center of a disk with hemispherical ends of precisely aligned load platens (0.5 inch [12 mm] diameter) in a specially designed point-loading jig (Reichmuth, 1968). For Travis Peak and Frontier tests, load was provided by a Soil Test 10,000 lb load frame, at a rate of 1 lb (454 gm) per second. Load and time were recorded on an X-Y recorder. For Canyon specimens, load was provided by a commercially available SBEL point-load test device, where load is applied with a hydraulic hand pump. The device has a load capacity of 80 kilopounds.

Disks were placed on the bottom anvil of the point-loading jig. The orientation of the disk was arbitrary, but disks were perfectly centered on the anvil by balancing the disk on the bottom anvil and visually checking to ensure that it was level. Travis Peak and Frontier disks were not confined laterally and were deformed dry, at room temperature. The top anvil unit was lowered onto the disk and a cylindrical weight was added to the top anvil unit, then the hydraulic ram was lowered onto the weight. Load was increased until the disk fractured. For Canyon samples, disks were confined laterally by a thin strip of tape wrapped around the sides of the plug in order to prevent the sample from falling apart after it broke. This was done to preserve delicate deformation structures near where the anvil indented the sample. The use of tape apparently has no effect on the orientation of induced fractures. After samples failed, fracture orientation was recorded relative to the MOL. Selected fractures were examined petrographically and with a scanning electron microscope.

The Soil Test load frame provides an approximately constant displacement rate for the load platens. The axial-load rate resulting from the applied displacement rate increases as the hemispherical platens deform the specimen surface, but the rate of increase decreases to a nearly constant rate as the specimen approaches failure. Ultimate loading rate, as well as magnitude of applied load at failure, depends on mechanical properties of the rock, but for specimens tested in this study loading rates fell within a relatively narrow range of between 0.8 and 5 lb (363 gm to 2.3 kg) per second. Most tests had loading rates of 2.5 ± 1 lb (1.1 ± 0.45 kg) per second. Over this range of loading rates induced fractures were predominantly single rather than multiple fractures. Optimum loading rates are sensitive to factors such as rock properties, anvil geometry, and specimen geometry, and different loading rates may be appropriate for tests of different rocks, or for tests with other systems. A certain amount of experimentation with loading rates is required.

Outcrop Strength Anisotropy Tests

Tests for strength anisotropy were carried out in the field on Frontier Formation sandstones. These tests initially involved uncontrolled loading of irregularly shaped samples having a range of sizes with a 16-lb sledge hammer. Such tests did not reveal preferred fracture directions. Tests where load was applied with a pointed metal rod and hammer also produced scattered results (fig. 139). Because these tests lack the regular specimen shape and controlled loading rate, they are only partly comparable to the laboratory tests. Moreover, petrographic examination of samples shows near-surface diagenetic and weathering-related porosity development. The microstructure, and probably the strength, of these samples is not directly comparable with subsurface specimens. The field tests are not discussed further, and they were not used in analysis of the axial point-load method.

Laboratory Test Results

Point-load tests on low-permeability sandstone core show marked strength anisotropy in soft Frontier Formation sandstone (Green River Basin, Wyoming) and moderate to weak anisotropy in hard Travis Peak Formation sandstone (East Texas Basin). Canyon sandstones showed moderate to strong strength anisotropy, depending on dominant cement type of sample tested.

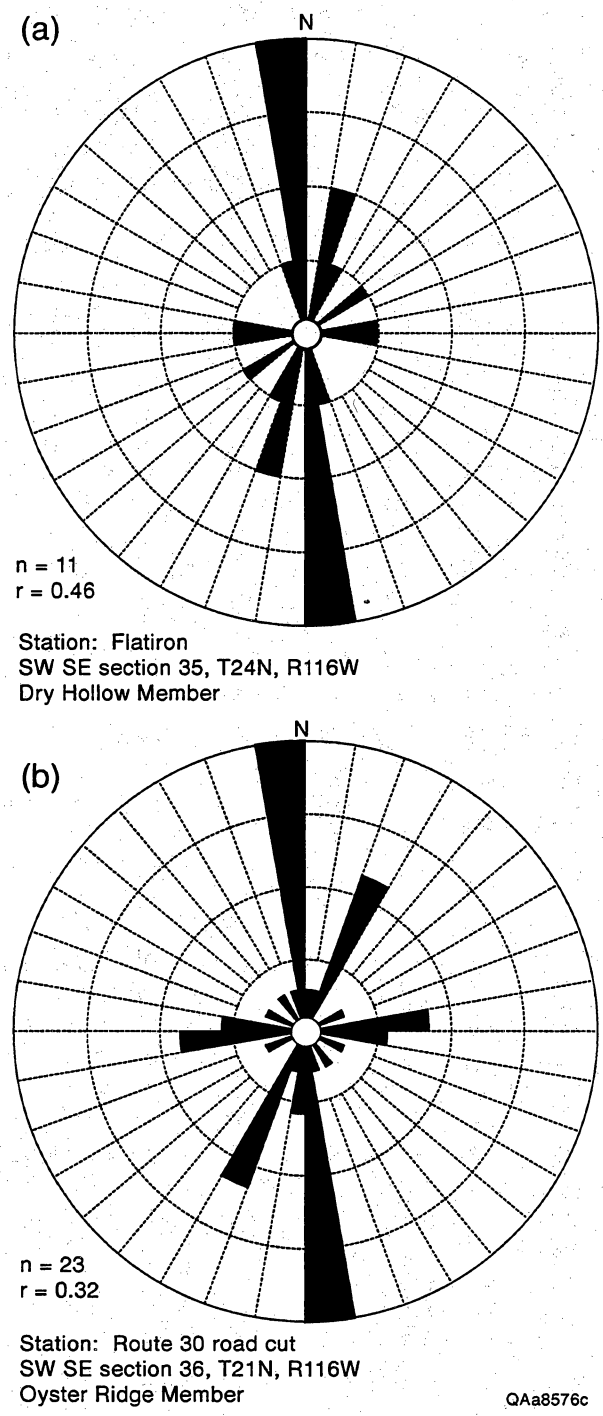

Figure 139. Rose diagrams of fractures created by dynamic loading, two Frontier Formation outcrops.

Comparing results of 328 Frontier and Travis Peak point-load tests with natural fractures, we found agreement in overall strike for some beds. The overall pattern of strength anisotropy in Frontier Formation samples suggests that this test is detecting a fabric more closely related to natural fracture strikes than to in situ stress (fig. 140). For both formations, when compared to stress-direction indicators, such as acoustic velocity anisotropy, anelastic strain recovery, wellbore breakouts, and hydraulically induced fractures, we found some agreement between test-induced fracture strike and inferred maximum horizontal stress direction.

Types of Induced Fracture

Induced fractures for these point-load tests fall into two categories: single fractures (figs. 141 and 142, table 17), in which two radial fracture segments emanate from the central point-load source in approximately opposite directions (i.e., segments define a single direction); and multiple fractures, in which two or more (usually three) fractures emanate from the center along different directions (fig. 142). Representative fractured disks showing single fractures are shown in figure 141, where single fractures have two distinct trends (northeastward and north-south). These trends are not clear for samples with multiple fractures, although generally one of the multiple fractures does follow the trend of associated single fractures.

Fifty percent (85 of 169) of disks from Frontier Formation core broke along a single, nearly planar fracture, with the rest developing multiple fractures. More than half (58%) of the 73 disks from the Holditch Howell No. 5 Travis Peak well broke along single fractures. In contrast, only 28 (35%) of the 80 Travis Peak samples from the Holditch SFE No. 2 well formed single fractures.

Loading rates for the tests varied slightly according to rock behavior. Rates, and the load at failure, generally increased with depth for all wells. Curvature of the load-time curves was pronounced at the beginning of loading, but loading became approximately linear at loads approximately one-half the failure load. Sharp drops in stress were frequently observed in the early part of loading, which probably reflect crushing of asperities on the specimen surface. Significant offsets (always load decreases) in load-displacement curves were observed later in loading for several Holditch SFE No. 4-24 samples. These are the result of macroscopic deformation, including pore collapse, grain crushing, grain displacement, elastic anvil penetration into the sample, and incipient radial fracturing and dilation around the tip of the loading anvil.

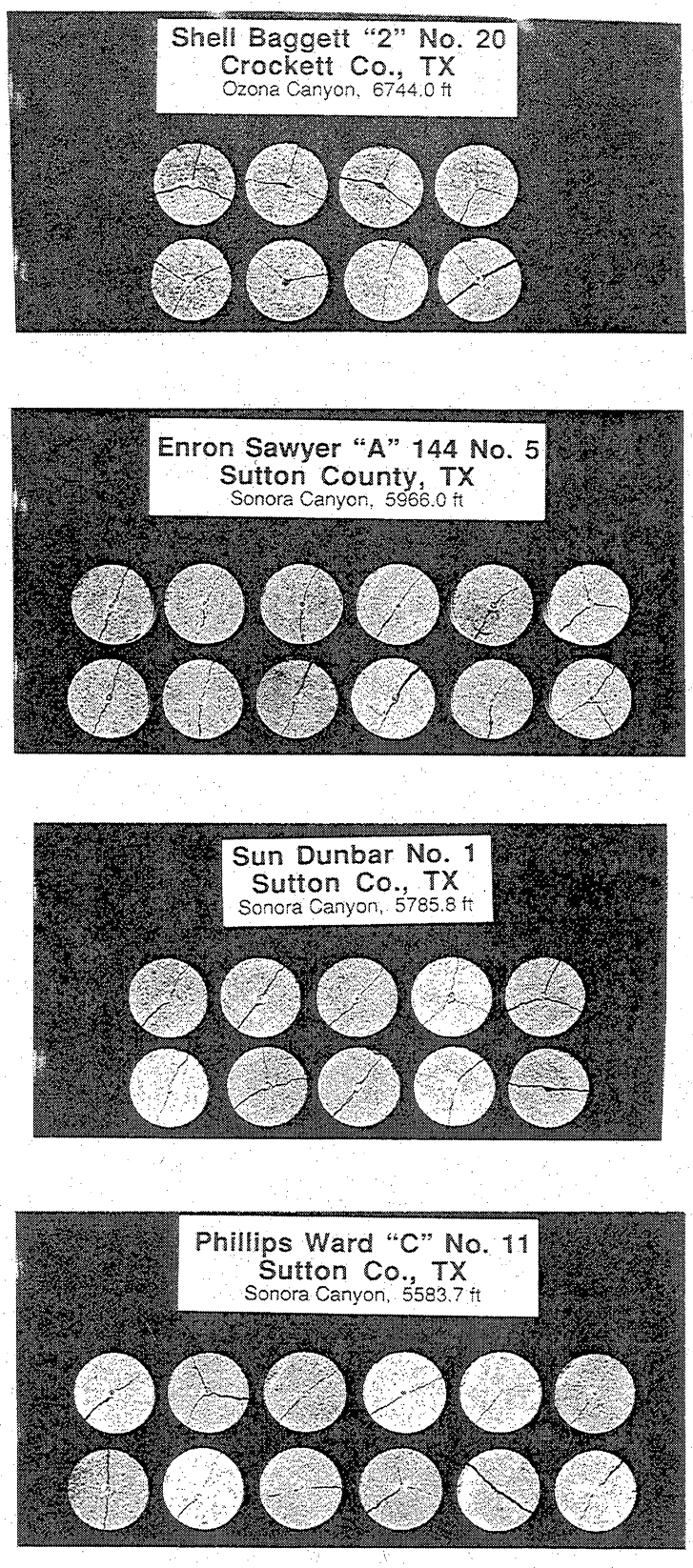

Figure 140. Representative test samples from Canyon Sandstone. Disks are 2.5 cm in diameter. North is to top of photographs.

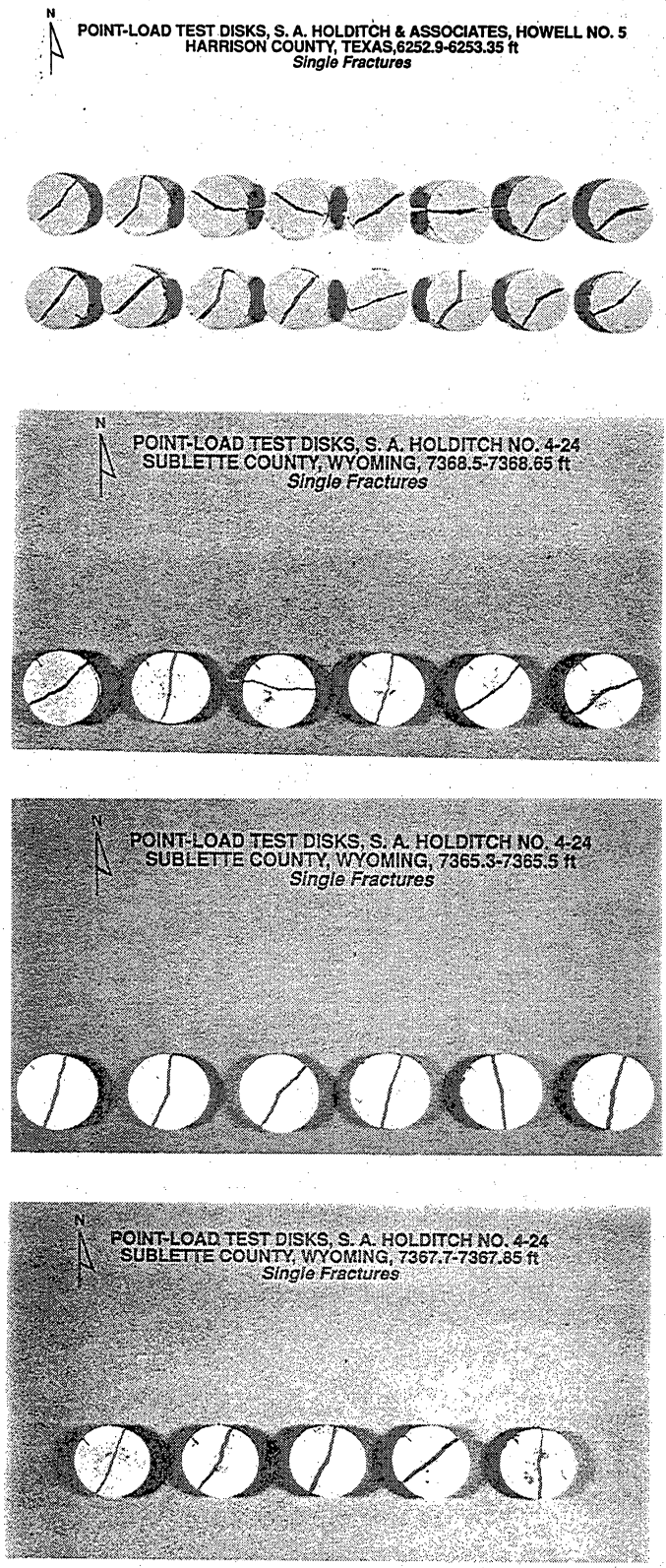

Figure 141. Photographs of disks with fractures induced by point-load tests. Specimens are oriented with north (0°) toward the top of the page. (a) Disks from Travis Peak Formation, 6252.9–6253.4 ft, Holditch Howell No. 5 well, Harrison Co., Texas. (b) Disks from Frontier Formation, 7365.3–7365.5 ft, 7367.7–7367.8 ft, 7368.5–7368.6 ft, Holditch SFE No. 4-24 well, Sublette Co., Wyoming.

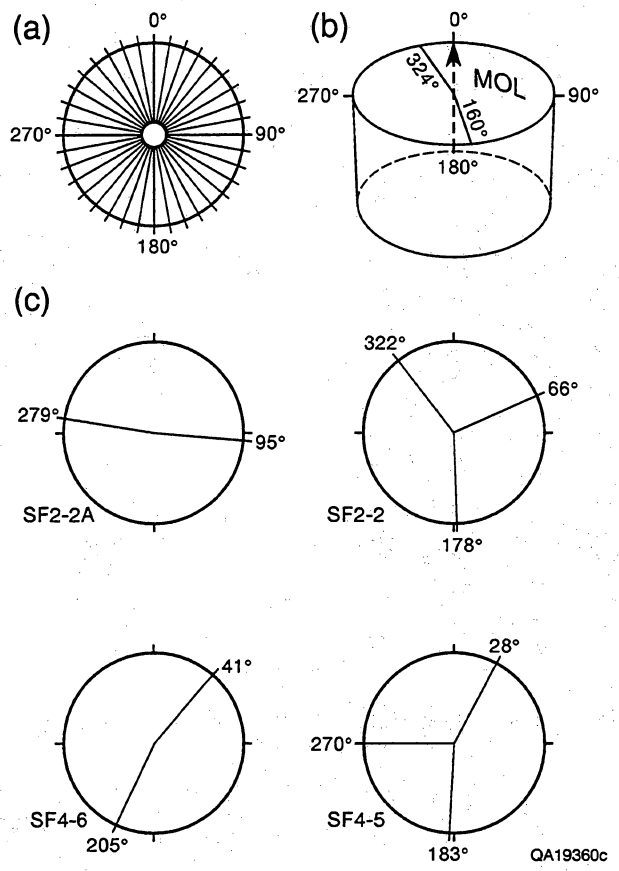

Figure 142. Diagram illustrating orientation convention and single and multiple fractures. (a) Orientation diagram. (b) Single fracture with arms oriented at 160° and 324°. From SFE No. 1, 6119.9–9120.3 ft, disk no. 10. (c) SF2-2A, single fracture, SFE No. 2, 9928.85–9929.1 ft, disk no. 2A; SF2-2, multiple fracture, SFE No. 2, 9928.85–9929.1 ft, disk no. 2; SF4-6, single fracture, SFE No. 4, 7365.3–7365.5 ft, disk no. 6; SF4-5, multiple fracture, SFE No. 4, 7365.3–7365.5 ft, disk no. 5.

Orientation Patterns

Rose diagram summaries on fracture directions in core material from the three Frontier and Travis Peak wells we studied are given in figures 143, 144, and 145. Two diagrams are shown for each sample depth: a diagram showing only single fractures, and a diagram showing the strikes of multiple fractures. Each depth represents data from several plugs at that depth. For most depths a well-defined direction can be identified for the single-fracture data, but no trend is evident in the highly scattered multiple-fracture data. In general, trends for the Frontier Formation are clearer than those of the Travis Peak sandstone.

In Travis Peak samples from the Holditch Howell No. 5 well (fig. 143), highly scattered single-fracture data indicate a plane of weakness that rotates from an approximately east-west strike at 6,120 ft (1,865 m) to an approximate northeast strike below 6,250 ft (1,904 m). Natural macro- and microfractures and maximum horizontal stresses measured in this interval also have eastward to northeastward trends (Laubach, 1989a). These results are consistent with natural microfracture control on fracture growth direction. Single-fracture trends from sample depths of 6,120 and 6,305 ft (1,865 and 1,922 m) have wide dispersion in fractures strike, and trends at these depths are obscure.

In Travis Peak samples from the Holditch SFE No. 2 well, induced fractures have widely scattered strikes (fig. 144) and a high proportion of multiple fractures. The most reliable samples from shallow depths show generally eastward and northeastward mean strikes, whereas samples at greater depths have northward and northwestward strikes (fig. 145g, i). Interestingly, sealed microfracture strikes having this orientation also occur in this depth range in the Travis Peak, suggesting that fractures having this strike may locally be present in the formation but that macrofractures of this orientation have not been sampled.

The tests show marked strength anisotropy in Frontier Formation sandstones (figs. 145 and 146), but samples from different beds have contrasting strikes, leading to an overall bimodal pattern of induced fracture strike. Our samples from the Holditch SFE No. 4-24 well are from three different sandstones. In samples from the upper sandstone (fig. 145a), fractures strike eastward. In the middle sandstone (fig. 145c, e, f, i) fractures strike northward to north-northeastward. In the lower sandstone, fractures strike eastward to east-southeastward (fig. 145k, m, o). Within an individual sandstone, the strikes of fractures created by point-load testing are highly reproducible.

The sharp transition (90° shift) in the strike of microfracture fabric for Frontier Formation sandstones in the interval between 7,370 and 7,380 ft (2,247 and 2,250 m) in Holditch SFE No. 4-24 is also indicated in acoustic wave velocity measurements on oriented core from this well (Walls and others, 1990). Their plot of azimuthal variations in compressional wave velocity is reproduced in figure 147. The compressional wave velocity is sensitive to microfracture fabric (Birch, 1961); wave velocity is highest in a direction parallel to the strike of microfractures.

The behavior indicated in figure 147 is consistent with the results of point-load tests that show that predominant microfracture planes change from almost east-west (approximately 100°) to north-south (0°) over this interval. There was also a substantial increase in the loading rates (and load at failure) for Holditch SFE

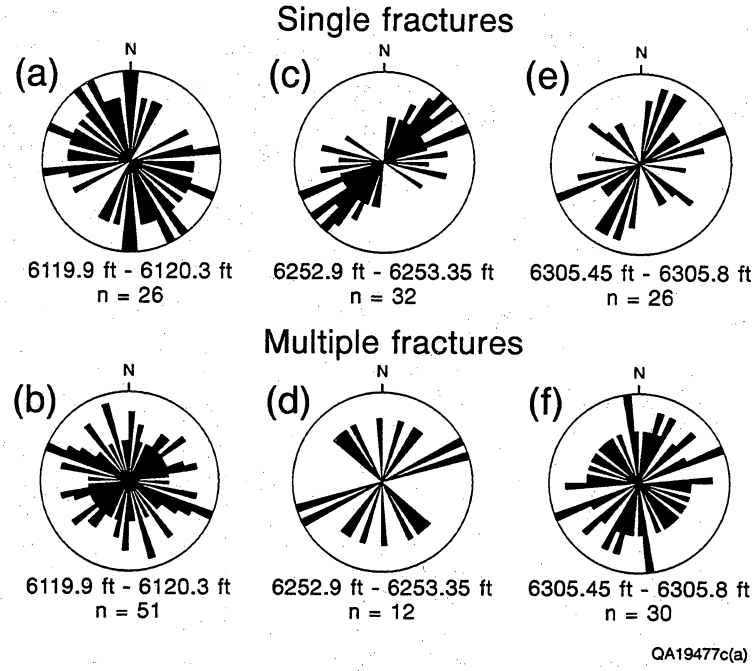

Figure 143. Equal-area rose diagrams of single and multiple fractures created in Holditch Howell No. 5 core. (a) Vector mean, 321°, maximum percentage (circle) 7.6%. (b) No preferred strike, circle 9.8%. (c) Mean 053°, circle 12.5%. (d) No preferred strike, circle 16.6%. (e) Mean 040°, circle 15.3%. (f) No preferred strike, circle 10%.

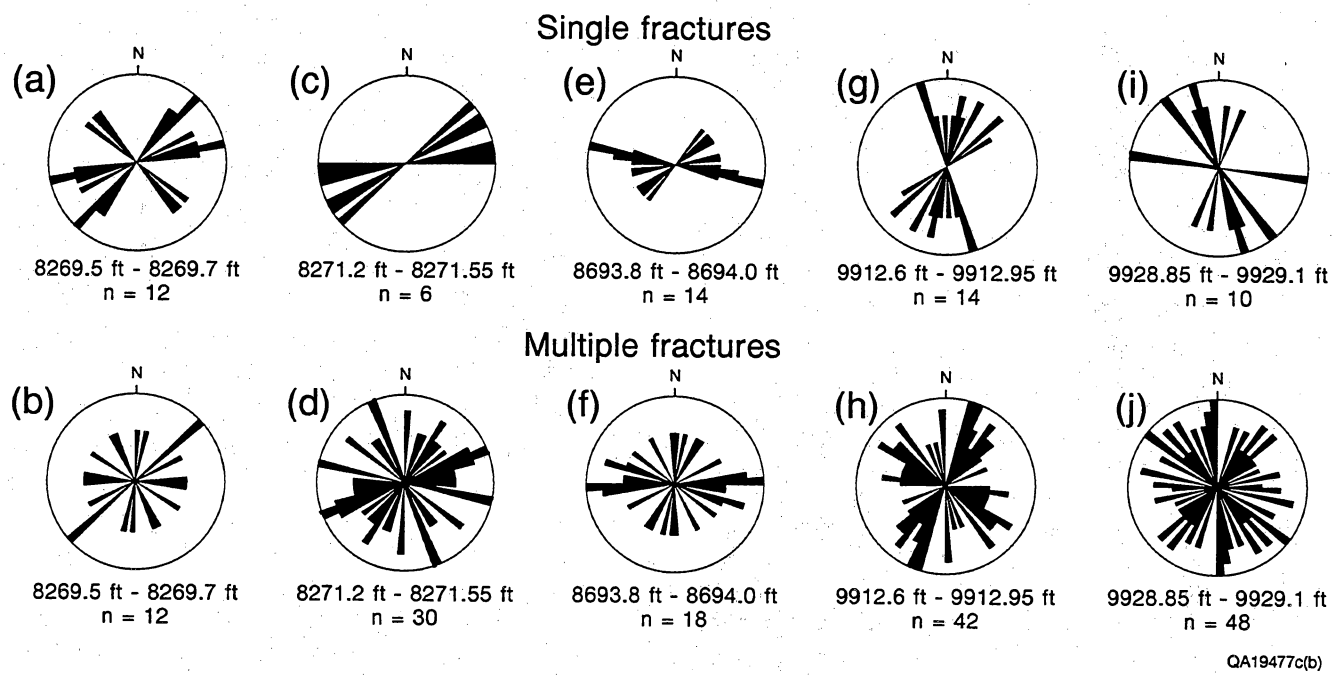

Figure 144. Equal-area rose diagrams of single and multiple fractures created in Holditch SFE No. 2 core. (a) Vector mean, 065°, maximum percentage (circle) 16.6%. (b) No preferred strike, circle 25%. (c) Mean 069°, circle 16.6%. (d) No preferred strike, circle 10%. (e) Mean 084°, circle 28.5%. (f) No preferred strike, circle 16.6%. (g) Mean 012°, circle 21.4%. (h) No preferred strike, circle 9.5%. (i) Mean 336°, circle 20%. (j) No preferred strike, circle 8.3%.

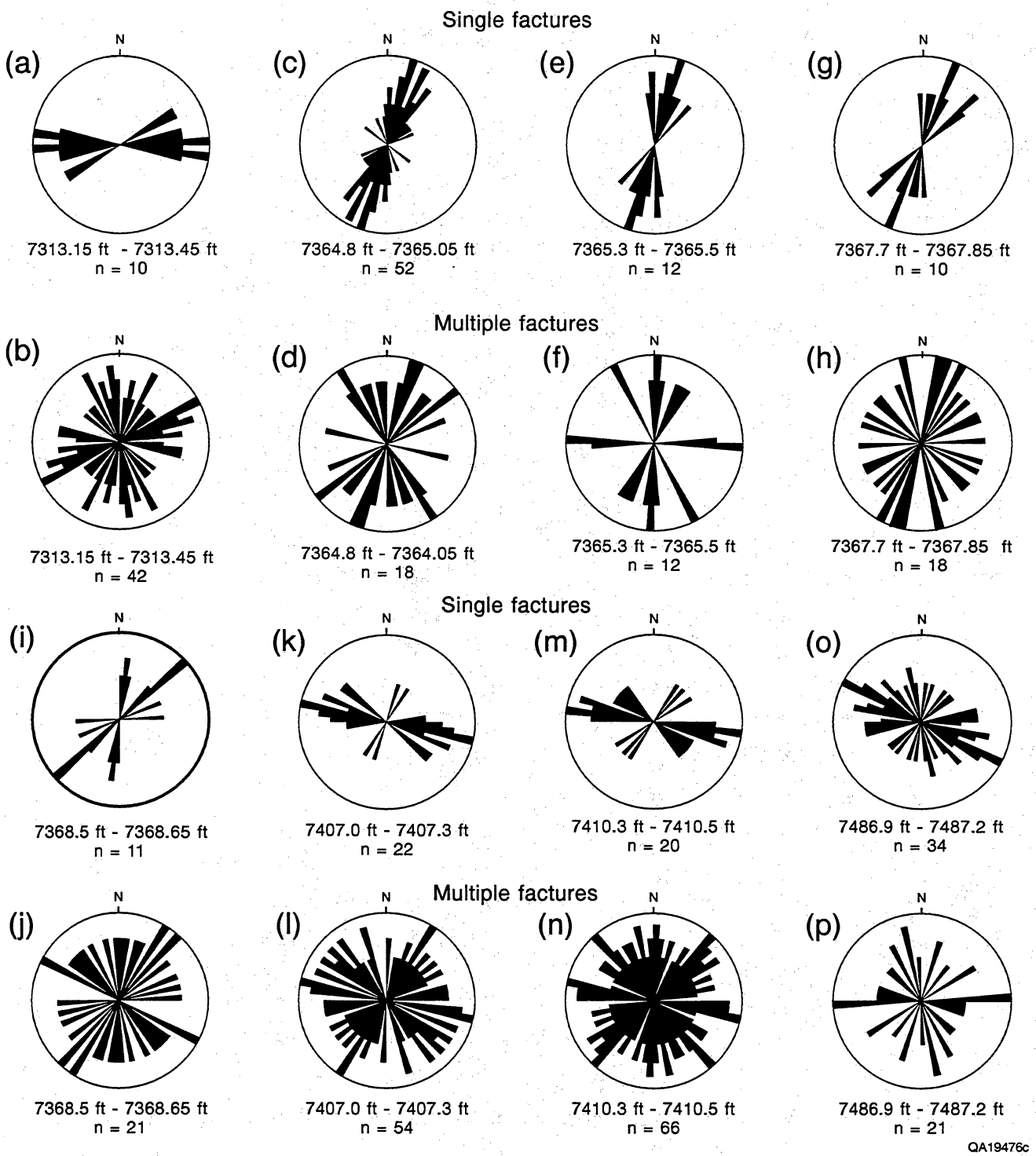

Figure 145. Equal-area rose diagrams of single and multiple fractures created in Holditch SFE No. 4-24 core. (a) Vector mean 085°, maximum percentage (circle) 20%. (b) No preferred strike, circle 9.5%. (c) Mean 020°, circle 19.2%. (d) Mean 11°, circle 11.1%. (e) Mean 012°, circle 25%. (f) No preferred strike, circle 16.6%. (g) Mean 26°, circle 30%. (h) No preferred strike, circle 11.1%. (i) Mean 037°, circle 36.3%. (j) No preferred strike, circle 9.5%. (k) Mean 284°, circle 22.7%. (l) No preferred strike, circle 7.4%. (m) Mean 285°, circle 20%. (n) No preferred strike, circle 6%. (o) Mean 293°, circle 14.7%. (p) No preferred strike, circle 19%.

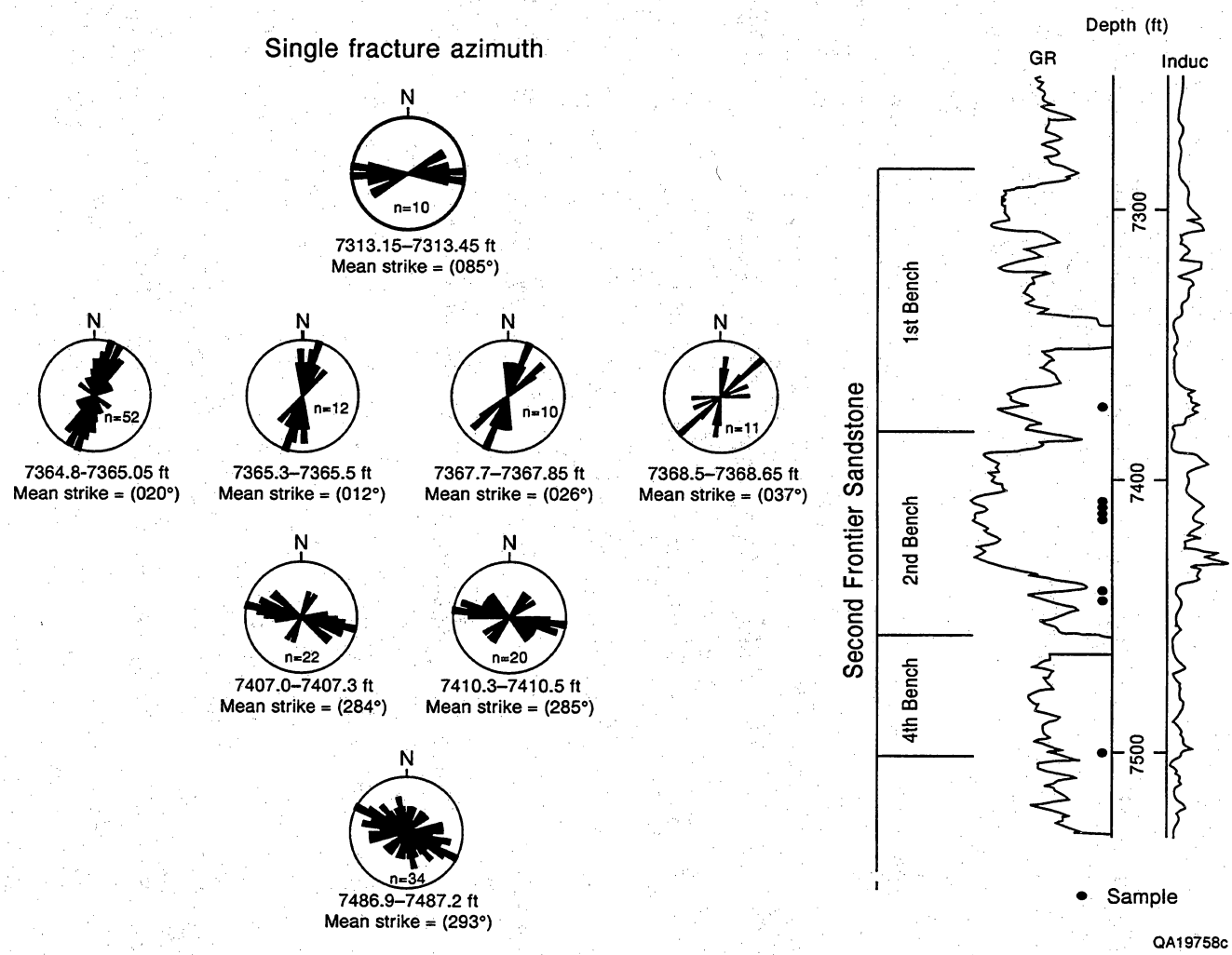

Figure 146. Point-load fracture strike versus stratigraphic position, SFE No. 4 well. Note shifts in fracture strike with depth.

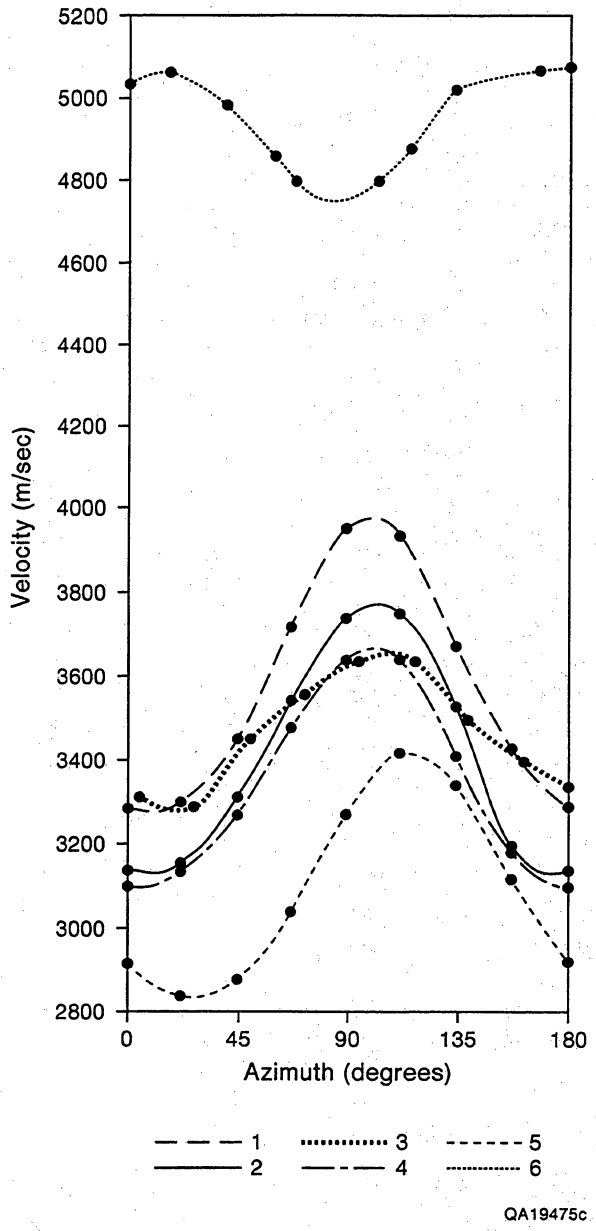

Figure 147. Compressional velocity versus azimuth, Holditch SFE No. 4-24 core, Frontier Formation (based on Hyman and others, 1991, from Clift and others, 1992). Curve 1, sample depth 7429.9 ft; 2, 7429.4 ft; 3, 7384.5 ft; 4, 7424.5 ft; 5, 7423.0 ft; 6, 7371.7 ft.

No. 4-24 specimens at depths greater than 7,380 ft (2,250 m). This increase is consistent with the increase, by almost a factor of two, in mean wave velocity over this depth range (fig. 147), which corresponds to an approximately fourfold increase in Young's modulus. This indirect indication of greater quartz cementation in this depth range is consistent with petrographic analysis of these samples. Moreover, limited scanned CL and petrographic analysis of closed microfractures indicates that some of these fractures in the Frontier Formation have northward strikes.

For some samples, Sonora Canyon point-load fracture directions for single fractures have preferred orientations that strike northeastward (figs. 148 through 151, table 18). In other samples, no preferred orientation is evident. Samples have either random or polymodal breakage patterns. For two Ozona Canyon cores and one Sonora core, strength anisotropy was compared to the strike of calcite-filled fractures. Parts of these cores were not oriented with respect to north, but strength anisotropy was compared to macrofracture strike in these cores. Results show that the induced fractures are not parallel to the calcite-filled macrofractures. This could mean that the preferred sample breakage (which is not pronounced in these specimens) reflects a cause such as core-expansion microfractures or residual stress that is unrelated to macrofractures. Alternatively, because there is evidence for more than one macrofracture event affecting these rocks, the rock anisotropy could be related to microfractures associated with a separate macrofracture event.

Petrographic and SEM Analysis of Test Specimens

Petrographic and scanning electron microscope (SEM) images of test specimens are summarized in figures 152 and 153. These SEM images show the characteristic indentation produced by the point-load anvils and the zone of induced microfracture that is created in the sample beneath the anvil. These results also show how grain-boundary fractures and other minute fractures coalesce in the area beneath the loading anvil to create throughgoing fractures. Numerous created microfractures are present in soft sandstones having moderate to strong strength anisotropy. Hard sandstones with weak or no strength anisotropy generally show few or no created microfracture arrays.

Interpretation of Fracture Strike

The cause of strength anisotropy indicated by point-load tests can be difficult to identify, but in rocks that lack preferred grain orientations, aligned microfractures are generally thought to be responsible (Reik and Currie, 1974; Lajtai and Alison, 1979; fig. 154). Tensile strength is a minimum in a direction normal to the

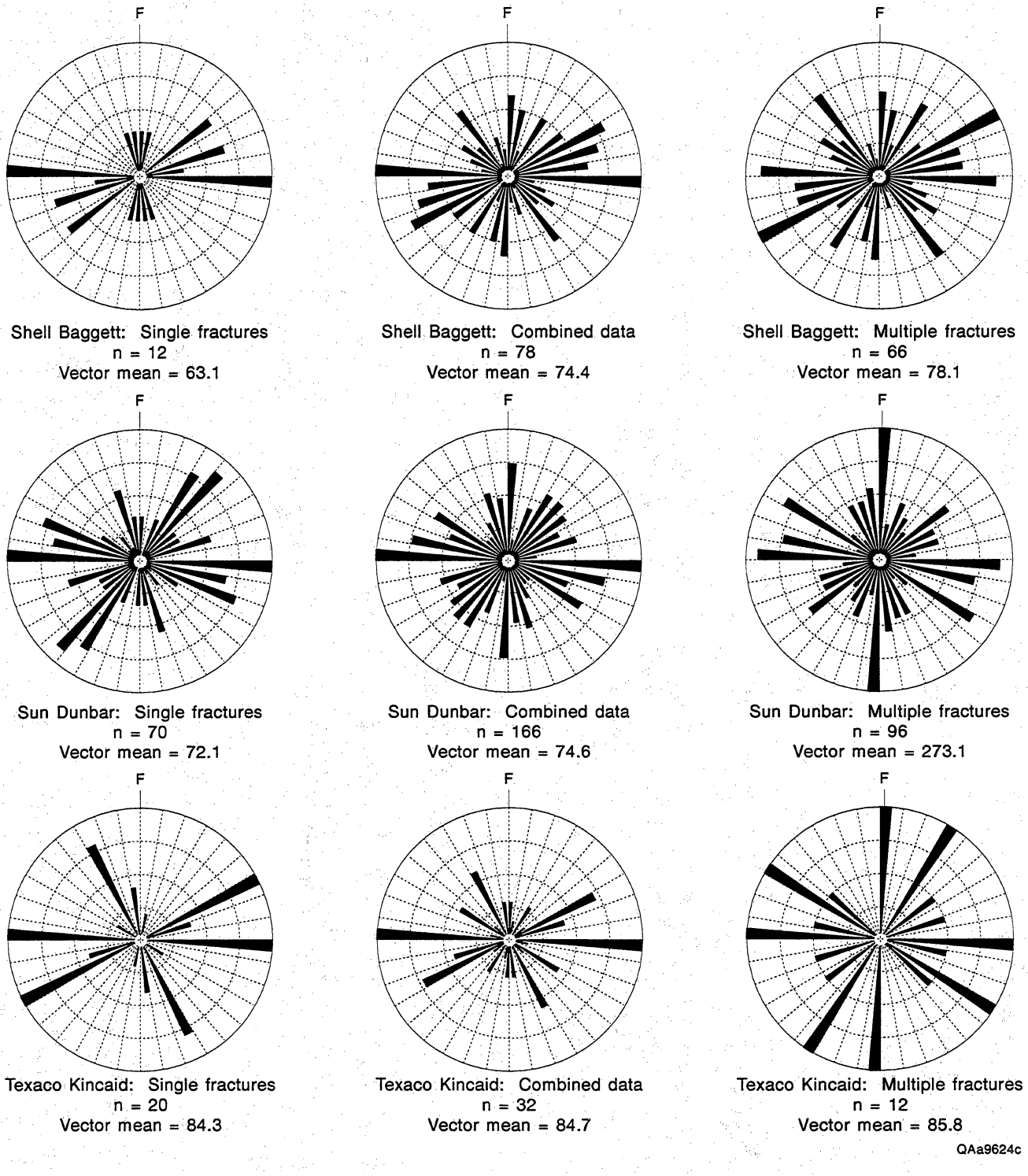

Figure 148. Point-load strength test results (unoriented core), Canyon Sandstone. North (F) on rose diagram is direction of natural macrofracture strike. Weak strength anisotropy is evident in single-fracture data, but anisotropy (direction of preferred sample breakage) is generally at a high angle to strike of nearby macrofractures.

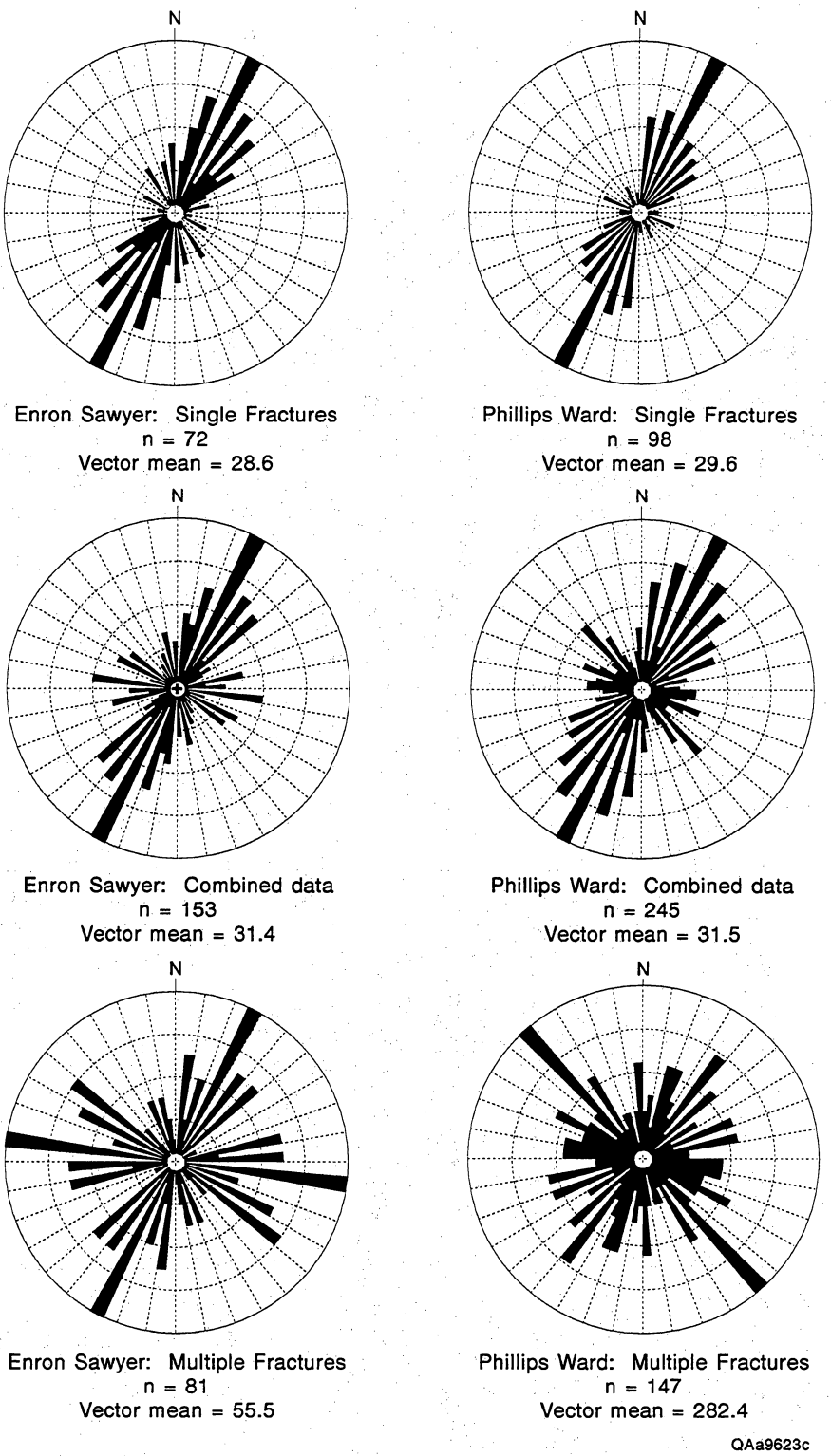

Figure 149. Point-load strength test results (oriented core), Canyon Sandstone. Single fractures strike northeast. No preferred orientation is evident in multiple-fracture data.

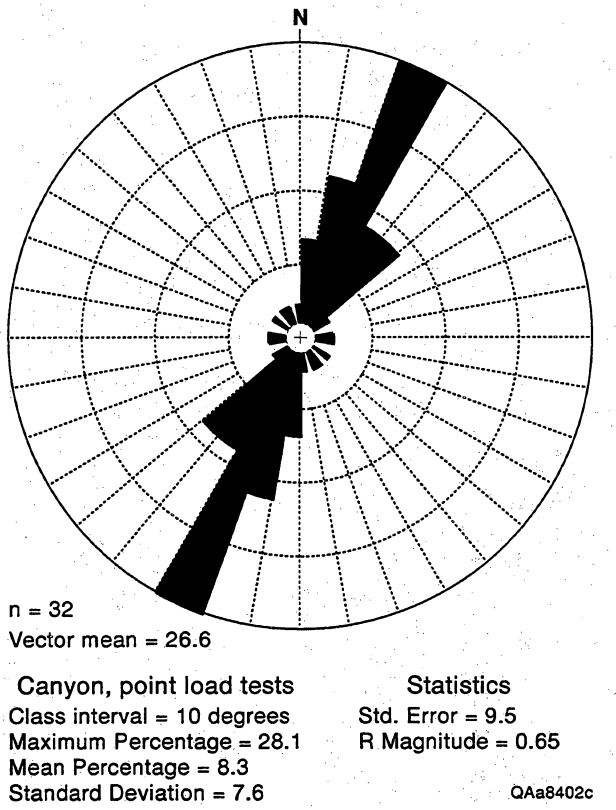

Figure 150. Point-load strength test results (oriented core), Canyon Sandstone. Enron Sawyer well single fractures.

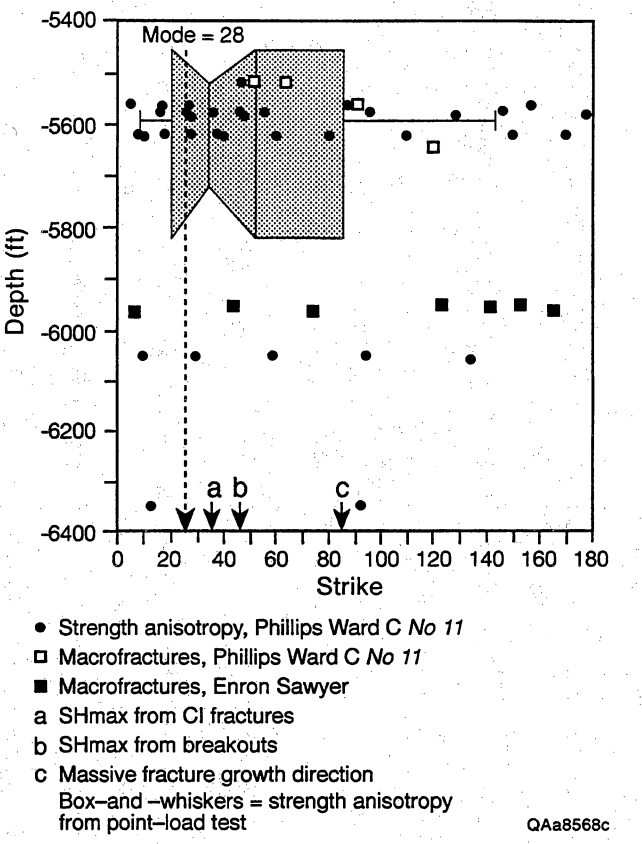

Figure 151. Comparison of strength anisotropy with macrofracture strike, stress directions, and hydraulic fracture growth direction. Box-and-whiskers plot shows interquartile range (box), median direction (line in notch), and range of data values on either side of median (whiskers) not more than 1.5 times interquartile range from box.

microfracture plane, and failure occurs along the plane of microfractures when a point load is applied in this plane (McWilliams, 1966; Friedman and Bur, 1974).

Petrographic and scanning electron microscope studies of point-load samples suggest that there are three possible causes of controls on fracture growth directions. First, microfractures smaller than 10 μm may grow and coalesce to produce the visible fractures that break the sample. This is consistent with previous petrographic searches for microfractures in point-load tested specimens, which indicate that fractures are chiefly submicroscopic (Lajtai and Alison, 1979). Microfractures with a range of sizes are visible petrographically in Travis Peak, Frontier Formation, and Canyon sandstones (Laubach, 1987, 1989a, b; Hyman and others, 1991; this report). Second, fracture orientation could be guided by a controlling flaw. Petrographic observations suggest that variations in grain size and cement distribution can control fracture initiation. Third, residual stress is a potential control on fracture growth direction.

Preferred Orientation and Natural Fractures

Because the origin of small fractures is disputable, interpreting microfracture fabrics is a challenging problem. Microfractures could be created by current or residual subsurface differential stresses, by deformation related to core relaxation, or by old natural fractures having strikes unrelated to present stresses. Natural microfracture arrays can be partly or completely preserved during burial, uplift, and diagenesis. Anisotropic residual elastic strain locked into the

Table 18. Data describing various aspects of Frontier and Travis Peak point-load-tested intervals.

Well and tested depth interval (ft)	APT Single fracture azimuth (°)	ASR Azimuth (°)	Thin section			Mechanical plugs		
			Depth (ft)	Mean grain size (mm)	Average porosity (%)	Depth (ft)	E (Mpsi)	ν
SFE NO. 1*								
6119.9–20.3 (ASR G)	321	68	6117.9	0.11	3.5	6116.5	4.9	0.05
6252.9–53.35	53		6253.3	0.11	8.0	6275.2	5.8	0.08
6305.45–05.8 (ASR Q)	40	99	6296.0	0.10	3.5	6297.1	4.7	0.02
SFE No. 2†								
8269.5–69.7	65		8270.5	0.11	0.8	8270.7	6.2	0.01
8271.2–71.55	69		8270.5	0.11	0.8	8270.7	6.2	0.01
8693.8–94.0	84		8700.8	0.11	0.3	8706.7	6.5	0.01
9912.6–12.95	12		9909.0	0.09	0.0	9913.2	7.3	0.01
9928.85–29.1	336		9930.0	0.17	1.3	9940.2	9.8	n.d.
SFE No. 4‡								
7313.15–13.45 (ASR 4)	85	67	7311.5	0.05	0.0	7332.1	6.3	0.2
7364.8–65.05	20		7363.6	0.11	0.0	7363.6	4.9	0.2
7365.3–65.5 (ASR 5)	12	34	7363.6	0.11	0.0	7663.6	4.9	0.2
7367.7–67.85 (ASR 6)	26	40	7363.6	0.11	0.0	7363.6	4.9	0.2
7368.5–68.65 (ASR 8)	37	47	7363.6	0.11	0.0	7363.6	4.9	0.2
7407.0–07.3	284		7407.6	0.11	1.8	7408.5	3.8	0.2
7410.3–10.5	285		7410.2	0.11	2.0	7409.9	4.7	0.2
7486.9–87.2	293		7479.5	0.07	0.0	7479.5	4.3	0.2

APT signifies axial point-load test
ASR signifies anelastic strain recovery sample; azimuth is maximum expansion direction
SFE No. 1 ASR data from CER and others, 1987
SFE No. 4 ASR data from CER, 1991a
* Dynamic moduli (E and ν) from CER and others, 1988
† Dynamic moduli (E and ν) from CER and others, 1989
‡ Dynamic moduli (E and ν) from SAIC, 1991
E Signifies Young's modulus
ν Signifies Poisson's ratio
Blanks signify no valid test in depth interval

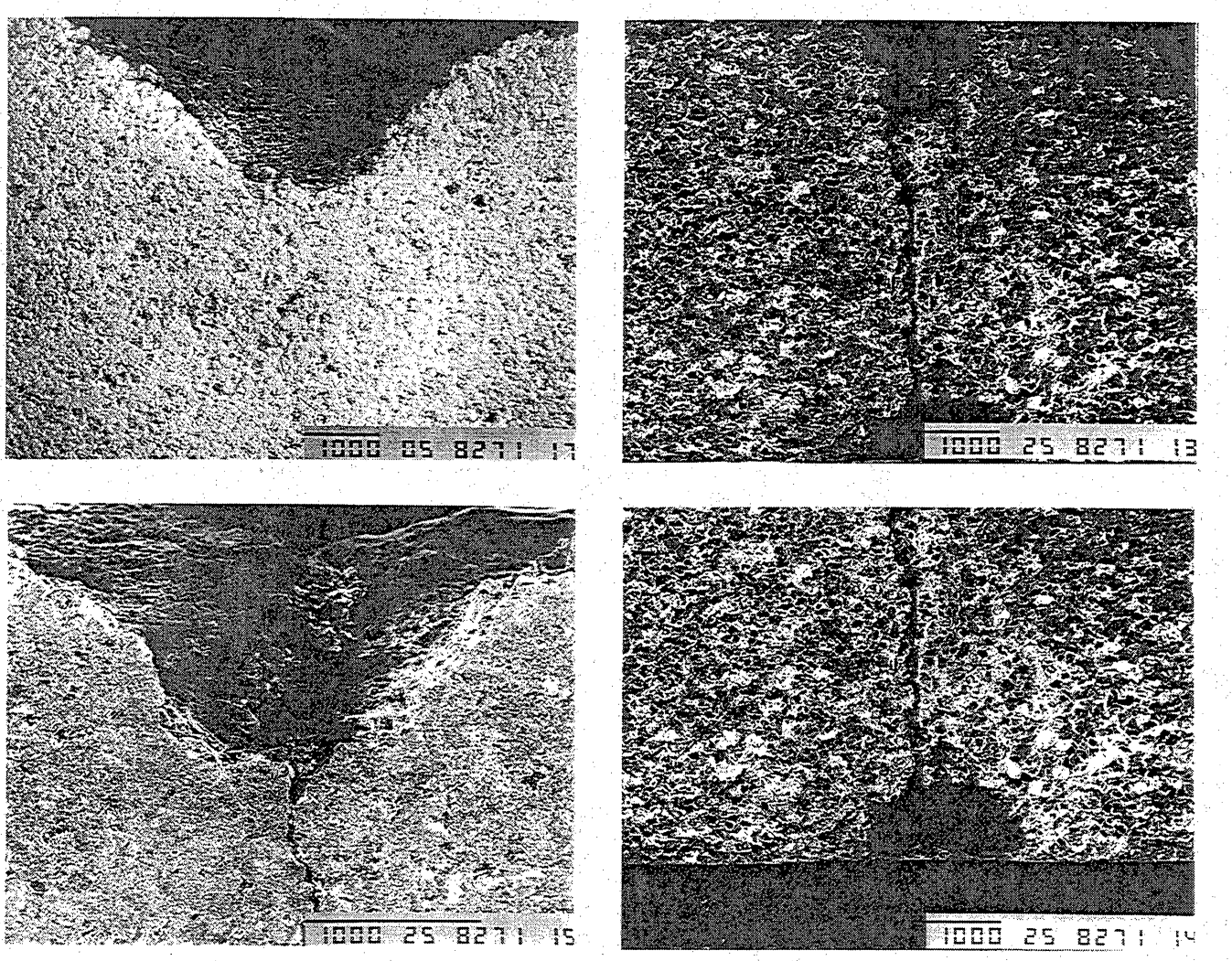

Figure 152. SEM images of point-load indentations. Scale in microns.

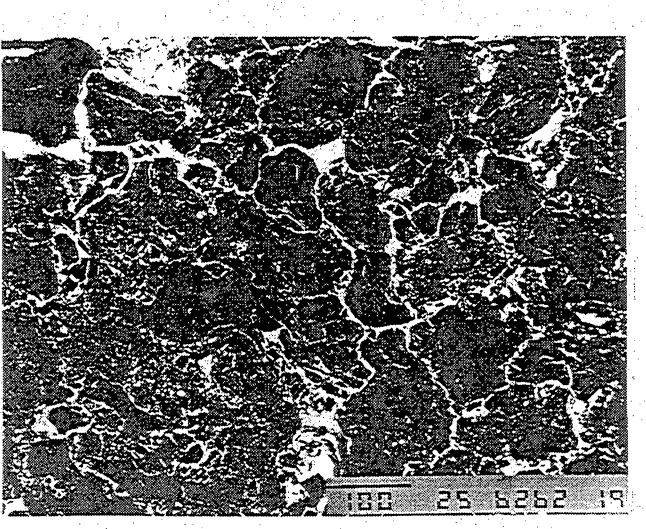

Figure 153. SEM image of fracture patterns beneath point-load indentations. Indentor aligned vertically. Light areas are fractures.

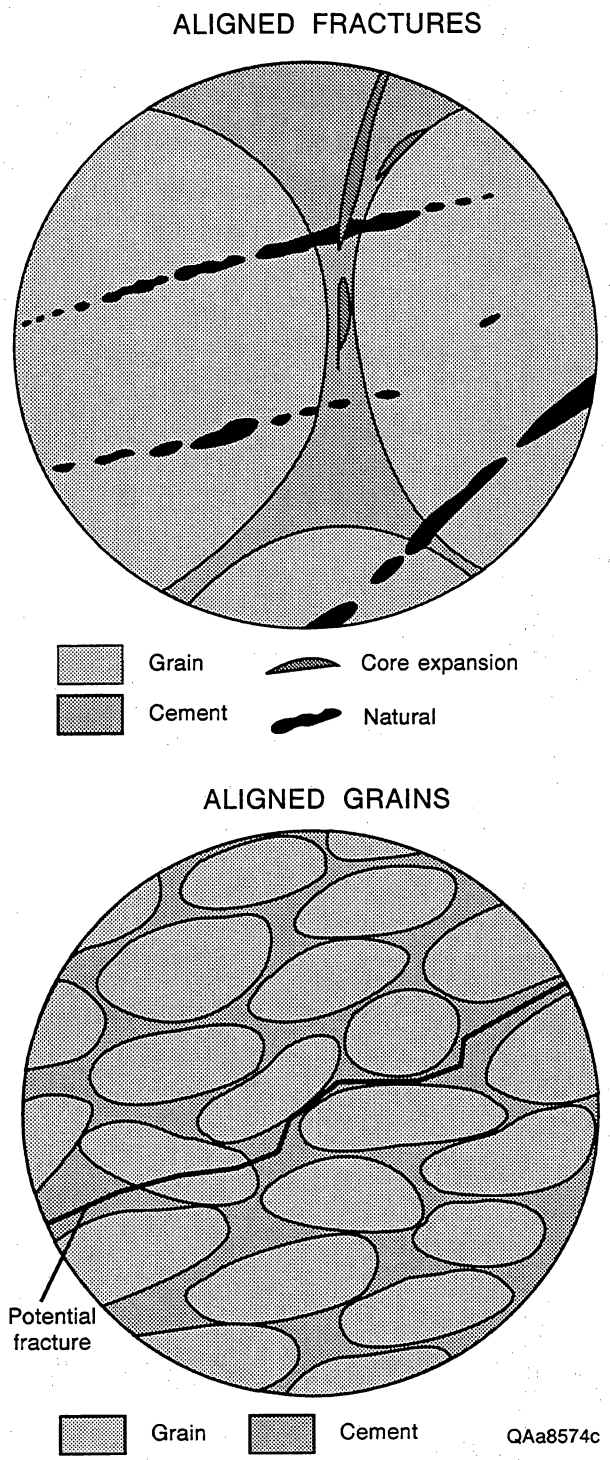

Figure 154. Diagram showing three microstructures that can govern point-load fracture direction. Natural fractures and core expansion fractures are dominant controls on strength anisotropy in the samples tested in this study.

natural grain-cement aggregate can cause strength anisotropy (Friedman and Logan, 1970; Reik and Currie, 1974). More than one natural fracture orientation may be present in a sample. Strength anisotropy studies of sandstone in outcrop have found unimodal and polymodal induced fracture directions that locally correspond to strikes of macroscopic joints (Lajtai and Alison, 1979). The microfracture fabric that causes strength anisotropy may therefore be fortuitously aligned with the present stress field.

In addition to the problem of separating natural microfracture anisotropy from that due to residual stress or fractures related to current stresses, a difficulty in using point-load fractures to infer in situ stress orientation is that microfracture fabric can result from two processes related to present in situ stress. First, fractures caused by current stresses may be ones that are open in the subsurface. Second, fractures can form as a result of elastic and anelastic strains during and after core recovery.

Strain relaxation associated with core removal is usually marked by core expansion that is measured with sensitive strain gauges (Teufel, 1983). It is commonly greatest in the maximum in situ stress direction, the result of the opening of microfractures oriented perpendicular to the direction of core expansion. Direction of maximum expansion is inferred to be the direction of maximum horizontal compressive stress (SHmax) in the subsurface. Pressure-dependent ultrasonic measurements on sandstones have been used to show that in some cases relaxation-related microfractures are aligned with SHmax determined by measuring core expansion (Sayers, 1990). However, acoustic velocity anisotropy may also be caused by microfractures that existed in subsurface rock prior to coring. Under appropriate experimental conditions, microfractures that existed in situ or that were created by core expansion can be detected by point-load tests. Successful point-load tests therefore have advantages and limitations similar to those of acoustic anisotropy tests for detecting stress-related microfracture fabrics; accurate interpretation of results requires petrographic or other information to distinguish relaxation-induced microfractures from natural microfractures.

In two Travis Peak samples where point-load and anelastic strain recovery samples were taken from the same core piece, induced-fracture strike and stress directions inferred from core expansion directions diverge by 17 degrees and 31 degrees, respectively (table 19). Since core expansion is expected to produce a microfracture fabric at right angle to the direction of core expansion, it is possible that point-load tests of these samples are detecting microfractures created by core expansion. On the other hand, point-load-induced fractures and natural macrofractures and petrographically documented microfractures in Travis Peak

Table 19. Orientation statistics for Canyon Sandstone point-load tests.

Well		Std. error*	R magnitude†	Rayleigh‡
Baggett "2" No. 20:	**Single**	**37.03**	**0.305**	**0.3259**
	Combined	25.17	0.181	0.0767
	Multiple	30.54	0.164	0.1676
Dunbar No. 1:	**Single**	**25.26**	**0.189**	**0.0802**
	Combined	35.02	0.089	0.2671
	Multiple	204.53	0.020	0.9607
Kincaid "D" No. 7:	**Single**	**37.16**	**0.240**	**0.3150**
	Combined	33.32	0.214	0.2278
	Multiple	67.71	0.172	0.6985
Sawyer "A" 144 No. 5:	**Single**	**7.54**	**0.573**	**0.0000§**
	Combined	11.00	0.292	0.0000
	Multiple	65.51	0.067	0.6930
Ward "C" No. 1:	**Single**	**8.17**	**0.469**	**0.0000§**
	Combined	15.02	0.172	0.0007
	Multiple	107.10	0.032	0.8567

*Standard error of vector mean
†Magnitude of resultant (degree of orientation)
‡Rayleigh's test of uniformity
§Nonuniform distribution

sandstones strike eastward to northeastward, so old natural microfractures could also be controlling induced-fracture strike. In four Frontier Formation samples, differences in maximum expansion direction and point-load fracture strike are small (10°, 14°, 18°, 22°), so it seems unlikely, for these specimens, that microfractures created by core expansion (at least as inferred from these anelastic strain recovery tests) are those detected by point-load testing, since these directions should be at right angles rather than parallel.

In Travis Peak and Frontier Formation samples some induced fractures parallel inferred SHmax directions, and some are at right angles to that direction. Hyman and others (1991) interpret a bimodal pattern of velocity anisotropy from these rocks to reflect both natural and induced microfracture fabrics. In some samples, this velocity anisotropy also corresponds to permeability anisotropy (Hyman and others, 1991). The northeastward-trending strength anisotropy in some Sonora Canyon samples parallels SHmax directions measured in the same wells. This is consistent with microfractures induced by in situ stresses being responsible for strength anisotropy. Sample breakage is not in the expected direction for microfracture arrays caused by core expansion. At least some mineralized macrofractures strike at a high angle to observed sample breakage directions.

The bimodal pattern of Frontier Formation induced-fracture orientation is consistent with the influence of old natural microfractures that are not necessarily aligned with current stress directions. Samples have small velocity anisotropy (~4% for some Frontier sandstones) and low values of differential core strain (20–30 με). Natural fractures in the Frontier Formation in outcrop near the wells we sampled have northward, northeastward, and eastward strikes, with predominant strike directions that shift from bed to bed (Laubach, 1992c). This pattern of shifting natural fracture strike direction is similar to the shift in induced fracture strike we found in the three sandstones we tested. These results show that natural microfracture fabrics could be responsible for induced fracture anisotropy. However, while petrographic studies revealed that sealed and open microfractures are present in these samples and some are aligned with sample breakage direction, there is no direct observational evidence in the form of clearly reactivated microfractures that such microfractures control the strike of fractures created in tests.

Deformation Behavior

Thin sections prepared from selected post-test specimens provide some insight into variations in observed point-load test results that can be qualitatively related to differences in test material behavior. In softer rock such as Frontier Formation sandstones, a localized zone of crushed grains is observed in the immediate vicinity of the point-load indentation. Adjacent to this zone is an array of small, randomly oriented extension microfractures. Larger microfractures extend away from the indentation point, and presumably, microfracture coalescence led to ultimate specimen failure. In harder Travis Peak sandstones, especially in heavily quartz-cemented, rigid specimens, there was little grain crushing and load-anvil penetration. These specimens broke suddenly, and there is no evidence for development of a microfracture zone and microfracture coalescence. Similar processes were documented with SEM back-scattering electron images in rock samples deformed by Thiercelin and Cook (1988). Macroscopic deformation near the indenting anvil is consistent with numerous prefailure stress drops in Frontier sandstone specimens from Holditch SFE No. 4-24 samples. Optical microscopy and SEM observations suggest that these stress drops are likely to be due to crushing and/or microfracture generation near the loading anvil.

Deformation behavior has implications for modes of fracturing in point-load tests and causes of preferred or random induced-fracture strike. Flaws, such as microfractures, grow under the influence of applied tensile stresses at a rate proportional to the stress level. The energy required to create a new fracture surface is on the order of $K^2_{Ic}/2E$, where K_{Ic} is the critical stress intensity factor for the propagation of tensile cracks (the Mode I fracture toughness) and E is Young's modulus (Grady and Kipp, 1987). When a load is applied at a sufficiently slow rate, open microfractures such as fresh cracks grow easily, local tensile stresses do not increase significantly above this critical level, and deformation is largely accommodated by growth of only these "low strength" fractures. Eventual coalescence of microfractures produces a macroscopic failure plane that is aligned with the predominant orientation of preexisting microfractures. When load is applied rapidly, tensile stress levels may increase more rapidly than can be accommodated by the growth of preexisting microfractures, to levels sufficient to activate older, partly healed microfractures or to create new fractures. In this case fractures are unlikely to be influenced significantly by subtle microfracture fabric, and the orientations of the ultimate fractures will be more random than will more slowly applied loads.

When point loads are applied by means of a constant rate of load-anvil displacement, as was done in our tests, the rate of loading is inversely proportional to the rigidity of the test specimen. Load rates in softer Frontier Formation sandstones were accordingly lower than for the rigid quartz-cemented Travis Peak sandstones. The more systematic pattern of fracture orientations observed for Frontier Formation sandstone specimens may therefore be related to their relatively low rigidity. It is possible that a more consistent pattern of behavior could be observed in rigid quartz-cemented Travis Peak sandstones if lower anvil-displacement rates, and hence loading rates, were used.

Evaluation of Method

Axial point-load tests can be used as a tool for characterizing and evaluating strength anisotropy in low-permeability sandstone reservoirs. Our results show that the point-load test can detect strength anisotropy in typical low-permeability sandstones, but the success of tests and thus utility of the method may be greater in sandstones such as those of the Frontier Formation that contain abundant ductile grains or cements, allowing sample fracture at low stress levels. In the formations we studied, induced fracture strikes correspond to directions of acoustic and permeability anisotropy, directions of principal horizontal stresses, and natural fracture strikes. Point-load tests results are therefore potentially useful tools for evaluating reservoirs where fractures and in situ stresses can govern the success of exploration and development. Yet these tests have significant limitations.

An advantage of point-load tests is their low cost and ease of use. With oriented core and simple, relatively inexpensive equipment, point-load tests could be carried out in the field or at the well site. Because small (less than 1 inch [2.5 cm]) samples are used, sedimentary heterogeneities can be avoided that interfere with results of widely used stress-determination methods such as acoustic anisotropy and anelastic strain recovery. In principle, the small sample size used for this test permits analyses to be carried out on samples obtained from wireline-conveyed sidewall coring devices, but in practice this technique would be competing with other tests that might preclude the use of this destructive procedure. Because the point-load test is rapid, large numbers of samples can be processed in a short amount of time, permitting detailed evaluation of variations in strength-anisotropy fabrics throughout a core. A technician could carry out tests of core at the well site on a foot-by-foot basis, and not interfere with field-based core analysis (appendix 2).

A major drawback of this technique is that the physical cause of anisotropy is not always apparent. Our study shows that point-load tests are sensitive to

natural microfracture fabrics, but these tests are also sensitive to preferred grain orientations in sandstone and (apparently) to residual stress or microfractures caused by core expansion that are too small to detect or at least to effectively map with SEM imaging devices (fig. 154). Petrographic evaluation of the causes of strength anisotropy and the origins of microfractures is crucial, yet such analysis does not always have a satisfactory result. Calibration of the technique with microfracture data derived from petrographic or SEM observations may provide a solution to this problem, but if usable microfracture data are available, point-load methods may not be needed.

As a consequence of uncertain causes of strength anisotropy, stress directions cannot be directly inferred from the results of point-load tests. As with other core-based methods that have been used to infer stress directions based on the presumed existence of microfracture arrays, to be interpreted correctly the origin of strength anisotropy must be documented petrographically or by some other method that is independent of orientation comparison, and results need to be compared with in situ stress measurements, such as wellbore breakout azimuth, in order to use point-load information to accurately infer stress directions. This result highlights potential interpretation problems with other core-based anisotropy methods, such as anelastic strain recovery. Whole-core stress-direction measurement techniques, such as acoustic velocity anisotropy measurements or on-site monitoring of anelastic core strain release, are susceptible to interference from sedimentary, diagenetic, or structural heterogeneity that can compromise these tests. Results of our study show that these heterogeneities may not be at all apparent, even at the scale of optical microscopy. At a minimum, thorough analysis of samples for natural microfracture fabrics should be undertaken before the results of any of these core-based methods are used to deduce stress directions.

Conclusions: Determining Fracture Strike

In low-matrix-permeability gas sandstone plays, fracture orientation information is commonly not available because costly borehole-imaging logs and whole core are rarely acquired in more than a few wells in an area, and fractures are rarely intersected by wellbores. Natural fracture strikes in nearly all major tight gas sandstone plays either are undetermined or have been measured satisfactorily only in small areas (table 1; appendix 1). Yet studies of fractures in outcrops of reservoir-facies sandstones show that fracture orientation can shift with disconcerting abruptness over short vertical and lateral distances (Laubach, 1992a) (fig. 155). Numerical models described in this report, sealed microfracture strike information, axial point-load results, and macrofracture data from extensively cored and logged research wells suggest that similar patterns exist in the subsurface. Three indirect methods to measure fracture strike are proposed.

(1) If synkinematic cement is present, systematic microfracture mapping with scanned CL images permits bed-by-bed documentation of fracture orientation even in core where macrofractures are absent. Quartz cement is synkinematic in the four formations we studied, and we found evidence that parts of the Mesaverde Group have synkinematic quartz. We speculate that much quartz cement is inherently synkinematic in that the processes that lead to cementation also promote fracture. Photomultiplier-based imaging of electron beam-induced luminescence (scanned CL) detects quartz-filled microfractures in quartz-cemented sandstones that are mostly not visible using standard petrographic methods. Because small samples can be used to get fracture strike, this approach can be applied to samples obtained from wireline-conveyed rotary sidewall coring devices, permitting more fracture-strike data to be collected at reduced cost. Examples show that strike of subvertical opening-mode microfractures is a good guide to macrofracture orientation.

(2) Fractures in coalified wood and thin coal beds or coal inclusions within sandstones are an overlooked source of information on sandstone fracture strikes. Coal intervals or inclusions in these sandstones are probably mainly coalified wood rather than actual thin coal seams. Fractures in the thin coal intervals have close spacing (less than 10 cm [4 inches]), so they are readily sampled by vertical cores. Such features are widespread in fluvial and certain nearshore facies of marine sandstones. Travis Peak and Frontier sandstones contain these structures, but Canyon sandstones do not. Oriented coal fractures in our sandstone cores are too sparse to fully test this approach, but numerical modeling and regional mapping of fractures in coal beds show that this approach can lead to constraints on fracture patterns in sandstones. Relating coal-fracture mineralogy to diagenesis is a necessary step in such an analysis.

(3) Axial point-load tests show that sandstones have strength anisotropy. In some cases, strength anisotropy corresponds to natural fracture trends, but in others it may reflect in situ stress, residual stress, or some other cause. The ease of application of the method is offset by uncertain interpretation of the cause of the strength anisotropy. For tests carried out with relatively compliant testing devices, the technique works best in soft sandstones such as parts of the Frontier that lack abundant quartz cement. In this respect the technique is complementary to scanned CL imaging of quartz-sealed microfractures, which appear to be most prevalent in hard, quartz-cemented sandstones.

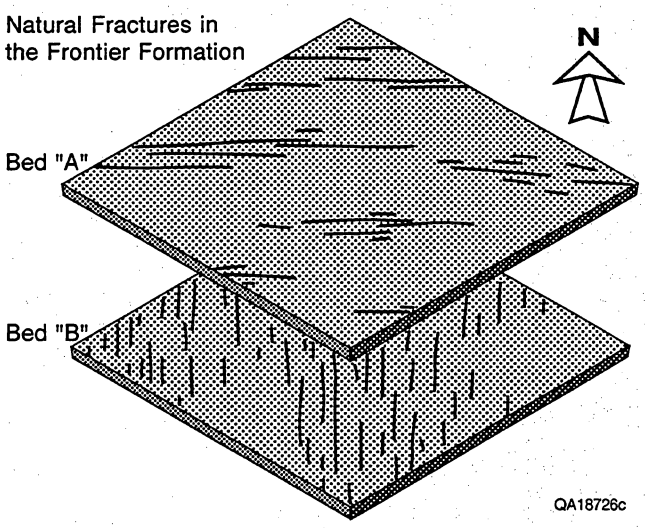

Figure 155. Natural fracture strike can shift abruptly from bed to bed, as well as laterally within a bed. Methods described in this report can be used to map such shifts in fracture strike. This example is based on patterns observed in Frontier Formation outcrops near Kemmerer, Wyoming.

Prospects for Utilization

Petrographic and scanned CL analyses of microfracture strike provide the capability to systematically map natural fractures in subsurface sandstones. These methods are not subject to the sampling bias and lack of data that plague macrofracture-based studies, and they can be carried out rapidly and inexpensively. Formerly, no methods allowed systematic measurement of fracture orientations on a bed-by-bed basis. Consequently, the potential exists for these methods to reveal the variability of fracture patterns that exists in the subsurface (fig. 150).

The ability to measure and map fractures in cored wells on a bed-by-bed basis will enable the explorationist or development geologist to improve fracture maps in areas of sparse data. This can lead to better appreciation of patterns of fracture strike and the location of fractured areas, helping to narrow the limits of possible fracture patterns in a given area. It could also verify fracture genesis models and lead to better forecasting of fracture patterns. Benefits of the application of this approach include lowered well costs and more accurate and certain targeting of natural fractures. Basic natural fracture information in most low-permeability sandstone plays is currently exceedingly sparse (appendix 1). Moreover, fracture information needs to be collected independently from in situ stress data (fig. 156). In other words, the orientation of maximum horizontal stress (SHmax) should *not* be assumed to be parallel to the strike of open natural fractures. The character of fracture surfaces, which are commonly rough and partly mineral-lined, the high stiffness of many quartz-cemented sandstones, and the low contrast between maximum and minimum horizontal stress that is present in many areas all suggest that parallelism between stress directions and open fractures need not generally be the case. Using the approaches described here, together with independent stress direction measurement methods, allows this goal to be met.

The risk associated with inadequate characterization of fracture strike is clear. Fractures could be overlooked or missed, or—just as importantly—their discovery could be too expensive to justify the search. Effective definition of subsurface fracture patterns requires higher-resolution maps of fracture strike than are currently available, and thus mapping procedure must be improved by application of the methods described in this report.

Currently, lack of reliable methods to map fracture strike hinders optimized well placement or efficient directional drilling, yet current sparse fracture-strike data may be adequate for many of today's development practices. However, the real portent is for *future* drilling

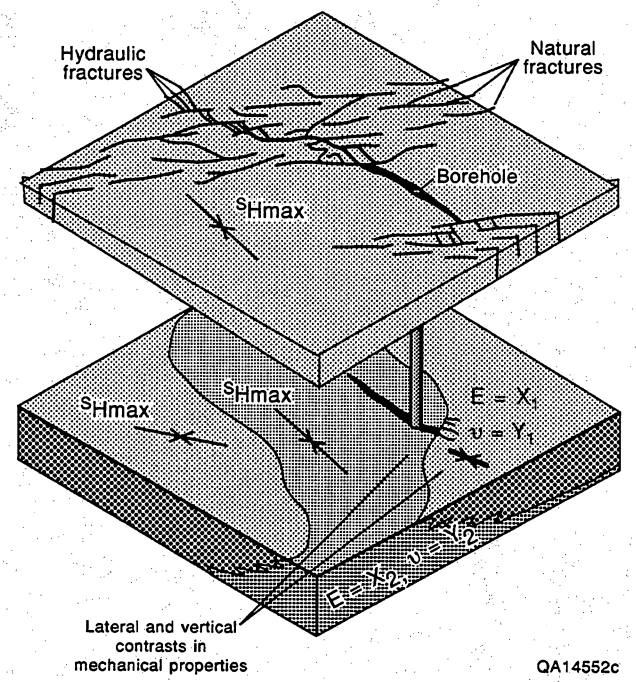

Figure 156. Independent measurements of rock properties, stress directions, and fracture strike are needed to design advanced reservoir development strategies. Prior to this study, natural fracture strike measurement depended on chance encounters with macrofractures. Consequently, fracture strikes are typically poorly determined in reservoir sandstones. Diagram shows hydraulic fracture growing from a well into a fracture swarm. Three independent data sets are needed to design a strategy to deal with this scenario. E, Young's modulus; ν, Poisson ratio; SHmax, maximum horizontal stress.

and hydrocarbon production. According to Perry (1994), development drilling in tight gas sandstones must be increasingly successful if production from this resource is to grow steadily into the next century. Yet over time exploration will tend to be in more technically challenging lower quality reservoirs and deeper reservoirs. Accurate targeting of high-deliverability zones within otherwise low-quality reservoir rocks is one way that desired production goals from these resources could be met (National Research Council, 1994). In low-quality reservoir rocks deliberate searches for natural fractures and associated high-deliverability zones may be a key—or perhaps the only—viable exploration or development method.

Overall Study Conclusions and Implications

- By categorizing diagenesis based on the temporal relations of authigenic mineral precipitation and fracture movement, highly cemented sandstones can be subdivided into those dominated, volumetrically, by pre-, syn-, and postkinematic cements. Diagenesis and fracturing can be coupled processes that operate simultaneously to create a fractured layer, or they may be additive processes that operate sequentially. This categorization leads to useful insights about the properties of fractures and their relation to sandstone framework porosity.

- Fracture-prone layers of several different types exist in highly cemented sandstone. Prekinematic cements that localize fractures can be identified with conventional geophysical logs if their composition is distinctive enough. Fractured beds associated with synkinematic quartz cement have favorable characteristics as drilling targets because they tend to preserve fracture porosity in the most highly cemented sandstones. However, geophysical well log approaches for identifying and mapping this cement type are hindered by lack of methods to quantify cement volume. Methods

based on borehole-imaging logs and combinations of acoustic and other logs (an application of data normally collected for stress profile logs) can identify thin, fracture-prone beds in quartz-cemented rocks. However, the current propensity of beds to fracture is only a useful indication of the likelihood of fracture occurrence if the diagenetic context of fracture development is known.

- Fracture porosity is mainly controlled by the diagenetic history of the rock; that is, timing of diagenesis relative to fracture opening. Diagenesis information can be used to predict the degree of natural fracture occlusion by cement. In the case of synkinematic cement, competition between fracturing and fracture sealing determines the porosity and connectivity of the intrafracture porosity network. Even sandstones that have virtually all of their matrix porosity occluded by synkinematic cement may retain substantial fracture porosity. An estimate of the probable degree of postkinematic mineral occlusion of fracture porosity can be obtained from study of the appropriate rock framework authigenic cement volume. High volumes of postkinematic cement in a bed may be an indication that fractures are occluded. Our results show that natural fractures in sandstones also have profiles rougher than those predicted from rock tests. These profiles are also generally rougher than assumed in modeling studies.
- A breakthrough technique that uses photomultiplier-based imaging of electron beam-induced luminescence (scanned CL) to detect quartz-filled microfractures in sandstones having synkinematic quartz cement permits fracture strikes to be mapped in areas of the wellbore where no macrofractures are present. Because small specimens can be used to get fracture strike with the scanned CL method, this approach can be applied to samples obtained from wireline-conveyed rotary sidewall coring devices, permitting more fracture-strike data to be collected at reduced cost. This report also describes the use of fractures in coal inclusions and those created in axial point-load tests as methods to acquire indirect evidence of macrofracture strike.

Verification: Field Examples

The descriptions presented earlier of fracture abundance, fracture porosity, and fracture strike in GRI and GRI-industry experimental wells confirm that the indirect approaches that we developed are useful for improving characterization of these critical fracture attributes. Applying the new diagenetic classification and microstructural data retrospectively to the GRI wells in these four formations provides field verification that these methods provide new and useful insights for fracture characterization.

Nevertheless, verification using wells and formations that were not part of the observational data base is desirable. Moreover, to fully test the ideas presented in this report, horizontal-well data are preferable to vertical-well data. Collecting such data was beyond the scope of this project, so we used publicly available information collected in Mesaverde Group sandstones as part of DOE's Multiwell Experiment in Colorado to test the applicability of our approach. This is a useful data set because descriptions and photomicrographs of mineralized fractures collected in vertical wells at the site have been published (Pittman and Sprunt, 1986). Subsequently, a near-horizontal (slant) well was cored in part of the formation (the SHCT experiment). One of us participated in core recovery for the slant well, and a description of some aspects of core fractures has been published (Lorenz and Finley, 1991). It was possible to apply our classification approach to these rocks by inspection of fracture photomicrographs and descriptions in Pittman and Sprunt (1986). Although useful to testing the classification applications of this study, these data sets do not include the comprehensive comparisons of rock-framework cement and fracture mineralogy that we recommend, nor do they use scanned CL microstructure analysis introduced in this report.

The geology of the Multiwell site has been described in detail elsewhere and is not repeated here. Dutton and others (1993) cite many of the relevant regional and local fracture and diagenesis descriptions. From inspection of information in Pittman and Sprunt (1986), we infer a fracture/diagenesis history for the fractured intervals they describe that is similar to that of the Ozona Canyon sandstones. However, we interpret the degree of synkinematic quartz cementation to be more advanced than that of the Ozona Canyon. It more nearly resembles the cementation/fracture microstructure of the upper Travis Peak Formation.

Our technique leads us to predict that the fracture stratigraphy of this part of the Mesaverde Group at the Multiwell site consists of beds having open, quartz-lined fractures that are concentrated where synkinematic quartz cement is prevalent. In beds having substantial postkinematic cement, fractures will be variably to completely filled with postkinematic carbonate cements. Beds that lack late carbonate cements are therefore prospective for containing open, quartz-lined fractures. The latter case is what was found in subhorizontal sandstone core from the SHCT well.

In this interval, open quartz-lined fractures are present. Elsewhere in the unit, beds having significant postkinematic carbonate cements also have completely filled fractures.

Well-placement and drilling-direction decisions at the Multiwell site were not based on predictions of where open fractures would exist. In fact, conventional core analysis provided no basis for predicting the location of open fractures despite data from three closely spaced, extensively cored vertical wells. Our interpretation of published observations and successful prediction of the drilling result are verification of the applicability of our approach to fracture porosity analysis. Our approach could be further tested by examining samples with scanned CL methods to verify that fracture drilling direction could have been successfully guided by sealed microfracture analysis.

Applying Results of This Study

The results of this study can be applied by operators to evaluate prospects for horizontal drilling in highly cemented sandstone formations. The results of this study should be relevant to parts of most tight gas sandstone plays. Data required to apply these results include samples of the formation sufficient to characterize cement sequence and microstructure. Such data can normally be acquired from sidewall or full-diameter core. If macrofractures are present, they should also be analyzed, but their presence is not required in order to evaluate beds for cement sequence or microfracture strike.

By using microstructures to evaluate the timing of fracturing, the proper categorization of cements relative to movement history can be carried out. The presence of a few macrofractures in core will greatly improve the reliability of this assessment. Cement volumes should then be compiled on a chart such as figure 5 in order to characterize volumes of pre-, syn-, and postkinematic cement. Results of this study suggest that areas having synkinematic quartz cement and slight or no overprint (low volume) of postkinematic cement will be most prospective for having open fractures. Such information can be used to predict areas where natural fractures are likely to be capable of transmitting fluid. Development drilling and reservoir simulation would be enhanced (fig. 157).

Scanned CL evidence taken from oriented core or sidewall cores in areas of dense synkinematic quartz cement can provide information on local fracture orientation that can guide choice of the direction to drill.

Implications

Low-matrix-permeability natural gas reservoirs in sandstones, generally defined as sandstone formations with in situ gas permeability values of 0.1 millidarcy or less, are important parts of the U.S. natural gas resource base, constituting about 27 percent (349 Tcf of 1,295 Tcf) of the technically recoverable lower 48 supply (National Petroleum Council, 1992). According to one recent projection, technologically advanced methods to access gas in these reservoirs will be required in the future in order to achieve desired production levels (Perry, 1994). Natural fractures are widespread in these reservoirs, and they may be responsible for local areas of high deliverability. Where natural fractures play a role in gas deliverability, lack of reliable methods to systematically map natural fracture strike, fracture porosity, and other fracture attributes has hindered efficient development of the resource through optimized well placement or directional drilling. As exploration and development increasingly moves into more technically challenging, diagenetically altered, deeper reservoirs where natural fractures are key to successful completions, low-cost, site-specific, accurate information on fracture attributes will be critical to reducing well costs and increasing well recoveries. Diagenesis information can greatly augment the usefulness of direct observations of fractures for exploration and development planning.

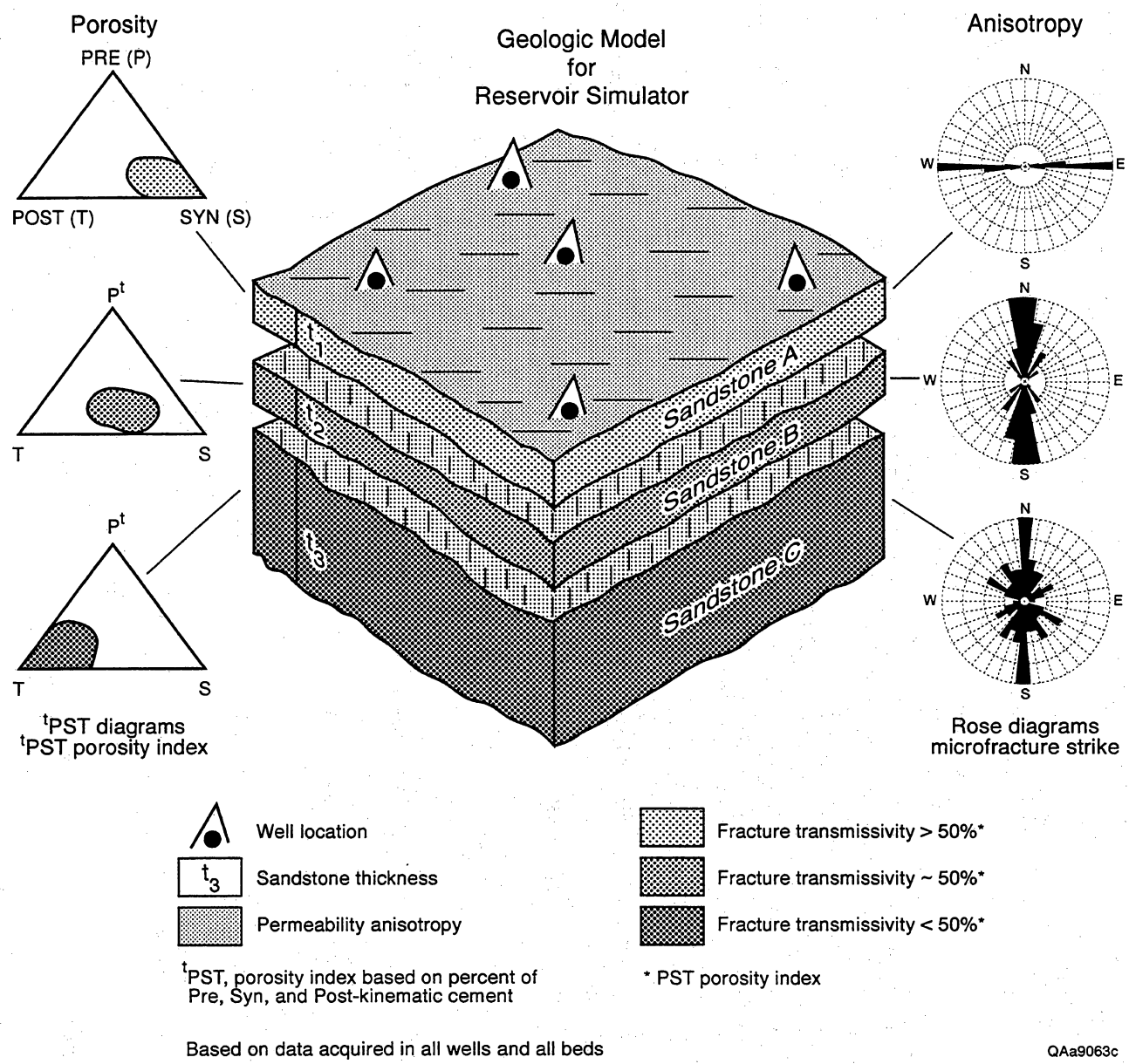

Figure 157. Conceptual geological model for input into reservoir simulator. Fracture transmissivity on a layer-by-layer basis and anisotropy are potentially estimated from observations of diagenetic textures (PST index) and microstructures.

Acknowledgments

This study was supported by the Gas Research Institute under contract number 5082-211-0708, John Hansen, Project Manager. We would like to acknowledge the companies and operators that supported this research by providing access to core. Much of the work reported here was carried out in collaboration with S. P. Dutton. The cooperation of K. L. Milliken in conducting CL analyses is greatly appreciated. P. P. Nelson, Department of Civil Engineering, The University of Texas at Austin, provided access to rock test laboratory facilities. J. Holder, Center for Earth Science and Engineering at UT-Austin, collaborated on point-load testing. D. D. Schultz-Ela, Bureau of Economic Geology, performed numerical modeling. L. Krystinik, B. Blakeney-DeJarnett, Union Pacific Resources, and J. Lorenz, Sandia National Laboratory, cooperated in Frontier Formation outcrop fracture studies. H. S. Hamlin and P. W. Dickerson, and research assistants Sabine Boardman, Barbara A. Marin, and Thomas E. Hoak aided in aspects of the research. We appreciate reviews of this report by J. Hansen, S. P. Dutton, and R. Tyler and editorial comments from Jeannette Miether and Amanda R. Masterson. Word processing and design were by Susan Lloyd. Figures were drafted by the Bureau's cartographic staff under the supervision of Richard L. Dillon and Joel L. Lardon. David M. Stephens provided text illustration photography.

References

Aguilera, R., 1980, Naturally fractured reservoirs: Tulsa, PennWell Books, 703 p.

Amadei, B., and Illangasekare, T., 1994, A mathematical model for flow and solute transport in non-homogeneous rock fractures: International Journal of Rock Mechanics and Mining Sciences and Geomechanics Abstracts, v. 31, no. 6, p. 719–731.

Baek, Hwanjo, and Laubach, S. E., 1994, Fracture mechanics property evaluation, Canyon Sandstone, *in* Geology of a stratigraphically complex natural gas play: Canyon sandstones, Val Verde Basin, southwest Texas: The University of Texas at Austin, Bureau of Economic Geology, topical report no. 94/0167 prepared for the Gas Research Institute, p. 95–114.

Baek, Hwanjo, Laubach, S. E., and Nelson, P. P., 1994, Fracture toughness and crack morphology of a variably cemented sandstone, *in* 1994 Society for Experimental Mechanics Spring Conference and Exhibits, p. 153–158.

Bahat, D., 1991, Tectonofractography: Berlin, Springer-Verlag, 354 p.

Barton, N., and Choubey, V., 1977, The shear strength of rock joints in theory and practice: Rock Engineering, v. 10, no. 1, p. 1–54.

Baumgardner, R. W., Jr., 1991, Comparative lineament analysis of the San Juan Basin: relationships between lineament attributes and coalbed methane production, *in* Ayers, W. B., Jr., Kaiser, W. R., Laubach, S. E., and others, Geologic and hydrologic controls on the occurrence and producibility of coalbed methane, Fruitland Formation, San Juan Basin: The University of Texas at Austin, Bureau of Economic Geology, topical report prepared for Gas Research Institute under contract no. 5087-214-1544, p. 153–179.

Baumgardner, R. W., Jr., Tye, R. S., Laubach, S. E., Diggs, T. N., Herrington, K. L., and Dutton, S. P., 1988, Site selection for GRI cooperative tight gas field research, volume II: geologic characteristics of selected low-permeability gas sandstones: topical report No. GRI-88/0180 prepared for the Gas Research Institute under contract no. 5082-211-0708, 194 p. plus appendix.

Bentz, L. M., 1992, Pecos Slope field, U.S.A.: Permian Basin, New Mexico, *in* Foster, N. H., and Beaumont, E. A., compilers, Stratigraphic traps III: American Association of Petroleum Geologists, Treatise of Petroleum Geology, p. 129–153.

Bieniawski, A. T., and Hawkes, I., 1978, Suggested method for determining tensile strength of rock materials: International Journal of Rock Mechanics and Mining Sciences and Geomechanical Abstracts, v. 15, no. 3, p. 99–103.

Birch, F., 1961, The velocity of compressional waves in rocks to 10 kilobars, Part 2: Journal of Geophysical Research, v. 66, p. 2199–2444.

Bodnar, R. J., and Bethke, P. M., 1984, Systematics of stretching of fluid inclusions 1: Fluorite and

sphalerite at 1 atmosphere confining pressure: Economic Geology, v. 79, p. 141–161.

Bodnar, R. J., Binns, P. R., and Hall, D. L., 1989, Synthetic fluid inclusions-VI. Quantitative evaluation of the decrepitation behavior of fluid inclusions in quartz at one atmosphere confining pressure: Journal of Metamorphic Geology, v. 7, p. 229–242.

Branagan, P. T., 1992, Current status and flow test procedures for SHCT-1: CER Corporation memorandum to distribution, January 16, 1992. (Addendum of January 24, 1992.)

Brashear, W. W., 1961, Lips field, *in* Wagner, C. R., and others, eds., Oil and gas fields of the Texas and Oklahoma Panhandles: Panhandle Geological Society, p. 181–183.

Broadhead, R. F., 1984, Stratigraphically controlled gas production from Abo red beds (Permian), east-central New Mexico: New Mexico Bureau of Mines and Mineral Resources, Circular 183, 36 p.

Broch, E., and Franklin, J. A., 1972, The point-load strength test: International Journal of Rock Mechanics, Mineral Science, v. 9, p. 669–697.

Brown, C. A., Smagala, T. M., and Haefele, G. R., 1986, Southern Piceance Basin model—Cozzette, Corcoran, and Rollins sandstones, *in* Spencer, C. W., and Mast, R. F., eds., Geology of tight gas reservoirs: American Association of Petroleum Geologists Studies in Geology No. 24, p. 207–219.

Brown, S. R., and Scholz, C. H., 1985, Broad bandwidth study of the topography of natural rock surfaces: Journal of Geophysical Research, v. 90, p. 12,575–12,582.

Burley, S. D., Mullis, J., and Matter, A., 1989, Timing diagenesis in the Tartan reservoir (UK North Sea): constraints from combined cathodoluminescence microscopy and fluid inclusion studies: Marine & Petroleum Geology, v. 6, p. 98–102.

CER Corporation, 1991a, Summary of open-hole data acquisition and field operations, S. A. Holditch & Associates SFE No. 4-24: topical report prepared for Gas Research Institute, unpaginated.

_____ 1991b, Summary of open-hole data acquisition and field operations, Maxus H. T. Glasgow No. 2: unnumbered topical report prepared for the Gas Research Institute under contract no. 5091-221-2130, variously paginated.

_____ 1991c, Summary of open-hole data acquisition and field operations, Phillips Ward C-11: unnumbered topical report prepared for the Gas Research Institute under contract no. 5091-221-2130, variously paginated.

CER Corporation, and S. A. Holditch & Associates, 1988, Staged Field Experiment No. 1: advancements in Travis Peak formation evaluation and hydraulic fracture technology: Gas Research Institute report no. GRI-88/0077, 223 p.

_____ 1989, Staged Field Experiment No. 2: application of advanced geological, petrophysical and engineering technologies to evaluate and improve gas recovery from low-permeability sandstone reservoirs; v. 1: report no. GRI-89/0140, 178 p.

_____ 1991, Staged Field Experiment No. 3: application of advanced technologies in tight gas sandstones—Travis Peak and Cotton Valley Formations, Waskom Field, Harrison County, Texas: Gas Research Institute report no. GRI-91/0048, 253 p.

Cheung, P. S. Y., 1984, Fracture detection using the sonic toll: Proceedings, 8th International Symposium of Société pour l'avancement de l'interprétation des diagraphies: Paris.

Clift, S. J., Laubach, S. E., and Holder, Jon, 1992, Strength anisotropy in low-permeability sandstone gas reservoirs: application of the axial point-load test: Gulf Coast Association of Geological Societies Transactions, v. 42, p. 61–72.

Collins, E. W., Hovorka, S. D., and Laubach, S. E., 1992, Fracture systems of the Austin Chalk, North-Central Texas, *in* Schmoker, J. W., Coalson, E. B., and Brown, C. A., eds., Geological aspects of horizontal drilling: Rocky Mountain Association of Geologists, p. 75–88.

Collins, E. W., Laubach, S. E., Dutton, S. P., and Hill, R. E., 1992, Depositional environments, petrology, and fractures of the Atoka Davis sandstone: a low-permeability, gas-bearing sandstone of the Fort Worth Basin, North-Central Texas, *in* Cromwell, D. W., Moussa, M. T., and Mazzullo, L. J., eds., Southwest Section, American Association of Petroleum Geologists, Publication SWS 92-90, p. 221–230.

Collins, P. L. F., 1979, Gas hydrates in CO_2-bearing fluid inclusions and use of freezing data for estimation of salinity: Economic Geology, v. 74, p. 1435–1444.

Corbett, K. P., Friedman, M., and Spang, J., 1987, Fracture development in mechanical stratigraphy of Austin Chalk, Texas: American Association of Petroleum Geologists Bulletin, v. 71, p. 17–28.

Cornell, F. L., 1991, Engineering improvements for Red Fork fracturing: Journal of Petroleum Technology, February, p. 132–137.

Craddock, D. L., Goza, B. T., and Bishop, J. C., 1983, A case history—fracturing the Morrow in southern Blaine and western Canadian Counties, Oklahoma, *in* Proceedings, 1983 Society of Petroleum Engineers Production Operation Symposium, SPE Paper No. 11567, p. 197–202.

Currie, J. B., 1974, Study examines fracture porosity and permeability in stratigraphic traps: Oil and Gas Journal, June 24, p. 178–181.

David, C., Bernabe, Y., and den Brok, B., 1994, Compaction, strength, and the amount of cement in hot-pressed quartz samples: preliminary experimental results (abs.): Eos, v. 75, p. 593.

Dickenson, R. G., 1992, Table Rock field-Frontier Formation, an overpressured reservoir, *in* Mullen, C. E., ed., Rediscover the Rockies: Wyoming Geological Association Guidebook, p. 139–144.

DuChene, H. R., 1989, Fracture reservoirs in the San Juan Basin, Colorado and New Mexico, *in* Lorenz, J. C., and Lucas, S. G., eds., Energy frontiers in the Rockies: Albuquerque Geological Society, p. 101–109.

Dula, W. F., 1981, Correlation between deformation lamellae, microfractures, macrofractures, and in situ stress measurements, White River uplift, Colorado: Geological Society of America Bulletin, v. 92, p. 37–46.

Dunn, D. E., LaFountain, L. J., and Jackson, R. E., 1973, Porosity dependence and mechanism of brittle fracture in sandstones: Journal of Geophysical Research, v. 78, p. 2403.

Dutton, S. P., 1994, Influence of provenance and burial history on diagenesis of Upper Cretaceous Frontier formation sandstones, Green River Basin, Wyoming: Journal of Sedimentary Petrology, v. 63, no. 4, p. 271–284.

Dutton, S. P., Clift, S. J., Hamilton, D. S., Hamlin, H. S., Howard, W. E., Akhter, M. S., and Laubach, S. E., 1993, Major low-permeability-sandstone gas reservoirs in the continental United States: The University of Texas at Austin, Bureau of Economic Geology Report of Investigations No. 211, 221 p.

_____ 1990, History of quartz cementation in the Lower Cretaceous Travis Peak Formation, East Texas: Journal of Sedimentary Petrology, v. 60, no. 2, p. 191–202.

_____ 1992, Evolution of porosity and permeability in the Lower Cretaceous Travis Peak formation, East Texas: American Association of Petroleum Geologists Bulletin, v. 76, no. 2, p. 252–269.

Dutton, S. P., Hamlin, H. S., and Laubach, S. E., 1992, Geologic controls on reservoir properties of low-permeability sandstone, Frontier Formation, Moxa Arch, Southwest Wyoming: The University of Texas at Austin, Bureau of Economic Geology, report no. GRI-92/0127 prepared for the Gas Research Institute, 199 p.

_____ in press, Geologic controls on reservoir properties of low-permeability sandstone, Frontier Formation, Moxa Arch, southwestern Wyoming: The University of Texas at Austin, Bureau of Economic Geology.

Dutton, S. P., and Land, L. S., 1988, Cementation and burial history of a low-permeability quartzarenite, Lower Cretaceous Travis Peak Formation, East Texas: Geological Society of America Bulletin, v. 100, p. 1271–1282.

Dutton, S. P., and Laubach, S. E., 1993, Comprehensive geologic basin analysis: application of a generic research approach to several tight gas sandstone formations: In Focus—Tight Gas Sands, v. 9, no. 1, p. 1–33.

Dutton, S. P., Laubach, S. E., Tye, R. S., Baumgardner, R. W., Jr., and Herrington, K. L., 1991a, Geologic characterization of low-permeability gas reservoirs, Travis Peak Formation, East Texas: The University of Texas at Austin, Bureau of Economic Geology Report of Investigations No. 204, 89 p.

Dutton, S. P., Laubach, S. E., Tye, R. S., Herrington, K. L., and Diggs, T. N., 1991b, Geological analysis of the Travis Peak Formation and Cotton Valley Sandstone, *in* Peterson, R. E., ed., Staged Field Experiment No. 3: application of advanced technologies in tight gas sandstones—Travis Peak and Cotton Valley Formations, Waskom Field, Harrison County, Texas: CER Corporation and S. A. Holditch & Associates, Inc., topical report no. GRI-91/0048 prepared for the Gas Research Institute, 253 p.

Dyer, J. R., 1983, Jointing in sandstones, Arches National Park, Utah: Stanford University, Ph.D. dissertation, 202 p.

Dyke, Chris, 1992, How sensitive is natural fracture permeability at depth to variation in effective stress?: conference preprints, Fractured and Jointed Rock Masses Symposium, p. 88–95.

Ekstrom, M. P., Dahan, C. A., Chen, Min-Yi, Lloyd, P. M., and Rossi, D. J., 1986, Formation imaging with microelectrical scanning arrays: Society of Professional Well Log Analysts, 27th Annual Logging Symposium Transactions, p. 1–21.

Engelder, Terry, 1982, Is there a genetic relationship between selected regional joints and contemporary stress within the lithosphere of North America?: Tectonics, v. 1, p. 161–177.

_____ 1985, Loading paths to joint propagation during a tectonic cycle: an example from the Appalachian Plateau, U.S.A.: Journal of Structural Geology, v. 7, no. 3/4, p. 459–476.

Fertl, W. H., 1990, Circumferential acoustic logs detect natural fractures and determine their orientation, *in* Hurst, A., Lovell, M. A., and Morton, A. C., eds., Geological applications of wireline logs: Geological Society of London Special Publication No. 48, p. 255–262.

Finley, R. J., 1984, Geology and engineering characteristics of selected low-permeability gas sandstones: a national survey: The University of Texas at Austin, Bureau of Economic Geology Report of Investigations No. 138, 220 p.

Finley, R. J., Laubach, S. E., Tyler, Noel, and Holtz, M. H., 1990, Opportunities for horizontal drilling in Texas: The University of Texas at Austin, Bureau of Economic Geology Geological Circular 90-2, 32 p.

Frantz, J. H., Jr., Hopkins, C. S., and Lancaster, D. E., 1993, Reservoir and stimulation evaluation of the Berea Sandstone Formation in Pike County, Kentucky: Society of Petroleum Engineers 1993 Joint Rocky Mountain Regional Meeting and Low-Permeability Reservoirs Symposium, SPE Paper No. 25896, p. 533–542.

Friedman, M., and Bur, T. R., 1974, Investigations of the relations among residual strain, fabric, fracture, and ultrasonic attenuation and velocity in rocks: International Journal of Rock Mechanics and Mining Sciences and Geomechanics Abstracts, v. 11, p. 221–234.

Friedman, M., and Logan, J. M., 1970, Influence of residual elastic strain on the orientation of experimental fractures in three quartzose sandstones: Journal of Geophysical Research, v. 75, p. 387–405.

Friedman, I., and O'Neil, J. R., 1977, Compilation of stable isotope fractionation factors of geochemical interest, *in* Fleischer, M., ed., Data of geochemistry: U.S. Geological Survey Professional Paper 440-KK, 12 p.

Gallagher, J. J., 1976, Fracturing of quartz sand grains: Proceedings, 17th U.S. Symposium on Rock Mechanics, Site Characterization, Snowbird, Utah, p. 2A41–2A48.

Gas Research Institute, 1992, Developing in-situ stress profiles: GRI Technical Summary, 8 p.

Goldstein, R. H., 1986, Reequilibration of fluid inclusions in low-temperature calcium-carbonate cement: Geology, v. 14, p. 792–795.

Gorham, F. D., Jr., Woodward, L. A., Callender, J. R., and Greer, A. R., 1979, Fractures in Cretaceous rocks from selected areas of San Juan Basin, New Mexico: exploration implications: American Association of Petroleum Geologists Bulletin, v. 63, p. 598–607.

Grady, D. E., and Kipp, M. E., 1987, Dynamic rock fragmentation, *in* Atkinson, B. E., ed., Fracture mechanics of rock: New York, Academic Press, 534 p.

Gudmundsson, Agust, 1983, Form and dimensions of dykes in eastern Iceland: Tectonophysics, v. 95, p. 295–307.

Hamlin, H. S., Clift, S. J., and Dutton, S. P., 1992, Stratigraphy and diagenesis of Sonora Canyon deep-water sandstones, Val Verde Basin, southwest Texas: American Association of Petroleum Geologists, Southwest Section Transactions, p. 209–220.

Hamlin, H. S., Clift, S. J., Dutton, S. P., Hentz, T. F., and Laubach, S. E., in press, Geologically complex gas reservoirs in slope and basin facies, Sonora and Ozona Canyon sandstones, Val Verde Basin, southwest Texas: The University of Texas at Austin, Bureau of Economic Geology.

Hanor, J. S., 1980, Dissolved methane in sedimentary brines: potential effect on the PVT properties of fluid inclusions: Economic Geology, v. 75, p. 603–609.

Hansen, J., 1993, Results of the Greater Green River basin natural gas technology workshop: In Focus, v. 9, no. 1, p. 37–38.

Helgeson, D. E., 1990, Characteristics of joint propagation in layered sedimentary rocks: The Rock Fracture Project Workshop, v. 1, p. F1–F5.

Henke, K. A., 1982, Origin of the late Paleocene–early Eocene Wilcox sandstones, Lobo trend, Webb and Zapata Counties, Texas: Texas A&M University, Master's thesis, 198 p.

_____ 1985, Reservoir characteristics of Lower Wilcox sandstones, Lobo trend, Webb and Zapata Counties (abs.): American Association of Petroleum Geologists Bulletin, v. 69, p. 265.

Hentz, T. F., 1992, Low-permeability, gas-bearing Cleveland formation (Upper Pennsylvanian), western Anadarko Basin: structure, paleoenvironments, and paleotectonic control on depositional patterns, *in* Cromwell, D. W., Moussa, M. R., and Mazzullo, L. J., eds., American Association of Petroleum Geologists, Southwest Section, Publication SWS 92-90, p. 231–252.

Higley, D. K., and Schmoker, J. W., 1989, Influence of depositional environment and diagenesis on regional porosity trends in the Lower Cretaceous "J" sandstone, Denver Basin, Colorado, *in* Coalson, E. B., ed., Petrogenesis and petrophysics of selected sandstone reservoirs of the Rocky Mountain region: Rocky Mountain Association of Geologists, p. 183–196.

Hills, J. M., and Galley, J. E., 1988, The Permian Basin region, general introduction, *in* Sloss, L. L., ed., Sedimentary cover–North American Craton: U.S. Geological Survey, Geology of North America, v. D-2, p. 261–267.

Hobbs, D. W., 1967, Formation of tension joints in sedimentary rocks: an explanation: Geological Magazine, v. 104, p. 550–556.

Hodgson, R. A., 1961, Regional study of jointing in Comb Ridge-Navajo Mountain Area, Arizona and Utah: American Association of Petroleum Geologists Bulletin, v. 45, no. 1, p. 1–38.

Hoshino, K., 1974, Effect of porosity on the strength of the clastic sedimentary rocks, *in* Advances in Rock Mechanics, Proceedings, 3rd International Society

for Rock Mechanics: Denver, Colorado, v. II, part A, p. 511–516.

Hower, T. L., 1990, Using depletion ratios to select and evaluate drilling locations in naturally fractured gas reservoirs: Society of Petroleum Engineers 65th Annual Technical Conference and Exhibition, p. 429–437.

Humphreys, B., and Lott, G. K., 1990, An investigation into nuclear log responses of North Sea Jurassic sandstones using mineralogical analysis, *in* Hurst, A., Lovell, M. A., and Morton, A. C., eds., Geological applications of wireline logs: Geological Society of London Special Publication No. 48, p. 223–240.

Hyman, L. A., Malek, D. J., Admire, C. A., and Walls, J. D., 1991, The effects of microfractures on directional permeability in tight gas sands: SPE/DOE Low-Permeability Reservoir Symposium, Denver, SPE Paper No. 21878, unpaginated.

International Society for Rock Mechanics (ISRM), 1981, The quantitative description of discontinuities in rock masses, *in* Brown, E. T., ed., Rock characterization testing and monitoring: ISRM suggested methods: New York, Pergamon Press, 211 p.

Jizba, D., and Nur, A., 1990, Static and dynamic moduli of tight gas sandstones and their relation to formation properties: topical report prepared for Gas Research Institute under contract no. 5089-211-1842.

Kimminau, S., 1994, Traceability—making decisions with uncertain data: The Log Analyst, v. 35, no. 5, p. 67–70.

Knipe, R., 1992, Faulting processes and fault seal, *in* Larsen, R. M., Brekke, H., Larsen, B. T., and Talleraas, E., eds., Structural and tectonic modelling and its application to petroleum geology: Amsterdam, Elsevier, NPF (Norwegian Petroleum Society) Special Publication 1, p. 325–342.

Kowallis, B. J., Wang, H. F., and Jang, B. A., 1987, Healed microcrack orientations in granite from Illinois borehole UPH-e and their relationship to the rock's stress history: Tectonophysics, v. 135, p. 297–306.

Kraig, D. H., Wiltschko, D. V., and Spang, J. H., 1987, Interaction of basement uplift and thin-skinned thrusting, Moxa Arch and Western Overthrust Belt, Wyoming: a hypothesis: Geological Society of America Bulletin, v. 99, p. 654–662.

Kulander, B. R., Dean, S. L., and Ward, B. J., Jr., 1990, Fractured core analysis: American Association of Petroleum Geologists, Methods in Exploration No. 8, 88 p.

Lacy, S. L., Ding, W. Z., and Joshi, S. D., 1992, Perspectives on horizontal wells in the Rocky Mountain region: Conference abstracts, Horizontal drilling symposium-domestic and international case studies: Rocky Mountain Association of Geologists, unpaginated.

Ladiera, F. L., and Price, N. J., 1981, Relationship between fracture spacing and bed thickness: Journal of Structural Geology, v. 3, no. 2, p. 179–183.

Lajtai, E. Z., and Alison, J. R., 1979, A study of residual stress effects in sandstone: Canadian Journal of Earth Sciences, v. 16, p. 1547–1557.

Lam, T. S. K., and Johnston, I. W., 1985, A scanning device to quantify joint surface roughness: Geotechnical Testing Journal, GTJODJ, v. 8, no. 3, p. 117–124.

Landes, K. K., 1970, Petroleum geology of the United States: New York, Wiley, 571 p.

Laubach, S. E., 1987, Mapping subsurface fracture trends (abs.): Eos, v. 68, no. 16, p. 299.

_____ 1988a, Fractures generated during folding of the Palmerton Sandstone, eastern Pennsylvania: Journal of Geology, v. 96, no. 4, p. 495–503.

_____ 1988b, Subsurface fractures and their relationship to stress history in East Texas Basin sandstone: Tectonophysics, v. 156, p. 37–49.

_____ 1989a, Paleostress directions from the preferred orientation of closed microfractures (fluid-inclusion planes) in sandstone, East Texas basin, U.S.A.: Journal of Structural Geology, v. 11, no. 5, p. 603–611.

_____ 1989b, Fracture analysis of the Travis Peak Formation, western flank of the Sabine Arch, East Texas: The University of Texas at Austin, Bureau of Economic Geology Report of Investigations No. 185, 55 p.

_____ 1991, Fracture patterns in low-permeability-sandstone gas reservoir rocks in the Rocky Mountain Region: SPE Paper 21853, SPE/DOE Rocky Mountain Regional Meeting/Low-Permeability Reservoir Symposium, Denver, p. 501–510.

_____ 1992a, Attributes of fracture networks in selected Cretaceous sandstones of the Green River and San Juan Basins, *in* Schmoker, J. W., Coalson, E. B., and Brown, C. A., eds., Geological studies relevant to horizontal drilling: examples from western North America: Rocky Mountain Association of Geologists, p. 61–74.

_____ 1992b, Advancements in hydraulic azimuth research, Green River Basin, Wyoming: In Focus—Tight Gas Sands, v. 8, no. 2, p. 12–22.

_____ 1992c, Fracture networks in selected Cretaceous sandstones of the Green River and San Juan Basins, Wyoming, New Mexico, and Colorado, *in* Schmoker, J. W., Coalson, E. B., and Brown, C. A., eds., Geological studies relevant to horizontal drilling: examples from western North America: Rocky Mountain Association of Geologists, p. 61–73.

Laubach, S. E., and Boardman, S. C., 1989, Multiple generations of fluid inclusions in Cretaceous quartz veins from the Gulf of Mexico basin (abs.): Geological Society of America, Abstracts with Programs, v. 21, no. 6, p. 64.

Laubach, S. E., and Jackson, M. L. W., 1990, Origin of arches in the northwestern Gulf of Mexico basin: Geology, v. 18, p. 595–598.

Laubach, S. E., and Lorenz, J. C., 1992, Preliminary assessment of natural fracture patterns in Frontier Formation sandstones, southwestern Wyoming: Wyoming Geological Association Guidebook, v. 48, p. 87–96.

Laubach, S. E., and Marin, B. A., 1992, Opportunities for horizontal drilling in fractured low-permeability sandstones, United States (abs.), *in* Horizontal Drilling Symposium: domestic and international case studies: Rocky Mountain Association of Geologists, unpaginated.

Laubach, S. E., and Monson, E. R., 1988, Coring-induced fractures: indicators of hydraulic fracture propagation direction in a naturally fractured reservoir, *in* Proceedings, 1988 Society of Petroleum Engineers Annual Technical Conference, SPE Paper No. 18164, p. 587–596.

Laubach, S. E., and Tremain, C. M., 1991, Regional coal fracture patterns and coalbed methane development: 32nd U.S. Symposium on Rock Mechanics: Rotterdam, Balkema, p. 851–861.

_____ 1994, Fracture swarms: potential targets for methane exploration in Upper Cretaceous sandstone and coal, northern San Juan Basin, Colorado, *in* Ayers, W. B., Jr., and Kaiser, W. R., eds., Coalbed methane in the Upper Cretaceous Fruitland Formation, San Juan Basin, New Mexico and Colorado: New Mexico Bureau of Mines and Mineral Resources Bulletin 146, p. 103–118.

Laubach, S. E., Clift, S. J., Hamlin, H. S., Dutton, S. P., Hentz, T. F., Baek, Hwanjo, and Marin, B. A., 1994, Geology of a stratigraphically complex natural gas play: Canyon Sandstones, Val Verde Basin, southwest Texas: The University of Texas at Austin, Bureau of Economic Geology, topical report prepared for the Gas Research Institute under contract no. 5082-211-0708, 135 p.

Laubach, S. E., Clift, S. J., Hill, R. E., and Fix, J. E., 1992a, Stress directions in Cretaceous Frontier Formation, Green River Basin, Wyoming: Wyoming Geological Association Guidebook, v. 48, p. 75–86.

Laubach, S. E., Hamlin, H. S., Buehring, R. L., Baumgardner, R. W., Jr., and Monson, E. R., 1990, Application of borehole-imaging logs to geologic analysis, Cotton Valley Group and Travis Peak Formation, GRI staged field experiment wells, East Texas: The University of Texas at Austin, Bureau of Economic Geology, topical report no. GRI-90/0222 prepared for the Gas Research Institute, 115 p.

Laubach, S. E., Mace, R. E., and Nance, H. S., 1995, Fault and joint swarms in a normal fault zone, *in* Rossmanith, H. P., ed., Mechanics of jointed and faulted rock; Proceedings of the International Conference on Mechanics of Jointed and Faulted Rock: Vienna, Austria, p. 331–336.

Laubach, S. E., Tremain, C. M., and Baumgardner, R. W., Jr., 1991, Fracture swarms in Upper Cretaceous sandstone and coal, northern San Juan Basin, Colorado: Potential targets for methane exploration, *in* Ayers, W. B., Jr., and others, Geologic and hydrologic controls on the occurrence and producibility of coalbed methane, Fruitland Formation, San Juan Basin: The University of Texas at Austin, Bureau of Economic Geology, topical report prepared for Gas Research Institute under contract no. 5087-214-1544, p. 199–140.

Laubach, S. E., Tyler, Roger, Ambrose, W. A., Tremain, C. M., and Grout, M. A., 1992b, Preliminary map of fracture patterns in coal in the western United States: Wyoming Geological Association Guidebook, v. 48, p. 253–267.

Laubach, S. E., Tyler, Roger, Schultz-Ela, D. D., and Tremain, C. M., 1994, Tectonic analysis of weakly deformed foreland areas: implications for improved coalbed methane and tight gas sandstone production (abs.): American Association of Petroleum Geologists national convention Abstracts, v. 3, p. 194.

Laubach, S. E., Vendeville, B. C., and Reynolds, S. J., 1992c, Patterns in the development of extensional fault-block shapes from comparison of outcrop-scale faults and experimental physical models, *in* Larsen, R. M., Brekke, H., Larsen, B. T., and Talleraas, E., eds., Structural and tectonic modelling and its application to petroleum geology: Amsterdam, Elsevier, NPF (Norwegian Petroleum Society) Special Publication 1, p. 231–241.

Laughrey, C. D., 1984, Petrology and reservoir characteristics of the Lower Silurian Medina Group reservoir sandstones, Athens and Geneva fields, northwestern Pennsylvania: Pennsylvania Geological Survey, 4th series, Mineral Resource Report 85, 126 p.

Laughrey, C. D., and Harper, J. A., 1986, Comparisons of Upper Devonian and Lower Silurian tight formations in Pennsylvania—geological and engineering characteristics: topical report prepared for Gas Research Institute under contract no. 5087-214-1544, p. 153–179.

Lawn, B. R., and Wilshaw, T. R., 1975, Fracture of brittle solids: Cambridge, Cambridge University Press, 523 p.

Lehne, K. A., 1990, Fracture detection from logs of North Sea chalk, *in* Hurst, A., Lovell, M. A., and Morton, A. C., eds., Geological applications of wireline logs: Geological Society of London Special Publication No. 48, p. 263–271.

Lemmlein, G. C., and Kliya, M. O., 1960, Distinctive features of the healing of a crack in a crystal under conditions of declining temperature: International Geological Review, v. 2, p. 125–128.

Lorenz, J. C., 1987, Reservoir sedimentology in Mesaverde rocks at the multi-well experiment site and east central Piceance Creek basin: Sandia National Laboratories report SAND87-0040, 40 p.

Lorenz, J. C., and Finley, S. J., 1991, Regional fractures II: fracturing of Mesaverde reservoirs in the Piceance Basin, Colorado: American Association of Petroleum Geologists Bulletin, v. 75, no. 11, p. 1738–1757.

Lorenz, J. C., and Hill, R. E., 1991, Subsurface fracture spacing: comparison of inferences from slant/horizontal core and vertical core in Mesaverde reservoirs: Proceedings, Joint SPE Rocky Mountain Regional Meeting/Low-Permeability Reservoir Symposium, SPE Paper No. 21877, p. 705–716.

_____ 1992, Measurement and analysis of fractures in core, *in* Schmoker, J. W., Coalson, E. B., and Brown, C. A., eds., Geological studies relevant to horizontal drilling: examples from Western North America: Rocky Mountain Association of Geologists, p. 47–59.

Lorenz, J. C., and Laubach, S. E., 1994, Description and interpretation of natural fracture patterns in sandstones of the Frontier Formation along the Hogsback, southwestern Wyoming: Sandia National Laboratory topical report prepared for the Gas Research Institute under contract no. SAND94-0153, 86 p.

Mallory, W. W., 1977, Fractured shale hydrocarbon reservoirs in southern Rocky Mountain basins, *in* Veal, H. K., ed., Exploration frontiers of the central and southern Rockies: Rocky Mountain Association of Geologists, p. 89–94.

Marin, B. A., Clift, S. J., Hamlin, H. S., and Laubach, S. E., 1993, Natural fractures in Sonora Canyon sandstones, Sonora and Sawyer fields, Sutton County, Texas: Society of Petroleum Engineers 1993 Joint Rocky Mountain Regional Meeting and Low-Permeability Reservoirs Symposium, SPE Paper No. 25895, p. 523–531.

Marshall, D. J., 1988, Cathodoluminescence of geological materials: Winchester, Massachusetts, Allen and Unwin, Inc., 146 p.

Mathieu, G., Yver, J., Cheung, P., Brie, A., Hornby, B., and Hsu, K., 1985, Applying sonic data: fracture detection: The Technical Review, v. 33, p. 69–79.

McQuillan, H., 1973, Small-scale fracture density in Asmari Formation of southwest Iran and its relation to bed thickness and structural setting: American Association of Petroleum Geologists Bulletin, v. 47, no. 12, p. 2367–2385.

McWilliams, J. R., 1966, The role of microstructure in the physical properties of rock: American Society of Mechanical Engineers (ASTM) Special Technical Publication STP 402, p. 175–189.

McWilliams, P. C., Kerkering, J. C., and Miller, S. M., 1990, Fractal characterization of rock fracture toughness for estimating shear strength, *in* Rossmanith, H. P., ed., Mechanics of jointed and faulted rock; Proceedings of the International Conference on Mechanics of Jointed and Faulted Rock: Vienna, Austria, p. 331–336.

Meckel, L. D., Jr., Smith, D. G., and Wells, L. A., 1992, Ouachita foredeep basins: regional paleogeography and habitat of hydrocarbons, *in* Macqueen, R. W., and Leckie, D. A., eds., Foreland basins and fold belts: American Association of Petroleum Geologists Memoir no. 55, p. 427–444.

Merewether, E. A., Blackmon, P. D., and Webb, J. C., 1984, The mid-Cretaceous Frontier Formation near the Moxa Arch, southwestern Wyoming: U.S. Geological Survey Professional Paper 1290, 29 p.

Middlebrook, M. L., Branagan, P. T., Hill, R. E., Kukal, G. C., Peterson, R. E., McDonald, T. S., and Aslakson, J. K., 1993, Reservoir evaluation and completion results from a horizontal well in the Mancos B, Douglas Creek Arch, Northwest Colorado, *in* Proceedings, 1993 Society of Petroleum Engineers Joint Rocky Mountain Regional Meeting and Low-Permeability Reservoir Symposium, SPE Paper No. 25924, p. 767–780.

Miller, W. K., Peterson, R. E., Stevens, J. E., Lackey, C. B., and Harrison, C. W., 1991, In-situ stress profiling and prediction of hydraulic fracture azimuth for the Canyon sands formation, Sonora and Sawyer fields, Sutton County, Texas, *in* Proceedings, 1993 Society of Petroleum Engineers Joint Rocky Mountain Regional Meeting and Low-Permeability Reservoir Symposium, SPE Paper No. 21848, p. 445–456.

Milliken, K. L., 1994, The widespread occurrence of healed microfractures in siliciclastic rocks: evidence from scanned cathodoluminescence imaging, *in* Nelson, P. P., and Laubach, S. E., eds., Rock mechanics: models and measurements, challenges from industry: Rotterdam, Balkema, p. 825–832.

Milliken, K. L., and Dickenson, W. W., 1994, Generation of apparent pressure solution fabrics by a brittle mechanism in quartz-rich sandstones (abs.):

Geological Society of America, Abstracts with Programs, v. 26, p. A-318.

Millison, C., 1962, Accumulation of oil and gas in northwestern Colorado controlled principally by stratigraphic variations, *in* Amuedo, C. L., and Mott, M. R., eds., Exploration for oil and gas in northwestern Colorado: Rocky Mountain Association of Geologists, p. 41–48.

Moore, C. H., 1983, The upper Smackover of the Gulf rim: depositional systems, diagenesis, porosity evolution, and hydrocarbon production: Louisiana State University, Applied Carbonate Research Program, Technical Series Contribution 12, 41 p.

Morrow, N. R., Brower, K. R., Shoxiang, M., and Buckley, J. S., 1990, Fluid flow in healed tectonic fractures: Journal of Petroleum Technology, v. 42, p. 1310–1318.

Moslow, T. F., and Tillman, R. W., 1986, Sedimentary facies and reservoir characteristics of Frontier Formation sandstones, southwestern Wyoming, *in* Spencer, C. W., and Mast, R. F., eds., Geology of tight gas reservoirs: American Association of Petroleum Geologists Studies in Geology No. 24, p. 271–295.

Multer, H. G., 1963, Geology of the Silurian producing zones in the Moreland Oil Pool, Wayne County, Northeast Ohio: Ohio Geological Survey Report of Investigations, v. 47, p. 1–42.

Myal, F. R., and Frohne, K. H., 1991, Slant-hole completion test in the Piceance Basin, Colorado: Rocky Mountain Regional/Low-Permeability Reservoir Symposium, SPE Paper No. 21866, p. 611–622.

_____ 1992, Drilling and early testing of a sidetrack from the Slant Hole Completion Test well—a case study of gas recovery research in Colorado's Piceance Basin: Society of Petroleum Engineers, SPE Paper No. 24382, p. 201–209.

Myers, R. C., 1977, Stratigraphy of the Frontier Formation (Upper Cretaceous), Kemmerer area, Lincoln County, Wyoming: Wyoming Geological Association 29th annual field conference guidebook, p. 271–311.

Nance, H. S., Laubach, S. E., and Dutton, A. R., 1994, Fault and joint measurements in Austin Chalk, Superconducting Super Collider Site: Gulf Coast Association of Geological Societies Transactions, v. 44, p. 521–532.

Narr, W., 1991, Fracture density in the deep subsurface: techniques with application to Point Arguello oil field: American Association of Petroleum Geologists Bulletin, v. 75, no. 8, p. 1300–1323.

Narr, W., and Suppe, J., 1991, Joint spacing in sedimentary rocks: Journal of Structural Geology, v. 13, p. 1037–1048.

National Petroleum Council, 1992, The potential for natural gas in the United States, source and supply, v. II: December, variously paginated.

National Research Council, 1994, Drilling and excavation technologies for the future: Washington, D.C., National Academy Press, 161 p.

Nelson, R. A., 1985, Geologic analysis of naturally fractured reservoirs: Houston, Gulf Publishing, 320 p.

Nelson, R. A., Lenox, L. C., and Ward, B. J., 1987, Oriented core: its use, error, and uncertainty: American Association of Petroleum Geologists Bulletin, v. 71, no. 4, p. 357–368.

Northrop, D. A., and Frohne, K. H., 1990, Insights and contributions from the Multiwell Experiment: a field laboratory in tight sandstone reservoirs: Journal of Petroleum Technology, v. 42, p. 722–779.

NSI Technologies, Inc., 1991, Well completion and hydraulic fracture treatment design and analysis of the Canyon sands (lower interval): topical report no. GRI-91-0165 prepared for the Gas Research Institute under contract no. 5091-221-2130, 192 p.

O'Brien, B. E., and Freeman, R. E., 1979, Lobo trend of south Laredo area, Webb and Zapata Counties, Texas: Oil and Gas Journal, v. 77, p. 158–176.

Ohio Geological Society, 1985, The New Clinton Collection—1985: Columbus, Ohio Geological Society, 243 p.

Olszak, W., Kajfasz, S., and Pietrzykowski, J., 1957, Ascertaining tensile strength by crushing cylinders: Concrete Construction Engineering, v. 9, p. 326–328.

Onash, C. M., 1990, Microfractures and their role in deformation of a quartz arenite from the central Appalachian foreland: Journal of Structural Geology, v. 12, p. 883–894.

Overbey, W. K., and Henninger, B. R., 1985, History, development, and geology of oil fields in Hocking and Perry Counties, Ohio, *in* The New Clinton Collection—1985: Columbus, Ohio Geological Society, p. 77–100.

Overbey, W. K., and Rough, R. L., 1971, Prediction of oil and gas bearing rock fractures from surface structural features: U.S. Bureau of Mines Report of Investigations, v. 7500, p. 1–14.

Oxford Instruments, 1993, EM applications note: scanning cathodoluminescence studies of siliciclastic rocks, 4 p.

Perry, K., 1994, Tight gas sands production: past—present—future: In Focus—Tight Gas Sands, v. 10, no. 1, p. 1–12.

Piscoran, P. L., and Schultz, R. A., 1994, Evolution of fracture sets and corresponding rock mass deformability (abs.): Eos, v. 75, p. 592.

Pittman, J. K., and Dickenson, W. W., 1989, Petrology and isotope geochemistry of mineralized fractures in Cretaceous rocks-evidence for cementation in a closed hydrologic system: U.S. Geological Survey Bulletin 1986-J, p. J1–J15.

Pittman, J. K., and Sprunt, E., 1986, Origin and distribution of fractures in Lower Tertiary and Upper Cretaceous rocks, Piceance Basin, Colorado, and their relationship to the occurrence of hydrocarbons, *in* Spencer, C. W., and Mast, R. F., eds., Geology of tight gas reservoirs: American Association of Petroleum Geologists Studies in Geology No. 24, p. 221–234.

Plumb, R. A., Herron, S. L., and Olsen, M. P., 1992, Influence of composition and texture on comprehensive strength variations in the Travis Peak Formation, *in* Proceedings, Society of Petroleum Engineers Annual Technical Conference and Exhibition, SPE Paper No. 24758, p. 985–998.

Potter, R. W., 1977, Pressure corrections for fluid inclusion Th based on the volumetric properties of the system NaCl-H_2O: USGS Journal of Research, v. 5, no. 5, p. 603–607.

Potter, R. W., Clynne, M. A., and Brown, D. L., 1978, Freezing point depression of aqueous sodium chloride solutions: Economic Geology, v. 73, p. 284–285.

Prezbindowski, D. R., and Larese, R. E., 1987, Experimental stretching of fluid inclusions in calcite—implications for diagenetic studies: Geology, v. 15, p. 333–336.

Price, N. J., 1966, Mechanics of jointing in rocks: Geological Magazine, v. 46, no. 2, p. 149–167.

Pyrak-Nolte, L. J., Myer, L. R., and Cook, N. G. W., 1985, Determination of fracture void geometry and contact area at different effective stress (abs.): Eos, v. 66, p. 903.

Queen, J. H., and Rizer, W. D., 1990, An integrated study of seismic anisotropy and the natural fracture system at the Conoco Borehole Test Facility, Kay County, Oklahoma: Journal of Geophysical Research, v. 95, p. 11,255–11,273.

Railroad Commission of Texas, 1980, Recommendation of the Railroad Commission of Texas that the geopressured Wilcox Lobo Formation be designated as a tight formation in Texas: Docket No. 20-75,144.

_____ 1990, Application of Texaco Producing, Inc., for the Commission's recommendation to the Federal Energy Regulatory Commission that the Guerra reservoir underlying certain portions of the McAllen Ranch (Guerra) field, Hidalgo County, Texas, be recognized as a tight gas sand: Docket No. 4-93,629.

_____ 1991, The application of Enron Oil and Gas Company for the recommendation before the Federal Energy Regulatory Commission that the lower Wilcox Sand interval underlying certain portions of Webb County, Texas, be recognized as a tight gas formation: Docket No. 4-96,631.

Reichmuth, D. R., 1968, Point-load testing of brittle materials to determine tensile strength and relative brittleness: Proceedings, 9th Symposium on Rock Mechanics, Golden, CO, p. 134–159.

Reik, G. A., and Currie, J. B., 1974, A study of relation between rock fabric and joints in sandstone: Canadian Journal of Earth Sciences, v. 11, p. 1253–1268.

Ritzma, H. R., 1962, Piceance Creek gas field, *in* Amuedo, C. L., and Mott, M. R., eds., Exploration for oil and gas in northwest Colorado: Rocky Mountain Association of Geologists, p. 96–103.

Rivers, T., Razack, T., M., Petit, J. P., and Rawnsley, K., 1992, Joint spacing: analogue and numerical modeling: Journal of Structural Geology, v. 14, p. 925–937.

Robinson, B. M., Holditch, S. A., and Lee, W. J., 1986, A case study of the Wilcox (Lobo) trend in Webb and Zapata Counties, Texas: Journal of Petroleum Technology, December, p. 1355–1364.

Roedder, Edwin, and Bodnar, R. J., 1980, Geologic pressure determinations from fluid-inclusion studies: Annual Reviews of Earth and Planetary Science, v. 8, p. 263–301.

Roedder, Edwin, 1962, Studies of fluid inclusions I. Low temperature application of a dual purpose heating and freezing stage: Economic Geology, v. 57, p. 1045.

_____ 1979, Fluid inclusions as samples of ore fluids, *in* Barnes, H. L., ed., Geochemistry of hydrothermal ore deposits: New York, Wiley, p. 684–737.

_____ 1984, Fluid inclusions: Washington, D.C., Mineralogical Society of America, Reviews of Mineralogy, v. 12, 644 p.

Roedder, Edwin, and Skinner, B. J., 1968, Experimental evidence that fluid inclusions do not leak: Economic Geology, v. 63, p. 715–730.

Sayers, C. M., 1990, Orientation of microcracks formed in rocks during strain relaxation: International Journal of Rock Mechanics, Mining Sciences, v. 27, p. 437–439.

Schrider, L. A., Watts, R. J., and Wasson, J. A., 1970, An evaluation of the East Canton oil field waterflood: Journal of Petroleum Geology, v. 22, p. 1371–1378.

Schultz-Ela, D. D., and Yeh, J., 1992, Predicting fracture permeability from bed curvature, *in* Tillerson, J. R., and Wawersek, W. R., eds., Proceedings of the 33rd U.S. Symposium on Rock Mechanics: Rotterdam, Balkema, p. 579–590.

Science Applications International Corporation (SAIC), 1991, Static and dynamic investigation on S. A.

Holditch's Staged Field Experiment (SFE) No. 4-24: SAIC final report no. 1-107-05-686-00, 12 p.

Scott, G. L., Brannigan, J. P., and Mitchell, S. T., 1983, Pecos Slope Abo Gas field, Chaves County, New Mexico, *in* Zidek, Jiri, ed., Guidebook for field trip to the Abo red beds (Permian), central and south-central New Mexico: Roswell Geological Society and New Mexico Bureau of Mines and Mineral Resources, 1 plate.

Self, G. A., Breard, S. Q., Rael, H. P., Stein, J. A., Thayer, P. A., and Easom, W. D., 1986a, Lockhart Crossing field: New Wilcox trend in southeastern Louisiana: Oil and Gas Journal, v. 84, p. 81–87.

Self, G. A., Breard, S. Q., Rael, H. P., Stein, J. A., Thayer, P. A., Traugott, M. O., and Easom, W. D., 1986b, Lockhart Crossing field: new Wilcox trend in southeastern Louisiana: American Association of Petroleum Geologists Bulletin, v. 70, no. 5, p. 501–515.

Shepherd, T. J., 1990, Geological link between fluid inclusions, dilatant microcracks, and paleostress field: Journal of Geophysical Research, v. 95, no. B7, p. 11,115–11,120.

Sinclair, S. W., 1980, Analysis of macroscopic fractures on Teton Anticline, northwestern Montana: Texas A&M University, Master's thesis, 102 p.

Sipple, R. F., 1968, Sandstone petrology: evidence from luminescence petrography: Journal of Sedimentary Petrology, v. 38, p. 530–554.

Sitler, G. F., 1985, East Canton-Magnolia oilfield, *in* Ohio Geological Society, Clinton Sandstone papers presented at the Ohio Oil and Gas Association Winter Meetings, 1961 to 1978—Abridged Reprint of 1980 Volume: Columbus, Ohio Geological Society, p. 41–51.

Smith, D. L., and Evans, B., 1984, Diffusional crack healing in quartz: Journal of Geophysical Research, v. 89, p. 4125–4135.

Snedden, J. W., and Kersey, D. G., 1982, Depositional environments and gas production trends, Olmos Sandstone, Upper Cretaceous, Webb County, Texas: Gulf Coast Association of Geological Societies Transactions, v. 32, p. 497–518.

Sowers, G. M., 1972, Theory of spacing of extension fractures: Geological Society of America Engineering Geology Case History No. 9, p. 27–53.

Sprunt, E. S., Dengler, L. A., and Sloan, D., 1978, Effect of metamorphism on quartz cathodoluminescence: Geology, v. 6, p. 305–308.

Sprunt, E. S., and Nur, Amos, 1979, Microcracking and healing in granites: new evidence from cathodoluminescence: Science, v. 205, p. 495–497.

Stearns, D. W., 1968, Certain aspects of fracture in naturally deformed rocks, *in* Rieker, R. E., ed., NSF Advanced Science Seminar in Rock Mechanics, Special Report: Bedford, Massachusetts, Air Force Cambridge Research Laboratories, AD 6693751, p. 97–118.

Szendi-Horvath, G., 1980, Fracture toughness determination of brittle materials using small to extremely small specimens: Engineering Fracture Mechanics, v. 13, no. 4, p. 955–961.

Tada, R., and Siever, R., 1989, Pressure solution during diagenesis: Annual Reviews of Earth and Planetary Sciences, v. 17, p. 89–118.

Teufel, L. W., 1983, Determination of the principal horizontal stress directions from anelastic strain recovery measurements of oriented core application to the Cotton Valley Formation, East Texas: Houston, TX, ASME Symposium on Geomechanics Proceedings.

Thiercelin, M., and Cook, J., 1988, Failure mechanisms induced by indentation of porous rocks *in* Cundall, P. A., Sterling, R. L., and Starfield, A. M., eds., Key questions in rock mechanics: Rotterdam, Balkema, p. 135–142.

Thomaidis, N. D., 1973, Church Buttes arch, Wyoming and Utah: *in* Wyoming Geological Association 25th annual field conference guidebook, p. 35–39.

Tuttle, O. F., 1949, Structural petrology of planes of liquid inclusions: Journal of Geology, v. 57, p. 331–356.

Tye, R. S., 1989, Stratigraphy and depositional systems of the Lower Cretaceous Travis Peak Formation, East Texas Basin: The University of Texas at Austin, Bureau of Economic Geology, topical report no. GRI-91/0128 prepared for the Gas Research Institute, 45 p.

Tyler, Noel, and Ambrose, W. A., 1986, Depositional systems and oil and gas plays in the Cretaceous Olmos Formation, South Texas: The University of Texas at Austin, Bureau of Economic Geology Report of Investigations No. 152, 42 p.

Verbeek, E. R., and Grout, M. A., 1983, Fracture history of the northern Piceance Creek Basin, northwestern Colorado, *in* Gary, J. H., ed., Proceedings of the 16th Oil Shale Symposium: Golden, Colorado School of Mines Press, p. 29–44.

Wach, P. H., 1977, The Moxa Arch, an overthrust model?: Rocky Mountain Thrust Belt, geology and resources, *in* Wyoming Geological Association 29th annual field conference guidebook, p. 651–664.

Walker, G., and Burley, S., 1991, Luminescence petrography and spectroscopic studies of diagenetic minerals, *in* Barker, C. E., and Kopp, O. C., eds., Luminescence microscopy, quantitative and qualitative aspects: SEPM, p. 83–96.

Walls, J. D., Hyman, L., Malek, D., and Admire, C., 1990, Improvements of formation evaluation and reservoir engineering in tight gas sands through selected core-analysis procedures: Core Lab contract report to the Gas Research Institute, 88 p.

Watts, R. J., Schrider, L. A., and Craig, J. G., 1972, Reservoir and production characteristics of the Clinton sand, East Canton oilfield, *in* Ohio Geological Society, Clinton Sandstone papers presented at the Ohio Oil and Gas Association Winter Meetings 1961 to 1978—Abridged Reprint of 1980 Volume: Columbus, Ohio Geological Society, p. 58–60.

Weimer, R. J., and Sonnenberg, S. A., 1989, Sequence stratigraphic analysis of Muddy (J) Sandstone reservoir, Wattenberg field, Denver Basin, Colorado, *in* Coalson, E. B., ed., Petrogenesis and petrophysics of selected sandstone reservoirs of the Rocky Mountain region: Rocky Mountain Association of Geologists, p. 197–220.

Weimer, R. J., Sonnenberg, S. A., and Young, G. B. C., 1986, Wattenberg field, Denver Basin, Colorado, *in* Spencer, C. W., and Mast, R. F., eds., Geology of tight reservoirs: American Association of Petroleum Geologists Studies in Geology No. 24, p. 143–164.

Whitehead, W. S., Gatens, J. M., III, and Holditch, S. A., 1989, Determination of in-situ stress profiles through hydraulic fracturing measurements in two distinct geologic areas: International Journal of Rock Mechanics Mining Science and Geomechanics Abstracts, v. 26, no. 6, p. 637–645.

Winn, R. D., Jr., Stonecipher, S. A., and Bishop, M. G., 1984, Sorting and wave abrasion: controls on composition and diagenesis in lower Frontier sandstones, southwestern Wyoming: American Association of Petroleum Geologists Bulletin, v. 68, p. 268–284.

Wu, H., and Pollard, D. D., 1991, Fracture spacing, density, and distribution in layered rock mass: results from a new experimental technique, *in* Proceedings, 32nd U.S. Symposium of Rock Mechanics, Oklahoma, p. 1175–1184.

Wu, S., and Groshong, R. H., 1991, Low temperature deformation of sandstones, southern Appalachian fold-thrust belt: Geological Society of America Bulletin, v. 103, p. 861–875.

Wuellner, D. E., Lehtonen, L. R., and James, W. C., 1986, Sedimentary-tectonic development of the Marathon and Val Verde basins, West Texas, U.S.A.: a Permo-Carboniferous migrating foredeep, *in* Allen, P. A., and Homewood, P., eds., Foreland basins: International Association of Sedimentologists Special Publication No. 8, p. 347–367.

Yin, Hezhu, and Dvorkin, J., 1994, Strength of cemented grains: Geophysical Research Letters, v. 21, no. 10, p. 903–906.

Yin, Peigui, Liu, Jie, and Surdam, R. C., 1992, Petrographic and petrophysical properties of the Almond Sandstone in the Washakie Basin: Wyoming Geological Association Guidebook, p. 191–205.

Zinkernagel, U., 1978, Cathodoluminescence of quartz and its application to sandstone petrology: Contributions to Sedimentology 8, 69 p.

Appendix 1. Fractures in Sandstone Natural Gas Reservoir Rocks

Table A1-1. Summary data on natural fracture information, tight gas sandstones.

	Fractures observed in core	Published core fracture description	Published account of anomalous production	Outcrop fracture description	Published account of horizontal well	Important fracture types		
						RE	LO	CO
"Clinton"-Medina	Y	a	1	N	N	5	5	2
Berea	Y	a	1	N	N	5	5	2
Cotton Valley	Y	a,c,g	1	N	N	5	5	2
Travis Peak	Y	b,c,d,e,f,g	1,h	N	N	5	Y	2
Olmos	—	N	—	—	N	Y,5	6	6
Wilcox deltaic	Y	N	—	—	N	2	6	6
Wilcox Lobo	Y	N	—	—	N	2	6	Y
Vicksburg	—	—	—	—	N	2	6	5
Cherokee/Red Fork	—	—	—	—	N	2	2	2
Cleveland	Y	a	—	—	N	2	2	2
Granite Wash	—	—	—	—	N	—	2	2
Davis	Y	b,c,d	Y	N	Y	5	4	2
Abo	Y	N,3	—	1	N	2	5	6
Morrow	—	N	—	—	N	2	2	—
Canyon	Y	8,a,c,d,g	1	N	N	5	5	2
Dakota	Y	3	—	N	N	6	6	2
Cliff House/Point Lookout	—	3	—	N	N	6	6	2
Pictured Cliffs	Y	a,c	Y,i	Y,j	N	6	6	2
Muddy (J)	Y	2,3	—	—	N	5	3	2
Mancos "B"	Y	a,c	—	—	Y	5	3	2
Mesaverde	Y	a,c	Y,i	Y,j,7	Y	5	6	2
Upper Almond/Blair	—	—	—	—	N	6	4,5	2
Frontier	Y	b,c,d,f,g	1,h	Y,j	N	5	5	2

Key

—	=	Unknown	b	=	Core study of subregional scale, numerous wells
Y	=	Yes	c	=	FMS or BHTV data are available
N	=	No	d	=	Published microstructural study
1	=	Limited study	e	=	Established "mechanical stratigraphy"
2	=	Limited information is available on topic	f	=	Basin-scale fracture study
3	=	Anecdotal evidence	g	=	Specific published data on in situ stress directions
4	=	Not definitive	h	=	Published account of anomalous treatment response
5	=	Probable	i	=	Production study of natural fractures
6	=	Unknown, suggested by structural setting	j	=	Published account of outcrop analog of reservoir fractures
7	=	Local	RE	=	Regional
8	=	In press	LO	=	Local fracture permeability in folds and fault zones
a	=	Core study in one or a few wells	CO	=	Reservoirs compartmentalized by small faults

Appendix 2. Analysis of Core Orientation and Fracture Sampling Success

This appendix presents information on the effectiveness of measuring macrofracture strike with whole core. Data are from eight Gas Research Institute (GRI) wells and industry-GRI cooperative research wells in the Sonora Canyon, Travis Peak, and Frontier formations (table A2-1). This data set is of interest because coring procedures and core recovery and handling were carried out largely by the same S. A. Holditch & Associates, CER Corporation, and Bureau of Economic Geology personnel using similar procedures. Data from oriented core are in part the basis for comparisons of microfracture and macrofracture orientations presented in the text of our report. The data set in this appendix substantiates the view that the process of obtaining oriented fractures using core from hard sandstone often falls below desired levels of success. Results presented in this appendix underline the need for the indirect fracture-strike mapping techniques described in the text.

Obtaining oriented macrofractures depends on (1) intercepting fractures in core and (2) orienting the core. The limitations of sampling near-vertical fractures in the subsurface are discussed in the main text. In cases where one fracture set is present, fracture spacing is regular, and fractures extend vertically across the interval of interest, the probability of encountering a fracture with vertical core is the ratio of the core diameter to the fracture spacing (Narr, 1991). Because natural fracture spacing is generally much greater than the core diameter, the probability of encountering fractures is inherently small. Natural fractures can also be mistaken for coring-induced fractures if fracture mineralization is not detected, and small fractures can be missed by inexperienced analysts during core description.

The challenge of orienting fractures that are encountered by drilling may seem slight compared to these sampling problems, but our results suggest that core orientation is generally not highly successful, further degrading the industry's ability to map subsurface fracture strikes. The causes of failure in core orientation relate to technical limitations and problems with individual core-orientation technologies, and interference with core orientation by the natural fractures themselves. To quantify the likelihood of accurately orienting core and the frequency of natural fracture occurrence in oriented intervals, we compiled data from CER well reports on eight wells of the Frontier, Travis Peak, and Canyon sandstones (table A2-1). These wells were drilled with the purpose of obtaining oriented core, and careful and relatively consistent core handling techniques were used.

Core is oriented by a variety of techniques that are summarized by Nelson and others (1987). All of these techniques were attempted in the wells we describe. One common orientation method uses a magnetic multiple-shot survey instrument to orient reference grooves on the core. Orientation measurements are taken at regular intervals during coring, and grooves are cut continuously. Failure can occur as a result of orientation instrument malfunction, relative movement between core barrel and orientation device, loss of scribe knives (and thus grooves on the core) due to wear, and breakup of core within the core barrel. Scribe knives are readily damaged, and core breakup is especially prevalent in hard, fractured sandstones.

Another core-orientation technique relies on using oriented borehole-imaging logs, such as borehole televiewers or Formation Microscanner, to identify individual features such as fractures or distinctive sedimentary structures that can be correlated between the log and the core. Such techniques require the fortuitous presence of unusual and distinctive features to be reliable. The technique also requires long sections of accurately reassembled core, so that orientation information related to features that are imaged with logs can be used to orient features in core. Dipmeter logs can be used in a similar way to orient an observed dipping feature in core. Application of dipmeter orientation requires high-quality log data and a continuous interval of core, as well as a fairly steeply dipping feature (>10 degrees).

Core can also be oriented using measurements of core magnetic properties, where results are correlated with a known magnetic standard such as Holocene magnetic north. As with log-based methods, exact reassembly of core segments is needed so that samples for magnetic core orientation can be taken over a range of depths to average out variations in magnetic signal.

Table A2-1. Core orientation success.

Operator	Philips	Enron Oil & Gas	S. A. Holditch	Mobil	S. A. Holditch	Terra Resources	Enron Oil & Gas	Wexpro
Well	Ward "C" #1	Sawyer 144A #5	SFE #1	SFE #3	SFE #4	Anderson Canyon 3-17	South Hogsback 13-A	Church Butte #48
Location	Sutton Co., TX	Sutton Co.,TX	Harrison Co., TX	Harrison Co., TX	Sublette Co., WY	Lincoln Co., WY	Lincoln Co., WY	Sweetwater Co., WY
Formation	Canyon	Canyon	Travis Peak	Travis Peak	Frontier	Frontier	Frontier	Frontier
Core recovered (ft)	201.1	281.0	468.5	373.6	322.0	159.9	273.2	85.6
Percent core recovered	58.0	99.0	89.0	78.9	75.0	72.0	79.0	99.0
Total sandstone (ft)	140.7	219.2	226.5	204.7	78.0	112.9	182.1	71.0
Attempted core orientation (ft)	201.1	27.6	418.8	83.5	178.2	136.0	114.1	85.6
Successful core orientation (ft)	133.9	19.0	58.1	34.7	165.6	23.8	53.6	72.0
Oriented core/total core (%)	66.6	6.8	12.4	9.3	51.4	14.9	19.6	84.1
Oriented sandstone (ft)	85.0	19.0	30.7	34.7	60.8	23.8	53.4	38.0
Percent oriented ss/total ss	60.4	8.7	13.6	17.0	77.9	21.1	29.3	53.5
Total natural fractures	23	57	36	55	30	18	20	8
Oriented natural fractures	4	8	6	51	22	0	0	3
Percent oriented /total natural fractures	17.4	14.0	16.7	92.7	73.3	0.0	0.0	37.5
Orientation techniques*	CHAMP	CHAMP	EMS, DMWD, PM	EMS	EMS	EM	EMS	EMS

*

EMS	electromagnetic survey instrument
EM	electronic multishot tool
PM	paleomagnetic core orientation
DMWD	directional-measurement-while-drilling tool
CHAMP	CHAMP downhole survey tool
SS	sandstone

Misorientation of core is caused by instrument error, error in data interpretation (Nelson and others, 1987), and breakup of the core. Instrument error includes error in compass reading, error in film reading, failure of electronic equipment, initial misalignment of orientation scribe and compass, or misalignment of scribe and compass due to drilling torque. Error in data interpretation includes miscorrelation between orientation measurement and core piece (a problem augmented by missing core or rubble), error in reading goniometer, and error in reading scribe. This last problem is especially pronounced when scribe marks curve or spiral. Nelson and others (1987) estimate that the minimum orientation errors from these combined factors is $\pm$11 degrees. Core breakup affects all orientation techniques and generally results in core orientation failure rather than in orientation uncertainty.

Accurate core orientation requires care in core cutting, recovery, layout, and marking. Careful techniques, described by Lorenz and Hill (1992), were used on the core in this study. To avoid misalignment or induced fracturing of core during processing, core was slowly extruded from core-barrel liners in the field using a hydraulic pump. Hydraulic recovery of the core from the barrel aids continuous reassembly of the core and preservation of small core fragments. To ensure full recovery of core reduced to rubble and preservation of core-segment orientation, water was flushed through the core barrel, forcing the core segments out into numbered trays. Core was reassembled, and rubble zones or spinoffs were noted. These techniques allowed a maximum proportion of the core to be oriented. To compare relative orientations of fractures in core, core reassembly was attempted even in unoriented segments. If scribe-based orientation methods were used, the principal scribe line (PSL) is marked on the assembled core. A straight master orientation line (MOL) is also marked. The MOL is marked the entire length of core, following the principal scribe line where it was visible and nonspiraling. The MOL and PSL are coincident where the PSL is straight. Deviation of the MOL and PSL is a measure of the rotation of the magnetic tool-face orientation.

The results of these procedures are summarized in table A2-1 and figure A2-1 for the eight wells. The table shows the total footage of core recovered, percent of core recovered, total amount of core that was attempted to be oriented, total amount of core that was successfully oriented, core-orientation technique, and total oriented-core footage. Additionally, because natural fractures tend to occur preferentially in sandstone beds, the total amount of sandstone recovered and amount of sandstone recovered from oriented intervals are also tabulated (table 2A-1 and fig. A2-2). These results demonstrate the difficulty of obtaining oriented core, even when careful handling procedures are used.

Percentage of oriented core per total core recovered and percentage of oriented sandstone per total amount of sandstone recovered were calculated as measures of core-orientation success. Proportion of oriented core ranges from 84 percent (Frontier Formation, Wexpro Church Butte No. 48 well) to 7 percent (Sonora Canyon, Enron Sawyer 144A No. 5 well). Proportion of oriented sandstone ranges from 78 percent (Frontier Formation, Holditch SFE No. 4 well) to 9 percent (Sonora Canyon, Enron Sawyer 144A No. 5 well). The proportion of oriented core in the two Travis Peak Formation wells is low (about 10 percent) despite (or because of) the large number of large fractures in these wells. The proportion of oriented core in the other wells studied shows substantial variation within a formation.

The percentage of oriented sandstone is greater than the percentage of oriented core in all but two wells (Wexpro Church Butte No. 48 and Philips Ward "C" No. 11). This suggests that sandstone is easier to orient than other rock types, possibly because it has better induration that inhibits coring induced fracturing and rubble formation, thereby allowing better core reassembly. In many industry applications, coring is focused on sandstone (i.e., reservoir) intervals, but in these wells, core orientation was attempted in shale and mudstone intervals to sample rocks that potentially are barriers to hydraulic fracture height growth.

The number of natural fractures and the number of oriented natural fractures are compared in table A2-1 and figure A2-3. The percentage of oriented fractures per total natural fractures in core ranges from 0 in two Frontier Formation wells (Terra Resources Anderson Canyon 3-17 and Enron South Hogsback 13-A) to 93 in a Travis Peak/Cotton Valley well (Mobil SFE No. 3). The percentage of oriented natural fractures is low for the two wells in the Canyon Formation, despite the large number of small fractures in these cores. Values range widely for wells of the Frontier and Travis Peak Formations. These results suggest that the success of orienting core and orienting fractures within a core does not strongly depend on the formation cored. Success in fracture orientation is generally low for all formations in which core orientation was attempted.

These results show that it is generally possible to obtain oriented core in these sandstones but that it is commonly not an effective means of obtaining oriented fractures. Partly this is the consequence of an additional sampling bias—core orientation is not attempted on all core runs, and features on borehole walls are commonly not distinctive enough for orientation purposes. In addition, the macrofractures themselves, or the highly indurated rocks in which they occur, interfere with the orientation procedure.

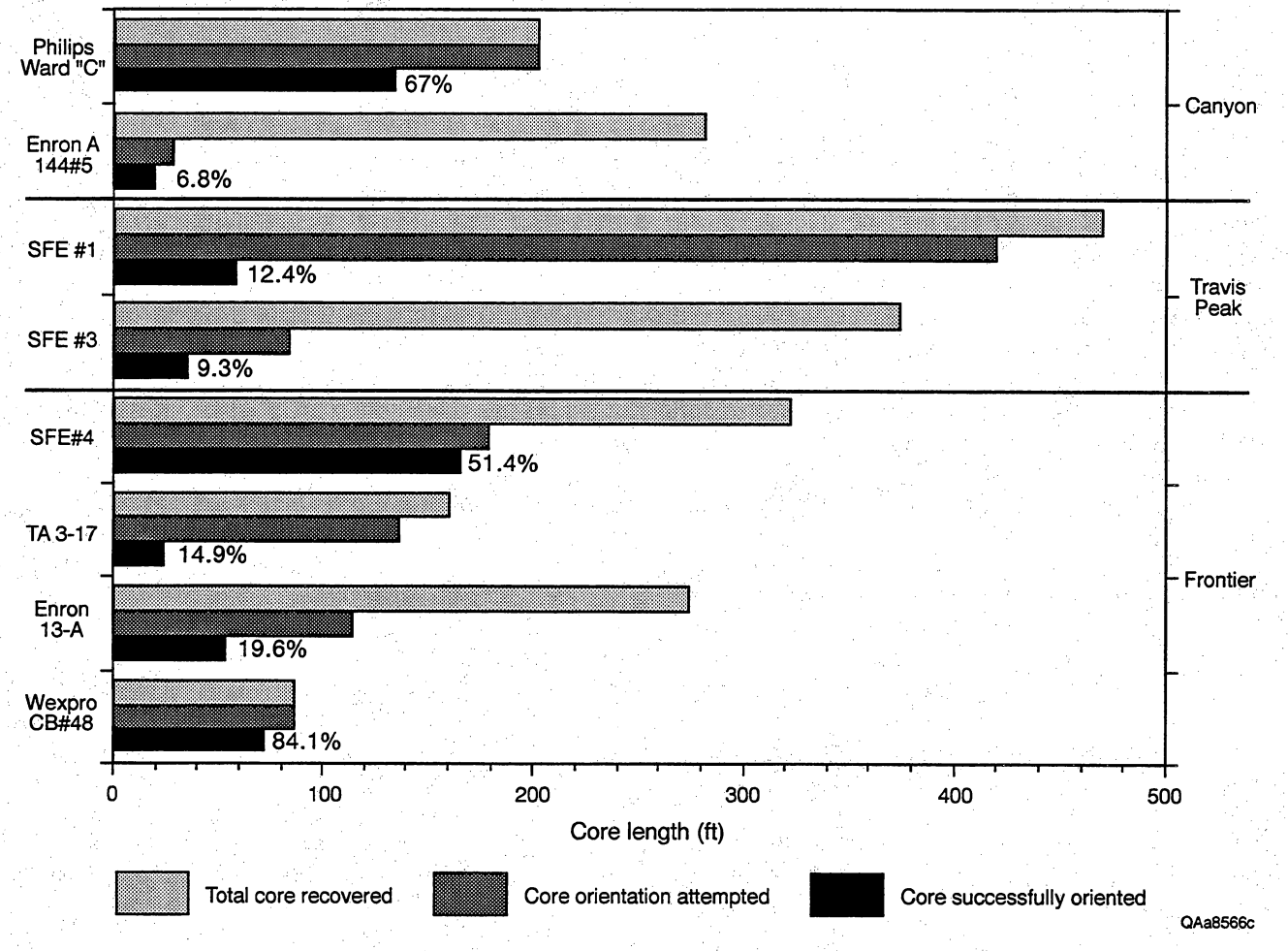

Figure A2-1. Total core recovered, core orientation attempted, and core successfully oriented.

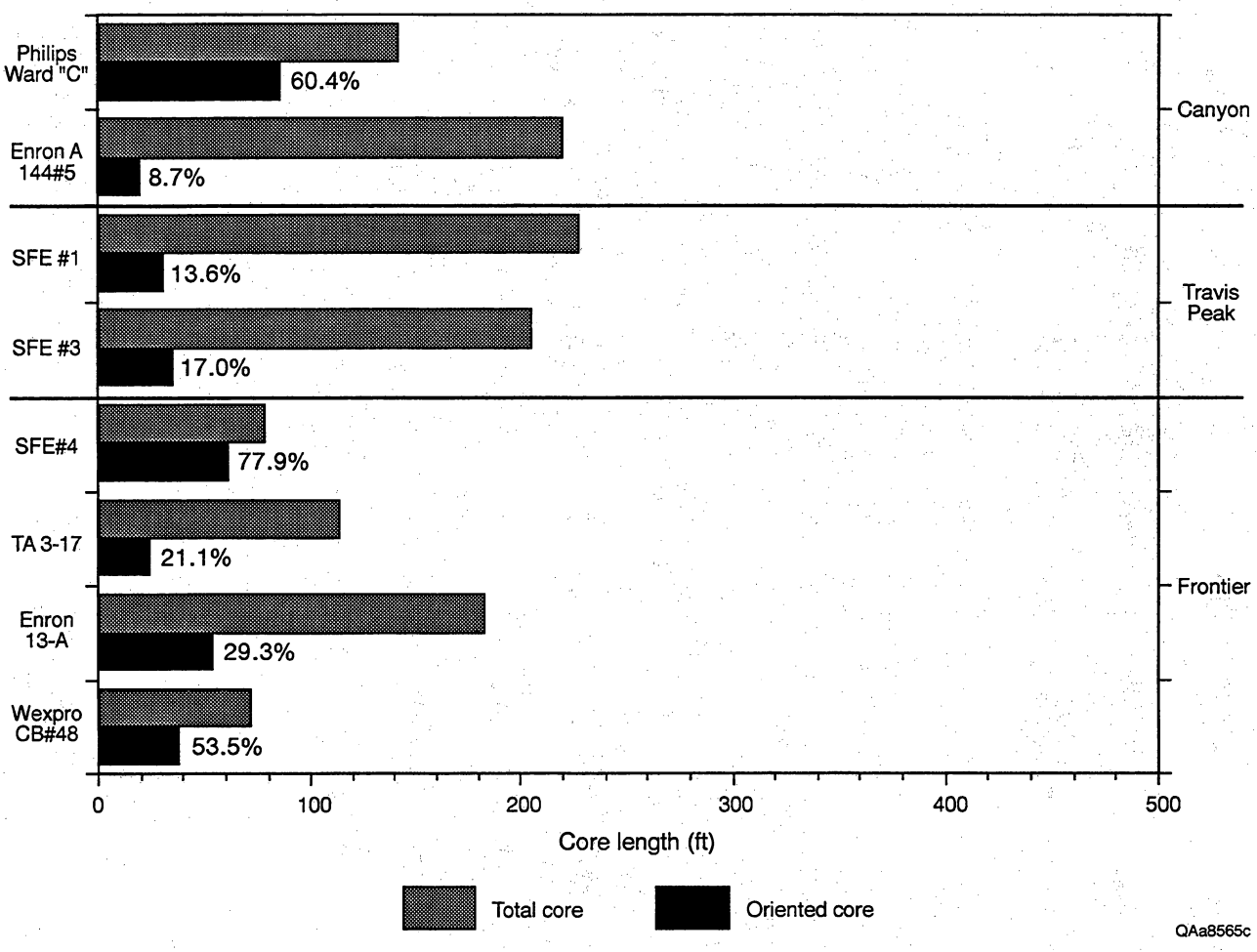

Figure A2-2. Total sandstone core versus footage of oriented sandstone.

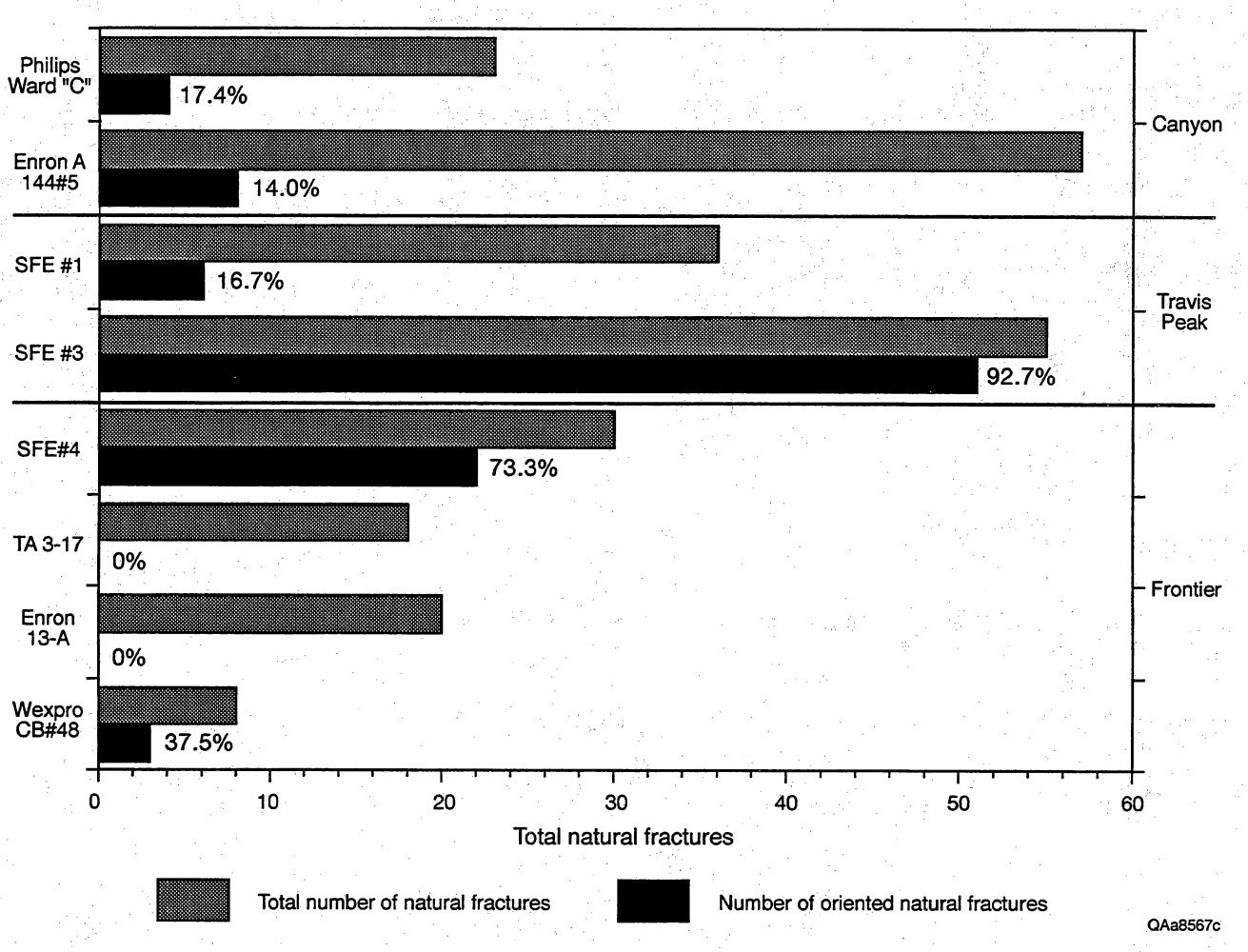

Figure A2-3. Total natural fractures in core versus number of oriented fractures.

Appendix 3. Fluid-Inclusion Data

Well	Section	Type	Diameter (μ)	Tim (°C)	Tfm (°C)	Th (°C)	NaCl eq. (wt %)
SFE #2	9871.5 A	C	14	-60	-10	168	13.99
		C	14	-60	-9	166	12.88
		C	7	-55	-6	164	9.21
	9914.0 A		30	-64	-11	157	15.04
			35	-63			
			45	-63	-8	174	11.71
			45	-64	-7	178	10.49
			33	-62	-9	160	12.88
			45	-63	-9	175	12.88
	9914.0 B1-1	B	6	-63	-7	137	10.49
		B	6	-63	-5	140	7.85
		B	6	-61	-7	135	10.49
		C	9	-63	-5	136	7.85
		B	4	-59	-5	130	7.85
		B	3	-62	-9		12.88
		C	6	-65	-9	146	12.88
		B	8	-70	-7	146	10.49
		B	3	-64	-9	147	12.88
		A	3	-63	-11	136	15.04
		A	2	-64	-10	120	13.99
		A	2	-64	-10	131	13.99
		A	2	-62	-8	139	11.71
	9914.0 B1-2	B	5	-62	-15	147	18.79
		B	5	-61	-12	150	16.04
		C	12	-62	-8	148	11.71
		C	15			143	
		B	5	-60	-3	162	4.94
		B	8	-65	-4		6.43
		C	10	-66	-5	135	7.85
		B	6	-67	-6		9.21
		B	10	-64	-3		4.94
		B	4			126	
		B	5			164	
		A	4		-11	158	15.04
		A	2	-70	-11	121	15.04
		A	5	-65	-9	124	12.88
		A	2		-10	175	13.99
		A	3	-67	-10	180	13.99
		A	2	-63	-9		12.88
		A	2	-64	-11	121	15.04
		A	5	-64	-13	180	16.95
		A	2	-64	-10	133	13.99
	9924.0 B1-3	C	13	-61	-8		11.71
		C	13	-61	-7		10.49
	9914.3 A	C	17	-73	-18	140	21.2
SFOT #1	10106 A1-1	C	17	-64	-9	158	12.88
		C	22	-62	-6	154	9.21
		C	7	-65	-8	150	11.71
		C	26	-54	-7		10.49
		C	8	-64	-7	153	10.49
		C	12	-64	-6	152	9.21
		C	15	-67	-5	152	7.85
		C	8	-64	-7	148	10.49
	10106 A1-2	C	17	-59	-8		11.71
		C	8	-58	-10		13.99
	10106 A2-1	C	13	-63	-10		13.99

QAa8583c

Appendix 3 (cont.).

		Diameter (μ)	Tfm (°C)	Th (°C)
Quartz	A-Type	4	-11	136
		2	-10	120
		2	-10	131
		2	-8	139
		4	-11	158
		2	-11	121
		5	-9	124
		2	-10	175
		3	-10	
		2	-9	
		2	-11	121
		5	-13	180
		2	-10	133
	B-Type	6	-7	137
		6	-5	140
		6	-7	135
		4	-5	130
		3	-9	
		8	-7	146
		3	-9	147
		5	-15	147
		5	-12	150
		5	-3	162
		8	-4	
		6	-6	
		10	-3	
		4		126
		5		164
	C-Type	14		168
		14	-9	166
		7	-6	164
		9	-5	136
		6	-9	146
		12	-8	148
		15		143
		10	-5	135
		13	-8	
		13	-7	
		17	-18	140
		17	-9	158
		22	-6	154
		7	-8	150
		26	-7	
		8	-7	153
		12	-6	152
		15	-5	152
		8	-7	148
		17	-8	
		8	-10	
		13	-10	
Calcite		30	-11	157
		45	-8	174
		45	-7	178
		33	-9	160
		45	-9	175

QAa8580c

Headquarters
Gas Research Institute
8600 West Bryn Mawr Avenue
Chicago, Illinois 60631-3562
312/399-8100

Washington Operations
Gas Research Institute
1331 Pennsylvania Avenue, N.W.
Suite 730 North
Washington, D.C. 20004-1703
202/662-8989